Mechanistic modelling of the links between environment, mosquitoes and malaria transmission in the current and future climates of West Africa

by

Teresa K. Yamana

S. B. Environmental Engineering Science
Massachusetts Institute of Technology (2004)

S.M. Civil and Environmental Engineering
Massachusetts Institute of Technology (2010)

Submitted to the Department of Civil and Environmental Engineering
in partial fulfillment of the requirements for the degree of
Doctor of Philosophy in the Field of Hydrology

at the

Massachusetts Institute of Technology
February 2015

Signature of Author: _____
Department of Civil and Environmental Engineering
January 29, 2015

Certified by: _____
Elfatih A. B. Eltahir
Professor and Associate Department Head of Civil and Environmental Engineering
Thesis Supervisor

Accepted by: _____
Heidi M. Nepf
Donald and Martha Harleman Professor of Civil and Environmental Engineering
Chair, Departmental Committee for Graduate Students

Mechanistic modelling of the links between environment, mosquitoes and malaria transmission in the current and future climates of West Africa

by

Teresa K. Yamana

Submitted to the Department of Civil and Environmental Engineering
on January 29, 2015 in partial fulfillment of the requirements for the degree of Doctor of Philosophy in the Field of Hydrology

ABSTRACT

Malaria transmission in West Africa is closely tied to climate, as rain fed water pools provide breeding habitat for the anopheles mosquito vector, and temperature affects the mosquito's ability to spread disease. This thesis presents a framework of highly detailed, spatially explicit mechanistic modelling to explore the relationships between the environment and malaria in the current and future climate of West Africa. A mechanistic model of human immunity was incorporated into an existing agent-based model of malaria transmission, allowing us to move beyond entomological measures such as mosquito density and vectorial capacity to analyzing the prevalence of the malaria parasite within human populations. The result is a novel modelling tool that mechanistically simulates all of the key processes linking environment to malaria transmission.

Simulations were conducted across climate zones in West Africa, linking temperature and rainfall to entomological and epidemiological variables with a focus on nonlinearities due to threshold effects and interannual variability. Comparisons to observations from the region confirmed that the model provides a reasonable representation of the entomological and epidemiological conditions in this region.

While current generation climate models agree that mean temperatures in West Africa will likely increase by 2 to 4^{o} C in the future by the end of the 21st century, they disagree on the magnitude and the direction of the change in rainfall. We analyzed the performance of CMIP5 climate models in simulating West African rainfall and temperature before selecting the most credible predictions of future climate. We used these predictions to simulate the expected change in malaria transmission in sensitive regions of West Africa. We found that the western subregion of West Africa is likely to become drier in the coming decades. The warmer temperatures will shorten mosquito life spans, and the drying will limit mosquito reproduction. As a result, we expect malaria transmission in this region to decrease. However, the eastern half of the region is expected to become wetter. In some areas, the positive effects of increased rainfall on mosquito

reproduction may surpass the negative effects of high temperatures on mosquito longevity, leading to a small net increase in environmental suitability for malaria transmission.

Thesis Supervisor: Elfatih A. B. Eltahir

Title: Professor and Associate Department Head of Civil and Environmental Engineering

Acknowledgements

I am so grateful to my advisor, Elfatih Eltahir, for his many years of guidance and encouragement. His generosity in time, advice and support has been invaluable to my growth as a scientist and as a person. I would also like to thank my graduate committee, Arne Bomblies, Bill Jobin, and Charlie Harvey who have provided so many important perspectives and ideas throughout my degree.

It has been such a wonderful experience being a part of the Parsons Laboratory community. Countless interactions at Friday breakfast or over the newspaper made every day more enjoyable. In particular, I'd like thank my cubicle-mates Jessie, Patricia and Dave for their friendship, coffee breaks and patience with my odd noises; my cohort of $6.5^{th} \pm 2$ year PhD students with whom I've shared so many experiences from studying for qualifying exams to farmshares to ski trips; my fellow February 2015 degree list candidates who kept me company during our many late nights of thesis writing these past few months.

Thank you to my friends and colleagues in the Eltahir research group: Noriko, Bec, Mariam, Mohamed, Mekki, Marc, Hamed, Eun Soon, Ross, Xin, Jeremy, Jonathan and Anjuli. It has been a privilege to work with such a diverse and hardworking group of people. I'd like to thank the CEE and Parsons administrators and support staff, especially Sheila Frankel, Kris Kipp, Joanne Batziotegos, Gayle Sherman, Vicki Murphy and Jim Long. Thanks to the faculty members of CEE and HSPH whose classes were a highlight of my graduate education.

I would like to thank my family for their constant encouragement and for all they have done to make this work possible. Thank you to my parents Misuzu and Ed who made me love school enough to spend two decades as a student. It has been such a treat to live in the same city as my brother Sean and his partner Amanda for the last few years. I am enormously grateful to Kabir, who has been unbelievably supportive in every aspect of my life. I cannot imagine a better partner and friend. Thank you to Salim for all the joy and excitement of this past year.

I am grateful to Jessie Berta-Thompson and Sean Yamana-Hayes for their assistance in preparing the figures and text of this thesis. Misuzu, Beth, Chris, Jessie, Zach, Jane and Waheed were extremely helpful in domestic matters during the final stages of my dissertation.

My friends from pika have continued to be an important and fun presence in my life – Kate, Gretchen, Johanna, Sarah, Marc, Kyle, Erin, Sam. The oddly large proportion of this group that preceded me in obtaining their doctorates provided encouragement and advice as I followed along. I look forward to continuing our annual reunions at AGU!

Thank you to my former students at Mother Caroline Academy, whose perseverance through high school and now college has been a true inspiration. Thank you to all my teachers and mentors who have inspired me and helped me to succeed, especially Dr. Bruce White from Vincent Massey Secondary School, Susan Murcott from MIT and the late Ron Rivera from Potters for Peace.

I'd like to thank the leaders and participants of my favorite extracurricular activities: Dance Party with Fen Tung, Chinese Painting with Qingxiong Ma, the Cambridge Symphony Orchestra, and the MIT Graduate Women's Reading Group.

This work was funded by the U.S. National Science Foundation and the Martin Family Society of Fellows for Sustainability.

Table of Contents

List of Figures

List of Tables

1 Introduction

1.1 Motivation

Malaria is one of the world's greatest public health challenges, with an estimated 3.2 billion people at risk of infection. In 2013, an estimated 198 million people were infected, leading to nearly 600,000 deaths (World Health Organization, 2014). 90% of these deaths occur in Sub-Saharan Africa, mostly in children under 5 years old. In addition to malaria's mortality and morbidity, the disease negatively impacts development in numerous ways including medical expenditures, lost wages and productivity, school absenteeism, discouragement of investment (Sachs & Malaney, 2002). This thesis focuses on West Africa, the region that currently has the highest rates of malaria deaths in the world (World Health Organization, 2014).

Malaria is a disease caused by the *Plasmodium* parasite and spread by *Anopheles* mosquitoes. In many areas affected by malaria, transmission is closely tied to climate, particularly to rainfall and temperature. In most of West Africa, malaria transmission occurs primarily in the wet season when rain-fed water pools form and serve as mosquito breeding sites. Temperatures affect the mosquito's ability to transmit the disease. The timing and severity of seasonal malaria outbreaks can vary year to year in response to interannual climate variability (M. Thomson *et al.*, 2006).

Despite the severity of the global malaria burden, there is much about the disease that remains unknown. Vector-borne diseases in the United States are monitored and controlled through an extensive network of vector surveillance and clinical reporting. High-quality meteorological data facilitates analyses linking environment to disease transmission. By contrast, the West

African countries affected by malaria have very limited data on the environmental and entomological drivers of malaria. Clinical data on infections, cases and deaths are improving but generally remain insufficient to assess trends (World Health Organization, 2014). Some of these gaps in data and knowledge can be addressed by mechanistic modelling. Using inputs of environmental data observed on the ground or by satellites, we can model expected hydrology (location, depth and persistence of water pools), entomology (mosquito population size, human biting rate, mosquito lifespan), and malaria transmission (infectious bites, new cases, disease prevalence).

In this thesis, we use a framework of highly detailed, spatially explicit mechanistic modeling to explore the relationships between the environment and malaria. The first goal of this work is to first establish relationships between environmental variables and indices of malaria transmission in the current climate. We consider the role of acquired immunity in shaping the response of malaria prevalence rates within a population, especially in the face of interannual variability. The second goal of this thesis is to predict the effect of climate change on malaria transmission in West Africa. We analyze the performance of the current generation of global climate models in simulating West African climate before selecting the most credible predictions of future climate. We use these predictions to simulate the change in malaria transmission regions of West Africa where the disease is most sensitive to changes in environmental conditions.

1.2 Literature review

1.2.1 Current distribution of malaria in West Africa

The spatial distribution of global malaria risk is shown in Figure 1.1 (Gething *et al.*, 2011). With an estimated 333 million people at risk of infection, West Africa has the highest rates of malaria infections and deaths in the world. In 10 of the 17 West African nations, prevalence rates were estimated to be over 20% (World Health Organization, 2014). The number of malaria cases per year estimated by the Malaria Atlas Project is shown in Figure 1.2 (Hay *et al.*, 2010).

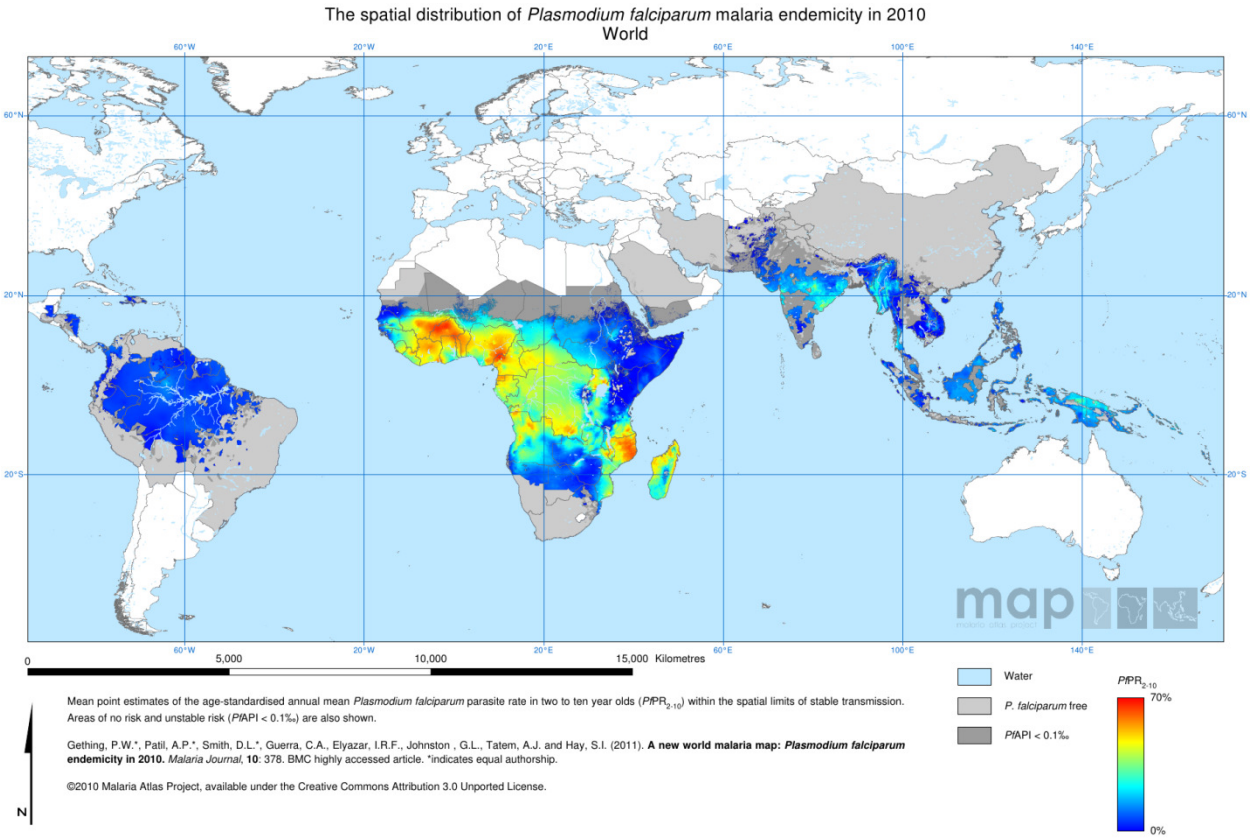

Figure 1.1 Malaria endemicity in 2010 estimated by the Malaria Atlas Project (Gething et al. 2011).

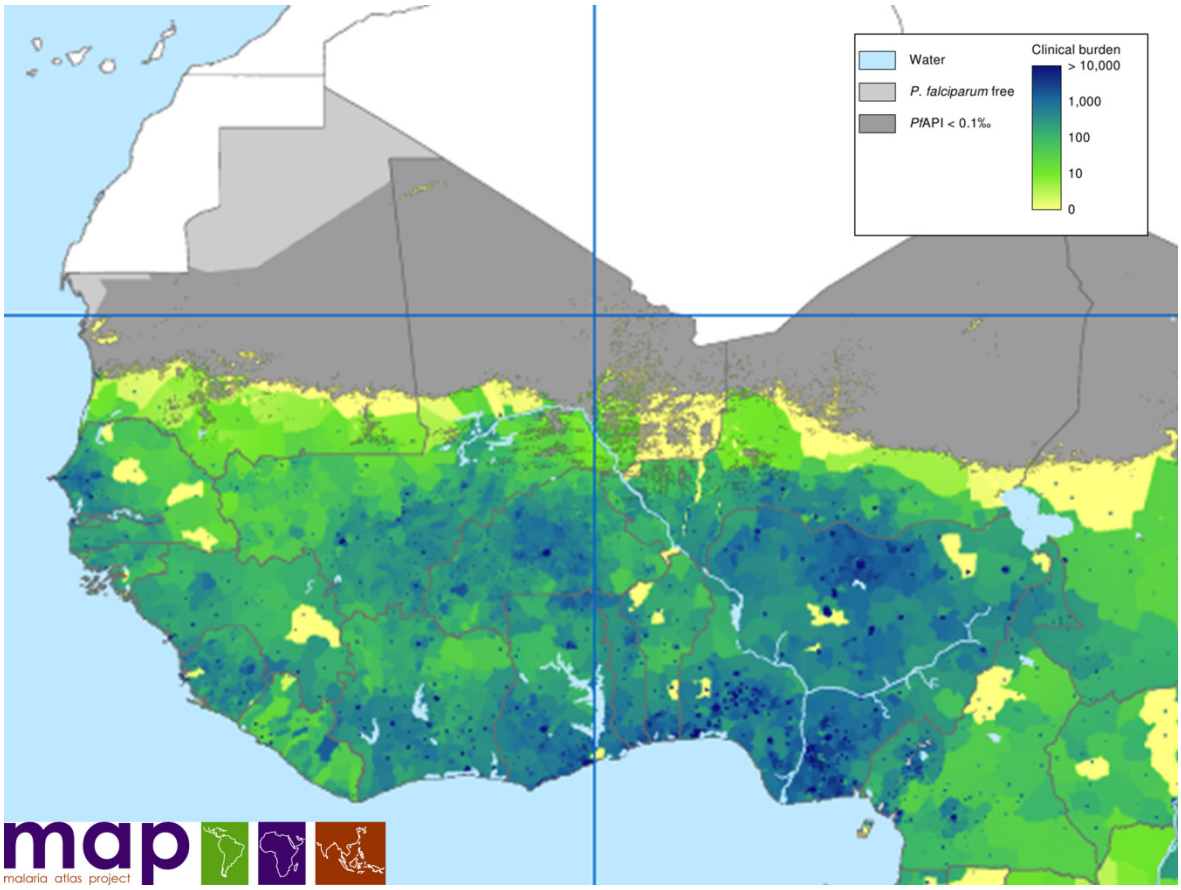

Figure 1.2 Estimated number of malaria cases per year. From Hay et al. 2010.

The climate of West Africa features strong north-south gradients in rainfall and temperature, resulting in a range of climatic zones, as shown in Figure 1.3. Comparing the prevalence estimates from Figure 1.1 to the climate zones, we see that malaria prevalence generally increases from north to south, with no malaria in the Sahara and increasing through the Sahelian, Sudano-Sahelian and Sudanian zones. The climate in the Guinean zone is highly suitable for malaria transmission, but some areas in this zone have prevalence levels that are lower than the climate suggests due to malaria control activities over the past decade (World Health Organization, 2014). Mosquito populations and therefore malaria transmission rates in the

Sahelian and Sudano-Sahelian zones follow the seasonal monsoon cycle. Transmission is interrupted during the dry season. The northern limit of malaria transmission varies from year to year, and the people living in this boundary area are especially vulnerable to infection as they lack immunity to the disease (Mouchet *et al.*, 2008).

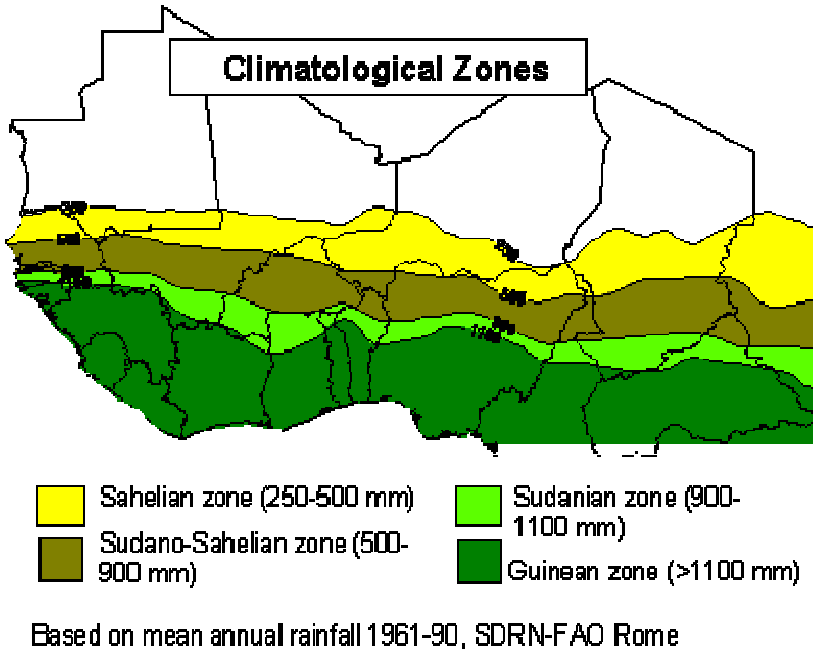

Figure 1.3 Climatological Zones of West Africa (FAO, 1998). The solid lines indicate annual average millimeters of rainfall. The white area above the 250 mm rainfall line is the Saharan zone.

1.2.2 Relationships between environmental variables and malaria transmission

The schematic shown in Figure 1.4 illustrates the relationship between climate, mosquito populations, and ultimately measures of malaria transmission. The squares are processes in the mosquito population and the pentagons are processes in the human population. These processes

are summarized here, and described in further detail below. Large scale climate processes, whether natural or influenced by greenhouse gas emissions, lead to distinct rainfall and temperature patterns. The rainfall forms water pools that allow the *Anopheles* mosquito vectors to reproduce and temperature influences the mosquito lifespan. These processes in turn determine the mosquito population size. Temperature also determines the duration of the parasite extrinsic incubation period (EIP) within the mosquito mid-gut. The mosquito population size and the EIP are reflected in the vectorial capacity, which is a measure of the environmental potential for disease transmission. Vectorial capacity drives the basic reproduction number (R_0), another measure of disease transmission, and the entomological inoculation rate (EIR), which is the number of infectious bites each human receives. The EIR is also affected by the level of immunity in the population and the parasite prevalence level in the population; these three quantities are strongly interrelated.

The connection between rainfall and malaria transmission has been observed for nearly a century (M. C. Thomson *et al.*, 1996). However, the relationship between rainfall and malaria transmission is highly nonlinear. Mosquitoes of the *Anopheles gambiae* complex, the primary malaria vector in Africa, breed in small, temporary pools of standing water. Increased rainfall often means that there are increased breeding sites available to female mosquitoes, which leads to an increased mosquito population, and thus malaria transmission. However, this is not always the case; excess rainfall can flood the small pools and disrupt developing larvae. A decrease in rainfall can also increase breeding habitats by slowing flowing water, as observed when pools formed along a river bed in Sri Lanka during a prolonged drought (Wijesundera Mde, 1988).

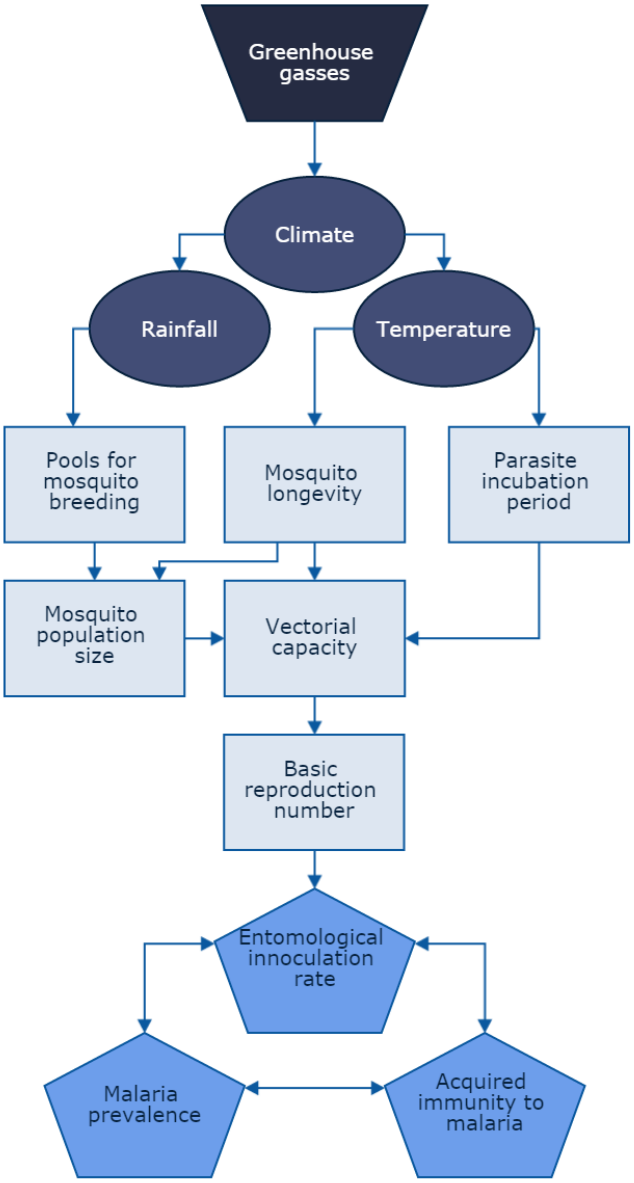

Figure 1.4 Schematic of the processes linking greenhouse gas emissions to malaria transmission

The temporal pattern of rainfall within the rainy season also plays an important role in mosquito abundance (Bomblies, 2012). In the Sahel, water pools are quickly emptied by evapotranspiration and infiltration. Water pools become productive breeding sites only if they persist for the duration of the aquatic stage of juvenile mosquitoes.

Temperature affects malaria transmission through mosquito longevity and the parasite's extrinsic incubation period. Mosquito survival is a function of temperature, with high temperatures increasing mortality by stressing the mosquitoes, and low temperatures limiting mosquito activity (W. Martens *et al.*, 1995). The extrinsic incubation period (EIP), which is the number of days *Plasmodium falciparum* requires within the mosquito in order to be transmitted to humans increases with temperature. Malaria transmission can only occur when mosquito survival is long enough to allow development of sporozoites. At low temperatures, the long extrinsic incubation period far exceeds the expected lifespan of mosquitoes, thus prohibiting disease transmission.

1.2.3 Defining measures of malaria transmission

There are a number of measures of malaria transmission that will be used throughout this thesis: vectorial capacity, basic reproduction number, entomological inoculation rate and prevalence. The quantities are defined here, and the relationships between them are outlined in Figure 1.4.

1.2.3.1 Vectorial capacity

The effects of rainfall and temperature are quantified through by the vectorial capacity (*VC)*, which is a measure of environmental suitability for malaria transmission. Vectorial capacity is defined as the average number of infectious bites per person originating from a single case of malaria if all vectors biting the original case were to become infected (Garrett-Jones & Grab, 1964). We compute *VC* using the following set of equations:

$$VC = ma^2D \tag{1.1}$$

where *m* is the number of female mosquitoes per human, a is the average number of bites taken by each mosquito per day, and *D* is the expected duration of infective life of the mosquito.

D is defined as the number of days an average mosquito will be infective and is a function of temperature, maximized at 28^{o}C. *D* is given by the following equation:

$$D = p^{EIP}/-\ln(p) \tag{1.2}$$

where *p* is the daily survival probability of the mosquito, and *EIP* is the extrinsic incubation period, defined as the number of days *Plasmodium falciparum* must be present within the mosquito before it can be transmitted to humans.

The survival of mosquitoes is given by:

$$p(T) = \exp\left(\frac{-1}{-4.4 + 1.31T - 0.03T^2}\right) \quad (1.3)$$

where T is the daily average air temperature in degrees Celsius (W. J. Martens, 1997). This function gives maximum longevity in the range of 20 to 25°C, and severe mortality at temperatures below 10°C and above 35°C.

EIP is given by:

$$EIP = 111/(T - 16) \quad (1.4)$$

where T is daily average air temperature in degrees Celsius (Detinova, 1962). Malaria transmission can only occur when mosquito lifespan exceeds the *EIP*.

Assuming the biting rate and mosquito density remain constant, inserting the temperature dependent values of *p* and *EIP* into the equation for vectorial capacity show that peak transmission occurs around 28°C. It follows that an increase in temperatures would be favorable for malaria transmission in areas where average temperatures were below 28°C, and unfavorable for transmission in areas above 28°C.

Temperature may also affect the vectorial capacity by changing the biting rate *a* and mosquito density *m*. Increasing temperature decreases the duration of the larval stage of *Anopheles* mosquitoes (Jepson WF, Moutia A, Courtois C., 1947), which could increase the proportion of larvae surviving to adulthood, thus increasing the mosquito density *m*. *Anophelines* have also

been reported to digest blood faster at higher temperatures, which would reduce the time between meals, thus increasing the biting rate *a* (Gillies, 1953).

1.2.3.2 Basic reproduction number

Another useful measure of disease transmission is the basic reproduction number R_0. This is defined as the total number of secondary infections resulting from a single case of malaria, assuming an entirely susceptible population. This can be thought of as the daily vectorial capacity integrated over the course of an infection, multiplied by the probability the parasite is transmitted:

$$R_0 = \sum_{t=0}^{len} VC(t) * b * c \tag{1.5}$$

The average length of disease in days is *len*, *VC(t)* is the vectorial capacity on day *t, b* is the probability a human with no immunity is infected when bitten by an infectious mosquito, and *c* is the probability a mosquito is infected when it bites an infected human.

In order for a disease to spread, R_0 must be greater than one. This means that on average, each infected person will infect more than one other person. If the R_0 is less than one, the disease will die out.

VC and R_0 are useful quantities for this study because they reflect only the environmental potential for malaria transmission. R_0 reflects a maximum value of disease spread. In practice, it

is almost impossible to measure R_0 in the field. If it were possible to track every case of malaria, we would find an effective reproductive number, R_{eff}, which is lower than R_0. In areas of intense transmission, R_{eff} is moderated by the limited number of susceptible individuals in the population, as well as acquired immunity to disease. However, areas with very low levels of malaria, such as the border between suitable and unsuitable climate or in a population where the disease is near elimination, R_{eff} approaches R_0 (Macdonald, 1956). This means that R_0 is most accurate when it is close to its threshold value of 1, making it a powerful tool to determine whether malaria will spread.

1.2.3.3 Entomological inoculation rate

The entomological inoculation rate, EIR, is defined as the number of infectious bites per person per unit time. This is a measure of both entomology and immunology; it depends on the vectorial capacity as well as the background prevalence level within a population. This index of transmission is frequently measured in the field. The biting rate is calculated either through human landing catches or household spraying. A sample of mosquitoes is then tested to find the proportion of bites that would have been infectious.

1.2.3.4 Prevalence

Malaria prevalence, or parasite rate, is defined as the proportion of a population that is infected with malaria at a given time. This is a straightforward measure that can easily be measured by testing blood samples from a subset of the population. Malaria prevalence is frequently reported for children aged 2-10 years old.

1.2.3.5 Immunity index

In this thesis, we refer to a quantity called the immunity index. This is a quantity we use in our model to indicate the level of acquired immunity in an individual, and is described in depth in Chapter 3. This index is a simplification of the very complex human immune response to malaria. However, we find it useful to discuss when analyzing our results as it provides a measure of both an individual's past exposure to disease, as well as his susceptibility to future disease.

1.2.4 Characterization of acquired human immunity to malaria

Naturally acquired immunity to malaria plays an important role in the transmission of the disease, but in many ways is still poorly understood. Acquired immunity to *Plasmodium falciparum* malaria develops in three stages. The first stage is protection from severe disease, and can develop in as few as one or two infections (Gupta *et al.*, 1999). The second stage is immunity to the clinical symptoms of malaria, and develops over the first years of childhood. The third stage is a partial protection against parasitization, and develops around adolescence. All three stages of immunity depend on constant transmission. When transmission decreases, immunity weakens (Schofield & Grau, 2005). While all three stages of immunity are important to the epidemiology of malaria, for the purposes of modelling disease transmission, we are only concerned with the immunity that protects against parasitization. This immunity potentially affects transmission by reducing the proportion of infectious mosquito bites that result in infection, decreasing the duration of disease and decreasing the infectivity of humans to mosquitoes.

Immune responses to the pre-erythrocytic stages have been shown to be effective at preventing blood-stage infection, forming the basis of the most advanced malaria vaccine to date (Agnandji *et al.*, 2011). Naturally occurring immunity is not believed to confer full protective immunity, and is often neglected in models of disease transmission (Smith, Maire *et al.*, 2006). However, adults become infected at lower rates than children, implying that immunity does provide a partial protection against infection (Bekessy *et al.*, 1976; Hoffman *et al.*, 1987).

Immunity decreases parasite levels in the bloodstream, and may lead to shorter duration of infection (Molineaux & Gramiccia, 1980). In a longitudinal study of recovery rates in Nigeria, the duration of disease in infants (625 days) was 10 times as high as in >44 year (52 days) olds, suggesting that acquired immunity increases the rate of disease clearance (Bekessy *et al.*, 1976). Others argue that there is little evidence to support this theory, assuming instead that immunity decreases the length of patent disease, without changing the length of subpatent infection (Maire *et al.*, 2006).

Gametocyte density has been correlated with the ability to infect mosquitoes, and there is evidence that infectivity to mosquitoes decreases with age (Bonnet *et al.*, 2003; Drakeley *et al.*, 2006; Githeko *et al.*, 1992). However other studies show no correlation, leading to a belief that beyond a bottom threshold of gametocyte density required for transmission of the parasite to mosquitoes, increased densities do not necessarily lead to enhanced transmission (Drakeley *et al.*, 2006). A study of infectivity to mosquitoes in a highly endemic African village found that <5, 5-15, and >15 year old age groups contributed equally to the malaria reservoir, indicating that people continue to be infectious despite having low levels of parasitaemia (Muirhead-Thomson, 1957). It has also been suggested that acquired immunity may decrease the infectivity of gametocytes (Buckling & Read, 2001; Drakeley *et al.*, 2006).

Beier *et al.* (1999) measured the relationship between the entomological inoculation rate (EIR) and malaria prevalence at 31 sites of varying transmission intensity across Africa. EIR is defined as the number of infectious bites on a person per unit time, and is a standard measure of malaria transmission. They noted a non-linear relationship between malaria prevalence and EIR. At low levels of EIR (<100 bites/person/year), prevalence was highly sensitive to EIR. However at high EIR (200-1000 bites/person/year), prevalence leveled at around 80% and was not sensitive to increasing EIR. These findings suggest that the saturation of malaria prevalence around 80% rather than 100% in areas of high EIR can be explained in part by the protective effects of acquired immunity.

Several seemingly paradoxical cases of increased mosquito abundances associated with lower human parasite prevalence have been reported (e.g. (Diuk-Wasser *et al.*, 2004; Gupta *et al.*, 1999; Snow *et al.*, 1997). These results have been attributed to several potential causes, but it is thought that human immunity may play a significant role in explaining these observations. In Mali, Diuk-Wasser *et al*. (2004) noted a decrease in malaria prevalence in villages with intensive irrigation and higher mosquito abundance. They suggested intraspecific competition of subadult mosquitoes for limited nutrients as an explanation as adult mosquitoes would be smaller, shorter-lived, and thus the vectorial capacity would be depressed. However increased levels of acquired immunity may have played a role in lowering the population prevalence in many of these observations.

1.2.5 Modeling immunity to malaria

Previous malaria models have incorporated acquired immunity. Dietz *et al*. (1974) developed a model that tracks temporal variation in malaria infections and the immunity level of populations

in northern Nigeria. That model has a compartmental structure and assumes perfect mixing, and was successfully used for vector control decision making during the Garki project, an extensive malaria control field campaign in the 1970s (Molineaux & Gramiccia, 1980). Many similar models with a compartmental structure exist with varying levels of complexity and assumptions regarding the mechanisms of immunity, for example Aron *et al*. (1988), Yang (2000), Filipe *et al*. (2007) Chiyaka *et al*. (2007), Águas *et al*. (2008) and Chitnis *et al*. (2008). Despite substantial differences in model structures, each of the models above have been parameterized in order to matched observed prevalence data.

Several recent models include individual-based humans. Smith and colleagues (Smith, Killeen *et al.*, 2006; Smith *et al.*, 2008) have developed an extensive stochastic individual-based model driven by the entomological inoculation rate (EIR), the number of infectious bites received by each human per unit time. This model includes modules for pre-erythrocytic immunity that decreases the frequency of infection (Smith *et al.*, 2006), and parasite regulating immunity at the blood stage that decreases the infectiousness of humans to vectors (Maire *et al.*, 2006; Ross *et al.*, 2006). Similarly, individuals in a model developed by Griffin *et al*. (2010) are infected according to the EIR derived from a corresponding compartmental model. This model includes representation for clinical immunity and infection-blocking immunity that developed based on the number of infectious bites received, as well as a parasite regulating immunity that is dependent on the individual's age. Gu *et al.* (2005) developed an agent-based model of humans and female mosquitoes to simulate the transmission of malaria incorporating human immunity for a population on the coast of Kenya.

1.2.6 Modelling studies predicting the malaria response to climate change

The effect of climate change on malaria transmission has been the subject of research and intense debate since the mid-1990s. The expansion of malaria into areas where transmission is currently limited is of significant concern, as people in these areas will be especially vulnerable to illness due to their lack of acquired immunity to the disease. This issue has been addressed using both biological/mechanistic models and statistical models (Parham & Michael, 2009; Rogers & Randolph, 2000). Early studies reported predictions of wide-spread increase in malaria transmission, including into Australia, Europe and the United States, with up to 300 million additional people at risk (P. Martens *et al.*, 1999; W. Martens *et al.*, 1995; Martin & Lefebvre, 1995; Tanser *et al.*, 2003). However, more recent studies estimating the global impact of climate change on malaria transmission seem to suggest a shift in distribution rather than a large net increase (Lafferty, 2009; Parham & Michael, 2009; C. J. Thomas *et al.*, 2004). In its 4th Assessment Report, the Intergovernmental Panel on Climate Change (IPCC) states that the local and global impacts of climate change on malaria are uncertain, and warrant further research (Confalonieri *et al.*, 2007).

While the relationships between temperature and malaria transmission are relatively well understood, modelling methods that have been used up to now to estimate the effect of climate change on malaria transmission are limited in their characterization of rainfall. They generally rely on rules for minimum threshold values, such as 80 mm rainfall per month for a number of consecutive months as used in the MARA/ARMA and MIASMA studies, with some models including an upper threshold, above which additional rainfall is expected to wash out breeding sites (Parham & Michael, 2009). However the processes by which rainfall is diverted into pools suitable for breeding is strongly dependent on the frequency, intensity and duration of rainfall

events, as well as site-specific topographical features, soil characteristics, and vegetation cover. This shortcoming is frequently mentioned by the authors and reviewers of such studies (McMichael *et al.*, 2006; Parham & Michael, 2009; Van Lieshout *et al.*, 2004). The IPCC emphasizes the importance of localized determinants of malaria transmission and notes the difficulty in making generalizations across settings (Confalonieri *et al.*, 2007). .

1.2.6.1 Biological Models of Malaria Transmission

Biological or mechanistic models relate environmental variables to malaria transmission based on known relationships. These models are often used to map areas climatically suitable for malaria transmission (P. Martens *et al.*, 1999; Tanser *et al.*, 2003; C. J. Thomas *et al.*, 2004). The advantage of such models is that they give a clear understanding of how environmental variables drive changes in malaria transmission, and can account for feedback process and non-linear relationships involved in disease transmission (Parham & Michael, 2009). A limitation of this approach is that in order to be credible, they must be properly parameterized, which requires a significant amount of knowledge of the *Plasmodium*, mosquito, and human biology.

In an early study, Martin and Lefebvre (1995) used a climate suitability model called the Malaria Potential Occurrence Zone (MOZ) to estimate how the global potential for malaria transmission would respond to a changing climate. MOZ classified areas as having no malaria, seasonal potential transmission or perennial potential transmission based on a minimum and maximum temperature thresholds and a minimum moisture requirement. MOZ was applied to climatic output from 5 general circulation models (GCMs), and changes from baseline results were analyzed. All five scenarios resulted in an increase of areas with seasonal potential transmission,

as the seasonal zones expanded into both currently malaria-free zones and areas currently designated as having perennial transmission potential.

MIASMA (Modelling framework for the health Impact ASsessment of Man-induced Atmosphere changes) (W. Martens, 1998) is an integrated assessment model developed in order to assess health impacts from global climate change and ozone depletion and has been used in a number of studies (Lindsay & Martens, 1998; P. Martens *et al.*, 1999; W. Martens *et al.*, 1995; Van Lieshout *et al.*, 2004). The malaria component of the model incorporates climate change by calculating the biological effect of increased temperature on mosquito mortality, mosquito biting rate, and parasite development, and by limiting malaria transmission to areas where daily precipitation is greater than 1.5 mm. The model also considers population growth, and its primary output is population living in areas climatically suitable for malaria transmission (P. Martens *et al.*, 1999). Based on climate predictions from GCMs, an early version of the model predicted that the temperature in 2100 would lead to a widespread increase in malaria risk, most notably in borders of currently endemic malaria areas, with the epidemic potential increasing by a factor of two in tropical areas, and by a factor of over 100 in temperate regions. They inferred that areas where *Anopheles* mosquitoes exist but malaria is not currently transmitted, such as Australia, the United States and Southern Europe would be at risk for malaria epidemics (W. Martens *et al.*, 1995), and the African highlands emerged as an area of special concern (Lindsay & Martens, 1998). A modified version of this model (P. Martens *et al.*, 1999) was used with climate predictions from HadCM2 and HadCM3 GCMs to estimate future populations at risk. Potential transmission increased in temperate zones. By 2080, the number of people at risk for malaria was expected to increase by 260-320 million for *P. falciparum* and 100-200 million for *P. vivax*. A subsequent study used results from MIASMA and further classified countries based

on their adaptive capacity to malaria in order to produce a more meaningful estimate of the number people with increased risk of disease (Van Lieshout *et al.*, 2004). Adaptive capacity was assigned based on countries' current vulnerability and malaria control status as determined by expert judgment and climate scenarios were obtained by downscaling output from four emissions scenarios of the HadCM3 GCM. In countries classified as vulnerable, the number of additional people at risk in 2080 ranged from 90-200 million, with the greatest increases occurring in Africa and Asia. Climate change was predicted to have little effect in the least developed countries where transmission is already highly favorable (Van Lieshout *et al.*, 2004).

Another climate suitability model was developed by Tanser at al. (2003). In order to be considered suitable for stable malaria transmission, each point had to have at least one month with rainfall of at least 80mm, and a minimum yearly temperature 5^{o}C. In areas fitting these criteria, months were deemed suitable if the 3-month moving average temperature was at least 19.5^{o}C plus the standard deviation of mean monthly temperature, and the 3-month moving average rainfall was at least 60mm. The model was applied over Africa using climate projections for 2100 using low emissions, medium-high emissions, and high emissions scenarios with the HadCM3 GCM. Population data from 1995 were overlaid on the resulting suitability maps in order to estimate the number of person-months at risk. They estimated an increase of 16-28% person-months at risk for stable transmission, due to a 5-7% increase in suitable area, and a 28-42% increase in person-months at risk due to a lengthened transmission season in areas where transmission already occurs. The change in disease distribution was mostly altitudinal, with little latitudinal change. Ethiopia, Zimbabwe and South Africa were projected to double in person-months of exposure due to increased suitability in the highlands and lengthened transmission seasons, while transmission was expected to decrease in countries in West Africa,

Namibia and Mozambique, due to a decrease in precipitation. A response to this paper described the study as "ill informed and misleading", arguing that the thresholds developed using only 15 African locations do not capture the spatial variability of disease, that the model's 63% sensitivity is insufficient to make predictions, and that the measure of person-months is not appropriate for measuring increases in transmission (Reiter *et al.*, 2004).

The MARA/ARMA (Mapping malaria risk in Africa/ Atlas du risque de la malaria en Afrique) (Craig *et al.*, 1999) classifies areas in Africa on a gradient of climatic suitability for stable malaria transmission from 0 (unsuitable) to 1 (highly suitable), based on mean temperature and rainfall. Temperatures outside of the 18-40^{o}C range are considered unsuitable for transmission, while temperatures between 22-32^{o}C are considered suitable. Temperatures between 18-22^{o}C and 32-40^{o}C are assigned a value of suitability based on a sigmoidal fuzzy membership curve. Similarly, areas with average monthly rainfall of 0 mm were unsuitable, 80 mm or greater were suitable, and values in between received a value between 0 and 1. Suitable rainfall and temperature conditions must coincide, and span five consecutive months, or three in North Africa where high temperatures allow rapid development of mosquito populations, in order to enable stable malaria transmission. Thus the minimum of the temperature and rainfall values was calculated for each point for each month, and the annual suitability index was defined as the highest value spanning five (or three in north Africa) consecutive months. The resulting map had good agreement with historical maps in southern Africa, Kenya and Tanzania. This model was applied to examine the effects of climate change on stable malaria transmission areas in Africa over the 2020s, 2050s, and 2080s (C. J. Thomas *et al.*, 2004). Climate projections at 0.5^{o} resolution were taken from the second generation Hadley Center coupled model (HadCM2) medium-high scenario ensemble mean. Projections for the 2020s showed declines in

transmission values in parts of Madagascar and southern East Africa, and only a small increase in highland malaria in northern South Africa. The length of transmission season increased in parts of South Africa and Namibia due to reductions in frost, but decreased in northern Botswana and Mozambique due to decreased rainfall. Transmission suitability decreased in the western Sahel due to increased temperatures. Changes in highland malaria were modest through the 2050s, but became more pronounced in many areas by the 2080s.

In another biological modeling exercise, Parham and Michael (2009) described the probability distribution of the number of mosquitoes as a Poisson distribution with mean $\lambda \div \mu$, where λ, the adult mosquito emergence rate, is a function of temperature and rainfall, while μ, the mosquito death rate, is a function of temperature. Rainfall was incorporated into the mosquito emergence rate through a non-linear model relating egg survival probability to rainfall. Mosquito death rates were based on the formulations of Martens (1998). The dynamics of malaria invasion to a naive population were explored, and a temperature window of 32-33^{o}C was identified optimal for the spread of malaria. The model was used with predictions from the HadCM3 GCM to estimate the response of malaria to climate change by 2080. They found that rainfall patterns are the main driver of malaria endemicity, invasion and extinction, while temperature dominates in transmission rates and disease spread, given that rainfall is sufficient to sustain a mosquito population.

The importance of diurnal temperature fluctuations to the extrinsic incubation period of malaria was examined by Paaijmans et al. (2009). Rather than using the Detinova equation for extrinsic incubation time (Detinova, 1962), Paaijmans et al. used a nonlinear thermodynamic model, which determined cumulative parasite development over 30 minute intervals. They found that when mean temperature is greater than 21^{o}C, diurnal temperature fluctuations slow parasite

development, while at mean temperatures less than 21^{o}C, diurnal fluctuations increase the rate of development. The implications of these findings are that studies using only the mean temperature underestimate the risk of transmission in low-temperature environments, and overestimate the risk in warm environments. These findings are important when considering climate change, as changes in diurnal temperature ranges may add to the effects of rising mean temperatures.

Bomblies and Eltahir (2010) used HYDREMATS to investigate the malaria response to climate shifts in the Sahel. The model was set up over Banizoumbou village in Niger, and was forced with climatological data (temperature, precipitation, wind speed and direction, relative humidity and radiation) representing two historically realistic climate change scenarios. In the first scenario, temperatures increased while rainfall decreased, while in the second, temperatures decreased and rainfall increased. The cooler, wetter scenario resulted in a significantly higher mosquito density; however this increase in mosquito populations did not translate directly into an increase in malaria transmission, as the cooler temperatures extended the EIP, limiting transmission. This study highlighted the importance in considering the joint effects of rainfall and temperature in modeling malaria transmission. They also showed that temporal patterns of rainfall distribution are important in determining the mosquito response to climate.

1.2.6.2 Statistical Models of Malaria Transmission

Statistical models find associations between environmental factors and field observations of a metric of malaria transmission, and then use these relationships to estimate transmission under new climatic conditions. This type of model does not consider the causal relationships between environmental variables and transmission. While this approach limits the understanding of the

system, it allows a wider range of variables, and does not require estimation of unknown parameters.

One statistical model mapped current *P. falciparum* areas using maximum likelihood methods with nine variables: the monthly mean, maximum and minimum of temperature, precipitation, and saturation vapor pressure (Rogers & Randolph, 2000). Compared to actual malaria distribution, the resulting map was 76% accurate. When the model was applied to predictions from the HadCM2 medium-high and high scenarios for 2050, few changes were observed. Suitable habitats extended into the southern United States, Turkey, Turkmenistan, Uzbekistan, and habitats within Brazil and China expanded. An estimated 23 million additional people were estimated to be exposed under the medium-high scenario, while high temperatures under the high scenario resulted in 25 million fewer people exposed.

Peterson (2009) applied an ecological niche model to predict future distribution of two major malaria vectors, *Anopheles gambiae sensu strictu* and *Anopheles arabiensis,* in Africa. The ecological niche model was created by finding non-random associations between known points of vector occurrence and environmental data which included annual mean temperature, mean monthly maximum and minimum temperature, annual precipitation, and topographic data, and interpolating them to unsampled regions based on geographical information systems (GIS) environmental data. Future *Anopheles* distributions were predicted by applying changes in climate as predicted by HadCM3 and the Canadian Center GCM (CGCM1) to current climate, and using the ecological niche model to calculate suitable areas. West Africa was expected to become less suitable for both species, while regions in eastern and southern Africa were expected to become more suitable. Currently, over 30 million people live in areas that are expected to become more suitable for *A. gambiae*, and 14 million in areas becoming more

suitable for *A. arabiensis*. Areas that are expected to become less suitable for vectors currently have a population of 78-111 million for *A. gambiae* and 135-171 million for *A. arabiensis*. In a similar study, Tonnang et al. (2010) predicted that the boundaries of *Anopheles* mosquitoes in Africa would shift southward and eastward.

Gething et al. (2010) put previous estimates of the effects of climate change into perspective by comparing them to historical changes in R_0. A historical map of malaria endemicity in 1900 (Lysenko & Semashko, 1968) was compared to a map of *P. falciparum* endemicity in 2007 created by using 8,938 parasite rate surveys and applying a geostatistical model to create a continuous surface of malaria transmission (Hay *et al.*, 2009). The difference between the two maps showed that global malaria transmission has decreased substantially, both in geographic range and endemicity. Since this decrease in malaria occurred despite observed increases in global temperature, the authors argue that over the past century, non-climatic factors such as disease control, economic development and urbanization were more important than climate in defining the range and intensity of malaria transmission. The decrease in transmission was quantified in terms of the basic reproductive number, R_0. They found that over the earth's surface, 75% of the area experienced a decrease in R_0 of over an order of magnitude, and 12% by less than an order of magnitude. By comparison, the most dramatic estimates of increased transmission due to climate change (Lindsay & Martens, 1998; P. Martens *et al.*, 1999) would lead to an increase of R_0 by a factor of three. They also calculated that the application of key intervention measures such as drug treatment, insecticide treated bednets and larvicide could decrease R_0 by an order of magnitude, suggesting that the effective use of such measures could counteract any increase in transmission due to climate change.

1.2.7 Skill of GCMs in modelling current and past West African Climate

The Intergovernmental Panel on Climate Change (IPCC) reports that the coupled ocean-atmosphere general circulation models (also global climate models; GCMs) used for the 4th Assessment Report (AR4) have systematic errors in modelling African climate (Christensen *et al.*, 2007). The 5th IPCC Assessment Report (AR5) focuses on a newer generation of climate models participating in the Coupled Model Intercomparison Project Phase 5 (CMIP5) (Taylor *et al.*, 2012). These include coupled ocean-atmosphere GCMs as well as more complex earth system models (ESMs) that simulate biogeochemical processes in addition to climate physics. The CMIP5 models were found to simulate global climate more accurately than the AR4 models, but they continue to exhibit biases in the monsoon location and intensity (Flato *et al.*, 2013).

Cook and Vizy (2006) assessed the ability of the 18 AR4 GCMs to simulate the climatology of the West African monsoon system. Models were judged based on their ability to reproduce a number of important characteristics of the monsoon system. The first requirement was the placement of the intertropical convergence zone (ITCZ) over the African continent during northern-latitude summer. Eight of the models incorrectly place the ICTZ and its associated rainfall over the Gulf of Guinea rather than over land, and were eliminated from further analysis. Another criterion that was assessed was the models' ability to simulate the precipitation dipole anomaly currently observed between the Guinea coast and the Sahel, which is considered to be a prominent mode of interannual variability in the monsoon system, and has been linked to sea surface temperature anomalies in the Gulf of Guinea. Of the remaining 10 models, 6 were able to reasonably recreate the dipole. Based on their analyses, GFDL_0, GISS_EH, MIROC(medres) and MRI were selected as the models that best represent climate processes in West Africa.

Hoerling et al. (2006) used ensembles of GCMs to investigate the mechanisms behind the drought observed in the Sahel in the late twentieth century, and assessed the ability of ocean-atmosphere coupled GCMs to simulate this observed drying. By forcing GCMs with observed sea surface temperatures, they were able to simulate the drought, and thus concluded that the decrease in rainfall was driven by an increased difference in temperature between the North and South tropical Atlantic Ocean. However of 18 AR4 coupled model simulations, only two, both from the Geophysical Fluid Dynamics Laboratory, were able to simulate the drying. This indicates limitations in the ability of current ocean-atmosphere GCMs to accurately simulate patterns of sea surface temperatures relevant to rainfall in the Sahel.

Mariotti et al. (2011) compared current and future precipitation and temperature over the African continent simulated by the ECHAM5 global model to projections for the regional climate model RegCM3 driven by ECHAM5 boundary conditions. The temperature biases of both models were of similar magnitude compared to observations. Precipitation bias patterns differed between the two models, and the regional model did not provide a systematic improvement over the global model. The patterns of temperature change by the late 21st century were similar in the two models. However, the precipitation signals differed in West Africa. En Nino-Southern Oscillation (ENSO) sea surface temperature anomalies in the equatorial Pacific and local changes in soil moisture were both found to contribute to the precipitation change signal. The precipitation response to soil moisture than stronger in the regional model than in the global model, and the different representations of soil-moisture feedbacks played a larger role in explaining the difference between the two projections than the differences in response to ENSO anomalies.

Giannini et al. (2013) proposed a mechanism to explain projected changes in precipitation as well as differences in predictions between models. Warmer tropical sea surface temperatures increase the temperature threshold required for convection, leading to dry conditions similar to those of an El Nino year. However, the subtropical North Atlantic Ocean can provide the moisture required for convection if the warming there exceeds warming of the global tropical oceans. Differences in precipitation signals between models can be attributed to differences in relative warming between these two ocean areas.

1.2.8 GCM projections of future West African Climate

The median temperature increase predicted by AR4 GCMs increase between 3^{o}C and 4^{o} C across Africa, with good agreement between models (Christensen *et al.*, 2007). However precipitation responses are much more uncertain, with highly contradictory results between models (Christensen *et al.*, 2007). In an analysis of climate simulations from the AR4 models, 14 out of 18 predicted an increase in rainfall over the Sahel throughout the first half of the 21st century, which is consistent with simulated changes in the relevant SSTs (Hoerling *et al.*, 2006).

Of the four models deemed by Cook and Vizy (2006) to give reasonable representations of current climate, three were used to simulate changes in the West African Monsoon in the 21st century. The first, GFDL_0, simulated significant drying in the Sahel beginning around 2050, followed by drying along the Guinean Coast by the end of the century. By contrast, MIROC (medres) showed drying on the Guinea coast, accompanied by increased precipitation in the Sahel. The MRI model showed the least change in precipitation, with an increase in frequency

of dry years in the Sahel, and a small increase in precipitation on the Guinean coast (Cook & Vizy, 2006).

The newer CMIP5 models continue to show a spread in predicted precipitation over the Sahel (Roehrig *et al.*, 2013). This has been interpreted as the result of differences in the atmospheric circulation changes between models (Collins *et al.*, 2013).

1.3 Thesis structure

Chapter 2 provides a description of HYDREMATS, the model used in this thesis. Improvements in the model's representation of mosquito survival are discussed, as are improvements in model efficiency. Improvements to the model's representation of human immunity to malaria are described in Chapter 3.

Chapter 4 is a first-order assessment of climate change impacts on malaria transmission in West Africa. Projected changes in temperature and rainfall from 19 GCMs were screened for a best case and worst case scenario in terms of malaria transmission. Changes in vectorial capacity were simulated for 5 ecoclimate zones. We determined that even under the worst case climate scenario, we did not expect to see a major increase in malaria in West Africa.

Chapter 5 presents modelling of current malaria transmission. We identify the parts of West Africa where malaria infection rates are most sensitive to changes in vectorial capacity. We then simulated malaria transmission for 12 locations within the sensitive region. Simulated entomology and parasite prevalence were compared to observational data.

Chapter 6 provides a more refined analysis of the initial assessment of climate change. The skill of GCMs was assessed in order to select the most credible projections of future climate. These projections were applied to the locations studied in Chapter 5 in order to assess the impact of climate change on malaria transmission.

2 Model Description and Improvements

The work presented in this thesis uses the Hydrology, Entomology and Malaria Transmission Simulator (HYDREMATS), a mechanistic model of malaria transmission developed to simulate village-scale responses of malaria transmission to interannual climate variability in semi-arid desert fringe environments such as the Sahel. In this chapter, I describe the model, as well as work conducted as part of this thesis to improve the model in two areas: increased model efficiency and the incorporation of the effects of relative humidity on mosquito survival. Improvements were also made to the immunity component of the model; these are described separately in Chapter 3.

2.1 Model description

The development of HYDREMATS is described in detail in Bomblies *et al*. *(Bomblies et al., 2008)*. In brief, the model is a physics-based hydrology model coupled with an individual based entomology model that is run at a spatial resolution on the order of 10 meters and a temporal resolution of around 1 hour. The hydrology component explicitly represents water pools available as breeding sites to anopheline mosquitoes by simulating the flow of water into topographical low points and water loss due to evaporation and infiltration. The temperature of each water pool is computed by solving a system of energy balance and heat transfer equations (Bomblies *et al.*, 2008).

HYDREMATS can be separated into three components, shown in Figure 2.1: the hydrology component which explicitly represents pooled water available to anopheles mosquitoes as breeding sites, the entomology component, which simulates the location and status of individual

mosquitoes, and the immunology component, described in Chapter 3, which simulates malaria infections within humans and the effects of acquired immunity to disease.

The hydrology component of HYDREMATS is based on the land surface scheme LSX of Pollard and Thompson (1995). The model simulates momentum, energy and water fluxes within its vertical column of the atmosphere, six soil layers and two vegetation layers. Vegetation type and soil characteristics are required as model inputs, and strongly influence soil moisture and runoff in the model. Thicknesses and permeabilities of vertical soil layers are assigned to represent the soil structure observed in the Sahel, including the thin layer of low-permeability crust commonly observed in areas with sparse vegetation (Bomblies *et al.*, 2008).

Rainfall at each grid cell is partitioned between runoff and infiltration, based on a Hortonian runoff process governed by hydraulic conductivity and porosity of the soil. Unsaturated zone hydraulic conductivity is calculated as a function of soil moisture following Campbell's equation. Uptake of soil water from evapotranspiration is calculated based on climatic variables. Infiltration through the unsaturated zone is calculated using an implicit Richard's equation solver (Bomblies *et al.*, 2008). Richard's equation is described by:

$$\frac{\partial \theta(z,t)}{\partial t} = \frac{\partial}{\partial z}\left[K_u(\theta)\frac{\partial \varphi(\theta,z)}{\partial z} + K_u(\theta)\right] \qquad (2.1)$$

where θ = soil moisture [$cm^3\ cm^{-3}$]

$K_u(\theta)$ = unsaturated hydraulic conductivity [$m\ sec^{-1}$]

$\varphi\ (\theta,z)$ = head value [m]

z = elevation [m]

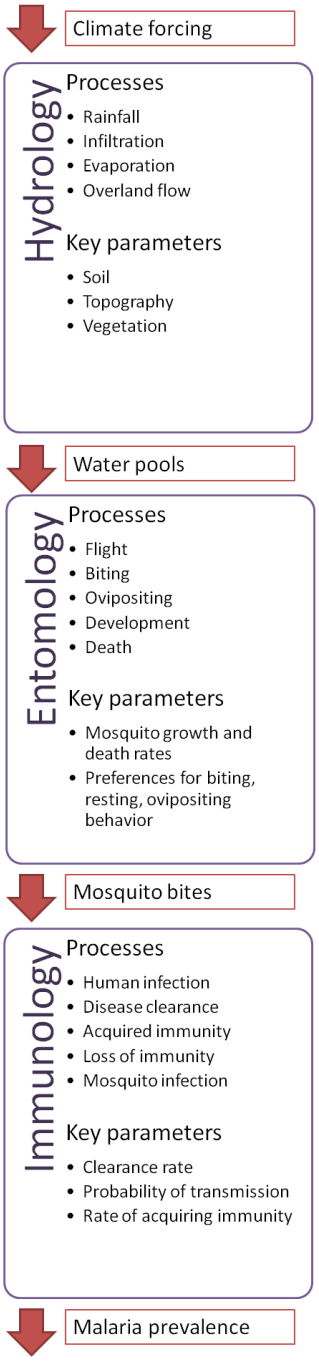

Figure 2.1 Schematic of HYDREMATS. This schematic diagram lists the major processes and key parameters represented by the Hydrology, Entomology and Immunology components of HYDREMATS. The arrows represent information that is passed from one component to the next

Overland flow is modeled using a finite difference solution of a diffusion wave approximation to the St. Venant equations following the formulation of Lal (1998). Flow velocity is represented by Manning's equation as a function of friction slope, flow depth, and the distributed roughness parameter n, which is derived from soil characteristics and vegetation type. The overland flow process is of critical importance for the modeling of water pool formation (Bomblies *et al.*, 2008). The overland flow process is described in greater detail in Section 2.2.1.

The meteorological inputs required by the model are temperature, relative humidity, wind speed and direction, incoming solar radiation, and rainfall. These variables are assumed to be uniform over the model domain in the simulations conducted in this thesis. Distributed rasters of vegetation, soil type, and topography are required at the grid resolution specified by the user. The hydrology component of HYDREMATS generates a grid of water depths and temperatures for each grid cell, for each timestep. These grids serve as the inputs for the entomology component of the model (Bomblies *et al.*, 2008).

The entomology component of HYDREMATS includes the aquatic and adult stages of the mosquito life cycle. Human agents are immobile, and are assigned to village residences, as malaria transmission in this region occurs primarily at night when humans are indoors (Service, 1993). Mosquito agents have a probabilistic response to their environment based on a prescribed set of rules governing dispersal and discrete events including development of larval stages, feeding, egg-laying and death. The model tracks the location, infective status and reproductive status of each female mosquito through time. The malaria parasite is transmitted when a mosquito bites an infected human, and takes a second bloodmeal from an uninfected human (Bomblies *et al.*, 2008).

In addition to the water pool inputs supplied by the hydrology component of the model, the entomology component requires air temperature, humidity, wind speed and wind direction. Air temperature and relative humidity influence mosquito behavior and survival, while wind speed and direction influence mosquito flight, both by physical displacement by wind, and by attracting mosquitoes to upwind blood sources. The location of village residences is required in order to assign the location of human agents (Bomblies *et al.*, 2008).

Each simulated female mosquito ready to oviposit begins to seek water. At each time step, she finds herself a new grid point. The probability that she will deposit her eggs at that point is called the probability of utilization, and is a function of the depth of water at that point, as shown in Figure 2.2. The probability of utilization is highest between parameter values *breedmin* and *breedcon*, reflecting the mosquito's preference for shallow water pools. The probability decreases linearly from *breedcon* to *breedmax,* which is the maximum pool depth considered suitable for *Anopheles* breeding. Mosquito eggs hatch and advance through four stages of larval development at rates dependent on water temperature, nutrient competition and predation given by Depinay et al. (2004). Surviving larvae pupate and emerge as adult mosquitoes. The duration of the aquatic stage of *Anopheles gambiae* mosquitoes ranges from roughly 8 to 24 days, depending on temperature (Depinay *et al.*, 2004). All aquatic stage mosquitoes in a pool that dries up are killed, emphasizing the importance of pool persistence for mosquito breeding (Bomblies *et al.*, 2008).

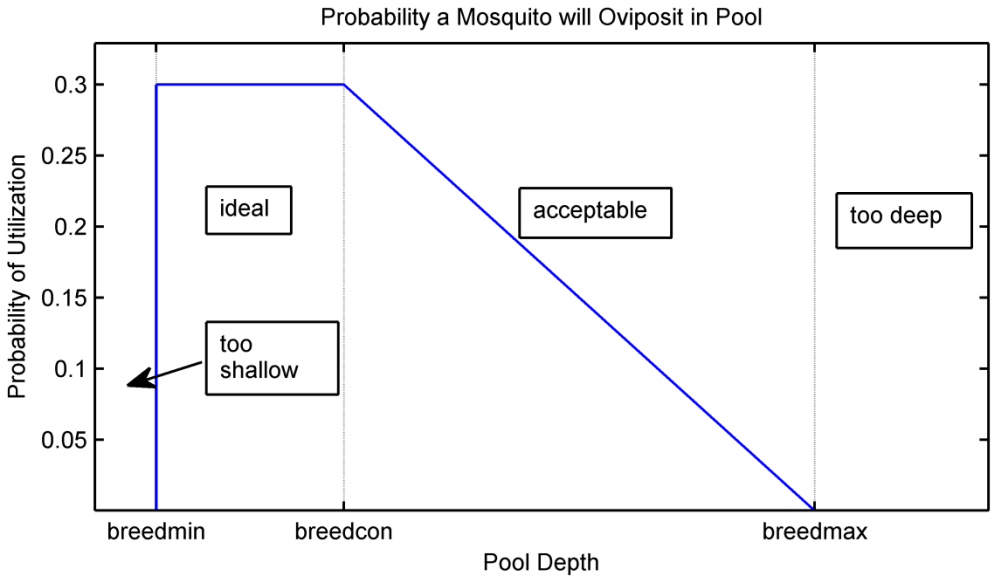

Figure 2.2 Probability of pool utilization

Adult female mosquitoes follow a cycle of seeking human bloodmeals, feeding, resting, and ovipositing for the duration of their lifespan (Figure 2.3). Mosquito flight velocity is assigned as a weighted random walk corrected for attraction to human agents and wind influence. Each human agent contributes to a plume of carbon dioxide that attracts downwind mosquitoes. The effective flight velocity, which incorporates resting time and direction changes within the model time-step, is assumed to follow a normal distribution with mean 15 m/hr and variance 25 m/hr. Mortality of adult mosquitoes is a function of daily average temperature, described in Equation 1.3, with no survival above a daily average temperature of 41^{o}C. The model outputs for each time step includes the number of live adult mosquitoes, their location and infective status, and the prevalence of malaria infections in humans (Bomblies *et al.*, 2008).

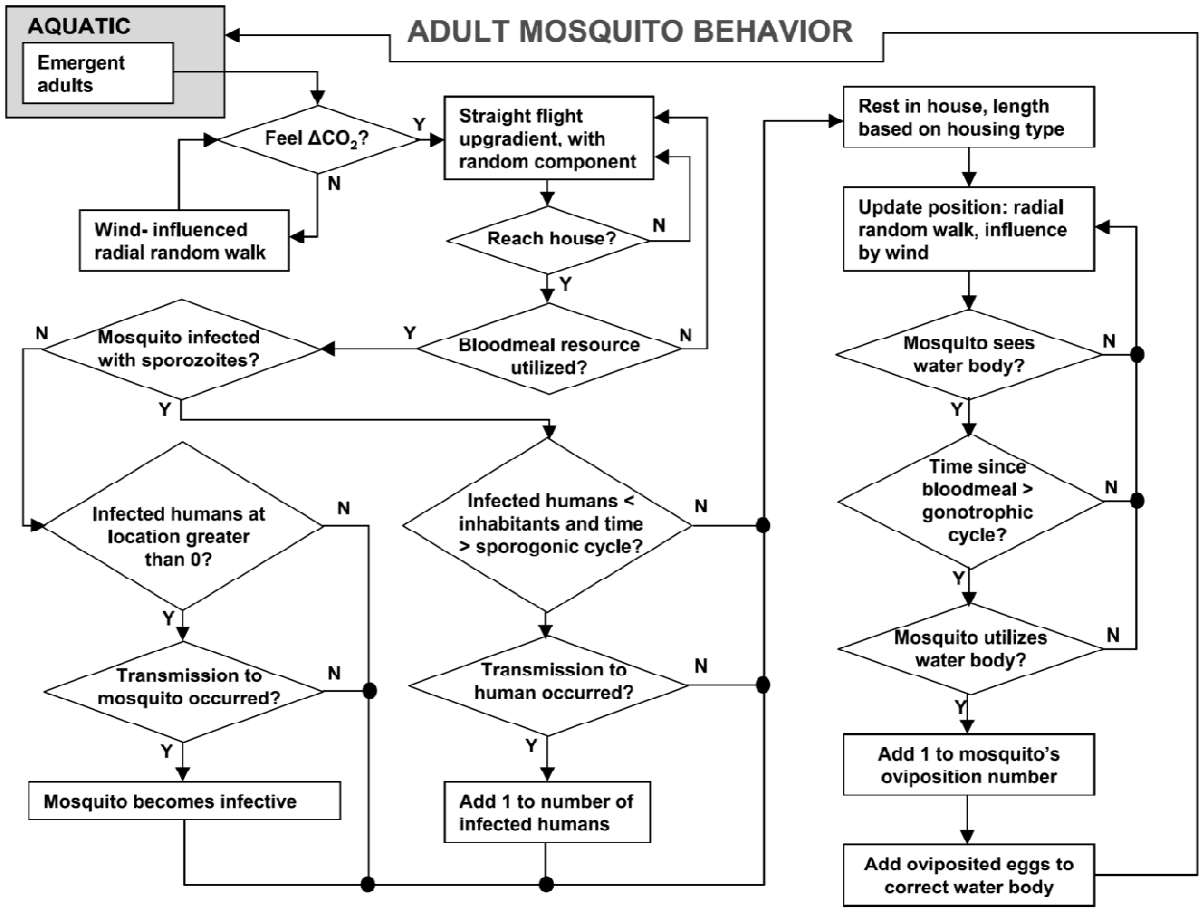

Figure 2.3 Adult mosquito simulation flow. During each timestep, the model updates each individual mosquito as she progresses through her life cycle. Mosquito attributes are updated as they interact with the environment and human agents. Reprinted from "Hydrolo Hydrology of malaria: Model development and application to a Sahelian village," by Bomblies A, Duchemin JB, Eltahir EAB. 2008. Water Resour Res 44.

2.1.1 Mosquito species

While previous studies using HYDREMATS focused on *Anopheles gambiae sensu lato* mosquitoes, in this thesis we assume that the model also reasonably simulates *Anopheles funestus*, another important vector in the wetter parts of West Africa. The primary difference

between the two types of mosquitoes is their breeding preference; members of the *A. gambiae* complex breed in small, temporary pools, while *A. funestus* breeds in larger and more persistent water bodies. Both types of pools are modelled in HYDREMATS and made available to mosquito agents. Although we do not currently distinguish between species of *Anopheles* mosquitoes, we can assume that smaller pools will be colonized primarily by *A. gambiae* while *A. funestus* will dominate at larger pools. The entomological parameters of the model are tuned using data for *A. gambiae*, as this complex has been studied much more extensively (Coetzee & Fontenille, 2004). However, we do not expect parameter values specific to *A. funestus* to be significantly different as the two types of mosquitoes have similar adult survival and dispersal behavior (Midega *et al.*, 2007) and are both primarily nocturnal, endophagic, and anthrophilic (Horsfall, 1943).

2.2 Improving model efficiency

2.2.1 Decreasing timestep of overland flow model

Overland flow is modeled using a finite difference solution of a diffusion wave approximation to the St. Venant equations following the formulation of Lal (1998). Flow velocity is represented by Manning's equation as a function of friction slope, flow depth, and the distributed roughness parameter n, which is derived from soil characteristics and vegetation type. The overland flow process is of critical importance for the modeling of water pool formation (Bomblies *et al.*, 2008).

The continuity equation for shallow flow is:

$$\frac{\partial h}{\partial t} + \frac{\partial (hu)}{\partial x} + \frac{\partial (hv)}{\partial y} - P + I + ET = 0 \quad (2.2)$$

where u and v are the flow velocities in the x and y directions, respectively, h is the water depth, P is precipitation, I is infiltration, and ET is evapotranspiration.

The momentum equations for the x and y directions are approximated as:

$$\frac{\partial H}{\partial x} = -S_{fx} \quad (2.3)$$

$$\frac{\partial H}{\partial y} = -S_{fy} \quad (2.4)$$

Where S_{fx} and S_{fy} are the friction slopes in the *x* and *y* directions, respectively, and *H* is the water depth *h* plus a reference elevation *z*.

A rearrangement of Manning's equation gives flow velocities as (Lal, 1998):

$$u = -\frac{h^{2/3}}{n\sqrt{S_{fx}}}\frac{\partial H}{\partial x} = \frac{-K}{h}\frac{\partial H}{\partial x} \quad (2.5)$$

$$v = -\frac{h^{2/3}}{n\sqrt{S_{fx}}}\frac{\partial H}{\partial y} = \frac{-K}{h}\frac{\partial H}{\partial y} \quad (2.6)$$

Where n is the Manning's roughness coefficient which determines resistance to overland flow and $K = \frac{h^{5/3}}{n\sqrt{S_f}}$ is analogous to the diffusivity coefficient in the heat diffusion equation, so that the governing equation can be rewritten as:

$$\frac{\partial H}{\partial t} = \frac{\partial}{\partial x}\left(K\frac{\partial H}{\partial x}\right) + \frac{\partial}{\partial y}\left(K\frac{\partial H}{\partial y}\right) \tag{2.7}$$

This equation is solved using the alternate-direction implicit (ADI) method described by Lal (1998).

The numerical stability parameter, ξ, for the diffusion equation is:

$$\xi = K[(\Delta x)^{-2} + (\Delta y)^{-2}]\Delta t \tag{2.8}$$

A stability analysis for overland flow on a relatively smooth plane with constant slope found the ADI method to become unstable for values of ξ>5 (Morita & Chie Yen, 2000). The topography used in our simulation is more complex than the smooth plane used in the analysis. The formulation of K causes it to become very large in within pools of water, where the slope in water level between adjacent grid cells is close to zero. We take the conservative stability criterion used for explicit numerical methods, $\xi \leq 0.5$. While the traditional approach is to use this criterion to limit the model timestep, the large values of K within water pools lead to prohibitively small timesteps. Furthermore, for the purposes of modelling mosquito habitat, we are more interested in the location and persistence of water pools than the exact dynamics of

water between grid cells within a given pool. Therefore, we impose an upper limit of K, which allows for a larger timestep while maintaining numerical stability.

Simulations were conducted, imposing upper limits on K of 5 m^2/s , 2.5 m^2/s and 0.25 m^2/s, corresponding with a timestep of 5 seconds, 10 seconds, and 100 seconds, respectively. These results are compared to a simulation where K is unconstrained, and the timestep ranges from 1 second to 0.05 seconds depending on maximum water depth. A comparison of various hydrologic outputs as well as the resulting mosquito populations showed that this approximation had only a small impact on the simulation. The normalized root mean square error (NRMSE) and the correlation coefficient (CC) of total infiltration, surface area of pools, volume of pools, and number of mosquitoes simulated over the model domain between the simulation with unconstrained K and simulations with upper limits on K are shown in Table 2.1. Based on these results, a maximum value of K=2.5 m^2/s was selected in order to maintain accuracy while increasing computational efficiency. During wet conditions, this results in a 200 fold decrease in the number of timesteps required by the overland flow module of HYDREMATS.

Table 2.1 Effect of limiting coefficient K on important model outputs.

	Kmax=5	**Kmax=2.5**	**Kmax=0.25**
Timestep	5 seconds	10 seconds	100 seconds
Infiltration			
NRMSE	0.9%	1.0%	1.5%
CC	99.1%	99.0%	97.8%
Surface Area of pools			
NRMSE	0.4%	1.2%	1.6%
CC	99.9%	99.1%	98.6%
Volume of pools			
NRMSE	3.4%	4.7%	13.1%
CC	99.7%	99.5%	97.9%
Number of mosquitoes			
NRMSE	1.9%	3.3%	3.6%
CC	99.9%	99.9%	99.6%

2.2.2 Decreasing model storage requirements

The hydrology component of HYDREMATS provides output information for every simulated hour. This includes the water depth and water temperature for each grid cell, which are used by the entomology component of the model as maps of larval sites. For a 2.5 x 2.5 km model

domain size, the memory requirements of the water depth and temperature output files are roughly 7.2 GB per simulated year. The model was modified such that when there are no water pools in the model domain, the hydrology component does not output pool information. At each time step, the entomology component then checks whether a pool output file exists; if not, the model assigns the pool depth for each grid cell as 0 mm. This greatly reduces the hard disk space required by the model, particularly during multi-year simulations in areas with long dry seasons.

2.2.3 Parallelization of entomology model

The entomology component of HYDREMATS updates the status of each adult mosquito at every hourly timestep. The processes considered at each timestep include flight, water-seeking, ovipositing, meal-seeking, biting, and disease transmission (Figure 2.3). Previously, the model cycled through the decision processes for every mosquito one at a time. However, adult mosquitoes simulated independently from one another, making this an ideal task for parallel computing. The entomology component of the model was converted from Fortran 77 to Fortan 90. The model code was then modified to allow the adult mosquito processes to be calculated in parallel using the OpenMP framework (Dagum & Menon, 1998). This allows the total number of adult mosquitoes to be divided among multiple processors. At the end of the parallel segment, the eggs laid in each grid cell on each thread are consolidated and the remainder of the entomology component runs in serial.

2.3 Incorporating the effects of humidity on mosquito survival

Low levels of relative humidity are known to decrease the lifespan of mosquitoes. However, HYDREMATS, like most current models of malaria transmission, did not account for the effects of relative humidity on mosquito survival. In the Sahel, where relative humidity drops to levels <20% for several months of the year, we expect relative humidity to play a significant role in shaping the seasonal profile of mosquito populations. Here, we present a new formulation for *Anopheles gambiae sensu lato (s.l.)* mosquito survival as a function of temperature and relative humidity and investigate the effect of humidity on simulated mosquito populations. Using existing observations on relationships between temperature, relative humidity and mosquito longevity, we developed a new equation for mosquito survival as a function of temperature and relative humidity. We apply this equation to the environmental data for two villages from the Sahel region of Africa and conduct numerical simulations of mosquito populations using HYDREMATS.

2.3.1 Background

2.3.1.1 Effects of humidity on mosquito longevity

Mosquitoes, like all insects, have a limited range of tolerable temperature and humidity (Wigglesworth, 1939). The high surface area to volume ratio of mosquitoes makes them especially sensitive to desiccation at low humidity levels.

Gaaboub *et al*. (1971) compared the survival of groups of female *Anopheles pharoensis* mosquitoes at 20^{o}, 26^{o} and 30^{o}C and found little difference in longevity between 50% and 90% relative humidity (RH) conditions at a given temperature. Bayoh and Lindsay (Bayoh, 2001)

measured the longevity of *An. gambiae sensu stricto (s.s.)* at 40%, 60%, 80% and 100% RH at 5°C intervals from 5°C to 40°C. Under the assumption that daily probability of survival is independent of mosquito age, there was little difference in survival between 60-100% RH, but survival was slightly reduced at 40% RH.

Molecular biology techniques applied to *An. gambiae s.s.* held at 42% RH (Liu *et al.*, 2011) and 30% RH (Wang *et al.*, 2011) found the mosquitoes had undergone physiologic responses to desiccation stress, decreasing their water loss. Mosquitoes held without food or water survived for an average of 15.6 hours at 30% RH compared to 26.2 hours at 70% RH (Wang *et al.*, 2011).

Recent studies on mosquito desiccation showed that extremely low levels of RH are fatal to mosquitoes when maintained for periods on the order of hours. These studies placed mosquitoes in vials without access to food or water and added a desiccant to reduce RH levels that are generally kept at <10% RH but not exactly specified. Several such studies found that no *An. gambiae s.s.* or *An. arabiensis* females survived for an entire day at <10% RH (Fouet *et al.*, 2012; Gray & Bradley, 2005) or <20% RH (Liu *et al.*, 2011). In a similar study, a small number of mosquitoes survived up to 30 hours at <10% RH, and acclimation to hot and dry conditions was shown to increase desiccation resistance (Gray *et al.*, 2009). However, in another study using the offspring of field captured mosquitoes held at <10% RH, 15% of S form *An. gambiae s.s.* and 23% of M form *An. gambiae s.s.* females survived for over 1 day, with 2 out of 30 M form individuals surviving for over 2 days (Lee *et al.*, 2009), suggesting that wild mosquitoes in arid regions may have higher desiccation resistance than laboratory colonies.

In summary, *An. gambiae* longevity does not appear to be substantially affected by relative humidity at ranges greater than 40%, but RH <10% is fatal, usually within hours. There is very little information on mosquito longevity in the range 10-40% RH.

2.3.1.2 Mosquito survival in malaria models

Many mechanistic models of malaria transmission, including HYDREMATS, use the Martens equation for survival as a function of temperature (Craig *et al.*, 1999; Ermert *et al.*, 2011; W. Martens *et al.*, 1995; Parham & Michael, 2009):

$$p(T) = \exp\left(\frac{-1}{-4.4 + 1.31T - 0.03T^2}\right) \quad (2.9)$$

where T is the daily average air temperature in degrees Celsius. This function gives maximum longevity in the range of 20-25^{o}C, and severe mortality at temperatures below 10^{o}C and above 35^{o}C. This curve, shown in Figure 2.7, was formed based on three data points (W. J. Martens, 1997).

The experiments relating survival to temperature conducted by Bayoh (2001) led to the development of two new formulations of survival probability of *Anopheles gambiae* to temperature, one by Ermert *et al.* (2011) and another by Mordecai *et al.* (2013), shown in Figure

2.7. The accuracy of these two formulations and the Martens equation were recently evaluated by Lunde *et al.* (2013).

Relative humidity has recently been incorporated into several models. Parham *et al.* (2012) developed a survival curve based on Bayoh's survival data (Bayoh, 2001). The Liverpool Malaria Model accounts for humidity by subtracting 10% from the daily probability of survival when 10 day accumulated rainfall is below 10mm (Ermert *et al.*, 2011). Lunde *et al*. (2013) use Bayoh's survival data by fitting a survival curve for each measured value of RH (40%, 60%, 80% and 100%), further adjusted by mosquito size and age. While these formulations for mosquito survival rates are improvements on previous formulations that considered only temperature, they do not reliably capture the effect of very low values of relative humidity (<40% RH) such as those observed during the dry season in the Sahel on mosquito survival. Here, we propose a new equation for mosquito survival incorporating current knowledge on the effects of relative humidity and temperature on survival.

2.3.1.3 Field observations

We investigated the effects of relative humidity on simulated mosquito population dynamics in two villages in Niger, West Africa. These two villages, Banizoumbou (13.53^{o} N, 2.66 ^{o} E) and Zindarou (13.43^{o} N, 2.92^{o} E), have been the subject of extensive field activities and numerical model simulations using HYDREMATS (Bomblies *et al.*, 2008; Bomblies *et al.*, 2009). The two villages are approximately 30 km apart, and there is little difference in climate between the two. Climate data for 2006 are shown in Figure 2.4. The rainy season in the region is dictated by the migration of the West African Monsoon. From approximately November through April, Harmattan winds from the Northeast bring dry air from the Sahara desert. From May through

October, the monsoon brings moist air from the Southwest (Sultan & Janicot, 2003). This shift in wind direction as measured in Banizoumbou and Zindarou in 2006 is shown in the upper left panel of Figure 2.4, where positive values of the meridional wind speed indicate wind blowing from the south, while negative values indicate wind blowing from the north. The moist air from the south leads to high relative humidity and rainfall as shown in the lower left and upper right panels of Figure 2.4, respectively.

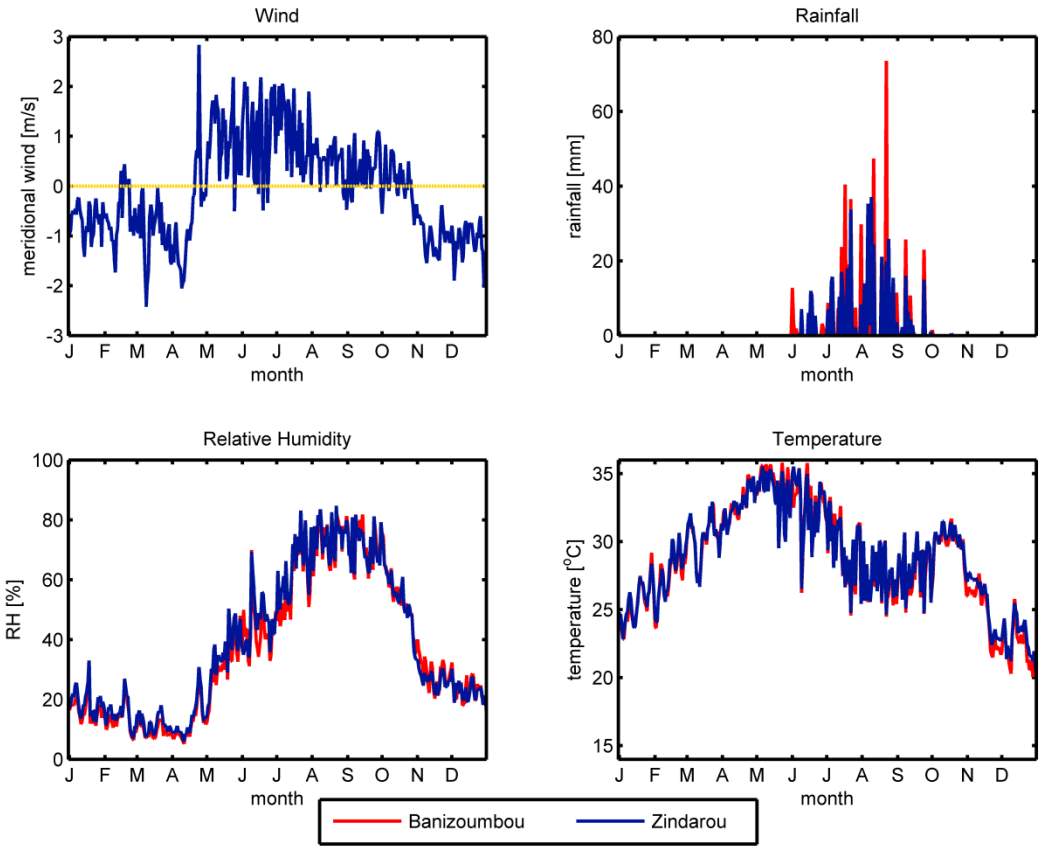

Figure 2.4 Climate in Banizoumbou and Zindarou. Ground observations of daily average meridional wind speed, daily total rainfall, and daily averages of relative humidity and temperature are shown for Banizoumbou (red) and Zindarou (blue) for the year 2006. Positive values (above the yellow line) indicate wind blowing from the south while negative values (below the yellow line) indicate wind from the north.

Despite similarities in climate, the two villages differ in their water availability. Banizoumbou is a typical Sahelian village with a deep water table (~25 meters), and surface water pools quickly dry up at the end of the rainy season. In contrast, Zindarou is located in the floodplain of an abandoned river system and is thus at a lower elevation (water table depth ~2.5 meters), allowing the groundwater to penetrate the land surface. This surface expression of ground water produces a wetter environment than is typically found in the Sahel allowing for high levels of mosquito breeding. The water pools in Zindarou persist for several months beyond the end of the rainy season, potentially extending the mosquito breeding season. Hydrological simulations of the two villages reflected this difference in pool availability, shown in Figure 2.5.

Mosquito collections were conducted as described in Bomblies *et al*. (2008) and Bomblies *et al*. (2009). Six CDC light traps were deployed overnight in each village once a month from December – May (dry season), and weekly from June – November (wet season). Female *Anopheles gambiae s.l.* and *Anopheles funestus* specimens, the important malaria vectors in this region, were identified by microscopy and counted. As shown in Figure 2.6, the observed number of anophelines followed a distinct seasonal cycle, increasing after the onset of monsoon rains in June, peaking in September, and returning to low levels by late October. No *An. funestus* were found in Banizoumbou, but a small number were found in Zindarou. The anopheline population in Zindarou did not persist beyond the end of the rainy season despite the continued availability of water pools for breeding. Bomblies *et al*. (2009) hypothesized that the observed drop in mosquito population, despite continued availability of breeding sites was due to the lack of nutrient availability for larvae, as the decline in population coincided with the end of

millet pollination. Here, we investigate whether the seasonal drop in humidity at the end of the rainy season could play a role in limiting mosquito populations.

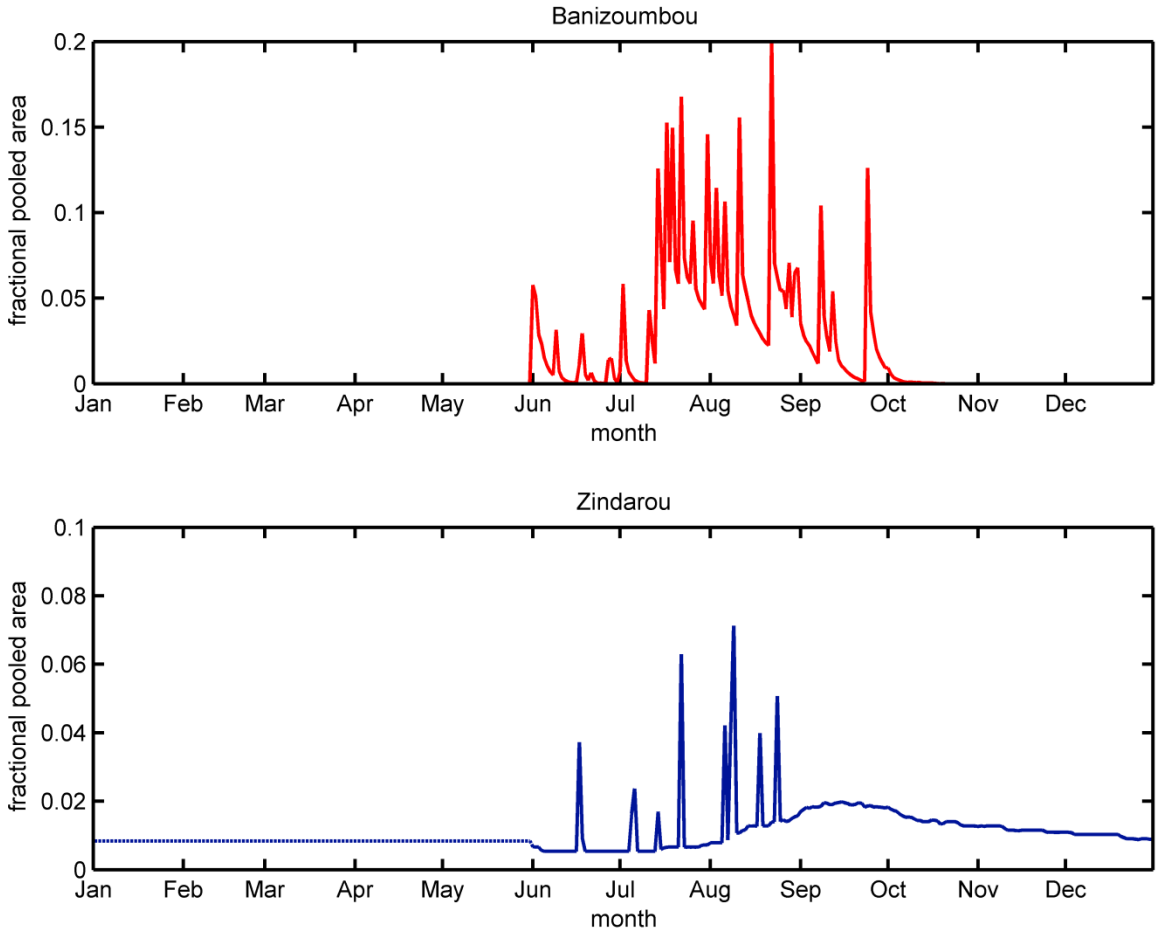

Figure 2.5 Simulated water pools as a fraction of total surface area in Banizoumbou (top) and Zindarou (bottom) in 2006. The dotted line from Jan – May in Zindarou indicates the assumption that permanent pools simulated in December persist through the dry season.

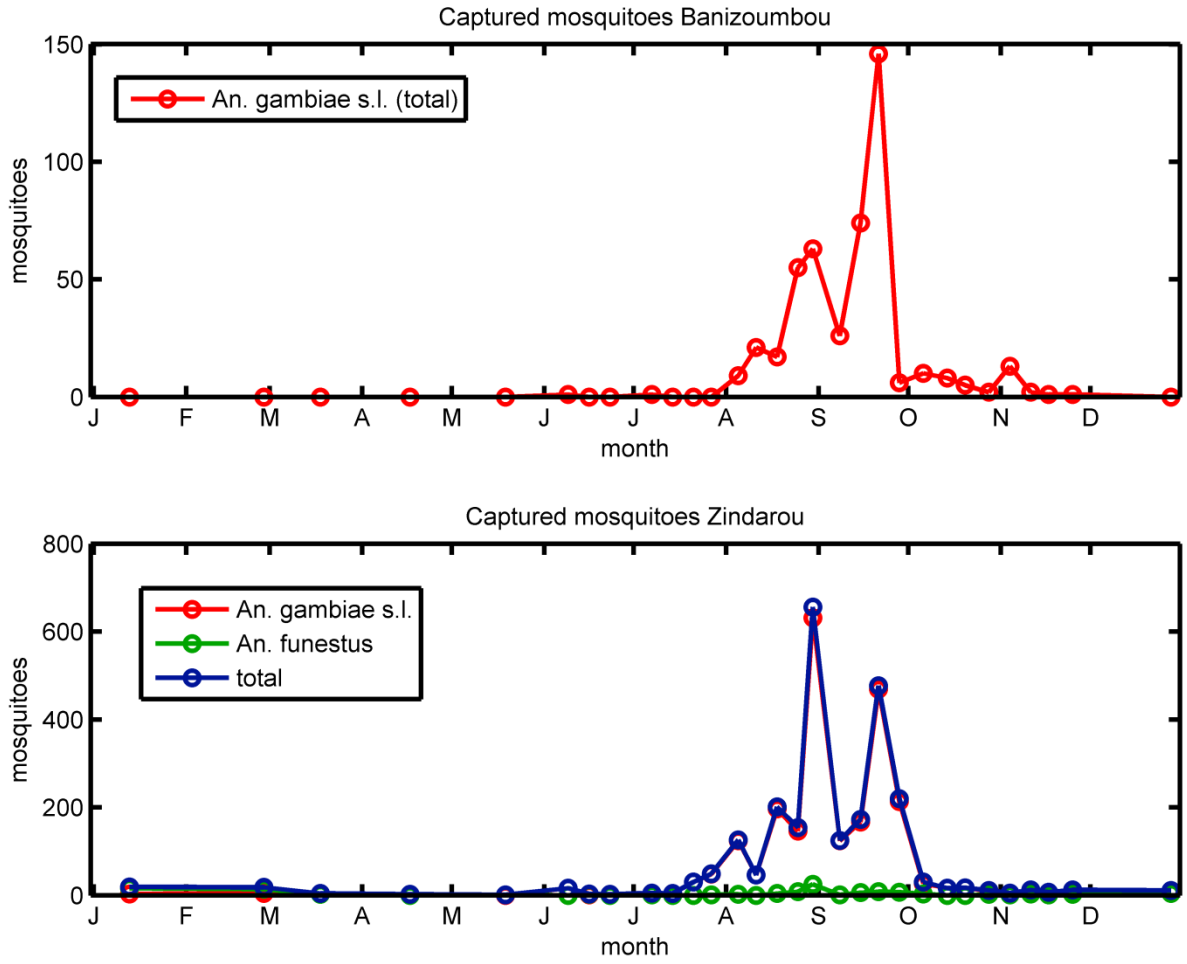

Figure 2.6 Mosquitoes captured by CDC light traps in Banizoumbou (top) and Zindarou (bottom) in 2006.

2.3.2 Development of new survival equation

2.3.2.1 Anopheline survival as a function of temperature

We based our formulation of anopheline survival on an existing relationship between temperature and survival, *p(T)*. In developing our equation for anopheline, we use the Martens equation (W. J. Martens, 1997) described above for *p(T)*. However, this equation can be

substituted by an alternative formulation for anopheline survival as a function of temperature. Two alternative equations have recently been developed using new survival data (Bayoh, 2001), which we will refer to as Bayoh-Ermert (Ermert *et al.*, 2011) and Bayoh-Mordecai (Mordecai *et al.*, 2013). The Martens curve and the two alternative curves are shown in Figure 2.7. These equations were recently evaluated by Lunde *et al*. (2013).

We make the assumption that the survival equation, *p(T)*, accurately describes *Anopheles gambiae* survival at high and moderate levels of relative humidity.

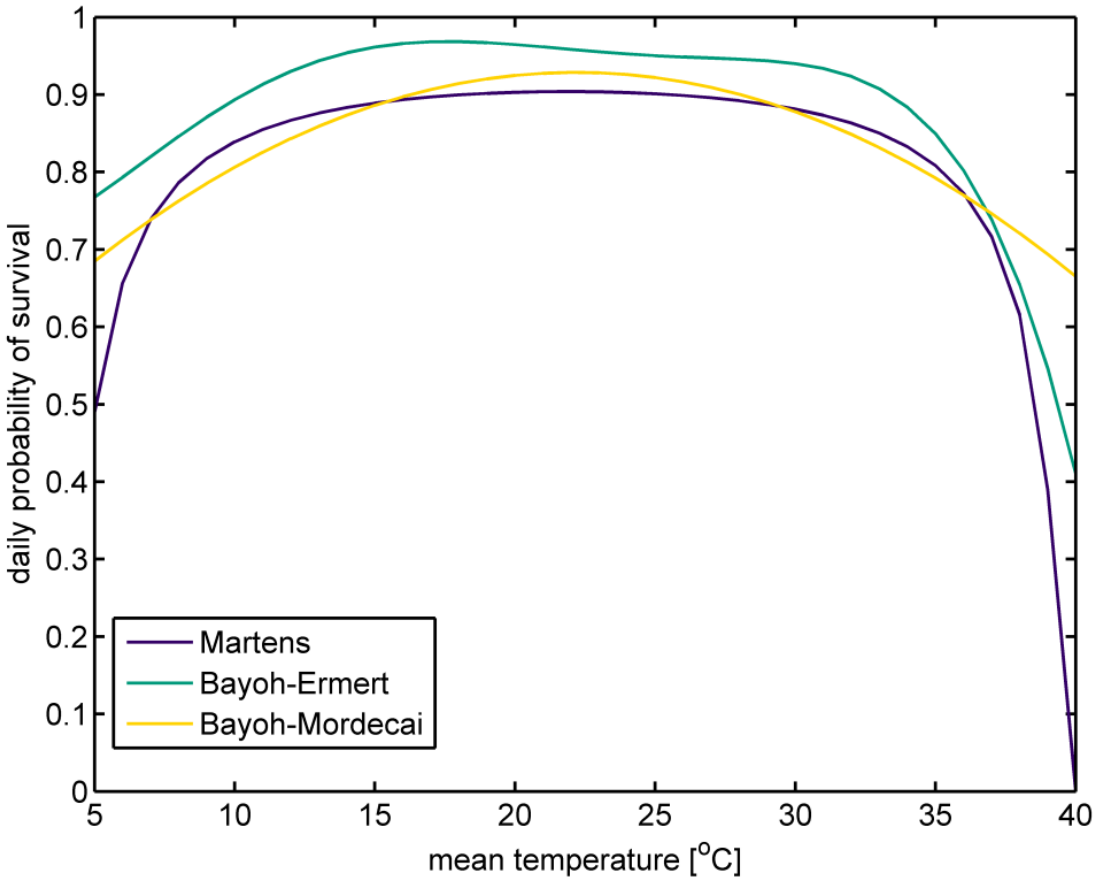

Figure 2.7 Three options for daily probability of survival, p(T).

2.3.2.2 Adding the effect of relative humidity

We then add the effect of relative humidity by multiplying the survival by a relative humidity stress factor *S*. The humidity stress factor was developed using the observations reviewed in the previous section, and listed in Table 2.2. As we summarized in the previous section, there are some data reported for mosquito survival at RH values ≥40% and < 10%. We assume that mosquitoes feel no humidity stress at daily average relative humidity greater than or equal to some value RH_S (S=0), and are stressed to the point of being unable to survive an entire day at critical daily average relative humidity RH_C (S=1). In the absence of data measuring mosquito longevity at relative humidity between 10% and 40%, we assume S decreases linearly from 1 at RH_C to 0 at RH_S.

Table 2.2 Observations of mosquito longevity used for development of the relative humidity stress factor

Species	**Temperature**	**RH**	**Reference**
An. pharoensis	20°C-30°C	50%, 90%	Gaaboub *et al*., 1971
An. gambiae s.s.	5°C -40°C	40-100%	Bayoh, 2001
An. gambiae s.s.	28°C	<20%,42%	Liu et al., 2011
An. gambiae s.s.	27°C	30%, 70%	Wang *et al.,* 2011
An. gambiae s.s.	28°C	<10%	Gray and Bradley, 2005
An. arabiensis	28°C	<10%	Gray and Bradley, 2005
An. gambiae s.s.	27°C	<10%	Gray *et al*., 2009
An. gambiae s.s.	26°C	5%	Fouet *et a*l., 2012
An. gambiae s.s.	28°C	<10%	Lee *et al*., 2009

The stress factor is then defined as follows:

$$S = \begin{cases} 1 \ , & RH < RH_C \\ \dfrac{RH_S - RH}{RH_S - RH_C} \ , & RH_C \leq RH \leq RH_S \\ 0 \ , & RH > RH_S \end{cases} \qquad (2.10)$$

The new equation for *An. gambiae* survival is given by:

$$\mathrm{p(T, RH)} = \mathrm{p(T)} \times (1 - \mathrm{S}) \qquad (2.11)$$

This assumes that temperature and relative humidity act independently on mosquito survival.

Mosquito survival as a function of temperature and RH are shown for RH_S=42% and RH_C=5% is shown in Figure 2.8. RH_S was set at 42% RH in order to reflect a decrease in longevity observed by Bayoh (Bayoh, 2001) at 40% RH compared to values ≥ 60% RH, and evidence that mosquitoes at 42% RH showed physiological signs of stress (Liu *et al.*, 2011). RH_C was set at 5% as several of the desiccation studies found that RH<10% killed all mosquitoes in one day (Fouet *et al.*, 2012; Gray & Bradley, 2005). While most of the experiments conducted to date relating mosquito survival to relative humidity and temperature focused on *An. gambiae s.s.*, we make the assumption that our model is valid for the *An. gambiae s.l.* complex. However, parameter values can be adjusted to reflect regional or species-specific differences in tolerance to arid conditions, or based on improved knowledge on mosquito longevity at RH <40%.

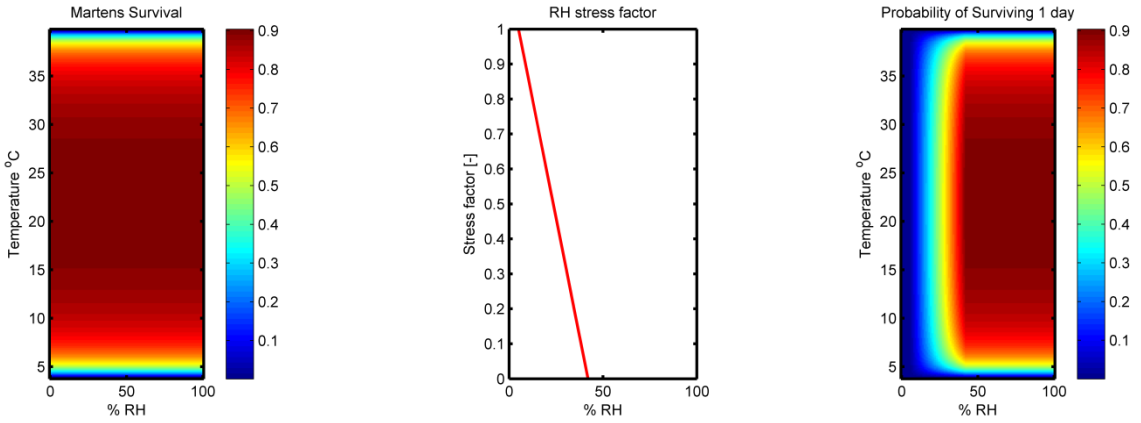

Figure 2.8 Martens survival equation (left), RH stress index (center) and daily survival probability of mosquitoes using the newly developed formula (right).

The first panel of Figure 2.8 shows the Martens survival curve, which is a function of temperature only. The second panel shows the RH stress factor calculated above. The third panel of Figure 2.8 shows the new equation for mosquito survival as a function of temperature and relative humidity.

The average lifespan of a mosquito can be calculated from the daily probability of survival: Lifespan=1/-ln(p).

Figure 2.9 shows a comparison of average lifespan using the Martens, Ermert Liverpool Malaria Model (dry season) and Parham equations and the new equation developed here when RH is held constant at 10%. At moderate temperatures (15-30^{0}C), only the new equation reflects the lethal effects of extremely low RH observed in desiccation studies (Fouet *et al.*, 2012; Gray & Bradley, 2005; Gray *et al.*, 2009; Lee *et al.*, 2009).

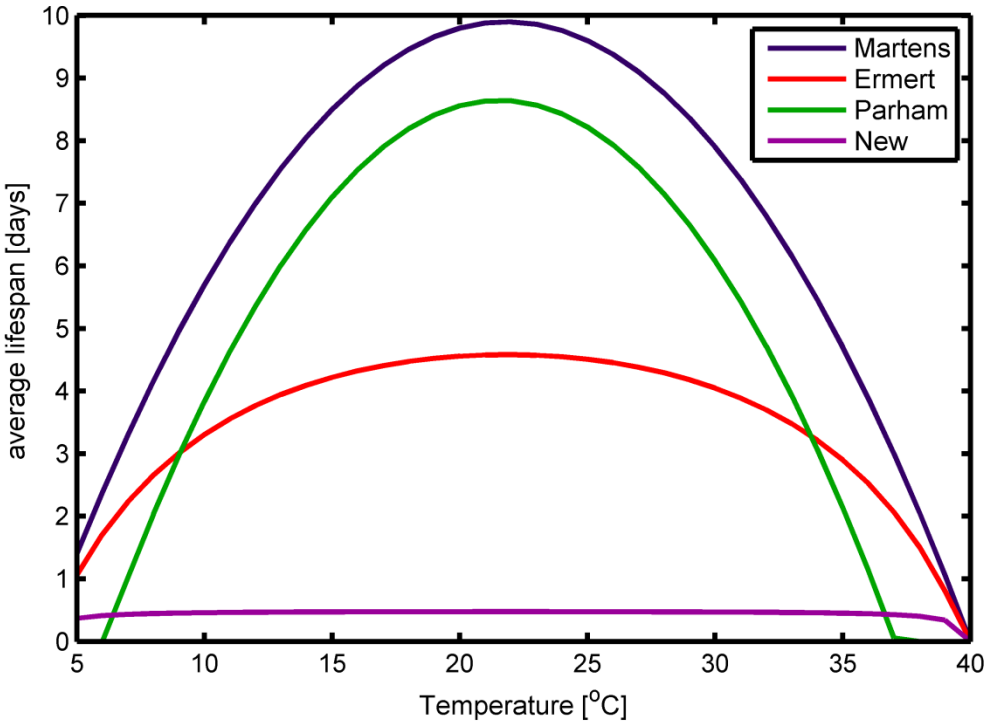

Figure 2.9 Average lifespan at 10% RH using various equations for mosquito survival.

We do not explicitly consider the possibility of aestivation, by which mosquitoes survive for long periods during the dry season. This mechanism for survival has been observed in several instances in *An. gambiae* in the Sahel (Lehmann *et al.*, 2010; Omer & Cloudsley-Thompson, 1970), but is still not well understood.

2.3.3 Testing new survival equation

We tested the impact of the new survival equation by conducting a simulation using HYDREMATS for Banizoumbou and Zindarou using field observations on temperature, wind, relative humidity, and rainfall for the year 2006. For each village, we conducted one simulation using the original Martens equation for mosquito longevity as a function of temperature only,

and 3 simulations using the new equation incorporating temperature and relative humidity using RH_S=42%, 40% and 35%, all at RH_C=5%. We also conducted a simulation for each village with RH_S=42% and RH_C=0%.

2.3.4 Results

The daily probability of mosquito survival calculated using the Martens equation and the new equation incorporating relative humidity are shown for each village in Figure 2.10. When mosquito survival depended only on temperature, as shown in the blue line of Figure 2.10, there was little seasonal variation in the probability of survival, which ranged between 0.78 and 0.90, reaching a minimum between April and July. This figure shows that temperature cannot explain the observed decrease in mosquito population at the end of the wet season. When relative humidity was included in the calculation of mosquito survival, we observed a highly seasonal pattern. During most of the wet season, relative humidity is high and therefore does not contribute to mosquito mortality. However, during the dry season, RH significantly reduces mosquito survival to values as low as 0.03 in late-March and early-April where relative humidity falls below 10%. The value of RH_S determines the extent of RH related mortality.

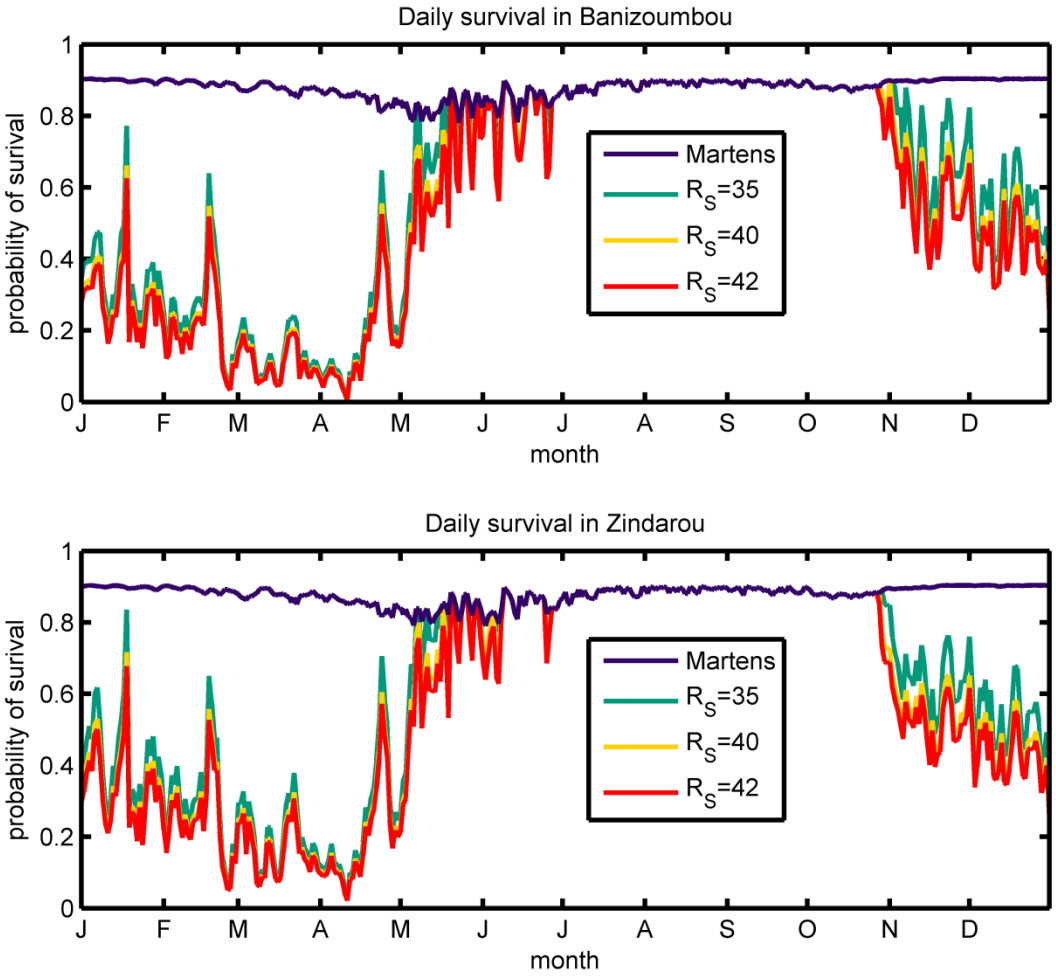

Figure 2.10 Daily probability of survival of mosquitoes using temperature and relative humidity data from Banizoumbou and Zindarou

Figure 2.11 compares the daily probability of survival as a function of temperature and relative humidity, *p(T,RH)*, using the three different equations for *p(T)* discussed in Section 2.3.2.1 and adjusted for relative humidity using parameters RH_S=42% and RH_C=5%. In the temperature range observed in Banizoumbou and Zindarou (20-35^{o}C), the three *p(T)* curves give similar survival probabilities, so there is little difference in the calculated *p(T,RH)*. The Bayoh-Ermert

equation leads to higher survival during the wet season, but the effects of relative humidity remain largely unchanged.

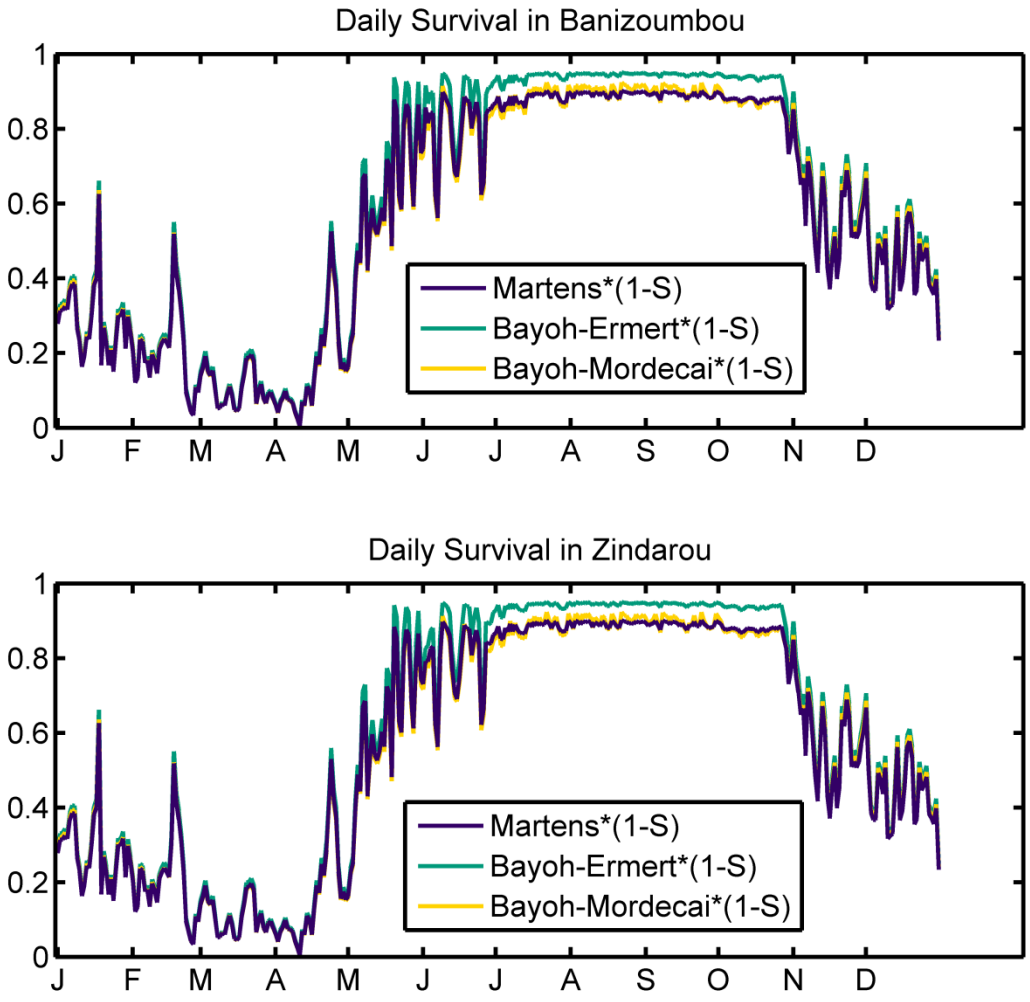

Figure 2.11 Daily probability of survival as a function of temperature and relative humidity, p(T,RH) using three different formulations for p(T).

The size of the mosquito population in each simulation is shown in Figure 2.12. In Banizoumbou (Figure 2.12, top panel), mosquito population levels were closely tied to rainfall.

There was little persistence of water pools beyond the end of the rainy season. Since the decrease in rainfall precedes the decrease in humidity, the addition of a stress factor at low levels of RH had minimal effect on mosquito populations. By contrast in Zindarou, where water pools persist for several months after the end of the rainy season, the size of the mosquito population was not limited by water availability. Temperature was also not a limiting factor at the end of the rainy season; in the simulation using the Martens equation for mosquito survival as a function of temperature, the mosquito population remained at high levels for the duration of the simulation (Figure 2.12, bottom panel, blue line). However, the incorporation of relative humidity into mosquito survival dramatically reduced the number of mosquitoes, beginning in late-October when the RH plummets. The choice of RH_S affected the results. In the simulations using RH_S=40% and 42%, the mosquito populations dropped dramatically starting on October 29th. When RH_S was set to 35%, there was no change in mosquito populations until November 4th, and the drop was somewhat more gradual than in the in the simulations with higher RH_S. There was little difference between simulations with RH_C=5% and RH_C=0% (see Figure 2.13).

The incorporation of relative humidity into simulations of mosquito populations substantially decreases mosquito longevity. In cases such as Zindarou where breeding sites are available beyond the end of the wet season, the drop in relative humidity could explain, at least in part, the rapid decline of the mosquito population in field observations. However, the timing of the decline of mosquitoes in the simulation (late October) occurred approximately four weeks after the decrease in captured mosquitoes (late September/early October), indicating that other factors likely played a role in limiting mosquito numbers.

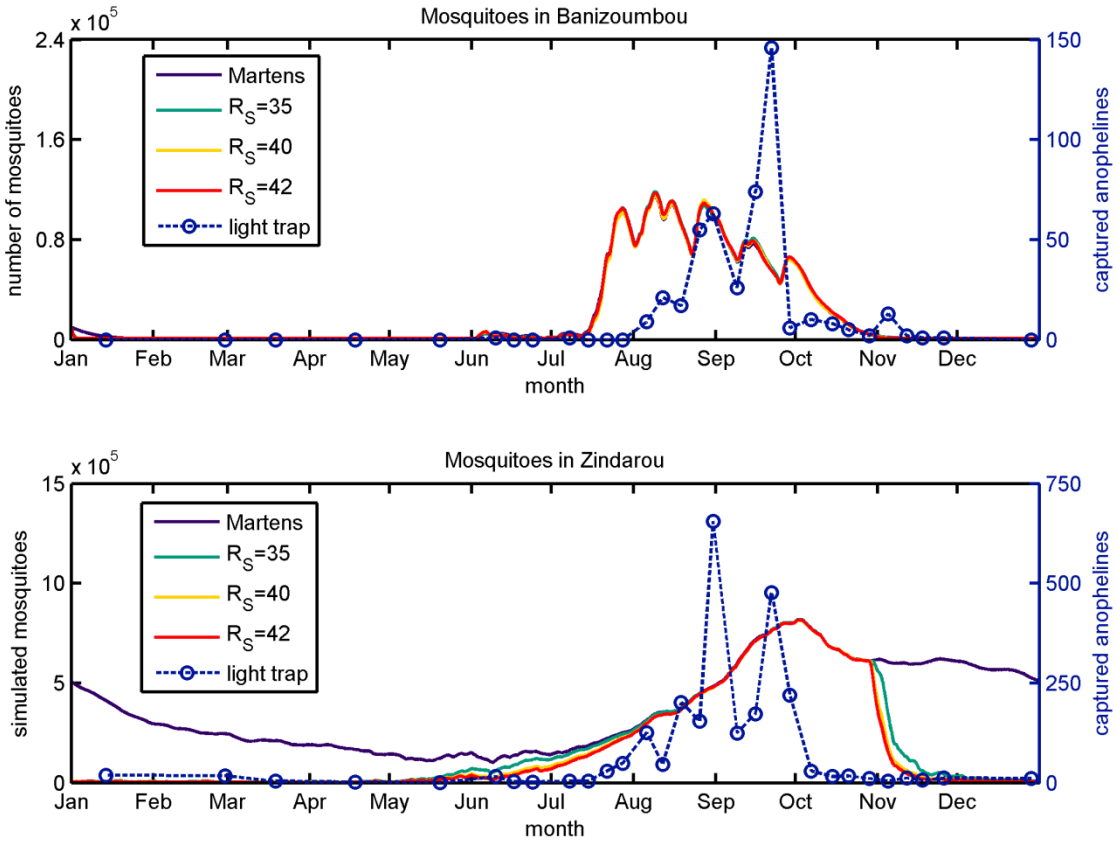

Figure 2.12 Simulated mosquitoes in Banizoumbou (top) and Zindarou (bottom) using the differing values of RHS. Mosquitoes captured by light traps are shown by the dashed line.

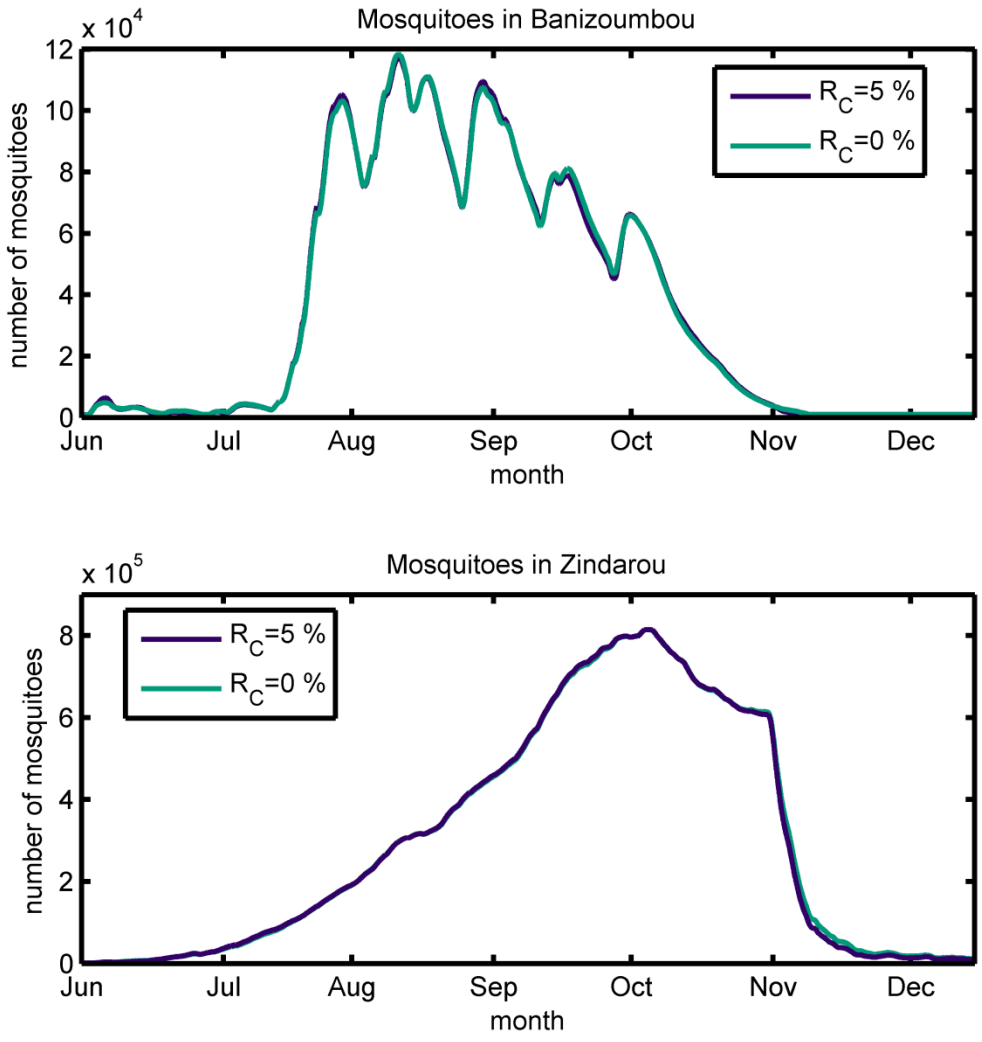

Figure 2.13 Sensitivity of results to critical value of RH

2.3.5 Discussion

The adverse effects of low humidity on mosquito longevity have been known for decades (Mayne, 1930). Here, we have taken a commonly used equation for mosquito survival as a function of temperature and added the effects of relative humidity. While other researchers have incorporated humidity into their models (Ermert *et al.*, 2011; Lunde *et al.*, 2013; Parham *et al.*, 2012), our equation is unique in that it reflects the fatal effect of the extremely low values of

relative humidity that are observed during the dry season in the Sahel. Using evidence from mosquito survival studies, we assumed that relative humidity does not affect survival rates at high and moderate values of RH, but at a value RH_S (~42% RH), survival decreases until a critical value RH_C (~5% RH) where it is assumed that no individual can survive for longer than 24 hours. In the two villages of the Sahel described here, daily averages of relative humidity remained below 30% for the majority of the dry season.

The primary mode of variability in mosquito populations in these villages features two distinct seasons; a wet season with a high population of mosquitoes and relatively high malaria transmission (July-November) and a dry season with a low population of mosquitoes and low malaria transmission (December – June). When we simulate mosquito populations using HYDREMATS parameterized with the Martens survival equation, it reproduces this mode of variability in Banizoumbou, where mosquito breeding sites were not available beyond the wet season, but it fails to reproduce the same mode in Zindarou, where breeding sites persist into the dry season. However, when we incorporate the constraints on survival due to humidity developed here into HYDREMATS, the model reproduces this observed mode of variability in both villages.

While the equation for mosquito survival developed here improved the model's ability to simulate the observed seasonal pattern of mosquitoes in Zindarou, the timing of the decline of captured mosquitoes preceded the drop in relative humidity by approximately 4 weeks, indicating that other factors must be playing a role in the mosquito decline. Other potential factors involved in this decline in mosquitoes could include a lack of nutrient availability for larvae and establishment of predator populations in the long-lasting water pools, which can be represented in HYDREMATS but were not included in the simulations for this study. Bomblies

et al. (2009) noted that the decline in mosquito population corresponded with the harvest of millet crops and hypothesized that aquatic stage mosquitoes may have depended on the availability of millet pollen. While anopheline larvae were found in the persistent water pools, it is possible that these pools become less attractive as breeding sites as the rainy season progresses, perhaps due to increased vegetation, turbidity or predator activity. Another possible explanation for the decline in mosquito captures could be the triggering of aestivation, where mosquitoes retreat to sheltered locations and cease regular activities, leading to a decrease in captured mosquitoes despite the continued presence of water pools.

In addition to the dramatic reduction in the mosquito population simulated in Zindarou as a result of low RH, mosquito longevity in individual mosquitoes plays an important role in malaria transmission dynamics. In order to transmit the parasite, a mosquito must survive long enough to bite an infected person, surpass the extrinsic incubation period of the parasite, roughly 6-10 days in warm climates (Detinova, 1962), and then bite a second (uninfected) person. This amplifies the effect of shortened lifespan, such that even a small decrease in lifespan can have a very significant effect on malaria transmission (Macdonald, 1956).

2.4 Conclusions

In this chapter, we describe improvements made to HYDREMATS in two areas: model efficiency, and mosquito survival. The efficiency improvements to HYDREMATS were critical for conducting multi-year simulations. The result is a much faster model that requires less hard disk space, and takes advantage of modern parallel computing platforms.

We proposed a new equation to describe mosquito survival as a function of temperature and relative humidity. We demonstrated that relative humidity can play a significant role in mosquito

survival and malaria transmission dynamics. In the Sahel, where dry season RH regularly drops to levels known to significantly decrease mosquito longevity, relative humidity can be as important as temperature and rainfall in determining the environmental suitability for mosquitoes and malaria transmission. The primary mode of variability in mosquito populations in these villages features two distinct seasons; a wet season with a high population of mosquitoes and relatively high malaria transmission and a dry season with a low population of mosquitoes and low malaria transmission. We showed that when we simulate mosquito populations using HYDREMATS parameterized with the Martens survival equation, it fails to reproduce the same mode in Zindarou, where breeding sites persist into the dry season. However, when we incorporate the constraints on survival due to humidity developed here into HYDREMATS, the model reproduces this observed mode of variability in both villages. Future modeling work should therefore account for these effects of relative humidity.

3 Extension of HYDREMATS to incorporate human immunological processes

3.1 Introduction

Individuals continuously exposed to malaria gradually acquire immunity that protects from severe disease and high levels of parasitization. Acquired immunity has been incorporated into numerous models of malaria transmission of varying levels of complexity. Most of these models require prescribing inputs of mosquito biting rates or other entomological or epidemiological information. Here, we present a model with a novel structure that uses environmental controls of mosquito population dynamics to simulate the mosquito biting rates, malaria prevalence as well as variability in protective immunity of the population. Findings from this chapter have been published in the journal Parasites & Vectors (Yamana *et al.*, 2013).

A simple model of acquired immunity to malaria is presented and tested within the framework of the Hydrology, Entomology and Malaria Transmission Simulator (HYDREMATS), a coupled hydrology and agent-based entomology model. This immunity model builds on the structure presented by Bomblies (2009). The combined model uses environmental data including rainfall, temperature, and topography to simulate malaria prevalence and level of acquired immunity in the human population. Simulated individual mosquitoes interact with their environment, become infected and transmit infection as they encounter humans and take blood meals. The model is used to demonstrate the effect of acquired immunity on malaria prevalence in two Niger villages that are hydrologically and entomologically very different. Simulations are conducted for the

year 2006 and compared to malaria prevalence observations collected from the two villages between December 2005 and February 2007.

3.2 Study location

Located only 30 km apart (see map, Figure 3.1), Banizoumbou and Zindarou are subject to the same general climate, shown in Figure 2.4, yet exhibit very different mosquito abundance. This difference in mosquito abundance has been shown to be the result of varying hydrological conditions between the two villages (Bomblies *et al.*, 2009). Regional average annual rainfall in this region of Niger is approximately 500mm and occurs exclusively during the summer monsoon (June – September), during which local mosquito populations increase significantly. Banizoumbou is typical of the Sahel, in that it is arid, has deep groundwater and has very little pooled water outside of the summer monsoon season. During the summer rainy season, water pools formed from rainfall runoff provide breeding habitiat for *Anopheles* mosquitoes. Zindarou, on the other hand, has shallow groundwater (depth to water table is ~1m) because it is located in a relic river channel known as the Dallol Bosso. The Zindarou villagers dig shallow garden wells to access water for their vegetable gardens, which exposes a large water surface area to continuous, perennial mosquito breeding. The pooling of rainfall during the summer rains is also exacerbated by the shallow groundwater, because infiltration causes the shallow groundwater table to rise, creating extensive surface expressions of groundwater (Bomblies, 2009). Not surprisingly, this leads to very high mosquito abundance. Figure 3.2 presents field observations of mosquito abundance in the two villages, showing significantly more mosquitoes in Zindarou than Banizoumbou for both 2005 and 2006.

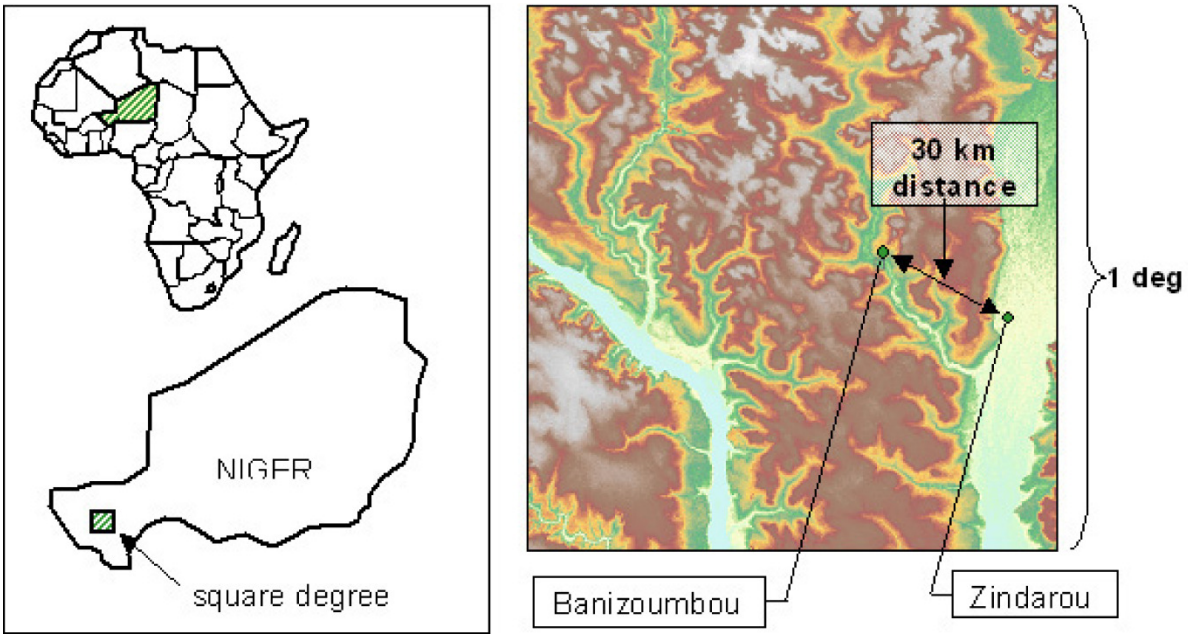

Figure 3.1 Location of the studied villages Banizoumbou and Zindarou, Niger. The right panel depicts topography within the HAPEX-Sahel square degree, the subject of an intensive international hydrology and climatology research project that took place from 1991 until 1993. The Niger River is seen in the bottom left of the domain, and the "Dallol Bosso" relict river basin is seen on the right. (From Bomblies et al., 2009)

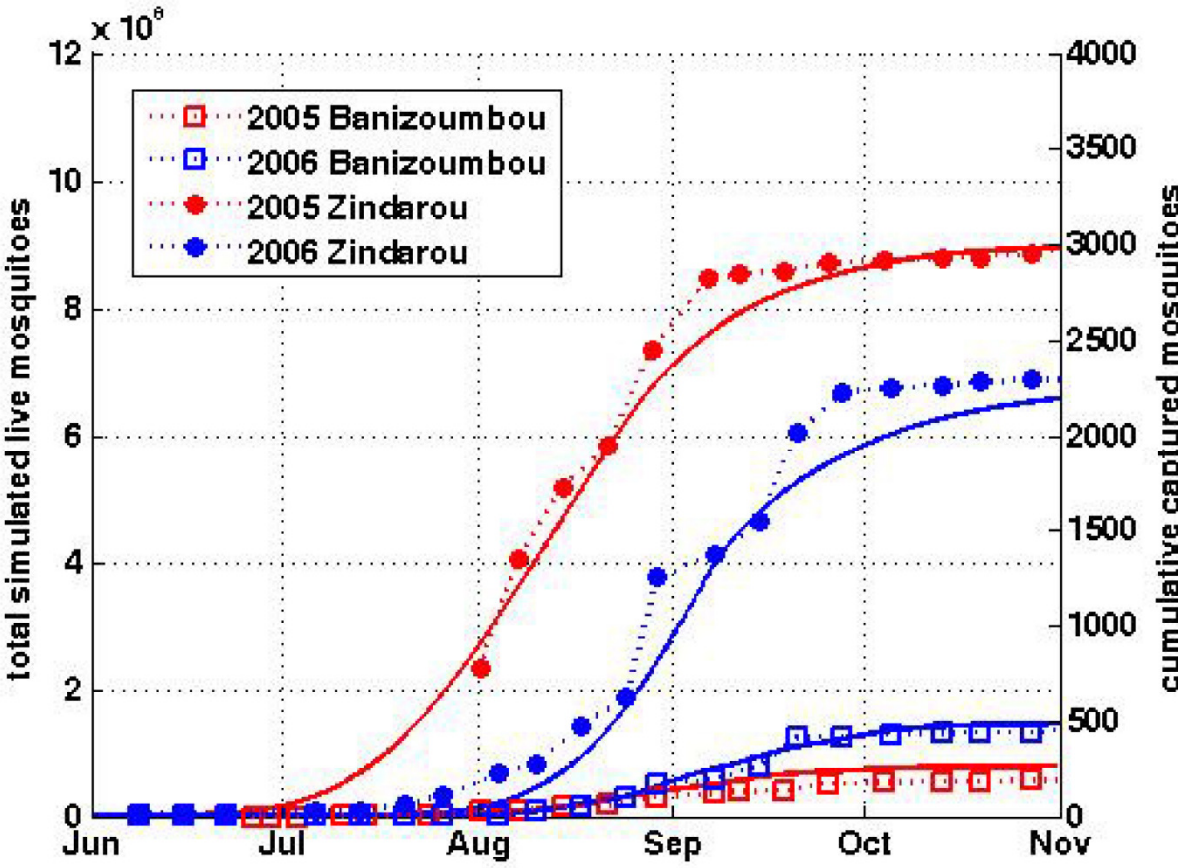

Figure 3.2 Modeled and observed Anopheles gambiae mosquito abundance in Banizoumbou and Zindarou. Mosquito abundance is very different in the two similarly sized villages, because of local hydrological differences. This is evident in the light trap captures (markers with dashed lines) and the simulation results (solid lines). (From Bomblies et al., 2009)

The hydrological differences between Banizoumbou and Zindarou and the associated differences in mosquito abundance as measured by CDC light trap captures were simulated by Bomblies *et al*. (2009) using the highly detailed coupled hydrology and entomology numerical model HYDREMATS (Hydrology, Entomology and Malaria Transmission Simulator) (Figure 3.2).

Here, we use HYDREMATS to investigate the levels of malaria prevalence in the two villages. We do this by extending HYDREMATS to include a representation of transmission of the

malaria parasite between humans and mosquitoes. An important aspect to malaria transmission is the semi-protective immunity to disease that is acquired as humans are exposed to infectious mosquito bites. The resulting immunity exerts a moderating effect on malaria transmission, and is expected to be a significant factor in shaping malaria propagation through the human/mosquito transmission cycle by a negative feedback mechanism. It follows that for accurate model representation of linkages between environmental variability and malaria prevalence, effects of human immunity must be considered.

3.3 Development of immunology component of HYDREMATS

The hydrology and entomology components of HYDREMATS were developed by Bomblies *et al*. (Bomblies *et al.*, 2008) as an agent-based model in which individual mosquitoes interact with their immediate environment. The model tracks the infection status in mosquitoes and humans. Malaria can be transmitted when a human is bitten by a sporozoite-infected mosquito. Mosquitoes become exposed to the parasite by biting infected humans. After ingesting a parasite, a mosquito becomes infectious after an extrinsic incubation period (EIP) of 111 degree-days above 16 degrees C (Detinova, 1962). At this point, the mosquitoes are able to transmit a new infection to the next human bloodmeal host, completing one cycle of transmission. If animal hosts are chosen for a bloodmeal instead of humans, no transmission occurs. Infections in mosquitoes persist for the remainder of the mosquito's lifespan, while human individuals clear the parasite at rate *r,* described below.

A simple model of malaria infections and human immunity was presented in Bomblies (2009). In this chapter, the immunology component of HYDREMATS (Figure 3.4) is extended to

provide a more detailed representation of malaria infections and acquired immunity within humans.

Since many details of immunity and malaria transmission remain unknown and thus are difficult to parameterize, we present a model with minimal parameters. Whenever possible, parameter values are taken from literature presented in Chapter 1. Where no exact value was given, we assumed parameter values that are deemed reasonable guesses. Of course, model results will depend on choice of parameters, and a perfect fit and parameterization is not a goal of this study. Rather, we seek to reproduce general observed trends with a simple model to help understand the effect of immunity in high resolution agent-based models and inform future malaria modeling efforts of such nature.

3.3.1 Previous formulation of acquired immunity

The representation human immunity developed Bomblies (2009) model aimed for simplicity. Human immunity is represented by the variable *imm*, which varies from 0 (immunologically naïve) to 1 (fully developed immunity). Each day, the immunity (*imm*) of any human agent that has received at least one infectious bite during the previous 24 hours is raised by parameter *s*, regardless of that human agent's infected status, up to a maximum of 1. In this formulation, *s* is set at 0.2. Immunity is then lost at 0.1% per day. These parameters were chosen based on the malaria prevalence observations made in Banizoumbou (Figure 3.5).

Each time a human agent is subjected to an infectious bite, the probability of infection is:

$$b = 1 - imm \tag{3.1}$$

A uniform random number is generated and compared to *b* to determine if the human agent has acquired the parasite from the infectious bite.

The duration of each malaria infection in humans is exponentially distributed with rate parameter, *r*, set to 0.0031, corresponding to a mean duration of infection of 320 days.

With this formulation, the variety of mechanisms of immune response to malaria infection are conveniently lumped together into one "immunity" process represented by a single variable *imm*, ignoring the exact details of the multitude of individual processes involved in the immune system.

3.3.2 New formulation of acquired immunity

The variation of immunity model developed in this chapter builds on the previous model, adding a more detailed representation of immunity mechanisms and parameter values that are more consistent with published data. The addition of immunity mechanisms adds a number of parameters. Whenever possible, parameter values are taken from literature.

As in the previous formulation, human immunity for each human individual is represented in HYDREMATS the index *imm*, which varies from 0 (immunologically naïve) to 1 (fully developed immunity). Each day, the immunity (*imm*) of any human individual that has received at least one infectious bite during the previous 24 hours is raised by parameter *s*, regardless of that human individual's infected status, up to a maximum of 1. The parameter *s* was reduced to 1/60 per infectious bite, reflecting the slow build up of immunity to parasitaemia through childhood and adolescence (Langhorne *et al.*, 2008). Immunity is lost at a rate of 0.019% per

day, corresponding to a half- life of ten years, reflecting the protective effects of immunity on the order of decades in the absence of exposure (Struik & Riley, 2004).

Each time a human individual is subjected to an infectious bite, the probability of infection is given by:

$$b = (bmin - bmax) * imm + bmax \quad (3.2)$$

where bmax and bmin are parameters reflecting the probability of infection with no immunity and full immunity, respectively.

A recent compilation of observed values of *b* gave a range between 0.01 and 0.49 (Ermert *et al.*, 2011). We reflect this range by setting bmax=0.5 and bmin=0.05. The non-zero value of bmin allows even fully immune individuals to contribute to the disease reservoir (Muirhead-Thomson, 1957).

In the previous formulation, the duration of a simulated human malaria infection was independent of an individual's immunity level. Here, the disease clearance rate was modified such that the duration of disease shortens as immunity increases. The duration of each infection is exponentially distributed with rate parameter, *r*, set to

$$r = (rmax - rmin) * imm + rmin \quad (3.3)$$

The value for *rmin* is set to 1/220 days^{-1}, which is consistent with the mean duration of infection found in immunologically naïve adults infected with malaria (Jeffery & Eyles, 1954). As we could not find a published estimate for *rmax*, we assume that full immunity doubles the clearance

rate and set *rmax* to 1/110 days^{-1}. The recovery rate is also affected by superinfection, the state of an individual having two or more concurrent malaria infections, following the assumption made by Macdonald (1950) and Dietz *et al*. (1974) that multiple infections can occur simultaneously and the duration of each infection is not affected by the presence of other infections. Thus each infection within a human is tracked separately and must be cleared independently at rate *r*.

We did not include an effect of immunity on the probability that a mosquito is infected when biting an infected human, due to the high uncertainty regarding the effect of acquired immunity on human infectivity to mosquitoes. However, this could easily be modified in the model, should more definitive information come to light.

HYDREMATS was modified so that each human in the village population is assigned an age, distributed according to local demographics as shown in Figure 3.3 (Niger. Bureau Central du Recensement & Niger. Ministère de l'Economie et des Finances. Sécretariat Général, 2005). The initial immunity level is proportional to an individual's initial age, reflecting the accumulation of immunity over time. Humans age as the model progresses, and at each time step, they are subjected to a probability of death equivalent to 0.0436/year. In order to maintain a constant population size, a new child is born into the model population each time a human dies.

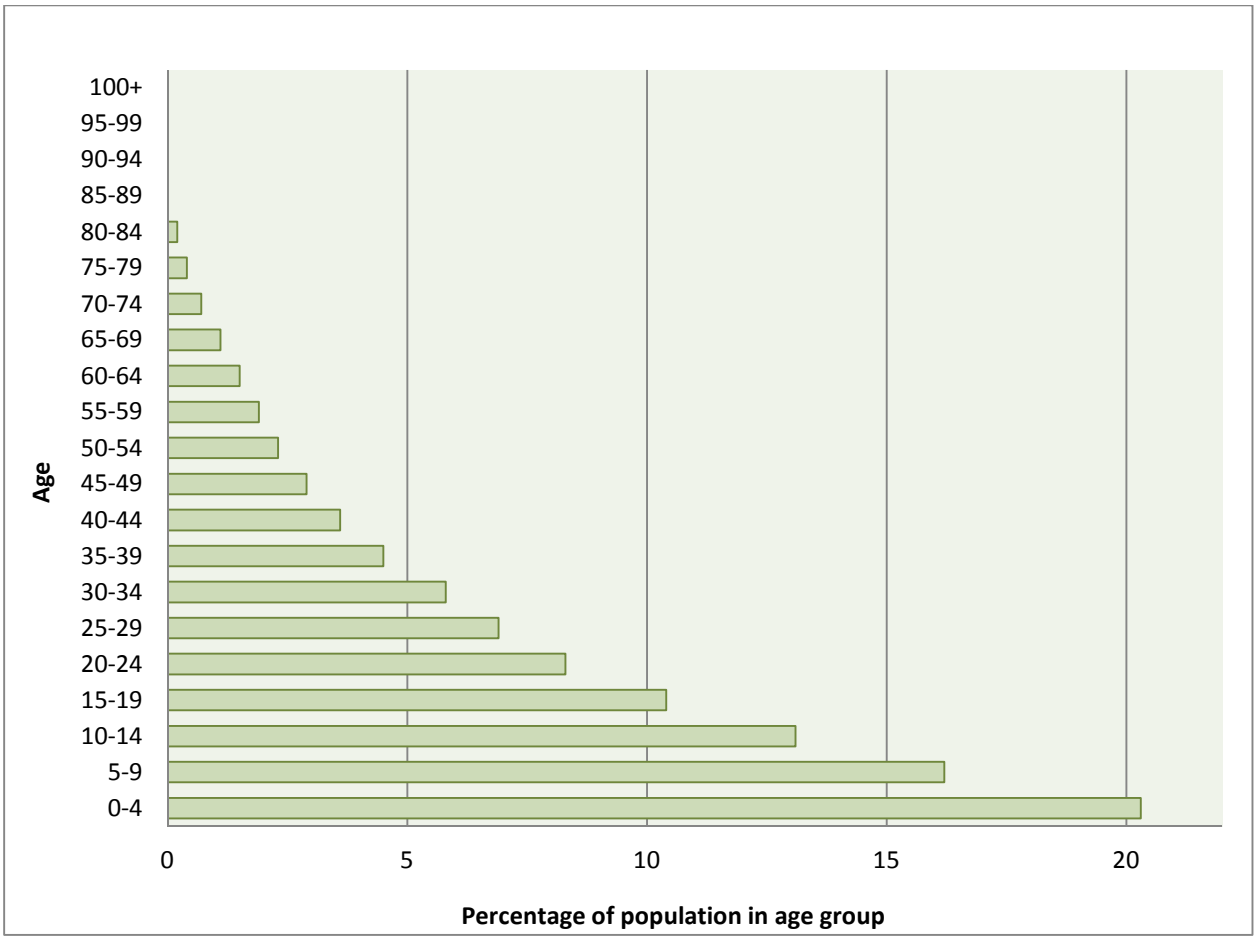

Figure 3.3 Population pyramid for Niger

Figure 3.4 shows a schematic of the malaria transmission model within HYDREMATS. Solid arrows represent the progress of individual human and mosquito individuals through infectious states, and dashed arrows indicate the transmission of malaria parasites through mosquito bites. The parameters for the immunity model are listed in Table 3.1. The sensitivity of disease prevalence to parameter values was assessed by perturbing each parameter by 10% and observing the effect on mean annual prevalence after 10 years of simulation in Banizoumbou.

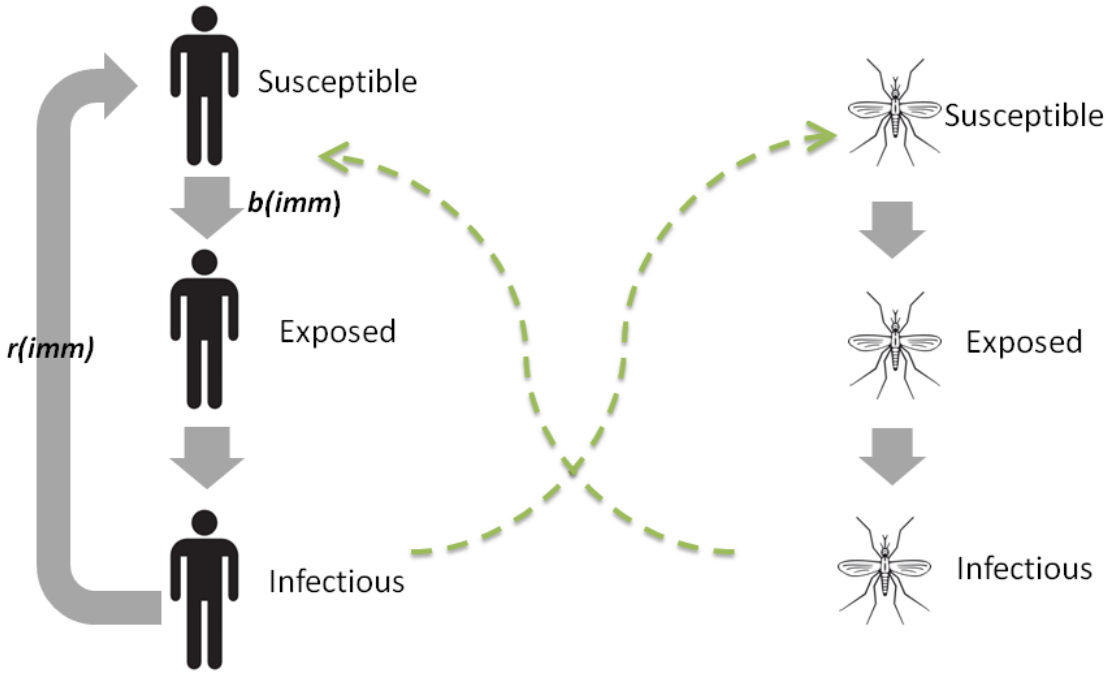

Figure 3.4 Schematic of the immunology component of HYDREMATS. HYDREMATS models individual mosquito human and mosquito agents. The solid arrows represent processes as individual agents become infected, dashed lines indicate the movement of malaria parasite through mosquito bites

With this formulation, malaria prevalence depends on resistance acquired over several years of repeated inoculations within a population. We stress that this is a very simple representation of a very complex and highly developed human immune response to the malaria parasite. Nevertheless, the model representation of immunity captures many of the important aspects regarding the role of immunity in malaria transmission. It allows the effects of immunity on malaria transmission to be incorporated into the model in a flexible and representative manner. This formulation allows simulated prevalence to be compared to observed prevalence while maintaining spatial structure.

Table 3.1 Parameters for immunology component of HYDREMATS

	Previous model	New model	Percent change in prevalence when parameter value in new model decreased by 10%
Minimum disease clearance rate parameter rmin	1/320 days	1/220 days	+35%
Maximum disease clearance rate parameter rmax	1/320 days	1/110 days	+5%
Rate of acquiring immunity s	0.2 per infectious bite	0.017 per infectious bite	-4%
Maximum probability a human is infected when bitten by infectious mosquito bmax	n/a	0.5	+1%
Minimum probability a human is infected when bitten by infectious mosquito bmin	n/a	0.05	0%
Rate of immunity loss	0.1% per day without infectious bite	0.019% per day without infectious bite	+6%

3.4 Simulations

To assess the importance of the difference in immunity between the two villages Banizoumbou and Zindarou, we first conduct a simulation for each village where the immunity level for each individual is static, remaining at 0.2 for the duration of the simulation. Climate forcing from 2006, recorded at the each village's meteorological station, was repeated twenty times in order to achieve a steady state in malaria prevalence and immunity. We then conducted a twenty year simulation in each village using the dynamic immunity model described above, where individuals acquire immunity as they accumulate infectious bites and lose immunity in the absence of inoculations.

3.5 Field observations of malaria prevalence

Field measurements of malaria prevalence were made in Zindarou and Banizoumbou between December 2005 and February 2007 by Jean-Bernard Duchemin and colleagues at Centre de Recherche Médicale et Sanitaire (Yamana *et al.*, 2013). The populations of Zindarou and Banizoumbou are roughly 500 and 1000, respectively, of which approximately 20% are under the age of 5 (Niger. Bureau Central du Recensement & Niger. Ministère de l'Economie et des Finances. Sécretariat Général, 2005). Bimonthly blood samples were taken from approximately 25 children aged one to five years old in each village. Resulting blood smears were analyzed microscopically for parasite presence. Children with observed or reported fever were sent to a local health clinic for treatment in accordance to national malaria treatment guidelines. Ethical clearance was obtained from the National Ethics Committee of Niger.

3.6 Results and Discussion

This study has simulated malaria transmission in two villages, Banizoumbou and Zindarou, Niger, which are subject to nearly identical climatic conditions, but are hydrologically very different. Mosquito captures in both villages during the 2006 rainy season show that abundance in Zindarou is approximately ten times that of Banizoumbou, and other years have shown the same order-of-magnitude difference in light trap captures (Bomblies *et al.*, 2008). However, the prevalence measured in the two villages was not significantly different, despite the order of magnitude difference in mosquito abundance. For the period February 2004 – December 2006, average prevalence was 0.54, 95% CI [0.50, 0.58] in Banizoumbou and 0.56, 95% CI [0.51, 0.61] in Zindarou. Bimonthly prevalence for the year 2006 is shown for both villages in Figure 3.5. The much higher vector population of Zindarou corresponds to very similar prevalence to that of Banizoumbou. This surprising result suggests that acquired immunity resists the malaria parasite within the human population, and that the high inoculation rate in Zindarou boosts immunity such that prevalence is moderated. Our simple immunity model captured this moderating effect, as shown by comparison of model results to prevalence as determined by blood smears in village children.

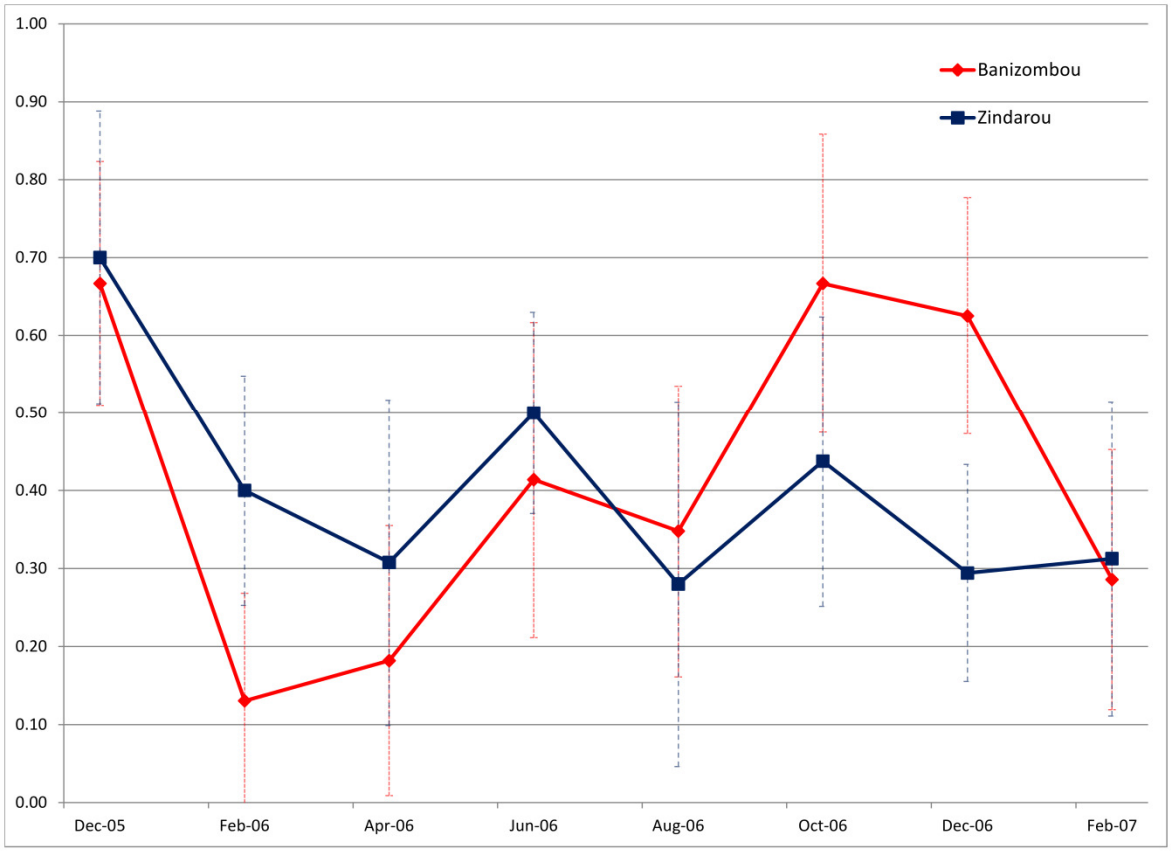

Figure 3.5 Observed prevalence in Banizoumbou (red) and Zindarou (blue), for the period December 2005 – February 2007. Error bars indicate 95% confidence intervals for each estimate.

We conducted two simulations for each village; one with static immunity where each person's immunity is set at a constant level of 0.2 throughout the simulation, and one with dynamic immunity where an individual's immunity level responds to infectious bites. Figure 3.6 shows the simulated prevalence in the static immunity simulation for the overall population (left panel) as well as for children under five (right panel). As expected, the increased mosquito activity in Zindarou led to higher rates of malaria transmission than in Banizoumbou, and as a result, the prevalence levels in Zindarou are much higher than in Banizoumbou. In both villages, there is a

strong seasonal signal in simulated prevalence, consistent with increased biting during the summer monsoon period, which peaks in mid-August in southern Niger. Because this simulation assigns the same immunity level to all human individuals regardless of their age, there is little difference in simulated prevalence between children and adults. The most notable difference is the lower minimum prevalence in children than in adults in both villages. This is the <5 age group and includes the continuous birth of malaria-free humans. Children born during the dry season are likely to remain free of infection until the following transmission season, thus lowering the average prevalence of this age group.

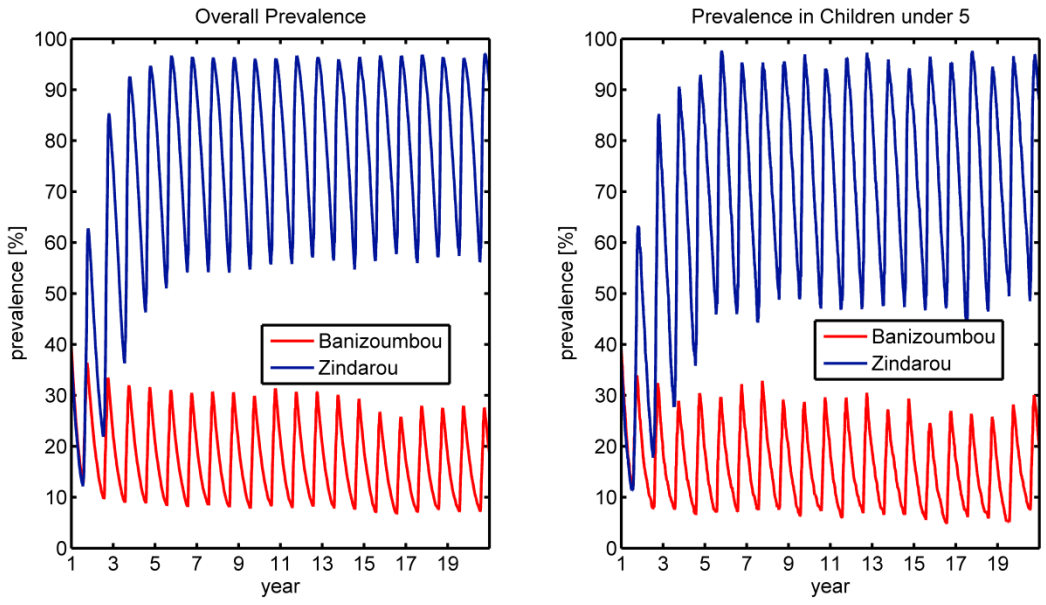

Figure 3.6 Simulated malaria prevalence using static immunity model. Banizoumbou is shown in red, and Zindarou is shown in blue. The left panel shows overall prevalence for all age groups, and the right panel shows prevalence for children under 5. In this simulation, 2006 climate forcing was repeated twenty times. The time step is years, and the cycle is annual. The peaks of each cycle correspond to late August.

In contrast to the static immunity simulations, the dynamic immunity model results in higher immunity levels in Zindarou than in Banizoumbou as a result of the greater mosquito population in Zindarou. The resulting simulated malaria prevalence for each village is shown in the left panel of Figure 3.7. Here, the difference in prevalence between the two villages is dramatically reduced. Banizoumbou has relatively low prevalence for the duration of the simulation. Zindarou initially has higher levels of prevalence, until the increased transmission raises population immunity and prevalence rates begin to decrease. The mean immunity levels in the two villages are shown in Figure 3.8. Mean immunity in both villages begins at 0.2, as individuals are given an initial value of *a* consistent with their age. In Banizoumbou, the mean immunity level decreases slightly to an equilibrium value between 0.16 and 0.18, while in Zindarou the level increases in response to greater numbers of infectious bites.

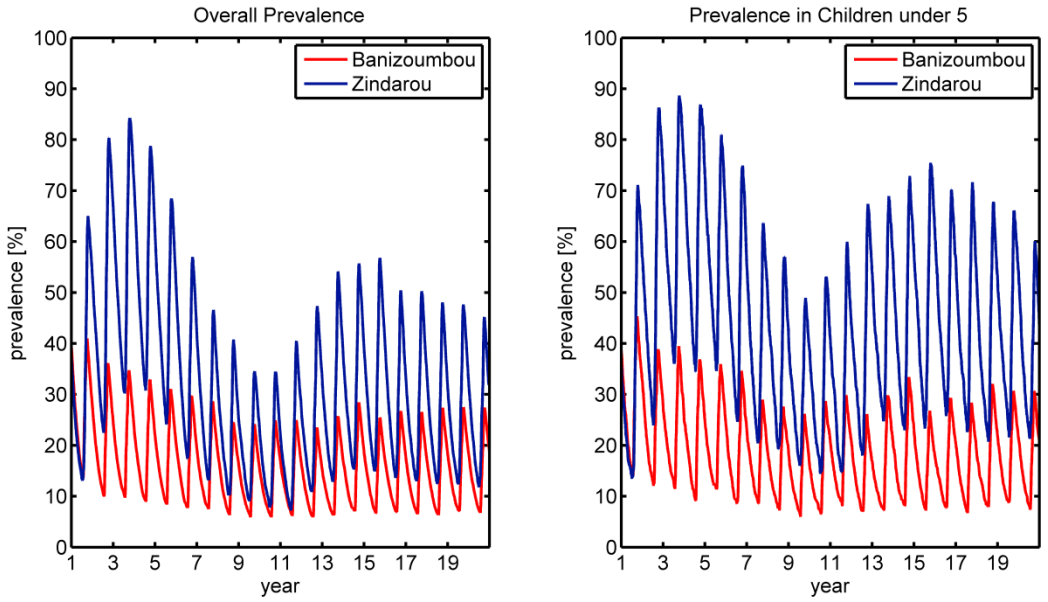

Figure 3.7 Simulated malaria prevalence using dynamic immunity model. Banizoumbou is shown in red, and Zindarou is shown in blue. The left panel shows overall prevalence for all age groups, and the right panel shows prevalence for children under 5. In this simulation, 2006

climate forcing was repeated twenty times. The time step is years, and the cycle is annual. The peaks of each cycle correspond to late August.

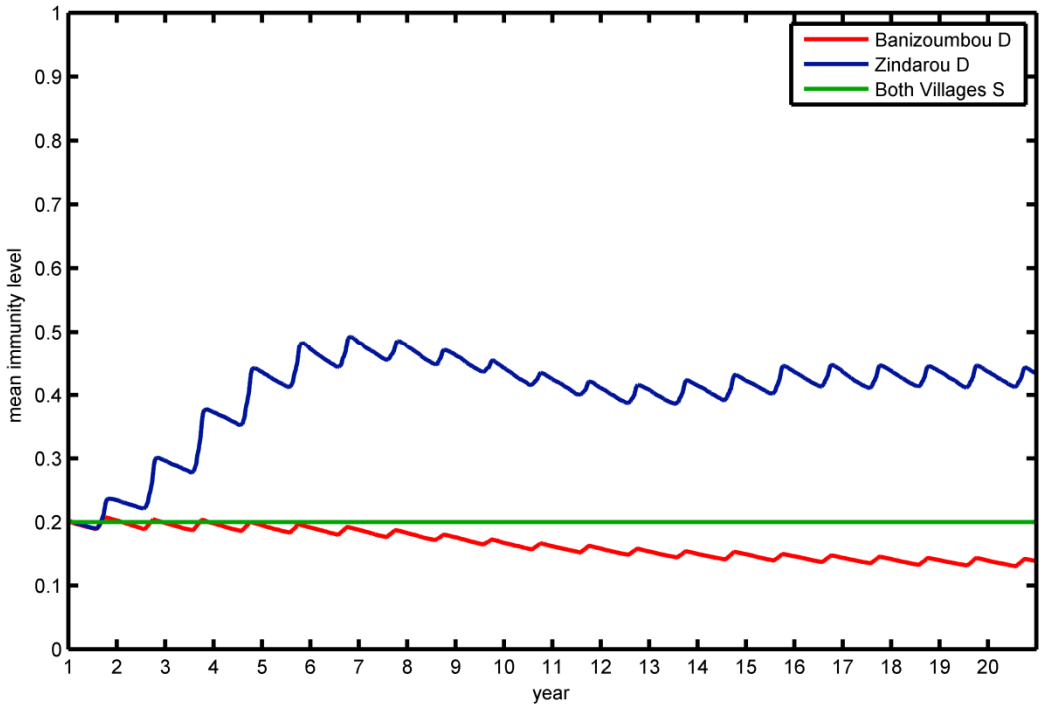

Figure 3.8 Simulated mean immunity level using the dynamic immunity model in Banizoumbou (red) and Zindarou (blue). In the simulations using static immunity, the immunity in both villages remained at 0.2 (green line) for the duration of the simulation.

We can also compare the malaria prevalence in children under five years old, shown in the right panel of Figure 3.7. In this age group, we see greater differences in prevalence between the two villages. In Banizoumbou malaria prevalence in the <5 year old group is very similar to prevalence in adults, as even adults do not have very high levels of immunity. In contrast, the higher inoculation rate in Zindarou leads to higher immunity in adults, so the prevalence in <5 year olds is higher than the general population.

The simulated prevalence levels in Zindarou were between 20% and 70%, which is consistent with the field observations of prevalence. However, the simulations in Banizoumbou underestimated prevalence, ranging from 8% in the dry season to 30% at the peak of the malaria season. As a result, our simulations show higher prevalence in Zindarou than in Banizoumbou, while field observations do now show a significant difference in prevalence between the two villages. Despite not perfectly replicating the observed prevalence in the two villages, our simulations support the hypothesis that acquired immunity to malaria dampens the difference in prevalence between the two villages that may have been expected given the difference in mosquito populations. In the static immunity simulations, the mean annual prevalence was 59 percentage points higher in Zindarou than in Banizoumbou. In the dynamic immunity simulation, the difference in prevalence between the two villages drops to 22 percentage points.

The improved ability of the model to simulate observed prevalence compared to prevalence without immunity underscores the importance of the negative feedback associated with immunity in the linkage of environmental variability and malaria. However, there are several factors that may be contributing to the difference between simulated and observed prevalence. One possible source of error is the parameterization of the entomology model. While the model properly reproduces relative differences observed in mosquitoes captured by light traps in each village (Bomblies *et al.*, 2009), it is not possible to compare the number of simulated mosquitoes to total mosquito population in the village. It is possible that both villages have more mosquitoes than are simulated under current parameterization. Another possible source of error is the parameterization of the immunity model. In our sensitivity analysis, we found that the model was most sensitive to disease clearance rate in people with no immunity (*rmin*). A longer mean duration of infection would lead to higher prevalence in both villages, especially in

Banizoumbou, where the lower immunity rates mean that the recovery rate is closer to *rmin* than in Zindarou, where higher immunity rates increase the recovery rate. While the parameter *rmin* was set to 1/220 day^{-1} based on data from immunologically naïve adults (Jeffery & Eyles, 1954), it is certainly possible that the clearance rate is different in the study population. For example, one study estimated the mean duration of infection in children 1-4 years old to be 625 days (Bekessy *et al.*, 1976). A third possible source of error is the sampling of village children for the prevalence data. Children testing positive for malaria at each bi-weekly sampling were treated with anti-malarial drugs. Because there were twice as many children in Banizoumbou compared to Zindarou, it was more likely for a child selected for testing in Zindarou to have been tested and treated in the past. Also, the relatively small sample size leads to a wide variance in prevalence estimates.

The model sensitivity analysis indicated greatest sensitivity to the value of *rmin*, with a 35% increase in prevalence when the minimum recovery rate was decreased by 10%. The duration of infection is important in sustaining malaria transmission in areas with low and highly seasonal transmission (Gu & Novak, 2005). Long infections carry the parasite over from one transmission season to the next. The sensitivity analysis showed low sensitivity to other parameter values, with no perturbation leading to more than 6% change in mean prevalence. Results of the sensitivity analysis are shown in Figure 3.9 and Table 3.1.

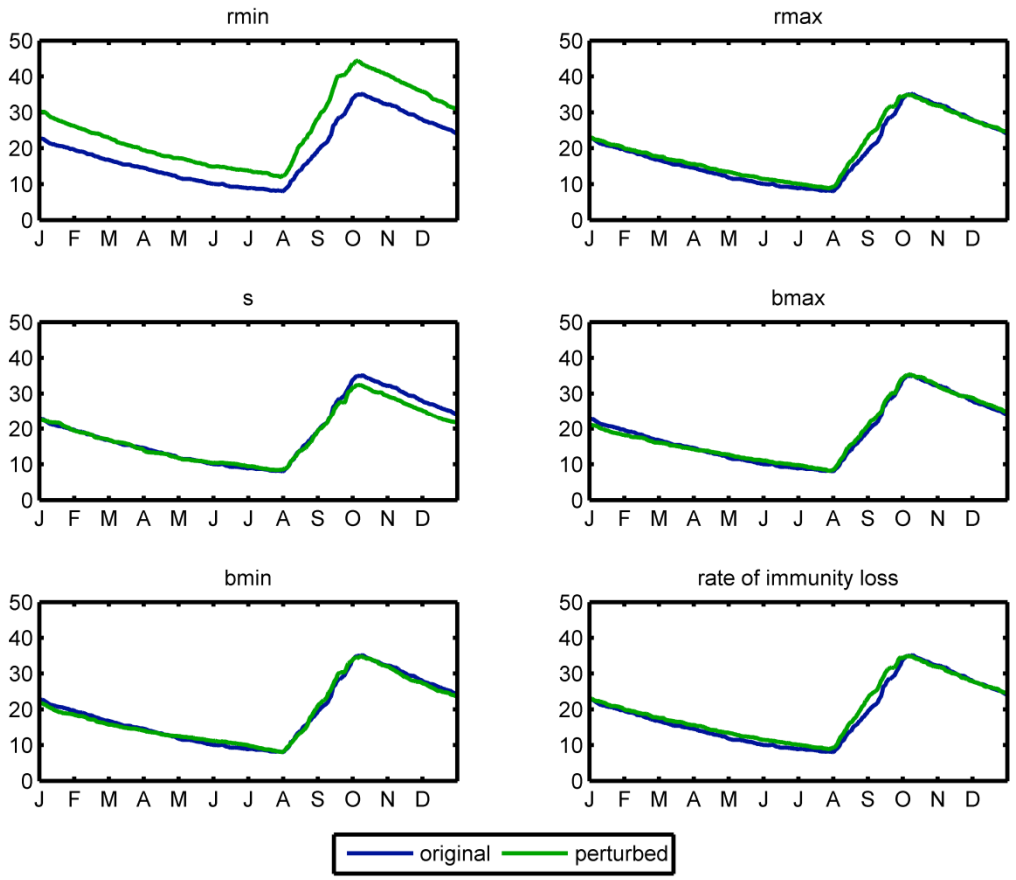

Figure 3.9 Sensitivity of model results to parameter values. Each parameter was decreased by 10%. Prevalence in Banizoumbou after 10 years of simulation under original parameterization (blue) and perturbed parameter (green) are shown.

The combined model we presented here, which includes a simple representation of acquired immunity, completes a mechanistic modeling linkage between hydrological variability and village-scale malaria dynamics. While malaria models incorporating immunity are not new, the presented model has a novel structure that allows the spatially- and temporally-varying environmental controls of mosquito population dynamics to determine prevalence as well as variability in protective immunity of the population. This is the only model to our knowledge

that provides an explicit link from environmental inputs to malaria prevalence through modelling hydrological, entomological and immunological processes.

While the simulation of overall village prevalence shown in this study could have been achieved using one of the many existing compartmental models of malaria transmission (Águas *et al.*, 2008; Aron, 1988; Chitnis *et al.*, 2008; Chiyaka *et al.*, 2007; Dietz *et al.*, 1974; Filipe *et al.*, 2007; Yang, 2000) driven by the time-series of mosquito biting rates simulated by HYDREMATS, we developed an individual-based model in order to provide a framework for using spatially-explicit individual based models to link environmental variability to malaria transmission in human populations, with the ultimate goal of simulating the impact of environmental changes (changes in regional climate, climate variability and land use) on malaria transmission in human populations at the village scale. By maintaining the spatial relationships between larval habitat and human population, we can simulate the effects of heterogeneous biting rates within communities (Kreuels *et al.*, 2008; Machault *et al.*, 2011). It also allows better environmental management by targeting water pools; pooled water some distance from a village will host far fewer subadult mosquitoes than pooled water close to the village or within the village itself because the proximity of pools to human hosts makes them much more easily accessible to ovipositing female mosquitoes and hence more likely to be utilized for breeding. By tracking the past exposure of each individual human, the individual-based approach provides a more realistic representation of the processes of malaria transmission than compartmental models.

The moderating effect of immunity on malaria prevalence has been shown by others. Dietz *et al.* (Dietz *et al.*, 1974) compared two Nigerian villages and found that despite significant differences in vectorial capacity there were only modest differences in malaria prevalence. This information

was used in developing the immunity and superinfection aspects of their malaria transmission model. An entomological and parasitological survey in The Gambia found a negative correlation between vector abundance and malaria prevalence, suggesting substantial differences in immunity between neighboring villages (C. Thomas & Lindsay, 2000). Macdonald (Macdonald, 1955) also emphasized the importance of acquired immunity in regulating malaria transmission in the context of field observations and modeling results, and cautioned against incomplete anti-malaria interventions that weaken a population's immunity, an effect that is now called rebound malaria and has been observed following interventions (Menendez *et al.*, 1997; Mockenhaupt *et al.*, 2007; Trape *et al.*, 2011). Our results are consistent with observations that large differences in EIR do not necessarily lead to changes in prevalence (Beier *et al.*, 1999).

When simulating malaria transmission in a village, it is useful to report simulated malaria prevalence as this is a common metric for field observations that can be compared with simulation results. However, our study shows that the acquired immunity level maybe a more useful metric in assessing the vulnerability of a village to malaria epidemics resulting from climate variability. In Zindarou, higher levels of mosquito populations led to more inoculations and higher immunity levels compared to Banizoumbou. If this region were to experience anomalously wet climate conditions that increases mosquito populations in both villages, we would expect a smaller increase in prevalence in Zindarou than in Banizoumbou, due to differences in the immunity level.

Acquired immunity is expected to play important role in shaping the effects of climate change on malaria transmission. If a population's immunity level is at an equilibrium value due to the vectorial capacity allowed by the current climate, changes in climate would disrupt this equilibrium until a new equilibrium is reached. This is especially of concern in areas where

vectorial capacity and EIR is currently low and as a result the population's immunity is weak; increased EIR could lead to major increases in malaria prevalence in these vulnerable populations.

3.7 Conclusion

A simple representation of malaria transmission and the acquired immunity to malaria was developed and embedded in an agent-based model of host-vector-parasite interactions surrounding two villages in Niger, allowing us to simulate prevalence in the two villages, and to observe the effects of acquired immunity. Although the simulated prevalence does not exactly match observations, it does show how acquired immunity dampens the effect of increased biting. Without the effects of immunity, Zindarou would have much higher prevalence than Banizoumbou. However, when we include the effect of immunity, prevalence in Zindarou significantly decreases and approaches Banizoumbou levels. This moderating effect of acquired immunity is consistent with field observations showing similar levels of malaria prevalence between the villages despite the observed differences in hydrological conditions and vector abundance. The modeling results suggest that the risk of malaria transmission in the community depends in part on the level of acquired immunity, which is determined by the hydrologically driven mosquito abundance over previous years. Higher levels of exposure to infectious bites in wet Zindarou leads to higher levels of immunity, providing villagers with greater protection from malaria epidemics associated with climate anomalies such as unusually wet years than those in dry Banizoumbou.

4 Projected Impacts of Climate Change on Environmental Suitability for Malaria Transmission in West Africa

4.1 Introduction

The response of malaria transmission to climate change has been the subject of research and intense debate since the mid-1990s, and has been investigated using both biological/mechanistic models and statistical models (Parham & Michael, 2009; Rogers & Randolph, 2000). While early studies reported predictions of a wide-spread increase in malaria transmission (P. Martens *et al.*, 1999; W. Martens *et al.*, 1995; Martin & Lefebvre, 1995; Tanser *et al.*, 2003), more recent studies suggest a shift in distribution rather than a large net increase (Ermert *et al.*, 2012; Lafferty, 2009; C. J. Thomas *et al.*, 2004).

Previous studies on this topic in West Africa have been limited by the relatively crude representation of processes dependent on rainfall in malaria models, as well as the great uncertainty in climate change projections in this region. While the relationships between temperature and malaria transmission are relatively well understood, modelling methods that have been used up to now to estimate the effect of climate change on malaria transmission are limited in their ability to address the effects of changes in rainfall. The primary malaria vectors in Africa, *Anopheles gambiae sensu lato* and *Anopheles funestus,* breed primarily in pools of water formed from rainfall. Few malaria models attempt to model the causal relationships between rainfall and mosquito breeding sites, relying instead on rules for minimum threshold values of rainfall required for malaria transmission to occur (Craig *et al.*, 1999; P. Martens *et al.*, 1999), with some models including an upper threshold of rainfall above which additional rainfall

is assumed to decrease mosquito density (Parham & Michael, 2009). Shaman et al. (2002) and Porphyre et al. (2005) use hydrological models link rainfall to the abundance of Culex and Aedes mosquitoes, which breed in floodwaters and serve as the primary vectors for several arboviruses. Montosi et al. (2012) use an ecohydrological model as well as a simplified linear model to calculate soil water content, which is then used to model malaria incidence. The processes by which rainfall is diverted into pools suitable for anopheles breeding are strongly dependent on the frequency, intensity and duration of rainfall events, as well as site-specific topographical features, soil characteristics and vegetation cover. The persistence of these pools depend on evaporation and infiltration rates; pools that dry out before adult mosquitoes emerge from eggs are not viable breeding sites.

Here, we bridge the gap between rainfall and corresponding mosquito abundances using the Hydrology, Entomology and Malaria Transmission Simulator (HYDREMATS) (Bomblies *et al.*, 2008). By mechanistically translating rainfall into water pools, we are able to simulate the effects of projected changes in climate on malaria transmission in West Africa. In addition, we address the high uncertainty of climate predictions in this region by estimating the impact of changes in rainfall over the full range predicted by current climate models.

4.2 Methods

4.2.1 Study area

The climate of West Africa is distinctively characterized by strong north to south gradients in both temperature and rainfall, shown in Figure 4.1 A-B. The climate is highly seasonal, dominated by the West African monsoon. We focus on the region bounded by 4^{o}N and 21.5^{o}N, and 18^{o}W and 16^{o}E, which we divide into 5 sub-regions (Zones 1 through 5 in Figure 4.1),

corresponding roughly to the following ecoclimate zones, respectively: Sahelo-Sahara, Sahel, Soudan, Soudano-Guinean, and Guinea Coast (Nicholson, 1993).

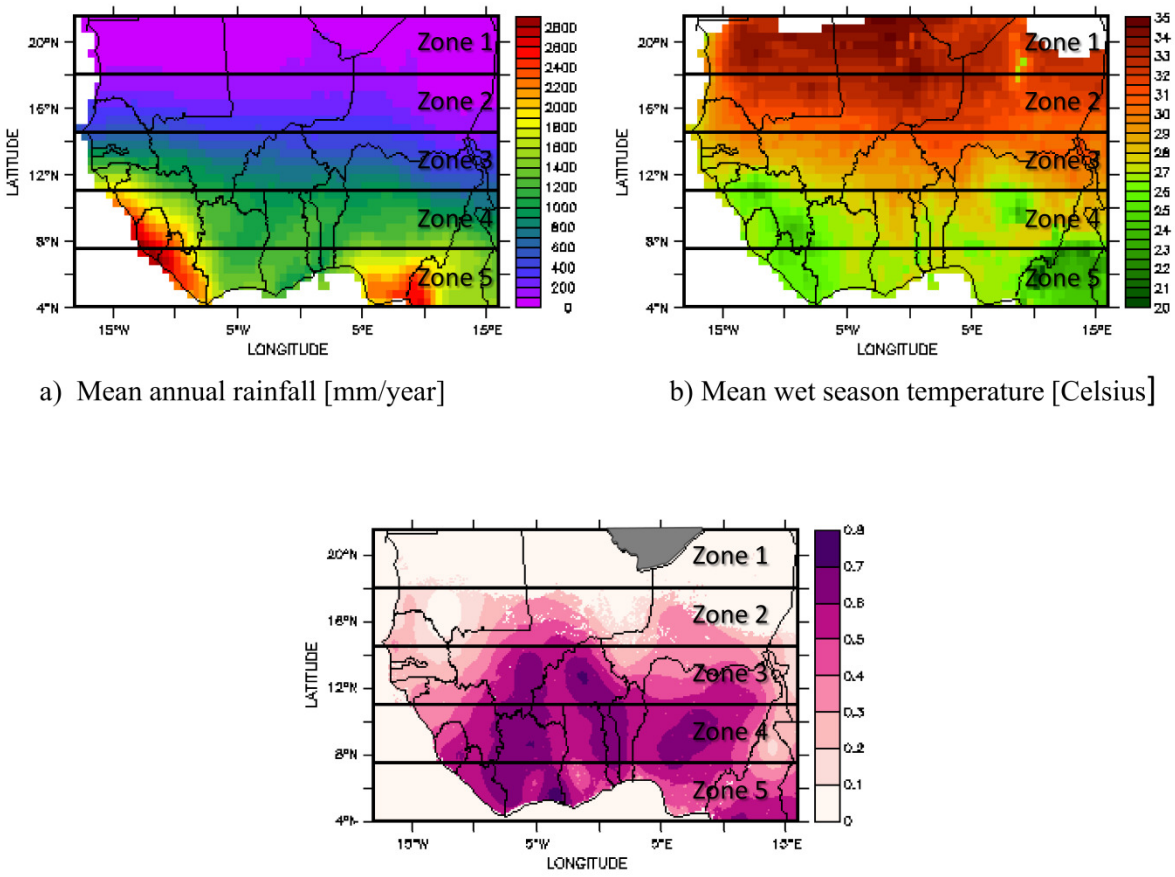

a) Mean annual rainfall [mm/year]

b) Mean wet season temperature [Celsius]

c) Mean parasite rate in children aged 2-10 in 2007

Figure 4.1 Baseline climate and malaria transmission conditions in West Africa. Zones 1-5 correspond roughly to the following ecoclimate zones, respectively: Sahelo-Sahara, Sahel, Soudan, Soudano-Guinean, and Guinea Coast (Nicholson, 1993). (A) mean annual rainfall in mm/year from CRU, 1980-1999 (Mitchell & Jones, 2005). (B) mean surface air temperature during the wet season from CRU, 1980-1999 (Mitchell & Jones, 2005). (C) Mean parasite rate in children aged 2-10 in 2007 estimated by Malaria Atlas Project (Hay *et al.*, 2009). White areas over land indicate unstable malaria transmission, and the grey area in Zone 1 indicates no malaria risk.

The baseline period for this study was 1980-1999, in keeping with the Intergovernmental Panel on Climate Change's Fourth Assessment Report (IPCC AR4) (Solomon *et al.*, 2007). The mean annual rainfall and wet-season temperature for each Zone were calculated for the baseline period using standard climate data from Climatic Research Unit time-series version 3.1 (CRU) data (Mitchell & Jones, 2005) and are shown in Table 4.1.

Table 4.1: Characteristics of the study zones.

	Ecoclimate zone[1]	**Annual rainfall 1980-1999 (mm)**[2]	**Mean wet season temperature 1980-1999 (^{o}C)**[2]	**Malaria transmission class 2007**[3]
Zone 1	Sahelo-Sahara	52	32.2	Unstable
Zone 2	Sahel	223	31.3	Unstable / moderate stable
Zone 3	Soudan	715	28.9	Moderate / intense
Zone 4	Soudano-Guinea	1286	26.8	Moderate / intense
Zone 5	Guinea Coast	1743	25.7	Intense

[1](Nicholson, 1993)

[2](Mitchell & Jones, 2005)

[3]Malaria endemicity class based on criteria outlined in (Hay et al. 2008) and calculated from mean parasite rate in children aged 2-10 in 2007 estimated by Malaria Atlas Project (Hay *et al.*, 2009)

We focus on this region because of its significant malaria burden. The spatial distribution of parasite rate in children aged 2 to 10 in 2007 estimated by the Malaria Atlas Project (Hay *et al.*, 2009) indicates that malaria burden increases roughly from north to south (Figure 4.1 C). Using the malaria endemicity classification proposed by Hay et al. (2008), Zone 1 experiences unstable transmission, Zone 2 is divided roughly equally between unstable and moderate stable transmission, Zone 3 is a mixture of moderate and intense stable transmission, and Zones 4 and 5 are primarily areas of intense transmission (Table 4.1). Malaria transmission in regions where transmission is classified as unstable is especially sensitive to effects of climate on vectorial capacity because human populations in these areas have little or no acquired immunity, and the infrastructure for malaria control is likely to be limited.

4.2.2 Design of numerical simulations: Baseline climate

The first step in estimating the potential impacts of climate change on environmental suitability for malaria transmission was to establish vectorial capacity under baseline conditions using HYDREMATS and current climate data. HYDREMATS is a fine resolution model that runs on the village scale. While this resolution allows us to simulate the details of mosquito breeding and malaria transmission, its high computational cost precludes the simulation of large geographic areas. However, West Africa is well known for its pronounced north-south climate gradient (Figure 4.1), whereas climate conditions are relatively constant moving from east to west (Eltahir & Gong, 1996; Nicholson, 1993). We therefore approximated the *VC* for each Zone by simulating conditions for a single hypothetical village with climate conditions that are representative of that Zone. We conducted a seven-year simulation at each of the five representative locations under baseline climate conditions.

4.2.2.1 Data used for current climate simulations

Environmental data sources used in the current climate simulations are summarized in

Table 4.2. The CRU data set and other monthly precipitation data available for 1980-1999, the baseline period, are of insufficient temporal resolution to be used with HYDREMATS, which requires as an input a rainfall series with an hourly resolution. To represent the role of fine scale variability of rainfall in the process of formation of breeding pools, we therefore disaggregated the CRU data into an hourly rainfall time series.

The spatio-temporal dissagregation of rainfall for hydrological applications is a well researched problem, and is often done using various statistical models parameterized by assumed or observed characteristics of finer scale rainfall events (Bo *et al.*, 1994; Mackay *et al.*, 2001; Margulis & Entekhabi, 2001; Segond *et al.*, 2007). Here, we take advantage of high resolution satellite observations of rainfall from the Climate Prediction Center Morphing Technique (CMORPH) data set, which gives ~8km resolution rainfall data every 30 minutes (Joyce *et al.*, 2004). After applying the bias-correction described in Yamana and Eltahir (2011), we use the hourly rainfall observations from CMORPH data at each village to disaggregate baseline CRU rainfall into realistic storm events. A bias correction factor was calculated for each location by comparing annual averages of University of East Anglia's CRU TS 3.1 high resolution gridded data set (Mitchell & Jones, 2005) to the corresponding CMORPH data, between 2003-2009, which is the period during which the two data sets overlap.

The hourly rainfall series were calculated using the following correction:

$$Rain(t,x,y) = CMORPH_{raw}(t,x,y) \ * \ \frac{CRU_{2003-2009}\,(x,y)}{CMORPH_{2003-2009}(x,y)} \qquad (4.1)$$

where $CRU_{2003\text{-}2009}$(x,y) and $CMORPH_{2003\text{-}2009}$ (x,y) are the mean annual rainfall from CRU and CMORPH respectively between 2003-2009 for each grid cell. The result is an hourly rainfall time series with mean annual rainfall equal to long-term observations from CRU, and patterns of hourly rainfall observations from CMORPH.

Temperature, wind speed, wind direction, and radiation data were taken from the ERA Interim data set (Dee *et al.*, 2011) for the grid cell containing each village being simulated; we assume uniform conditions within the 0.75 degree ERA grid cell. ERA Interim data were adjusted for HYDREMATS as follows. Wind speed was brought from 10 m to 2 m using the logarithmic wind profile for neutral atmospheric conditions (De Bruin & Moore, 1985):

$$u(z) = \frac{u^*}{k} \ln\left(\frac{z-d}{z_0}\right) \qquad (4.2)$$

Where $u(z)$ is the horizontal wind velocity at height z above ground, u^* is the friction velocity, k is Von Karmen's constant (≈0.41), d is the zero plane displacement height and z_0 is the roughness length. Assuming the dominant vegetation surrounding villages is cropland with height of approximately 1.5 meters, d is approximately 1.1 meters and z_0 is around 0.15 meters. The friction velocity is approximated using the wind speed at 10 meters given by ERA Interim:

$$u^* = \frac{u_{10}k}{\ln\left(\frac{10-d}{z_0}\right)} \qquad (4.3)$$

Table 4.2 Summary of data sources

	Data source	Spatial resolution	Temporal resolution	Reference
Baseline Climatology				
temperature	CRU TS 3.1	0.5 x 0.5 degree	1 month	Mitchell and Jones, 2005
rainfall	CRU TS 3.1	0.5 x 0.5 degree	1 month	Mitchell and Jones, 2005
Meteorological Inputs for HYDREMATS Simulation				
precipitation	CMORPH	~8km	30 min	Joyce et al., 2004
temperature	ERA-Interim	.75 x .75 degree	3 hour	Dee et al., 2011
wind speed	ERA-Interim	.75 x .75 degree	3 hour	Dee et al., 2011
wind direction	ERA-Interim	.75 x .75 degree	3 hour	Dee et al., 2011
surface radiation	ERA-Interim	.75 x .75 degree	3 hour	Dee et al., 2011
Other HYDREMATS inputs				
soil type	HWSD	~1km		FAO, 2009
vegetation	UMD landcover	1km		Hansen et al., 2000
topography	Computed from Envisat synthetic aperture radar and ground survey	10 m		Toutin and Gray, 2000; Bomblies et al. 2008
household locations	Quickbird image	0.6 m		Bomblies et al. 2008
Climate predictions				
Rainfall and temperature anomalies 2080-2099	Various climate models (See Table 2) from IPCC AR4 emissions scenario A1B	Range from 1.4 x 1.4 degree to 3.9 x 3.9 degree	1 month	IPCC, 2011

Wind and radiation data were linearly extrapolated from the 3-hour resolution provided by ERA to the 1-hour resolution required by HYDREMATS.

A comparison of the diurnal temperature cycles given by ERA Interim and ground observations at three locations across ecoclimate zones in our study region (Banizoumbou, Niger; Agoufou, Mali; and Djougou, Benin) indicated that while the reanalysis data gave good estimates of the daily mean temperature, the diurnal range was underestimated. The regression coefficients below were calculated using the diurnal temperature ranges of the three ground stations over one year and applied to daily ERA temperature ranges:

$$R_{corrected} = R_{ERA} \times 1.03 + 5.25\text{C}° \quad (4.4)$$

The maximum and minimum daily temperatures were then computed as the daily temperature mean from ERA plus or minus the corrected range divided by two. The hourly temperature was calculated assuming a sinusoidal curve during daylight hours and an exponential decrease between sunset and sunrise, as described in Paaijmans et al.(2009)

The dominant vegetation type at each location was obtained from the University of Maryland Land Cover Classification (Hansen *et al.*, 2000). Soil properties were taken from the Harmonized World Soil Database (Nachtergaele & Batjes, 2012). A thin layer of low-permeability soil is included in the model to account for soil crusting that occurs throughout West Africa under cultivated conditions (Morin, 1993). Water pools are lined with a clayey soil that slows infiltration (Desconnets *et al.*, 1997). We assumed typical topographical conditions and household locations as observed in Banizoumbou, Niger (Bomblies et al. 2008) that were held constant among Zones.

4.2.3 Design of numerical simulations: Future climate

After establishing baseline conditions, we repeated the simulations using future climate projections as inputs to HYDREMATS. We considered the entire range of predictions from the 19 General Circulation Models (GCMs) contributing to the A1B emissions scenario of the IPCC's 4th Assessment report (Solomon *et al.*, 2007). This scenario describes a future characterized by rapid economic growth, decreased heterogeneity among nations through increased interactions, capacity building and cooperation, and a balance between fossil fuel and alternative energy sources (Solomon *et al.*, 2007). The models differ greatly in their predictions of future climate in West Africa. This disagreement implies that at least some of the GCMs are substantially flawed in their representation of the climate in this region (Christensen *et al.*, 2007; Cook & Vizy, 2006). Therefore, we conducted a preliminary analysis to identify the GCMs that would maximize and minimize vectorial capacity in each Zone during 2080-2099, under the assumption that the true outcome will fall within the bounds set by these extreme scenarios. As discussed in detail in Section 4.3.1, we determined that the GCMs resulting in the wettest and driest climate projections would produce the maximum and minimum estimates of vectorial capacity (*VC,* given by Equation 1.1), respectively.

We conducted four simulations of future *VC* for each Zone. First, to highlight the impact of changes in rainfall, we simulated the predicted changes in rainfall only, while keeping baseline values of temperature and all other variables. Two 7-year simulations were conducted for each region, one using the driest outcome predicted by the models and one using the wettest outcome (referred to as dry and wet simulations, respectively). Next, to assess the combined impact of increased temperature and changing rainfall, we repeated the simulations with predicted

temperature increases included in addition to changes in precipitation (dry-hot and wet-warm simulations, respectively).

4.2.3.1 Data used for future climate simulations

Projected changes in rainfall and temperature between the baseline period (1980-1999) and the future (2080-2099) are provided by the GCM outputs. We assume that climate change will take the form of shifts in the north-south rainfall gradient, consistent with historical changes in rainfall regimes in this region (Bomblies & Eltahir, 2010; Irizarry-Ortiz *et al.*, 2003). The 2080-2099 precipitation time series were created by selecting a location directly north (for decreased rainfall scenarios) or south (for increased rainfall scenarios) of the representative village in each zone where the current rainfall is equal to the annual rainfall predicted by a GCM for 2080-2099, and disaggregating using CMORPH. For example, the village selected to represent Zone 2 is located at 15.05N, 8.33E, where the baseline rainfall is 259 mm/year. Applying the predicted changes from the GCMs, the dry scenario should have an average rainfall of 53 mm/year and the wet scenario should have an average rainfall of 366 mm/year. The rainfall time series for the wet scenario comes from a location south of our village, at 14.25N, 8.33E where current rainfall averages approximately 366 mm/year. Rainfall inputs for the dry scenario come from a location north of our village at 19.25N, 8.33E where current rainfall averages 54 mm/year. We again disaggregate the coarse resolution rainfall data by applying the hourly patterns of rainfall observed by CMORPH.

The increase in temperature for each zone was represented by adding the mean wet-season temperature increase of the GCM grid cell containing each village to each hourly data point used in the simulation of baseline climate. The remaining model inputs were not changed.

4.3 Results

4.3.1 Analysis of climate predictions from GCMs

Before conducting our numerical simulations, we analyzed GCM outputs to identify the predictions that would maximize and minimize *VC*. The uncertainty for predicted rainfall is much greater than for predicted temperature; while all of the models predict a temperature increase between 2 and 6°C, the predicted changes in rainfall differ in even their sign, and range from a decline of 400% to an increase of 260% (Figure 4.2). The wide range of possible rainfall outcomes underscores the importance of considering changes in rainfall when assessing future climates.

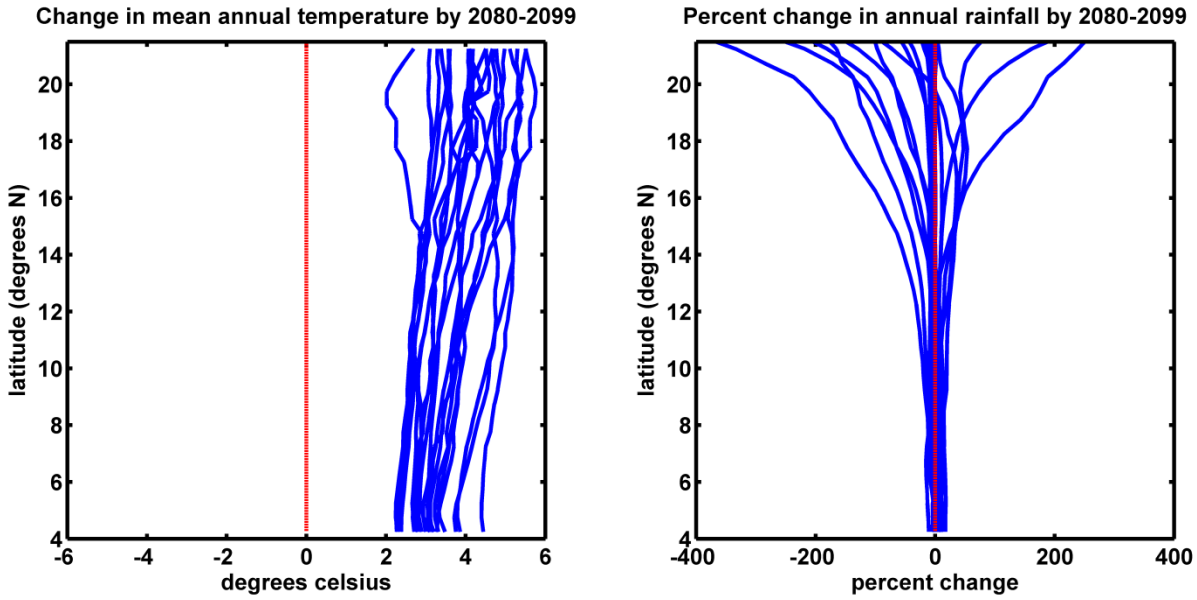

Figure 4.2 Predicted changes in temperature and rainfall, zonally averaged for each model. Each blue line is the zonally averaged change in temperature (left) and rainfall (right) predicted between the baseline period (1980-1999) and 2080-2099 by a single SRES A1B GCM, averaged zonally over land points between 18°W and 16°E.

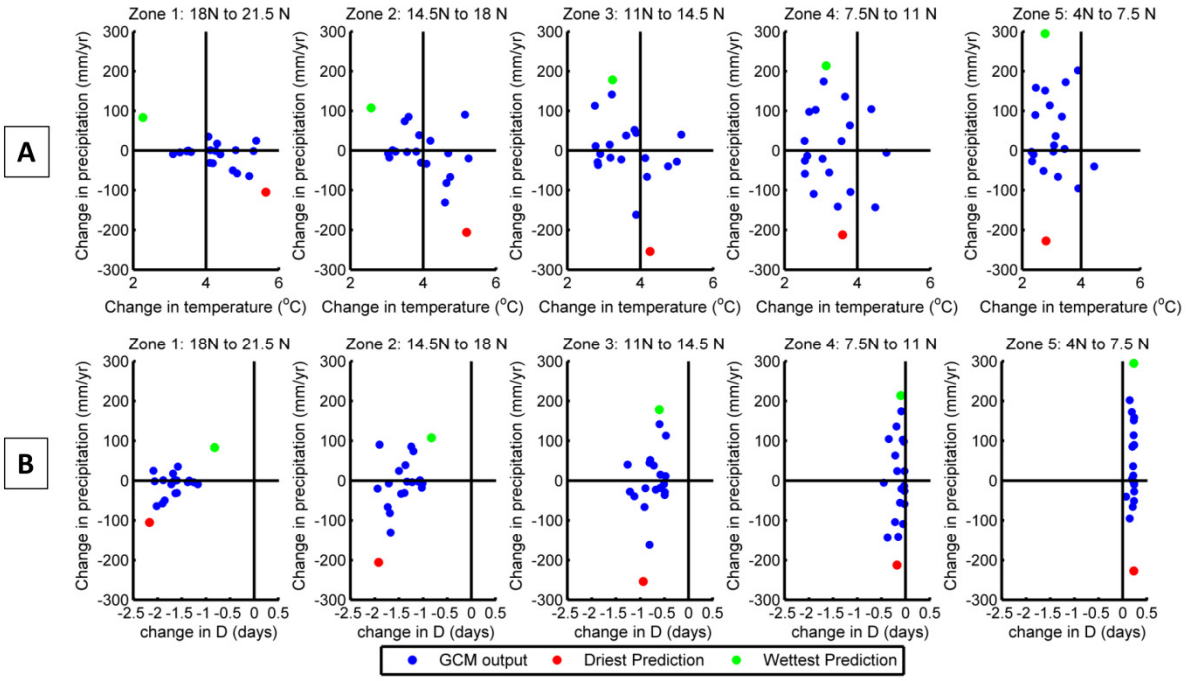

Figure 4.3 GCM predictions for changes in temperature, precipitation, and expectation of infective life. Each point represents the change in temperature and precipitation (A), or the change in the expectation of infective life (*D*, in days) and precipitation (B), predicted by each IPCC AR4 GCM.

The mean change in temperature and precipitation predicted by each GCM is shown in Figure 4.3 A. In Zones 1-3, which are currently drier and warmer than is optimal for malaria transmission, the conditions that would maximize *VC* would be the wettest and coolest prediction, whereas the driest and hottest prediction would minimize *VC*. In these regions, increases in precipitation are associated with less warming, as a wetter climate would lead to more evaporative cooling, counteracting some of the warming caused by greenhouse gasses. Similarly, decreases in precipitation are associated with greater warming. This association is less pronounced in Zones 4 and 5 as the relative change in precipitation is much smaller, thus

decreasing the impact of the change in evaporative cooling. The changes in the expectation of infective life, *D*, calculated from the predicted changes in temperature from each GCM are shown in Figure 4.3 A. In Zones 1 and 2, the wettest prediction also has the smallest decrease in *D*, and the driest prediction corresponds to the greatest decrease in *D*. In Zones 3, 4 and 5, we assume that the wettest and driest predictions will result in the highest and lowest predictions for vectorial capacity, respectively, as the percent change in precipitation between predictions varies more than the percent change in *D* caused by increased temperature. The projected changes in rainfall and temperature corresponding to the two extreme future climate change scenarios for each zone are summarized in Table 4.3. We did not investigate the accuracy of the climate models, but instead selected the most extreme predictions of climate change assuming that resulting simulations would indicate the upper and lower bounds of potential changes in vectorial capacity.

Table 4.3 Changes predicted between 1980-1999 and 2080-2099 by the wettest and driest GCMs for each zone.

	Wettest prediction			**Driest prediction**		
Zone	GCM[1]	Change in rainfall (mm)	Increase in rainy season temperature (^{o}C)	GCM	Change in rainfall (mm)	Increase in rainy season temperature (^{o}C)
1	NCAR	83	2.3	GFDL/NOAA	-105	5.6
2	NCAR	107	2.6	GFDL/NOAA	-206	5.2
3	ECHAM + HOPEG	178	3.2	GFDL/NOAA	-254	4.3
4	ECHAM + HOPEG	214	3.1	GFDL/NOAA	-212	3.6
5	NASA/GISS E-H	295	2.8	University of Tokyo – MIROC med-res	-227	2.8

[1](Solomon *et al.*, 2007)

4.3.2 Simulation results using HYDREMATS

The results of the simulations were analyzed in terms of the components of the equation for vectorial capacity. Projections of weekly average values over the representative seven-year simulation are shown in Figure 4.4 for simulations that accounted for changing rainfall only, and in Figure 4.5 for the simulations changing rainfall and temperature. Figure 4.6 shows the estimated percent change in *D*, *m*, and *VC* averaged over the length of the simulation for each zone.

4.3.2.1 Expected duration of mosquito infectivity

In the case of changing rainfall only, *D*, the estimated duration of mosquito infectivity, does not change, as it depends only on temperature. When we also simulate rising temperatures, *D* increases in Zones 4 and 5 because the temperature in these areas at baseline (1980-1999) is below the optimal temperature for transmission (Figure 4.5, column 1). The relative changes in *D* in Zones 1, 2 and 3 are highly seasonal (Figure 4.5). During the rainy summer months when malaria transmission can occur, the simulated temperature exceeds optimal levels for mosquito survival, resulting in a decrease in *D* and *VC*.

4.3.2.2 Mosquito density

In general, our simulations predict that increased rainfall will lead to more mosquitoes, although the magnitude of the change varies by region (Figure 4.4). Relative to baseline values, the greatest predicted increase in *m*, the number of female mosquitoes per human, occurs in Zone 1, where increased rainfall leads to greater persistence of water pools, and in Zone 4, where the earlier onset of the rainy season leads to higher peak values of mosquito populations. When rainfall is predicted to decrease, mosquito populations in all five zones decrease substantially from baseline values, particularly in Zones 1 and 2, which become too dry to sustain mosquito life, and Zone 3.

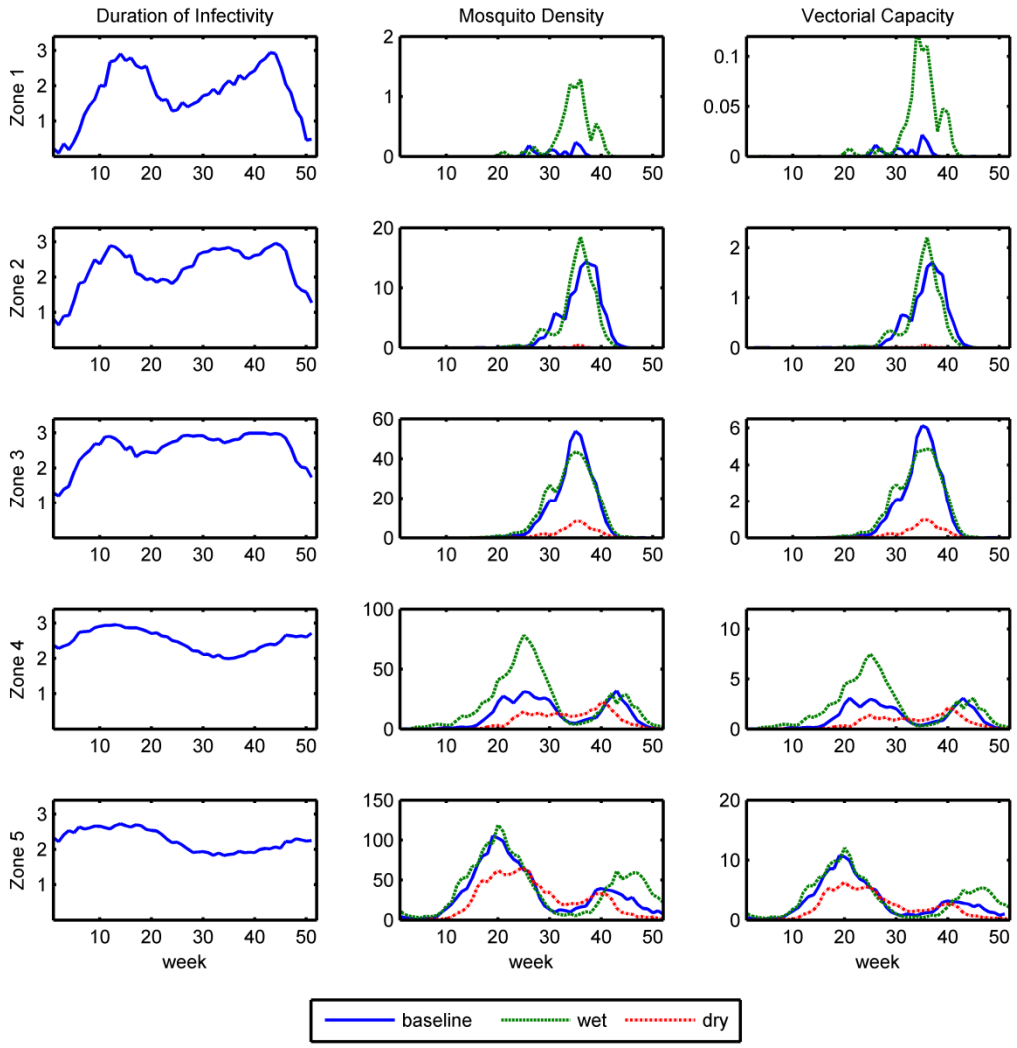

Figure 4.4 Simulated effect of changing rainfall predictions on D, m, and VC. Weekly average values based on simulations for D (the duration of infective life, column 1, in days), m (mosquito density, column 2, the number of mosquitoes per human), and VC (vectorial capacity, column 3, the average number of human inoculations of a parasite originating from a single case of malaria if all vectors biting the original case became infected) as a result of changes in rainfall only, from Zone 1 (top row) through Zone 5 (bottom row). Simulation-based estimates at baseline (1980-1999) and for 2080-2099 according to the wet and dry climate change scenarios for each zone are shown in blue, green, and red, respectively. D does not change between simulations because temperature is held constant.

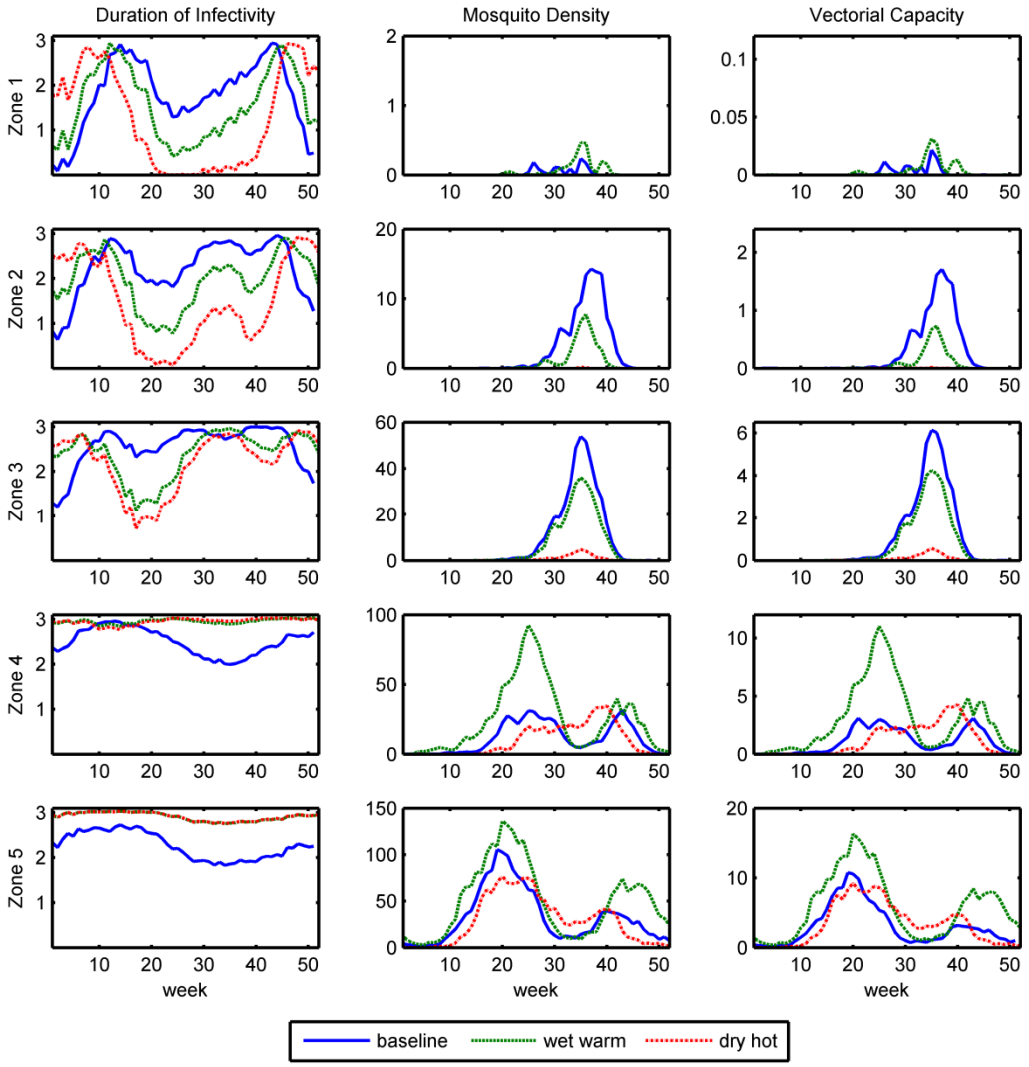

Figure 4.5 Simulated effect of changing rainfall and temperature predictions on D, m, and VC. Infective life (*D*, in days), mosquito density (*m*, the number of female mosquitoes per human), and vectorial capacity (*VC*), from Zone 1 (top row) through Zone 5 (bottom row). Weekly averages for baseline simulations (1980–1999) are shown in blue, and weekly averages based on wet-warm and dry-hot simulations for 2080–2099 are shown in green and red, respectively.

In many cases, the changes in *m* from baseline values predicted by simulations where only rainfall was changed (Figure 4.4) and simulations where both rainfall and temperature were changed (Figure 4.5) is small, as *m* depends primarily on rainfall. The potential impact of rising temperatures on mosquito density is more apparent in Figure 4.6, where we see that with increased rainfall and warming (wet-warm simulation), the overall effect on Zones 1, 4 and 5 is an increase in *m*; however in Zones 2 and 3, there is a net decrease in *m*. With warming and decreased rainfall (dry-hot simulation), high temperatures in Zones 1-3 amplify the estimated effect of decreased rainfall, further decreasing *m*. In Zones 4 and 5, the high temperatures reduce the estimated effect of decreased rainfall, leading to a smaller net reduction in *m*.

We use HYDREMATS to calculate the mosquito density, *m*, which is a function of the number of humans and the total number of mosquitoes. In general, the mosquito population in the village can be described by three different variables: total number of real mosquitoes in the village, total number of simulated mosquitoes in the model, and sampled real mosquitoes in discrete locations captured by light traps. It is not possible to observe the total number of real mosquitoes in the village in order to compare it with the total number of simulated mosquitoes. However, HYDREMATS has been shown to simulate a total number of mosquitoes that mimics the relative differences observed in mosquitoes captured by light traps between wet and dry years (Bomblies et al. 2008) and under different hydrological conditions (Bomblies et al. 2009).

We hold the number of humans and the configuration of residences constant among villages now and in the future, an assumption that affects *m*. This assumption allows us to isolate the impact of climate change on vectorial capacity while neglecting the potential impacts of the human population variability and change in space and time.

4.3.2.3 Vectorial capacity

As with the density of mosquitoes, in many cases accounting for changes in temperature, in addition to precipitation (i.e., in the wet-warm and dry-hot simulations, Figure 4.5) had a relatively small impact on *VC* (Figure 4.4), which highlights the importance of rainfall in assessing future *VC*. In the wet-warm scenario (Figure 4.6 top panel), there is an overall increase in *VC* in Zones 1, 4, and 5. In contrast, there is little change in *VC* from baseline in Zones 2 and 3 because the positive effect of increased rainfall on mosquito density is offset by negative effects of higher temperatures on both density and the duration of infectivity. In the dry-hot simulations (Figure 4.6 bottom panel), *VC* is reduced to zero in Zones 1 and 2 and substantially decreased in Zone 3, whereas there is a small increase in *VC* in Zones 4 and 5 because the positive effect of warmer temperatures outweighs the decrease in breeding sites with reduced precipitation. However, in almost all cases, the estimated percent change in *m*, which depends primarily on rainfall, is greater than the percent change in *D*, which depends on temperature only, thus adding further support for the importance of rainfall.

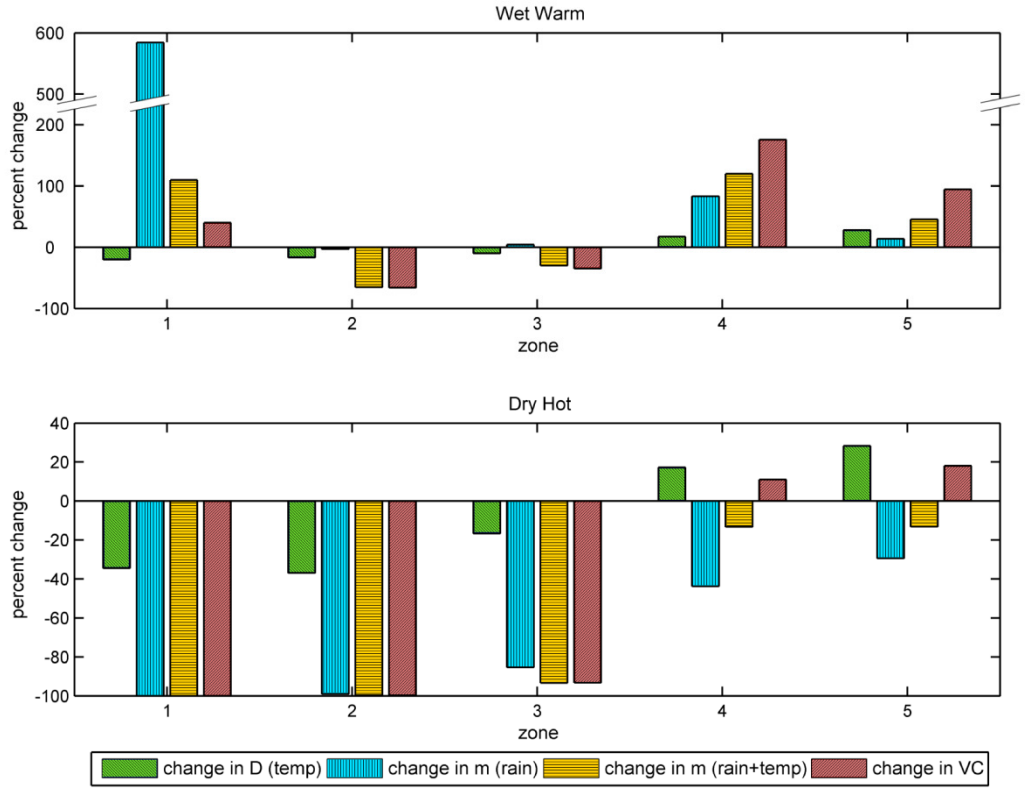

Figure 4.6 Summary of changes to expectation of infective life, mosquito density, and vectorial capacity averaged over 7-year simulations. Wet-warm (top) and dry-hot (bottom) scenarios in climatic zones 1 through 5 (Sahelo-Saharan to Guinea Coast, respectively). Note the abbreviated vertical axis in the top figure.

4.3.2.4 Simulation results using alternate extrinsic incubation period

In calculating the extrinsic incubation period (EIP), the lag time between when the mosquito ingests malaria gametocytes and when it becomes infectious to humans, we use Equation 1.4 developed by Detinova (1962). We also simulated the effects of climate change using an alternate formulation for *EIP* developed by Paaijmans et al. (2009). Simulations using the

alternate *EIP* generally had lower *D,* and thus lower *VC*, throughout West Africa, with the effect being most pronounced in the hottest regions (Zones 1 and 2). While the magnitudes of the values are lowered, the relative changes between the baseline climate and future climate were similar to those based on the main analyses.

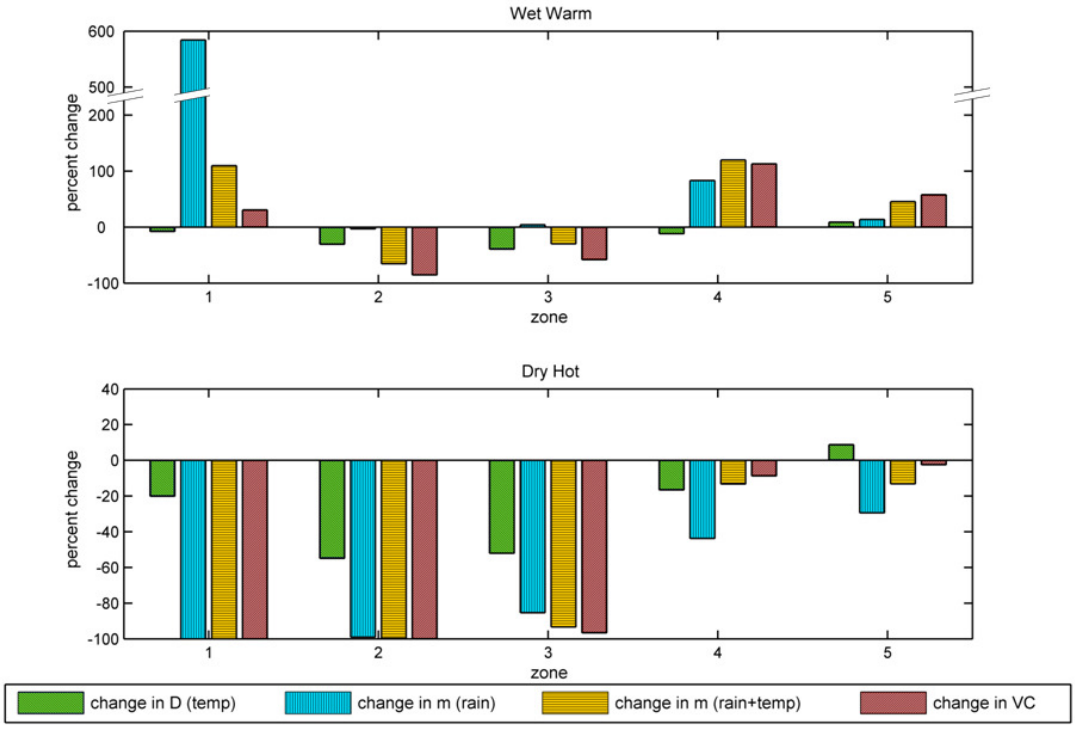

Figure 4.7 Summary of changes to D, m, and VC using the alternate EIP. Mean changes in vectorial capacity over 7-year simulations for the wet-warm (top) and dry-hot (bottom) climate change scenarios for climatic zones 1 through 5 (Sahelo-Saharan to Guinea Coast respectively) using the Paaijmans (2009) equation for *EIP*. Note the abbreviated vertical axis in the top figure.

When we average the changes over the seven-year simulation period, shown in Figure 4.7, the results are again very similar to our original findings. The main differences are in the dry-hot scenarios in Zones 4 and 5; while the warming leads to slight increases in vectorial capacity using Detinova equation for *EIP*, there is a slight decrease in *VC* using the Paaijmans equation.

4.4 Discussion

We simulated the effects of projected changes in climate on malaria transmission in West Africa over a range of scenarios predicted by current climate models, and found that the potential impact of changes in rainfall patterns on malaria transmission may be as great as or greater than the potential impact of rising temperatures. However, our findings should be interpreted in light of model assumptions and limitations. We do not consider changes in extreme weather events, which would have an impact on the hydrology and water pool availability of the region. We also do not account for possible shifts in mosquito species, changes to vegetation that may occur as a result of climate change, or changes in non-environmental factors that will influence malaria transmission in this region, such as malaria control activities, access to health care, improved housing structures, migration, and changes in population density and land use. Our study was limited to rural settings where the primary mosquito breeding sites are formed from rainwater. The model was developed and tested in the semi-arid climate characteristic of Zones 1-3; it is possible that it does not fully represent some of the hydrological processes of the wetter Zones 4-5. Although we present results for an ensemble of future climate projections from AR4 GCMs, these projections represent the extremes of possible changes in rainfall and temperature and are not necessarily the most likely projections of future climate. In Chapter 6, we evaluate the

accuracy of each GCM for simulating past and current climate in the region to determine which predictions are the most plausible.

Our simulations suggest that changes in rainfall have a significant impact on mosquito populations and vectorial capacity in West Africa, particularly in the northern areas where breeding sites (water pools) currently are a limiting factor. Additionally, by comparing the predicted effect of changing rainfall alone to the combined effects of changing rainfall and increasing temperature, we demonstrated that temperature also plays an important role in determining the mosquito density and thereby influencing vectorial capacity. Our results stress the need to include rainfall in studies linking climate change and malaria. We also highlight the difficulty in making predictions of future environmental suitability for malaria in this region, as the GCMs differ greatly in their rainfall predictions. This also is a problem for projecting other impacts of climate change in Africa, for example, on water supplies (De Wit & Stankiewicz, 2006) and food security (Lobell & Burke, 2008). All research involving the impacts of changing rainfall in Africa should therefore take care in selecting appropriate rainfall predictions.

In the arid and semi-arid regions represented by Zones 1, 2 and 3, our simulations suggest that rising temperatures will move environmental conditions towards, and in some cases beyond, the upper limits tolerated by the *Anopheles* mosquito. However, if rainfall increases, the increased availability of breeding sites will tend to raise *VC*, somewhat offsetting decreases in *VC* due to increasing temperatures. Under the wettest future climate predicted by an IPCC climate model, our simulations suggest that the fringes of the Sahara desert will experience a small increase in *VC* despite extremely hot temperatures. However, in the Sahel region, the predicted impact of warming temperature dominates, and a decrease in *VC* is predicted even under the wettest future climate scenario.

Our simulations predict that the wetter and cooler Soudano-Guinean and Guinea Coast regions (Zones 4 and 5) will experience an increase in *VC* as a result of warming temperatures, regardless of changes in rainfall. The driest scenarios would lead to only a slight and seasonal increase in *VC*, while the wettest scenarios could lead to doubling or tripling of *VC*. However, malaria transmission in these zones is already classified as intense and stable, and thus, these areas would be less sensitive to changes in mosquito ecology and vectorial capacity than areas where malaria transmission is unstable (Hay *et al.*, 2009). Children living in such areas experience many malaria infections in their first years of life, and quickly develop immunity to severe disease (Gupta *et al.*, 1999). Therefore, malaria incidence in these areas is likely to be limited primarily by the number of susceptible individuals within the population, rather than inoculation intensity or vectorial capacity. Consequently, even tripling *VC* would not necessarily lead to a significantly higher burden of malaria (Reiter, 2008).

By contrast, Zones 1, 2 and 3 represent areas where malaria is unstable, or seasonally stable with lower intensity, and are therefore more sensitive to changes in *VC*. Even under the wettest conditions predicted by GCMs, our simulations predict that *VC* will decrease in Zones 2 and 3, while simulations of the hottest and driest scenarios predict the near elimination of mosquito populations in these zones due to a lack of breeding areas and intolerably hot temperatures. Although a 40% increase in *VC* is predicted in Zone 1 under the wet-warm scenario, vectorial capacity would still be too small to sustain malaria transmission in this zone.

4.5 Conclusions

Our simulations suggest that changes in rainfall will be important in shaping the impact of climate change on malaria transmission, and therefore must be considered in order to accurately

project the environmental suitability for malaria transmission in future climates. The disagreement among GCM projections for changes in rainfall makes the future of vectorial capacity in West Africa highly uncertain. However, despite this uncertainty, our analysis suggests that we should not expect increases in malaria transmission due to climate change in areas where transmission is currently unstable or stable at low levels. In addition, although we predict a significant increase in vectorial capacity in the two southern zones of our study area, we do not necessarily expect increases in malaria cases, as these areas already have intense stable transmission and are therefore relatively insensitive to changes in vectorial capacity.

In Chapter 6, we analyze the skill of current climate models and select climate projections based on model performance in West Africa, with a focus on regions that we have determined *a priori* to be sensitive to changes in vectorial capacity. Additionally, in Chapter 6 we use the immunology component of HYDREMATS to link changes in climate and vectorial capacity to changes in malaria incidence.

5 Simulating malaria transmission in the current climate of West Africa

5.1 Introduction

In this chapter, we simulate the relationship between current environment and malaria transmission, assuming no malaria control, at twelve locations across West Africa. Because HYDREMATS was originally developed and calibrated to simulate conditions specific to the semi-arid climate of southwestern Niger (Bomblies *et al.*, 2008), we compare simulated variables to a number of data sources from wetter and drier locations to determine whether the model can accurately simulate malaria transmission in these settings.

Most malaria models rely on assumptions of equilibrium states. However, we show that the climate, entomology, and malaria transmission dynamics vary substantially from year to year. The climate in our study area is highly seasonal, and mosquito populations and malaria transmission are mostly limited to the wet season. Mosquito populations are depleted during the winter dry season and must be reestablished at the beginning of each wet season. As a result, vectorial capacity and the basic reproduction number in any year depend primarily on the climate of that year. In contrast, variables relating to the malaria parasite including the entomological inoculation rate, disease prevalence and human immunity level depend on conditions in previous years as well. Untreated malaria infections clear slowly, and can carry over from one transmission season to the next. The EIR depends not only on the mosquito biting rate, but also on the background prevalence level. Human immunity to malaria, which affects disease transmission and clearance rates, depends on past exposure to the disease, integrating the

infectious bites over a person's lifetime. Periodic epidemics associated with higher than average rainfall may maintain a reservoir of parasite within the population in an area where the disease would have otherwise died out. The malaria indices are therefore dependent on the assigned initial conditions, and incorporate information from previous years.

Given these challenges, the assumption of equilibrium conditions greatly simplifies the dynamics of transmission. We consider the role of interannual variability by comparing the results of an equilibrium simulation, where the climate of a single year is repeated until the system reaches a steady state, to multiyear simulations forced by observed time series of environmental data.

Simulation results are pooled and general relationships between the environment and important indices of malaria transmission are developed.

5.2 Identifying regions where malaria prevalence is sensitive to changes in vectorial capacity

The relationships between vectorial capacity and malaria prevalence are nonlinear. At very low levels of vectorial capacity corresponding to basic reproduction number (R_0, the number of secondary infections generated from a single initial infection in a fully susceptible population, see section 1.2.3.2) values less than 1, changes in environmental suitability do not affect malaria prevalence rates because the values are still too low to allow transmission. At very high levels of vectorial capacity, or R_0 values in the tens or hundreds, prevalence is again less sensitive to changes in environmental suitability because inoculation rates are already very high, and rate of disease transmission is limited more by the number of susceptible individuals and other factors such as acquired immunity to malaria, than by vector populations. However, when R_0 is close to

one, disease transmission can be limited by the environmental factors affecting the vector populations and the parasite development rate. At these levels, malaria prevalence is most susceptible to changes in vectorial capacity. These are the areas that are most likely to experience a change in malaria transmission dynamics as a result of climate change.

Gething et al. (2011) related R_0 to prevalence using equilibrium properties of a simple malaria transmission model:

$$R_0 = \frac{(1-\mathrm{Pr})^{-\propto}-1}{1-(1-\mathrm{Pr})^{1+\propto}}\left(\frac{1+\propto}{\propto}\right)(1+\mathrm{S}*\mathrm{c}*(1-(1-\mathrm{Pr})^{1+\propto}))$$

where Pr is prevalence, α is a measure of heterogeneity in biting rates between humans, S is the expected number of human bites per mosquito lifetime, and c is the probability that a mosquito acquires the parasite after biting an infected person.

If we rearrange and differentiate this equation for $\frac{\partial Pr}{\frac{\partial(R0)}{R0}}$ we obtain the curve shown by the black line in Figure 5.1. We can then qualitatively divide the curve into sensitivity levels. An order of magnitude of change in R_0 in the high sensitivity region, whether due to climate change, malaria control, or regular interannual variability, will lead to the greatest change in prevalence, while an order of magnitude change in R_0 in the low sensitivity region will have less impact on prevalence.

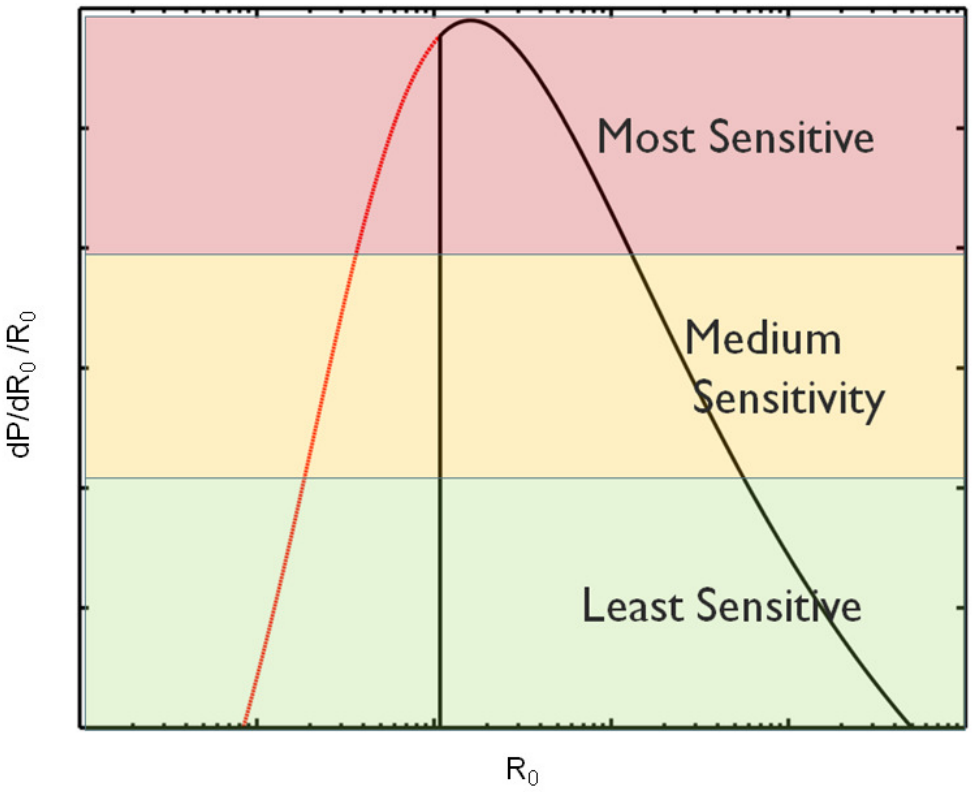

Figure 5.1 Derivative of prevalence with respect to fractional change in R_0.

If we know R_0 at a location, we can use this relationship to estimate the sensitivity of that location to increases in malaria prevalence due to changes in environmental conditions. While little data on R_0 currently exists, we can use spatial estimates of the reproductive number from the Malaria Atlas Project, shown in Figure 5.2 (Gething *et al.*, 2011). The Malaria Atlas Project's estimates were created by applying the equation shown above to prevalence estimates.

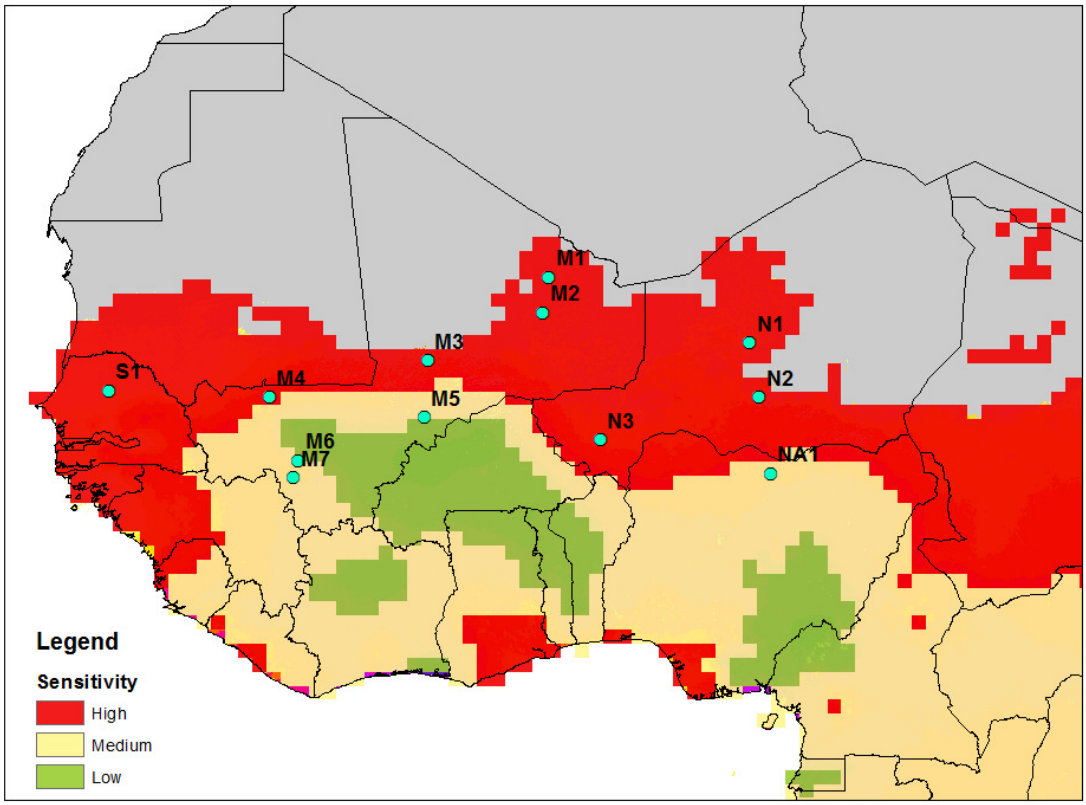

Figure 5.2 Sensitivity to changes in environmental suitability for malaria transmission. Labeled points indicate the sites selected for our experiments.

It should be noted that because most areas with malaria have some form of malaria control, the prevalence estimates are often lower than they would have been under natural equilibrium conditions. As a result, the estimates of the basic reproductive number are lower than true the $R_{0,}$ which is a function of environmental and entomological conditions, independent of control. A further limitation of estimating R_0 using prevalence data is that malaria is found only in locations with R_0 greater than 1. This method therefore cannot estimate R_0 values less than one. However, we can infer that the fringes of the current malaria transmission have values of R_0 slightly below one, and are therefore especially sensitive to changes in environmental conditions that could push R_0 over the threshold value of one and allow transmission to occur.

5.3 Design of numerical experiments

5.3.1 Simulation of baseline conditions at 12 locations

We selected 12 locations from areas in the high and medium sensitivity zones identified in Figure 5.2. For each location, we conducted a 15-year simulation, driven by environmental data from 1998 to 2012. The relatively long simulation length allowed us to explore some of the effects of interannual variability, particularly through the complex feedback processes between entomological inoculation rates (EIR, see section 1.2.3.3), acquired immunity to malaria, and disease prevalence. While a longer time period would have been preferable, we were limited by the availability of environmental data with sufficient temporal resolution. The mean weekly rainfall and temperature during this period is shown in Figure 5.3. Rainfall increases from north to south, both in the amount of rainfall per week and the number of weeks with rainfall. Wet season temperatures decrease from north to south.

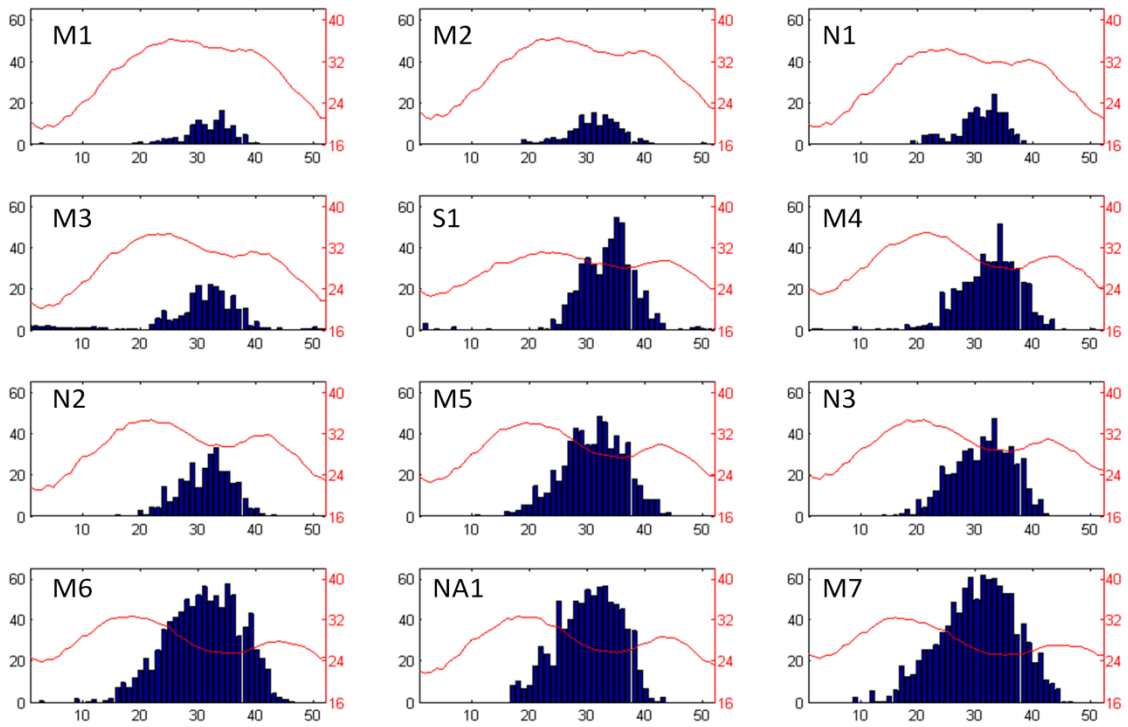

Figure 5.3 Mean weekly rainfall in millimeters (blue bars, left axis) and temperature in degrees Celsius (red line, right axis) in the 12 study locations, arranged from north (upper left corner) to south (bottom right corner).

Environmental data sources used in the current climate simulations are summarized in Table 5.1. We used high-resolution satellite observations of rainfall from the Climate Prediction Center Morphing Technique (CMORPH) Version 1.0 data set, which gives ~8km resolution rainfall data every 30 minutes (Joyce *et al.*, 2004), and has been found in multiple comparison studies to be one the most skilled satellite rainfall products currently available (Serrat-Capdevila *et al.*, 2014). CMORPH data is created by combining images from multiple passive microwave sensors, and interpolating them forward and backward in space and time based on cloud advection vectors calculated from geostationary infrared sensors (Joyce *et al.*, 2004).

Like most satellite products, CMORPH is known to have a positive bias compared to rain gauge data in West Africa, primarily due to overestimation of high-intensity rainfall (Gosset *et al.*, 2013). However, after a simple bias-correction, CMORPH can be used as in input to HYDREMATS to reasonably simulate water pools and mosquito populations (Yamana & Eltahir, 2011).

While Yamana & Eltahir (2011) used a single bias-correction factor for all rainfall estimates regardless of intensity, here we used a probability matching technique (Wolff *et al.*, 2005) so that the cumulative distribution function (CDF) of corrected hourly CMORPH data matched that of the ground observations. This method, described in Appendix A, is preferable to applying a single correction factor because the bias differs by rainfall intensity. Variations of the probability matching technique have recently been used to correct biases in CMORPH using rain gauge data (De Vera & Terra, 2012; Guilloteau *et al.*, 2014).

Table 5.1summarizes the data inputs for HYDREMATS. Temperature, wind speed, wind direction, and radiation data were taken from the ERA Interim data set (Dee *et al.*, 2011) for the grid cell containing each village being simulated; we assume uniform conditions within the 0.75 degree ERA grid cell. ERA Interim data were adjusted for HYDREMATS as follows. Wind speed data were converted from 10 m to 2 m elevation using the logarithmic profile described by Equations 4.2 and 4.3. ERA-Interim data were linearly extrapolated from the 3-hour resolution to the 1-hour resolution required by HYDREMATS.

The dominant vegetation type at each location was obtained from the University of Maryland Land Cover Classification (Hansen *et al.*, 2000). Soil properties were taken from the Harmonized World Soil Database (Nachtergaele & Batjes, 2012). A thin layer of low-

permeability soil is included in the model to account for soil crusting that occurs throughout West Africa under cultivated conditions (Morin, 1993). Because this study focuses on climate variables, we assumed typical topographical conditions and household locations as observed in Banizoumbou, Niger (Bomblies et al. 2008) that were held constant between locations.

The model's initial conditions for malaria prevalence levels were based on the Malaria Atlas Project (MAP; see Section 5.4.1.3) estimate for each location. Simulated humans are randomly infected at the beginning of each simulation to match the MAP estimate. Locations where MAP estimated no malaria prevalence were initialized as 5% prevalence. In order to maintain a background level of malaria parasite in the simulated population, the model simulates imported cases at a rate of 0.1% of the population per month. Each human's immunity level was initialized based on estimated EIR and the human's age. Using the MAP prevalence level, we estimated the EIR for each location. The immunity model assumes that roughly 60 infectious bites are required to confer full immunity. We used the EIR to estimate the number of years required to collect 60 inoculations, and then scaled the initial immunity according to age. For example in a location with EIR of 5 infections bites per year, full immunity is expected at age 12. A newborn is assigned an initial immunity of zero, a six-year old has initial immunity of 0.5, and everyone aged twelve or older has initial immunity of 1.

Table 5.1 Summary of data sources

	Data source	**Spatial resolution**	**Temporal resolution**	**Reference**
Baseline Climatology				
temperature	CRU TS 3.21	0.5 x 0.5 degree	1 month	Mitchell and Jones, 2005
rainfall	CRU TS 3.21	0.5 x 0.5 degree	1 month	Mitchell and Jones, 2005
Meteorological Inputs for HYDREMATS Simulation				
precipitation	CMORPH version 1.0	~8km	30 min	Joyce et al., 2004
temperature	ERA-Interim	.75 x .75 degree	3 hour	Dee et al., 2011
wind speed	ERA-Interim	.75 x .75 degree	3 hour	Dee et al., 2011
wind direction	ERA-Interim	.75 x .75 degree	3 hour	Dee et al., 2011
surface radiation	ERA-Interim	.75 x .75 degree	3 hour	Dee et al., 2011
Other model inputs				
soil type	HWSD	~1km		FAO, 2009
vegetation	UMD landcover	1km		Hansen et al., 2000
topography	Computed from Envisat synthetic aperture radar and ground survey	10 m		Toutin and Gray, 2000; Bomblies et al. 2008
household locations	Quickbird image	0.6 m		Bomblies et al. 2008

5.3.2 Simulating equilibrium relationships between climate and malaria transmission

In order to explore the basic relationships between climate and various measures of disease transmission without the complication of interannual variability, we simulated equilibrium conditions by repeating environmental inputs from a single year until the system reached a steady state. After calculating the mean annual vectorial capacity for the 15-year simulations at each of the twelve locations described in 5.3.1, we selected the year closest to the mean to serve as our equilibrium year.

In addition to simulating the mean year at each of the twelve sites, we conducted additional equilibrium simulations by repeating meteorological inputs for years resulting in R_0 values spanning from 0 to nearly 400, for a total of 33 equilibrium systems. The majority of these additional simulations (13) used meterological inputs for other years from sites N3, MA5 and NA1. These locations were selected because they covered a wide range of R_0 values that were not sampled by the mean year equilibrium simulations.

The environmental conditions of the twelve sites in our study area produced a maximum R_0 of 271. In order to test the immunity component of HYDREMATS functioned at higher transmission levels, we examined seasonal mosquito populations at higher levels than would have been found in our study area. Three simulations were conducted using environmental input from wetter locations, corresponding to Zones 4 and 5 from the experiment in Chapter 4. In another set of experiments, we artificially increased mosquito populations by manipulating environmental inputs from the year leading to the highest simulated R_0 in our original baseline simulations, site NA1 in 2001. Two of these experiments used modified the rainfall inputs from NA1, year 2001, to extend the rainy season by two weeks and four weeks, leading to a longer

period of mosquito breeding and thus higher R_0 and EIR. Another four experiments used hydrology output from the original NA1 year 2001 simulation, but altered the entomology component such that additional mosquitoes were added to the simulation, increasing the total number of mosquitoes by a factor of 1.2 to 4. These simulations with artificial rainfall or mosquito populations were used only as tests of the immunity component of the model.

5.3.3 Simulating malaria transmission at varying levels of rainfall and temperature

Our initial simulation of twelve baseline locations gave us relationships between annual rainfall and temperature and the corresponding entomological and immunological values. In order to further explore these relationships, we performed additional realizations at each location using hypothetical combinations of annual rainfall and temperature inputs for a total of roughly 1600 realizations. These additional simulations used northward and southward shifts in the rainfall gradient like those described Section 4.2.3.1. Temperature inputs were altered by adding between 0 and 6 degrees Celsius to the hourly time series used in the baseline conditions. The magnitudes of rainfall and temperature changes came from changes in climate predicted by CMIP5 climate models for the twelve baseline locations, as described in Section 6.4.1. We simulated temperature and rainfall combinations predicted by three climate models: CCSM4, MPI-ESM-MR and BNU-ESM, for two time periods: 2030-2060 and 2070-2100. In addition to these simulations, we used additional realizations where the change in temperature was from climate projections for the period 2030-2060 and the change in rainfall came from climate projections for the period 2070-2100. These simulations were the result of an error in pairing the temperature and rainfall predictions, but we include them here as realizations of plausible climate combinations.

Each of these additional simulations ran for 15 years at one of the twelve baseline locations. Figure 5.4 shows the combinations of rainfall and wet-season temperature that were simulated.

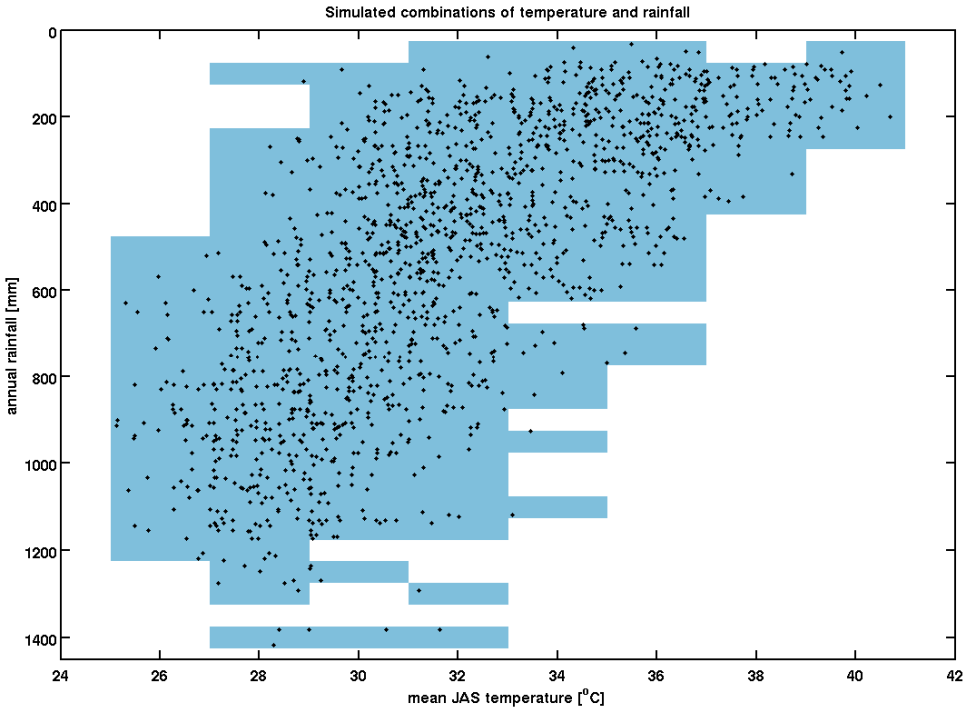

Figure 5.4 Annual rainfall and wet-season temperature used for simulations. Each point represents one year of simulation. The shaded areas are rainfall and temperature combinations in increments of 50 mm and 2 degrees Celsius with one or more simulations. The black points represent individual simulated years.

5.4 Results

5.4.1 Comparison of simulated variables to observational data

HYDREMATS has previously been shown to accurately represent observed hydrology and entomology in two villages in Southern Niger (Bomblies *et al.*, 2008; Bomblies *et al.*, 2009). Here, we compare simulated results to a number of additional data sources:

1. Hydrology, entomology and malaria prevalence from Banizoumbou and Zindarou, Niger
2. Entomology and malaria prevalence from Garki, Nigeria
3. Malaria prevalence estimates from the Malaria Atlas Project
4. The relationship between the entomological inoculation rate and prevalence from across Africa

5.4.1.1 Comparison to data from Banizoumbou and Zindarou, Niger

HYDREMATS was developed and calibrated through extensive data collection from 2005 through 2010 in two neighboring villages in Niger, shown on the map in Figure 3.1. Data sampling locations in one of the villages, Banizoumbou, are shown in Figure 5.5. Environmental data collected included one-hour resolution meteorological variables, spatially distributed soil, vegetation and topography values, and time-varying measurements of soil moisture, and the depths and temperatures of selected recurring water pools. Entomological variables collected included adult mosquitoes captured in CDC light traps and mosquito larva collected using a standard dipping method (Bomblies *et al.*, 2008; Bomblies *et al.*, 2009). In addition, malaria prevalence data were collected, as described at length in Chapter 3 (Yamana *et al.*, 2013).

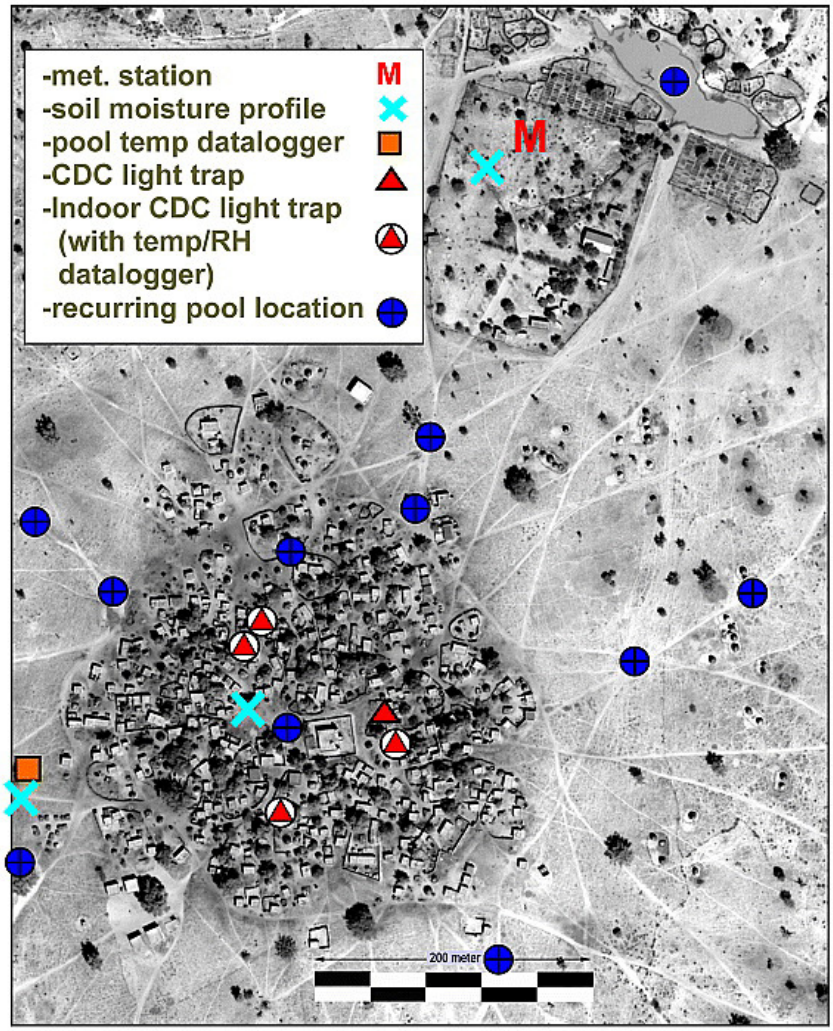

Figure 5.5 Data sampling locations in Banizoumbou, Niger. Reprinted from Bomblies et al., 2008.

The hydrology component of HYDREMATS was rigorously compared to field observations in Bomblies et al. (2008). Figure 5.6 shows that the model very closely reproduced volumetric water content measured in a millet field in Banizoumbou, Niger. Figure 5.7 shows the close relationship between simulated and observed water depths at three water pools known to be productive breeding sites.

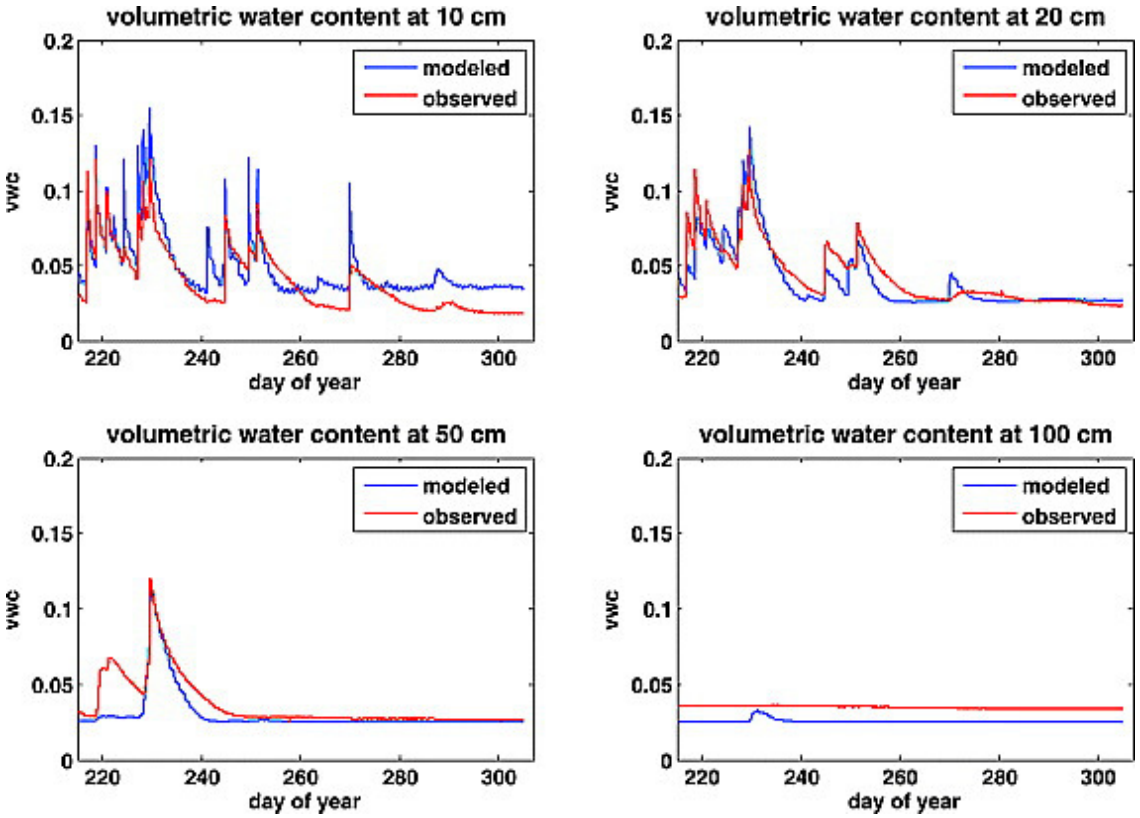

Figure 5.6 Field observations (red) and simulations (blue) of volumetric water content measured in Banizoumbou, Niger. Reprinted from Bomblies et al., 2008.

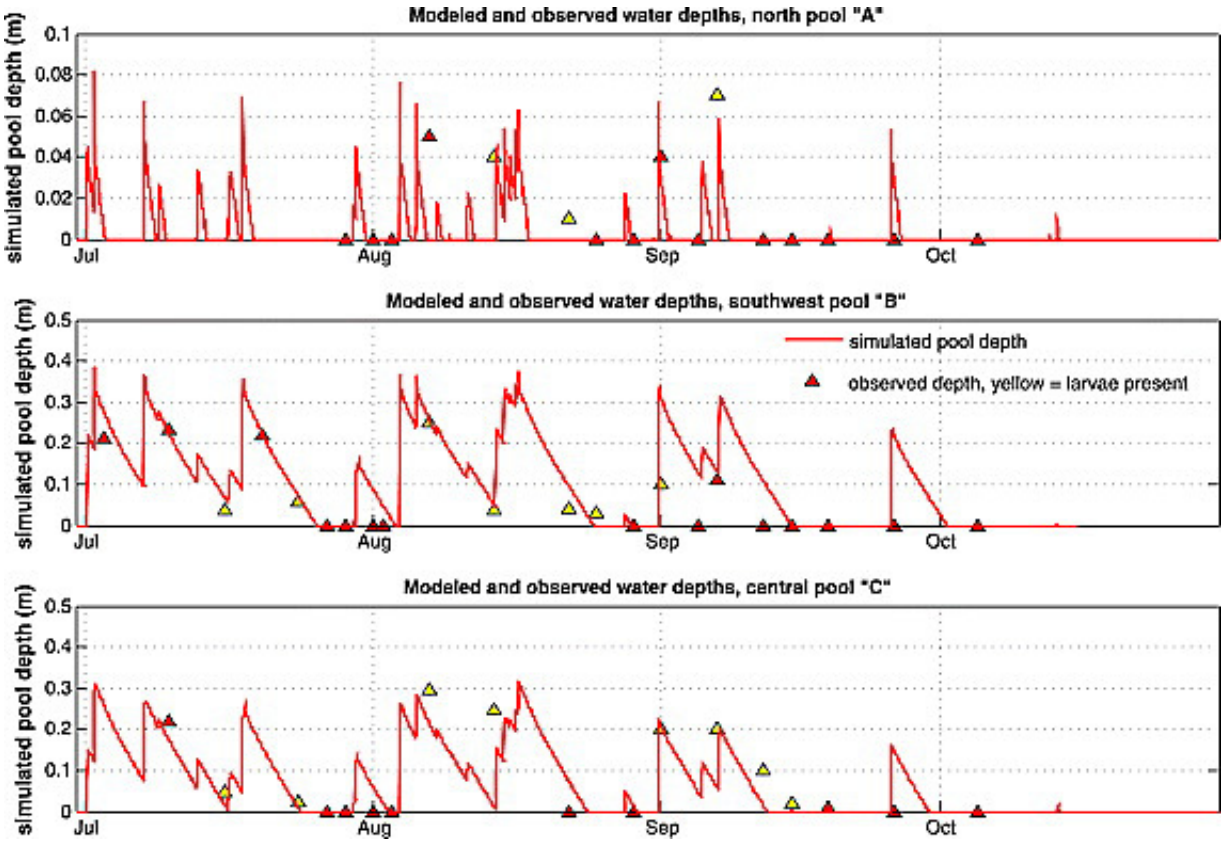

Figure 5.7 Observed and simulated water depths at three pools in Banizoumbou, Niger. Reprinted from Bomblies et al. 2008.

Figure 3.2 compared simulated to captured adult mosquitoes in 2005 and 2006 in Banizoumbou and Zindarou. HYDREMATS accurately simulated both the seasonality of mosquito populations, and the relative differences between the two villages. Malaria prevalence data were shown in Figure 3.5, and compared to simulation results shown in Figure 3.7. While the mosquito density was an order of magnitude higher in Zindarou than in Banizoumbou, the two villages had similar malaria prevalence levels (Yamana *et al.*, 2013). In Chapter 3, we were able to reproduce this effect using the improved immunity component of the model.

Comparison to data from the Garki Project

The Garki Project was a major effort to study malaria transmission and control by the World Health Organization and the Government of Nigeria from 1969 to 1976. The study location corresponds with site NA1 shown in Figure 5.2. The goals of the project were to study the epidemiology of malaria transmission in the Sudan Savanna climate zone, test intervention methods, and develop a model of disease transmission (Molineaux & Gramiccia, 1980). The study included four tiers of villages, shown in Figure 5.8. Malaria control interventions were applied to the inner villages. Villages outside of the intervention zone were monitored as non-intervention comparison locations. Mosquitoes were captured every 5 weeks during the dry season and every 2 weeks during the wet season using human landing catches. Human bait collectors were stationed at indoor and outdoor locations for the duration of the night and collected mosquitoes attempting a blood meal. Mosquitoes were also captured using pyrethrum spray collections and light traps. Captured mosquitoes were counted and analyzed in order to estimate the mosquito biting rate, EIR, mosquito age, and the sporozoite rate (proportion of mosquitoes infected by the *plasmodium* parasite). Age-specific malaria prevalence was measured for selected villages every 10 weeks using standard blood smear methods. Seroimmunological surveys were conducted every 6 months to test for the presence of antibodies to *Plasmodium falciparum* and other forms of the malaria parasite within the human population.

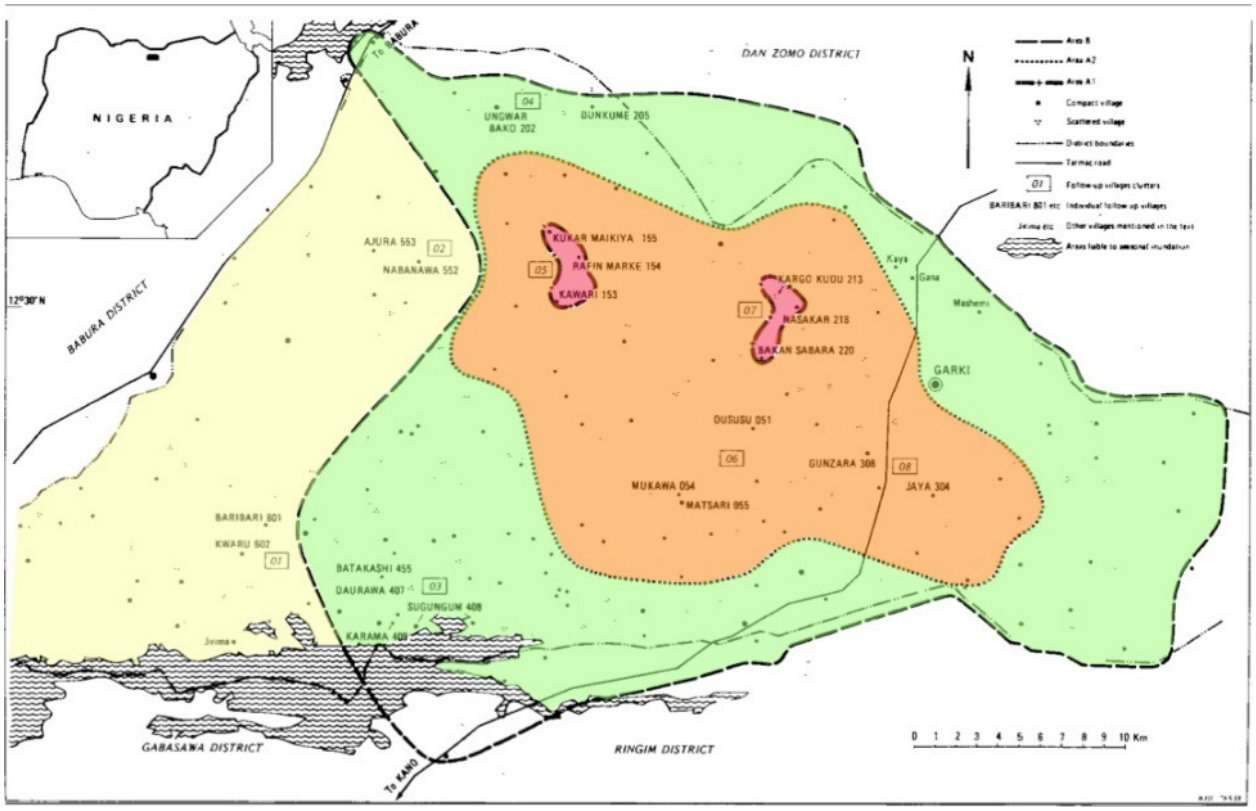

Figure 5.8 Location of the Garki Project. Reprinted from Molineaux & Gramiccia, 1980.

The following is a comparison between data collected from villages outside of the intervention area and corresponding variables simulated by HYDREMATS in our 15-year baseline simulation. Because the high-resolution environmental data sources required for HYDREMATS simulations did not overlap the Garki Project time period, we compare the results to the range of values simulated in our 15-year simulation. We are therefore more interested in reproducing general characteristics and timing of the seasonal cycle rather than specific values.

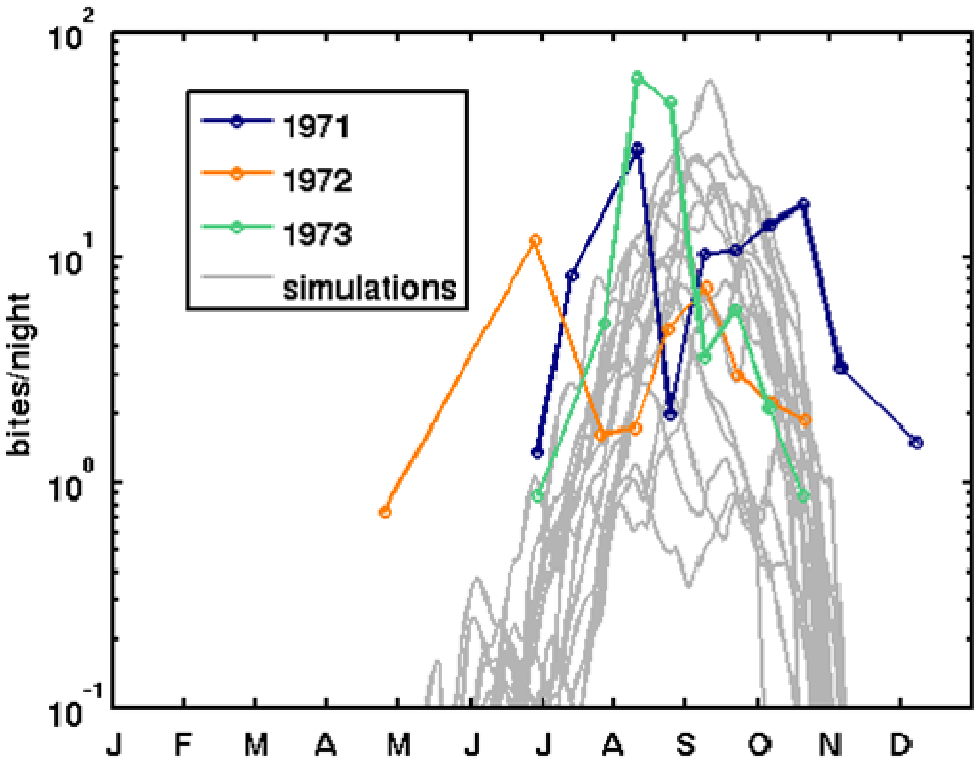

Figure 5.9 Mosquito biting rate in Kwaru, Nigeria, one of the non-intervention comparison villages in the Garki project. Colored lines show captured mosquitoes for 3 consecutive years. Grey lines show simulation results.

Figure 5.9 shows simulated and observed mosquito bites per person night from Kwaru, a non-intervention comparison village in the Garki district in linear scale on the left and log scale on the right. The mosquito biting rate differs from the entomological inoculation rate (EIR) in that it counts all bites, while EIR counts infectious bites. EIR is frequently estimated by multiplying the biting rate by proportion of captured mosquitoes testing positive for malaria sporozoites. Observations are shown in the colored lines, and the results of our multiyear simulations are shown in the grey dashed lines. Our simulations capture the main features of the biting cycle, with biting concentrated between day 200 and day 300.

Figure 5.10 shows prevalence by age for a cross-section of the population in the non-intervention villages at the end of rainy season. The observations, in red, show a characteristic age profile of malaria prevalence. Young children become infected at high rates until they begin to develop partial immunity to disease. This explains the sharp decrease in prevalence between the first few years of life and early adolescence. While the exact shape and magnitude of the prevalence profile varies by year and by location, HYDREMATS succeeds in simulating the basic characteristics of the age profile. In this simulation, children appear to develop immunity several years faster than the observed population.

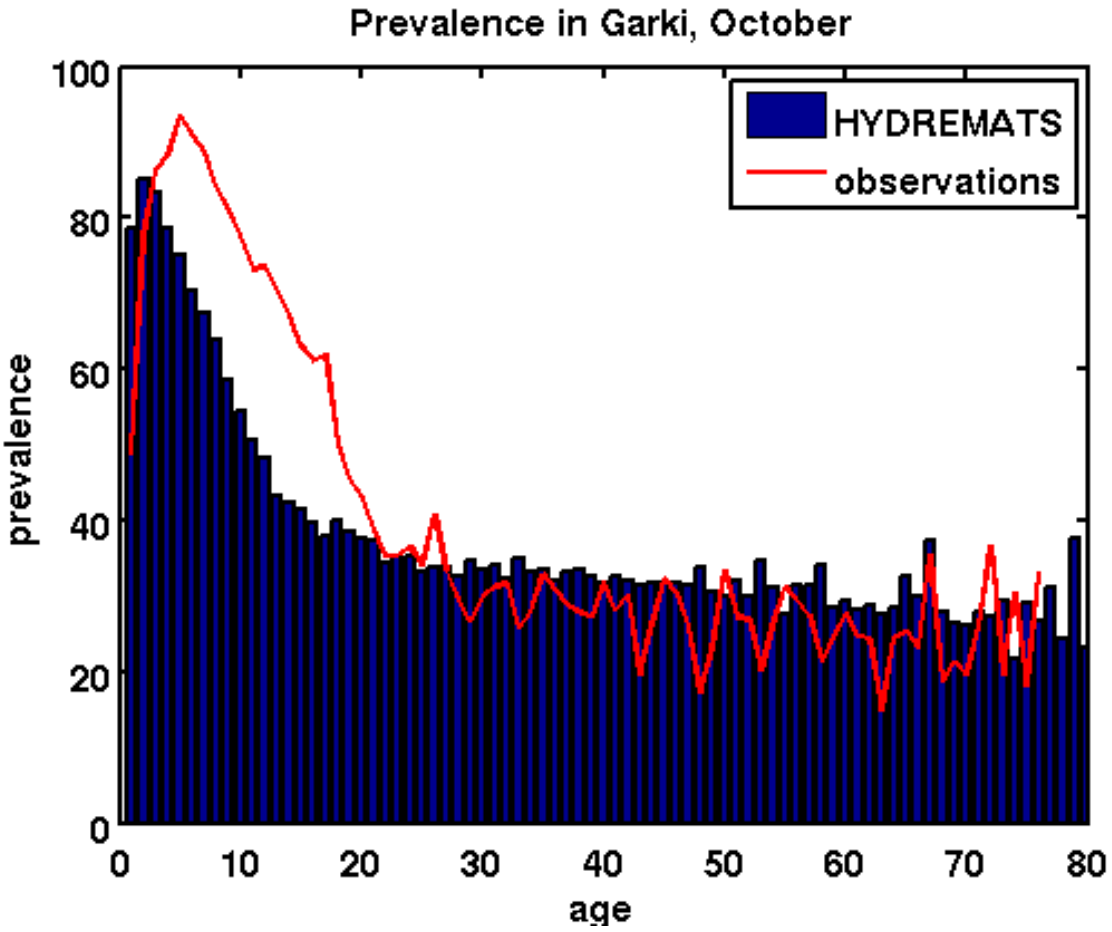

Figure 5.10 Malaria prevalence by age group

Finally, Figure 5.11 shows observed malaria prevalence in two non-intervention villages over five years. Simulated prevalence from our equilibrium simulation is shown in bright red for all ages and dark red for children aged 2-10. Again, while the specific prevalence value varies from year to year, HYDREMATS correctly simulates the timing of the seasonal cycle. The magnitudes of the simulated prevalence appear to be reasonable.

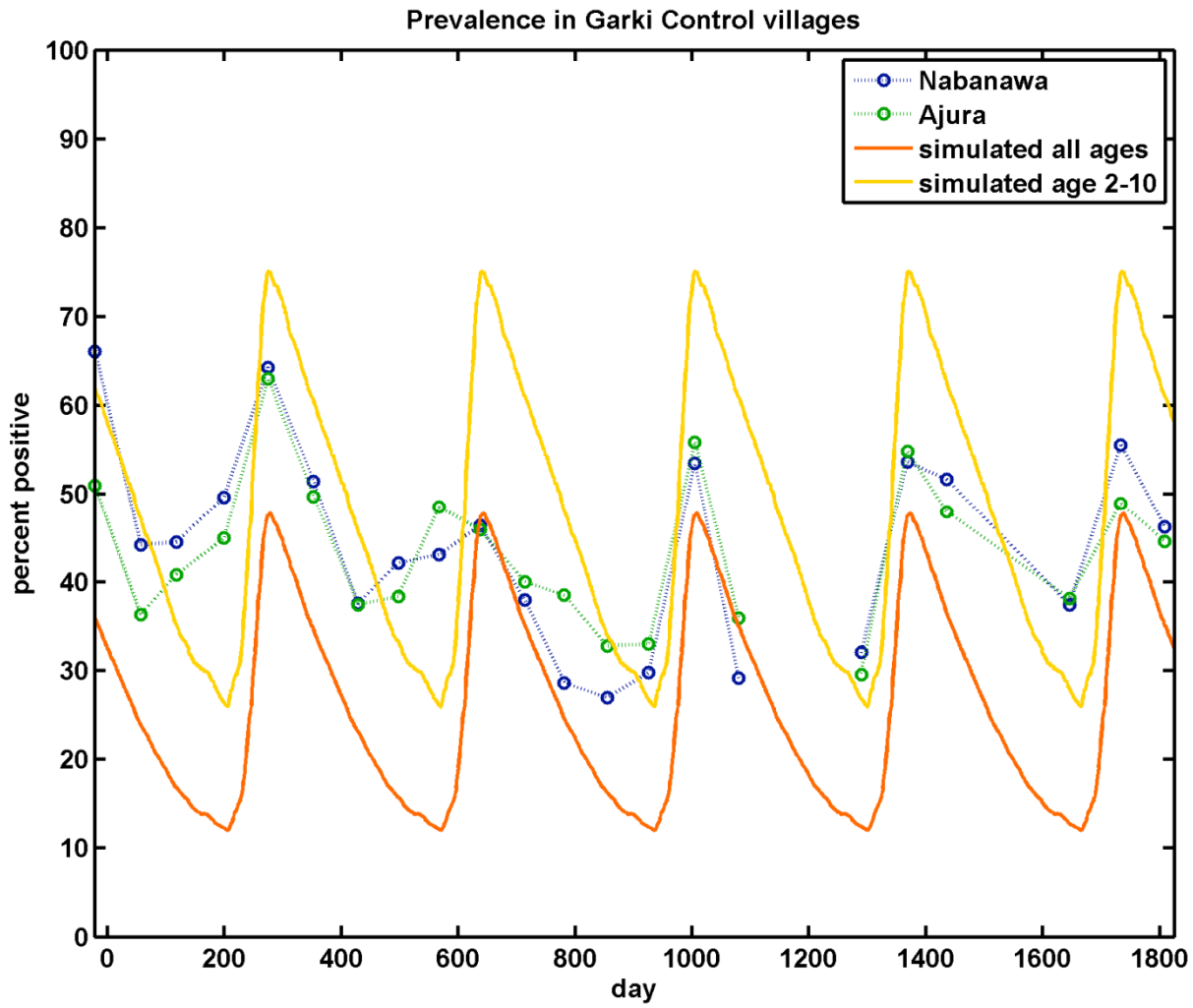

Figure 5.11 Prevalence in observed and simulated prevalence in the Garki district

5.4.1.2 Comparison to Beier data

Beier et al. compiled paired data from 31 locations across Africa and developed a relationship between the entomological inoculation rate (EIR), and malaria prevalence (Beier *et al.*, 1999). These paired data points originated from multiple countries including Kenya, Ethiopia, Tanzania, Republic of Congo, Burkina Faso, and Senegal, spanning a wide range of climate zones. The paired data points were selected by conducting a literature search with the following inclusion criteria: entomological data collected over at least one year with a minimum of monthly sampling over the transmission season, standard methods for estimating mosquito densities and sporozoite rates, and no vector control interventions. Inclusion criteria for the prevalence data included use of standard blood smear techniques and reporting by time period and age group. In instances where the original malaria prevalence data were reported for multiple time periods and age groups, the single highest prevalence value was selected. The analysis showed a linear relationship between prevalence and the logarithm of annual EIR. This log-linear relationship persisted when data were stratified by ecological zone as well as between east and west Africa, indicating that this is a fundamental relationship and independent of climate. These data therefore provide a test for the human immunity and malaria transmission component of HYDREMATS, which has been less extensively tested against observations than the hydrology and entomology components.

Since Beier et al. used the maximum prevalence value sampled over multiple age groups and time periods, we compared the data to the maximum simulated prevalence for the 2 to 10 year age group from our equilibrium simulations, shown in Figure 5.12. HYDREMATS was able to reproduce the observed linear relationship between EIR and peak malaria prevalence. There is very good agreement between our simulation results and observational data for a wide range of

epidemiological conditions, from 0 to over 300 infectious bites per person per year.

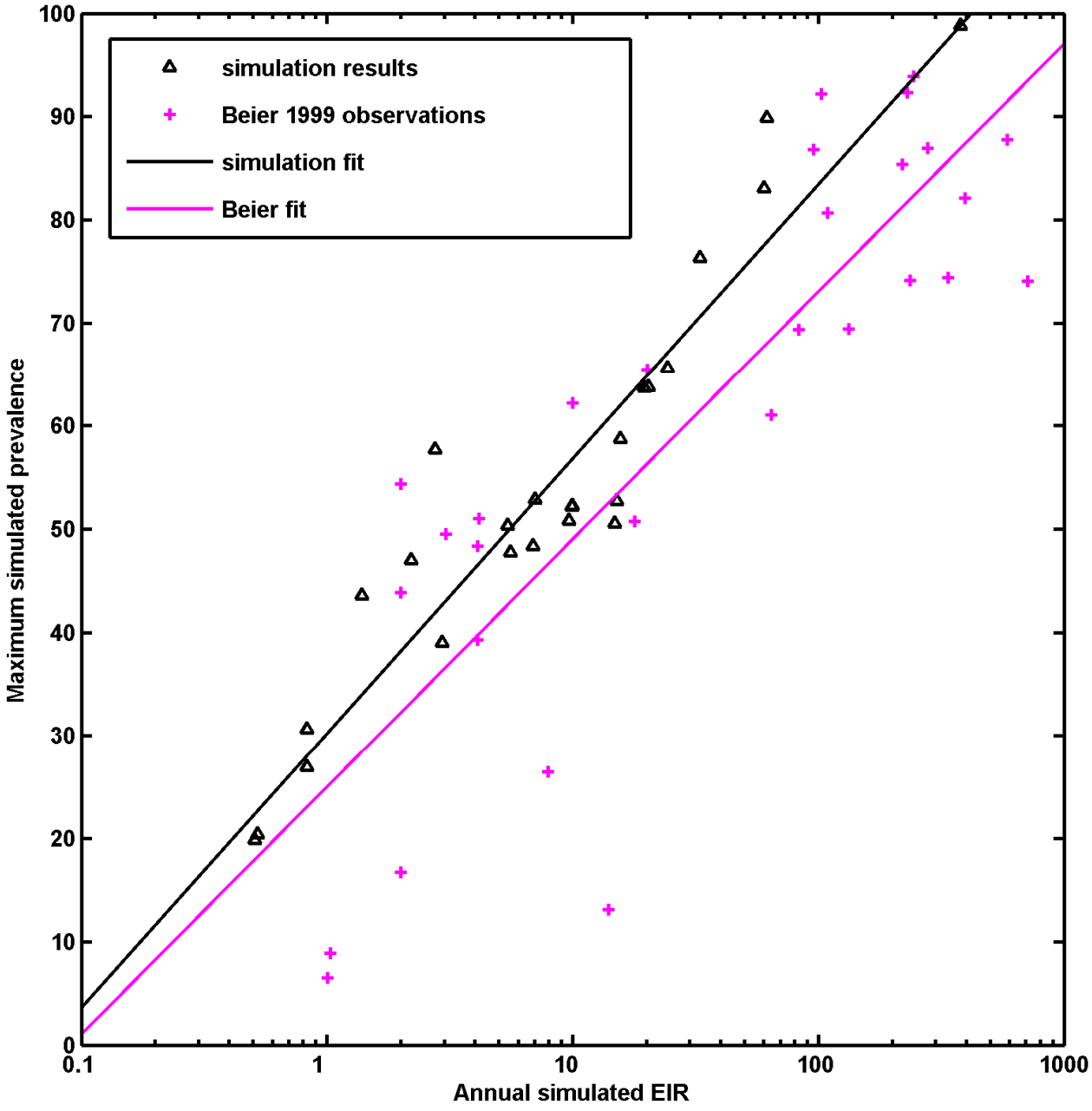

Figure 5.12 Observed (pink) and simulated (black) relationship between EIR and malaria prevalence

5.4.1.3 Comparison to data from the Malaria Atlas Project

The Malaria Atlas Project (MAP) is an effort based at University of Oxford to produce maps showing global estimates of various measures of malaria risk. MAP compiles and maintains a database of routine malaria prevalence surveys. The current maps use over 22,000 geo-referenced data points of malaria prevalence measured between 1985 and 2010 from across the 85 malaria endemic nations. Survey data that meet inclusion criteria are standardized to the 2 to 10 year old age group (Gething *et al.*, 2011).

Temperature and aridity masks were used to predict the limits of stable malaria. The aridity mask was formed by excluding areas classified as bare ground by the GlobCover land-cover classification product (Bicheron *et al.*, 2008), a remote sensing product derived from data collected by the European Space Agency's Environmental Satellite (ENVISAT), for the period between December 2004 and June 2006. The temperature masks excludes regions where low temperatures cause the extrinsic incubation period to exceed mosquito lifespan (Gething *et al.*, 2011).

Within the predicted limits of stable malaria transmission, these prevalence data are mapped to a global surface at a 5 km x 5km resolution using Bayesian inference and geospatial modeling (Gething *et al.*, 2011). The MAP estimate of malaria prevalence in children aged 2 to 10 years is shown as the colored surface in Figure 5.13. The overlaying circles show the prevalence during the peak malaria transmission season simulated by HYDREMATS in the equilibrium simulations.

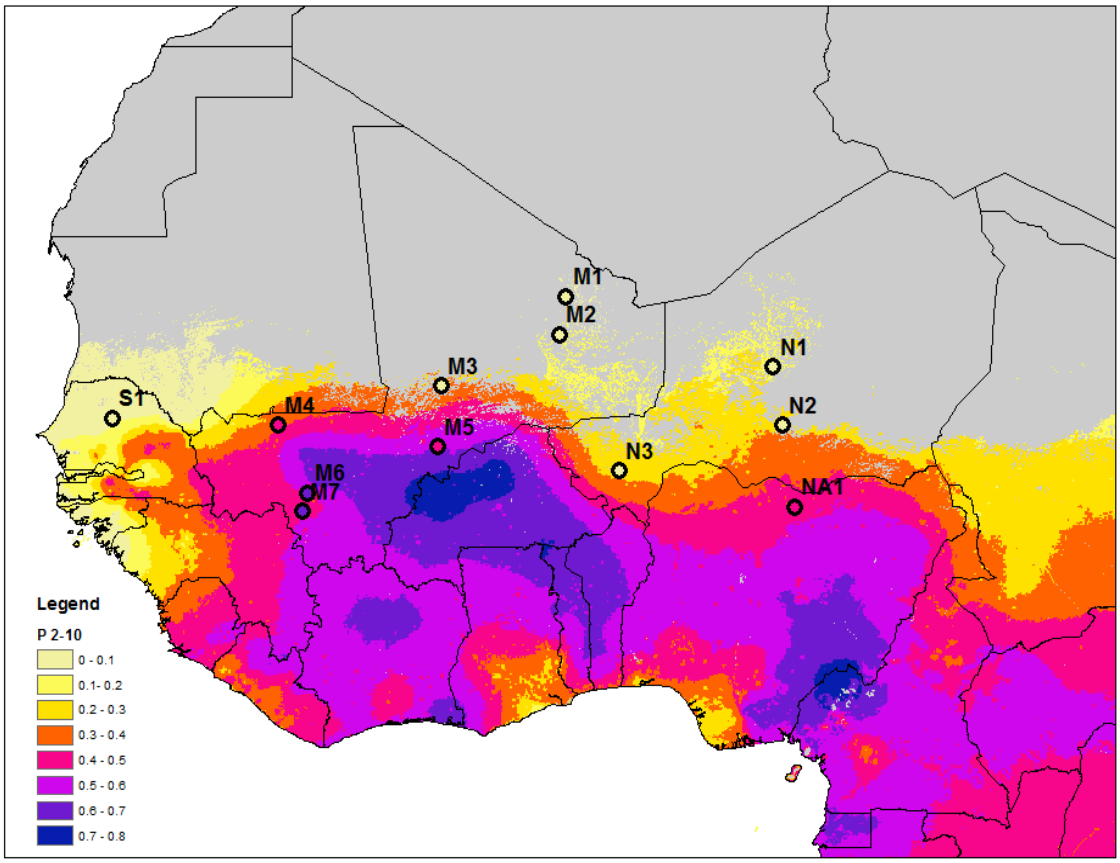

Figure 5.13 Malaria prevalence estimated by Malaria Atlas Project (colored surface) and simulated by HYDREMATS (circles)

Figure 5.14 compares simulated peak prevalence to the MAP estimate, with results of the equilibrium simulation on the right, and the mean of the multiyear simulation on the left. For the majority of the twelve locations, simulated results matched well with the MAP estimate. One outlier in the equilibrium results is the point S1, located in Senegal. This could be explained in part by Senegal's malaria control activities, which cause observed prevalence to be substantially lower than what would have been expected given the environmental conditions. Our simulations did not account for varying levels of malaria control between locations. Interannual variability is

likely playing a role as well, as is discussed in Section 5.4.5; the MAP estimates do not address seasonal and interannual variability in response to climate variability. Another discrepancy between simulations and MAP estimates are the three locations (N1, N2 and M3) where simulated prevalence was 0%, while MAP estimates levels between 10 and 30%. There are several additional explanations for this discrepancy. One is that in the sparsely population regions northern Niger and Mali, there are very few observations of malaria prevalence. In these regions, MAP estimates rely on statistical techniques using environmental covariates including rainfall, temperature, land cover, and rural versus urban classification. We therefore have less confidence in MAP estimates at high latitudes. Another explanation for the discrepancy is that while the equilibrium simulation had R_0 less than one leading to elimination of the parasite, all three of these locations had at least some years with R_0 greater than one. Transmission is therefore possible in these locations if the parasite is present in the population during years with R_0 greater than one. A third possibility for the discrepancy is that these locations may have had some form of permanent water source not accounted for in our simulations that could serve as mosquito breeding habitat in the absence of rain-fed water pools. This is likely to be true of M3, which lies on the banks of a tributary to the Niger River.

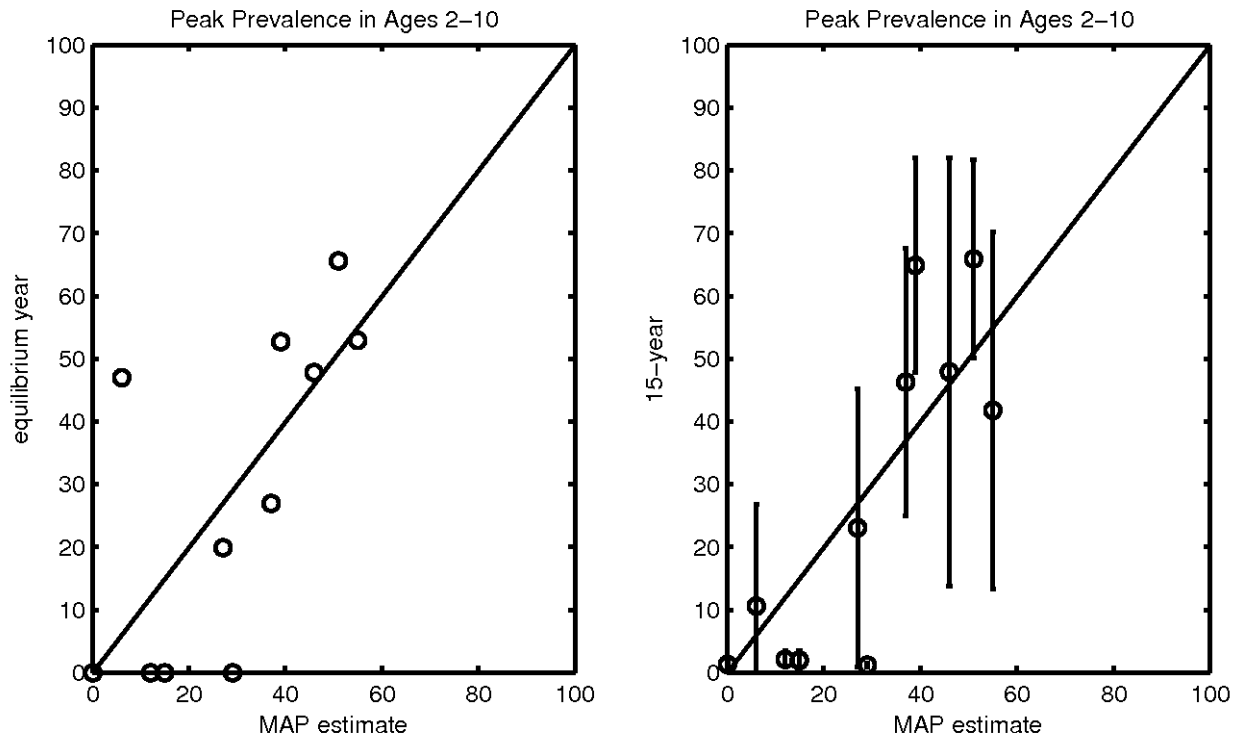

Figure 5.14 Simulated prevalence compared to MAP estimate. Error bars on for the multiyear simulation represent one standard deviation from the mean.

5.4.2 Classifying sites by levels of R_o and malaria transmission

The multiyear simulations showed high levels of interannual variability in R_0. As discussed in Chapter 1, R_0 is a significant measure of malaria transmission because it has a critical value of 1, below which malaria transmission is not sustained. Malaria transmission in villages where R_0 is always less than one would be limited to cases imported from outside the village. Villages where R_0 is always greater than 1 consistently have malaria transmission during the rainy season. Villages where R_0 is greater than 1 for some years and less than 1 during other years have epidemics of varying frequency and intensity.

Simulation results are summarized in Figure 5.15. Areas that had low suitability for malaria transmission include Sites M1 and M2 Northern Mali and N1 in Niger, where R_0 was less than 1 for most or all years. Simulated prevalence levels and EIR in these locations fell to near zero. Areas with moderate transmission potential include S1, M3, M4, N2 and N3. These areas had many years with R_0 spanning the sensitive area between 1 and 10, as well as occasional years with $R_0 < 1$ and $R_0 > 10$. Some of these sites could experience epidemics when conditions were suitable, but also had years with low transmission. Sites M5, M6 and M7 in southern Mali and site NA1 in northern Nigeria had R_0 greater than 10 for almost all years. These locations had the highest prevalence levels. Figure 5.16 shows the sites by transmission category and Figure 5.17 shows daily values of R_0, EIR, peak prevalence in children aged 2-10, and mean population level immunity index for a representative location in each of the three transmission categories.

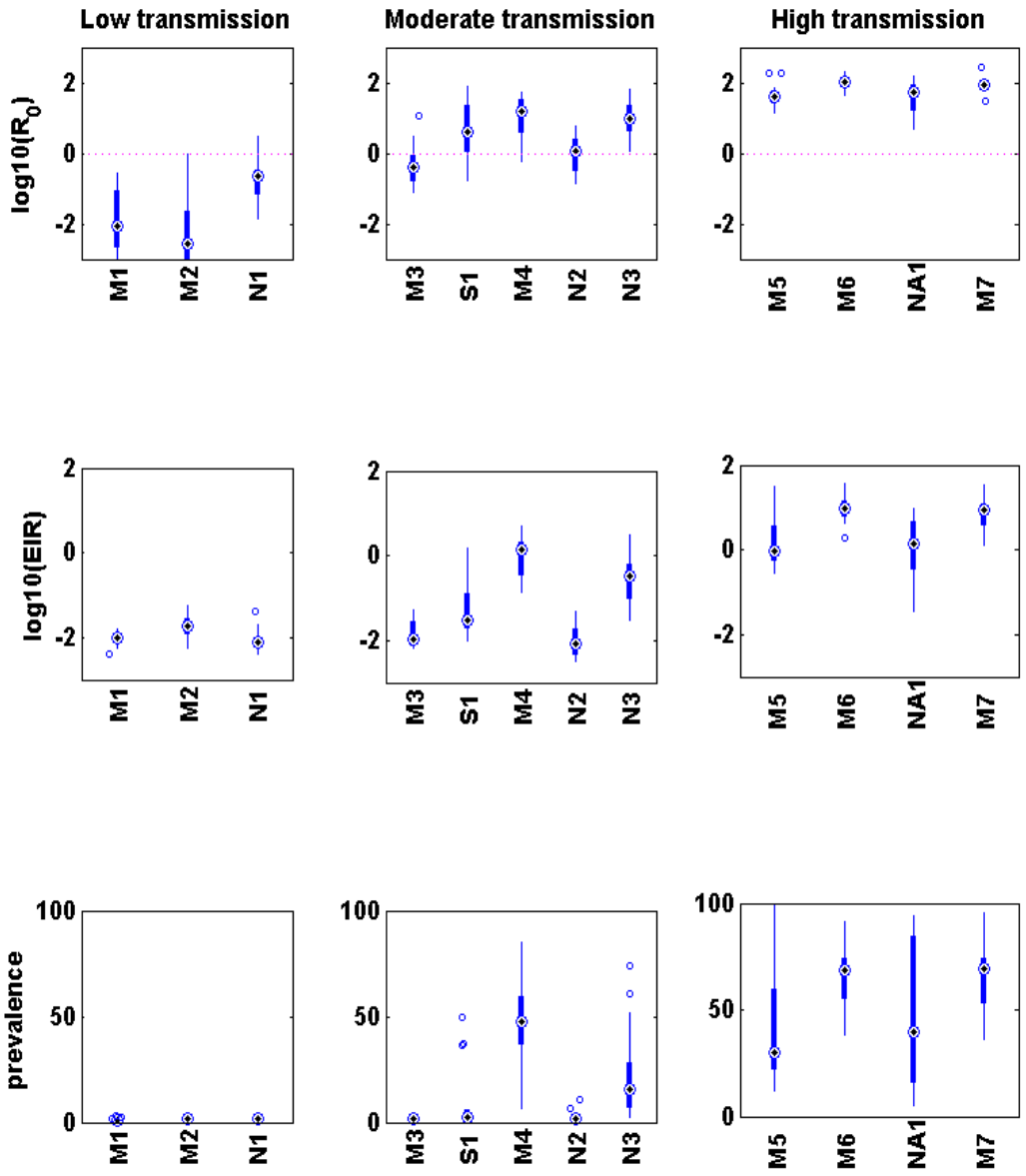

Figure 5.15 Summary of annual R_0, EIR and peak prevalence for each location. The three columns of subplots correspond to low (left column), medium (middle column), and high (right column) transmission potential categories. The center dot in each boxplot indicates the median value over the 15 year simulation, the extent of the solid box corresponds to the limits of the 25th through 75th percentile values, and the solid lines (whiskers) extend to include roughly 99% of values if the data were normally distributed. Data points outside of the whiskers are considered outliers, and are denoted by open circles.

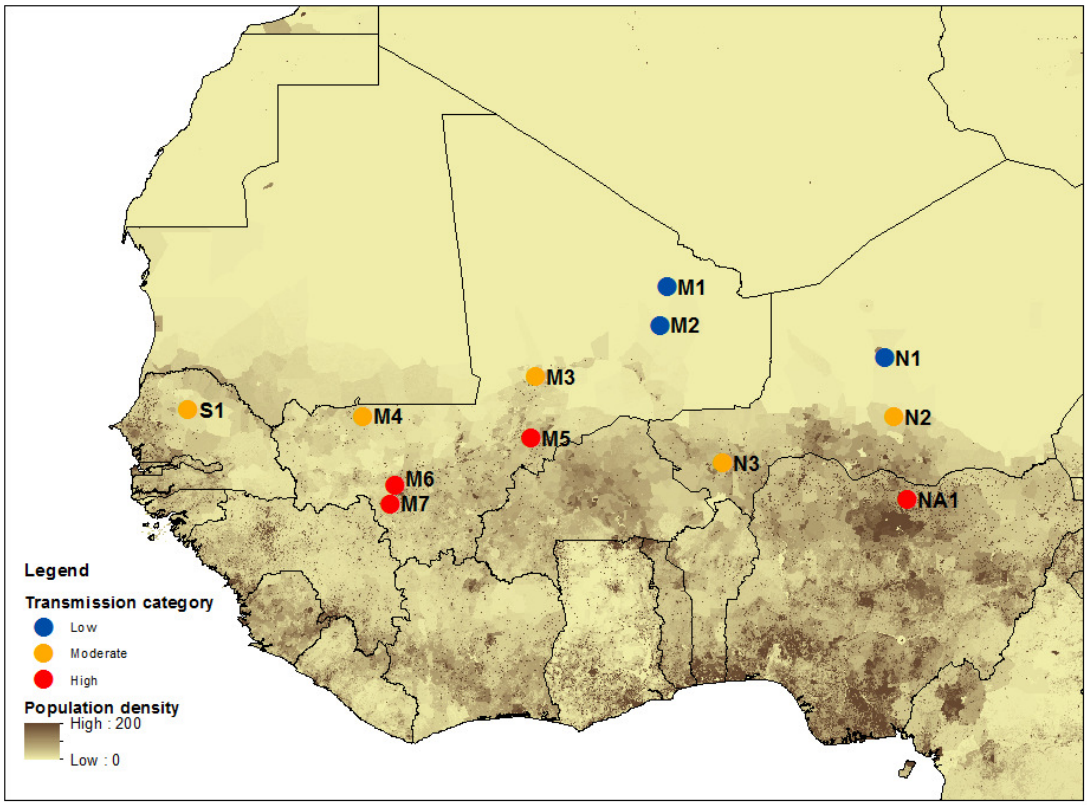

Figure 5.16 Malaria transmission category

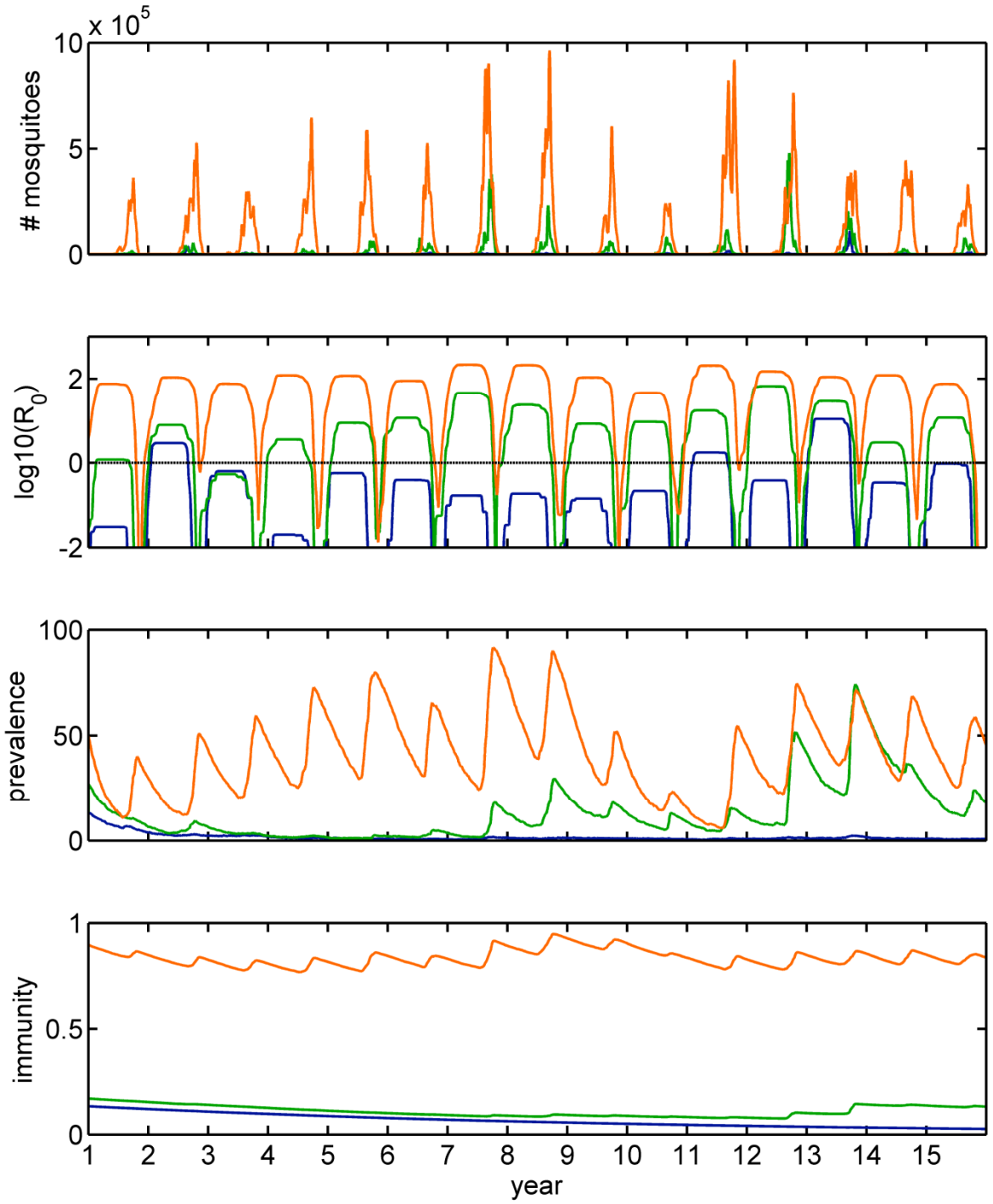

Figure 5.17 Daily values of R_0, EIR, prevalence and immunity in a low (blue), moderate (green), and high (orange) R_0 setting

5.4.3 Plotting results in rainfall-temperature space

The results of the 1575 simulated years were summarized in terms of annual rainfall, mean temperature between July-September (T_{JAS}), R_0, annual EIR, peak prevalence in children aged 2-10, and the mean immunity level in the population. The results were plotted as points in rainfall-temperature space, shown in Figure 5.18 to Figure 5.21. Each point represents the results from a single simulated year. The x-axis shows T_{JAS}, and the y-axis is annual rainfall. We see from the smooth color gradient in Figure 5.18 that R_0 closely follows temperature and rainfall; it was highest during wet and cool years (upper left quadrant) and lowest for hot and dry years (lower right quadrant). Malaria transmission can only be sustained at values of R_0 greater than one, corresponding to the red shaded points. In our simulations, R_0 was less than one for all years with T_{JAS} greater than 35.6 ^{o}C or rainfall less than 168 mm.

The entomological inoculation rate depends on both the vectorial capacity and the prevalence rate within the population. As a result, the EIR scatter plot shown in Figure 5.19 is closely related to the scatter plot for R_0.

Figure 5.20 shows the mean level of the immunity index within the simulated population for each point, and Figure 5.21 shows the peak prevalence level in children aged 2-10 year. We see a general pattern of high prevalence and high immunity under cool and wet conditions, and low prevalence and low immunity under hot and dry conditions. For nearly half of the points, climate suitability for malaria transmission was low, leading to prevalence levels below 10 percent. These two figures show more variability between years with similar climate than the R_0 and EIR maps show, reflecting the more complex dynamics of malaria infections within the human population.

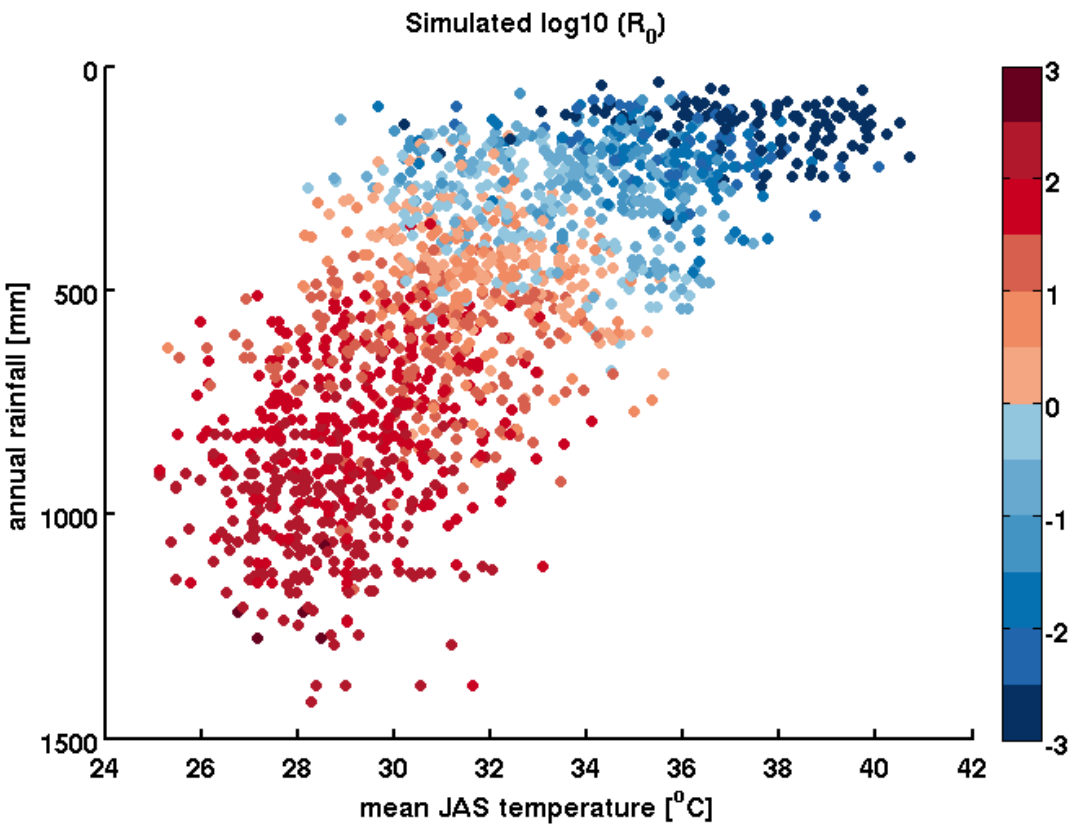

Figure 5.18 Simulated $\log_{10} R_0$ plotted as points in rainfall-temperature space. Each point represents the results of one year's simulation with annual average temperature indicated on the y-axis and average temperature from July through September on the x-axis.

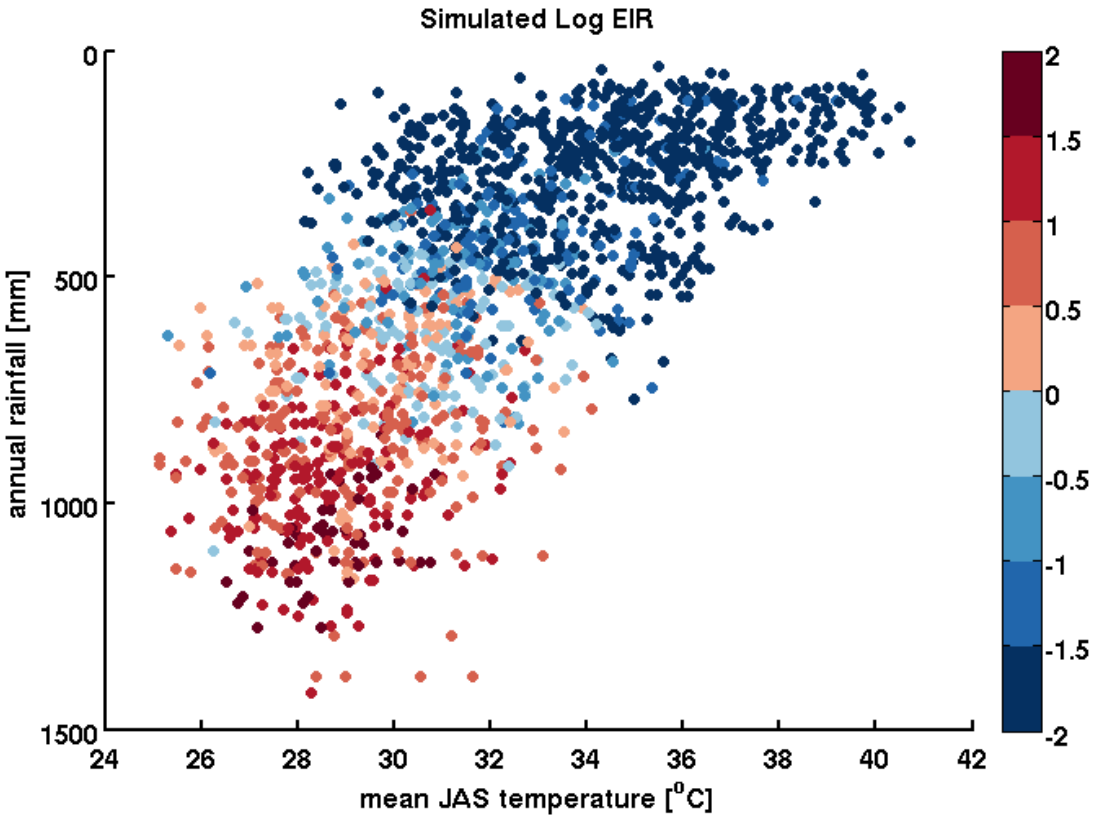

Figure 5.19 Simulated log EIR plotted as points in rainfall-temperature space. Each point represents the results of one year's simulation with annual average temperature indicated on the y-axis and average temperature from July through September on the x-axis.

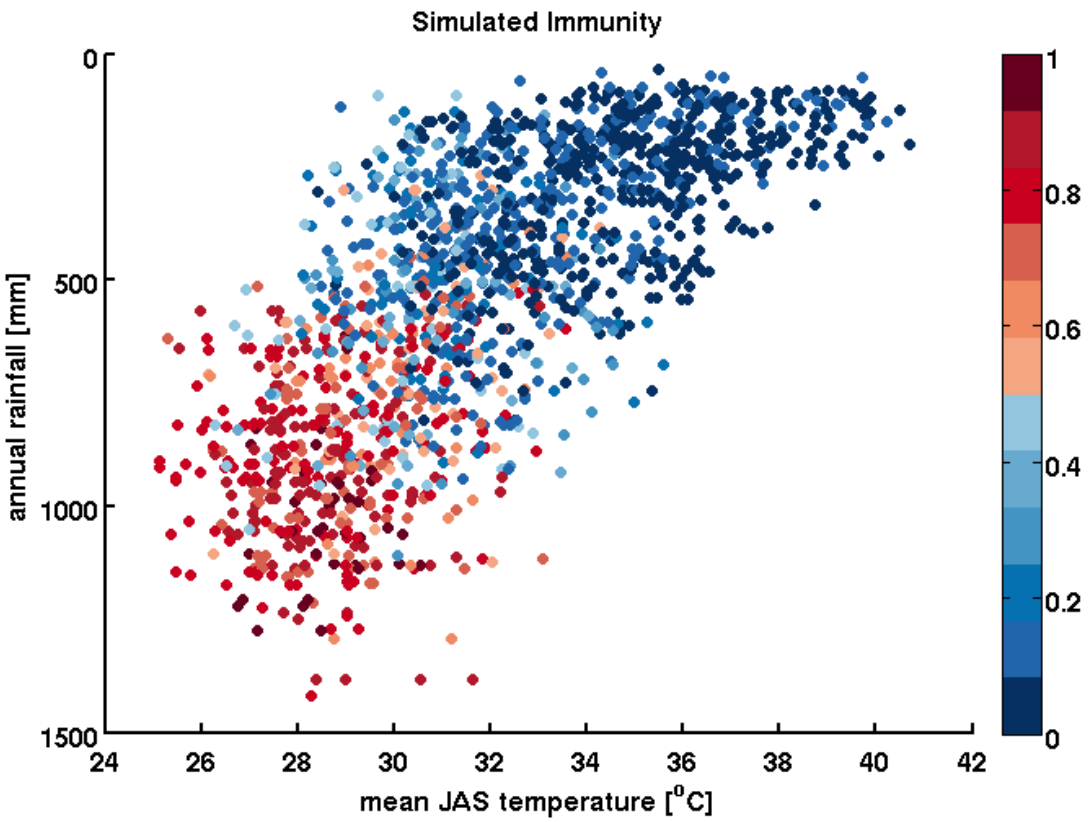

Figure 5.20 Simulated population mean immunity index plotted as points in rainfall-temperature space. Each point represents the results of one year's simulation with annual average temperature indicated on the y-axis and average temperature from July through September on the x-axis.

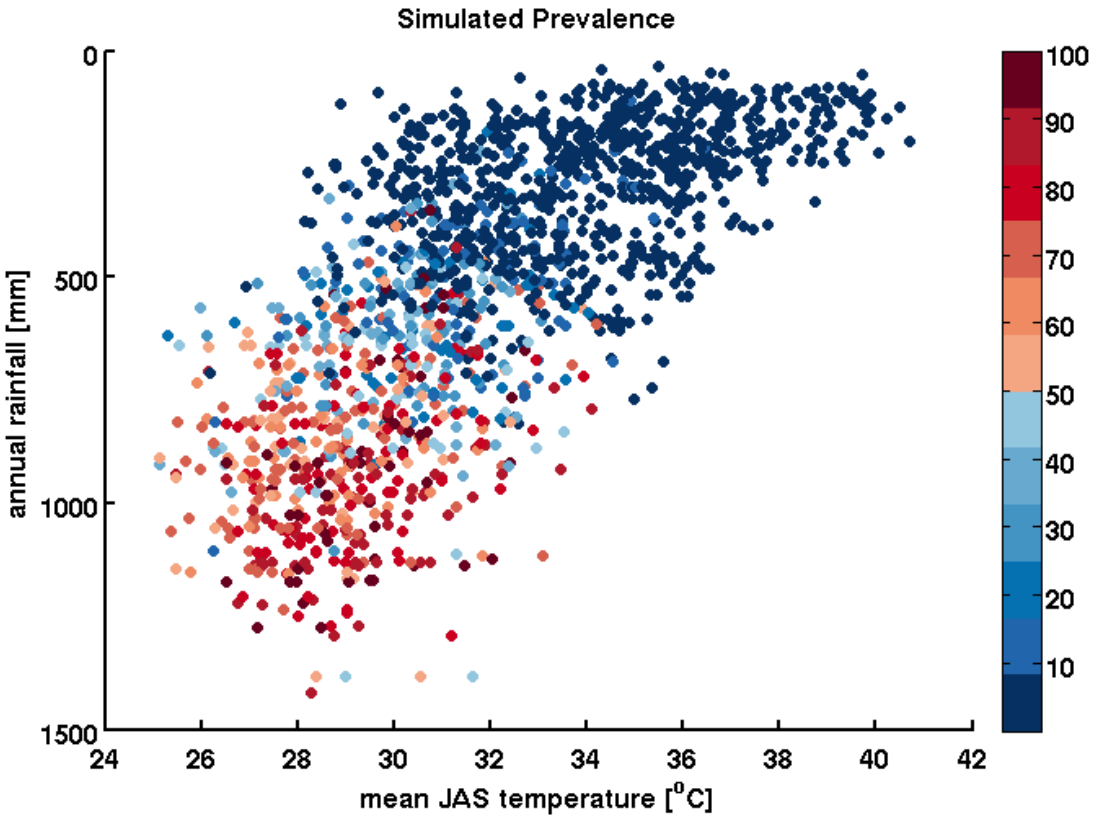

Figure 5.21 Simulated peak prevalence in children aged 2 to 10 plotted as points in rainfall-temperature space. Each point represents the results of one year's simulation with annual average temperature indicated on the y-axis and average temperature from July through September on the x-axis.

Interannual variability in climate and malaria transmission indices can be visualized by plotting results for a single location in rainfall-temperature space and observing the spread between years. For example, the figures below show the four transmission indices in rainfall-temperature space for three locations: a low transmission site (Figure 5.22), a moderate transmission site (Figure 5.23), and a high transmission site (Figure 5.24). Each point summarizes one year of the multiyear simulation for that location.

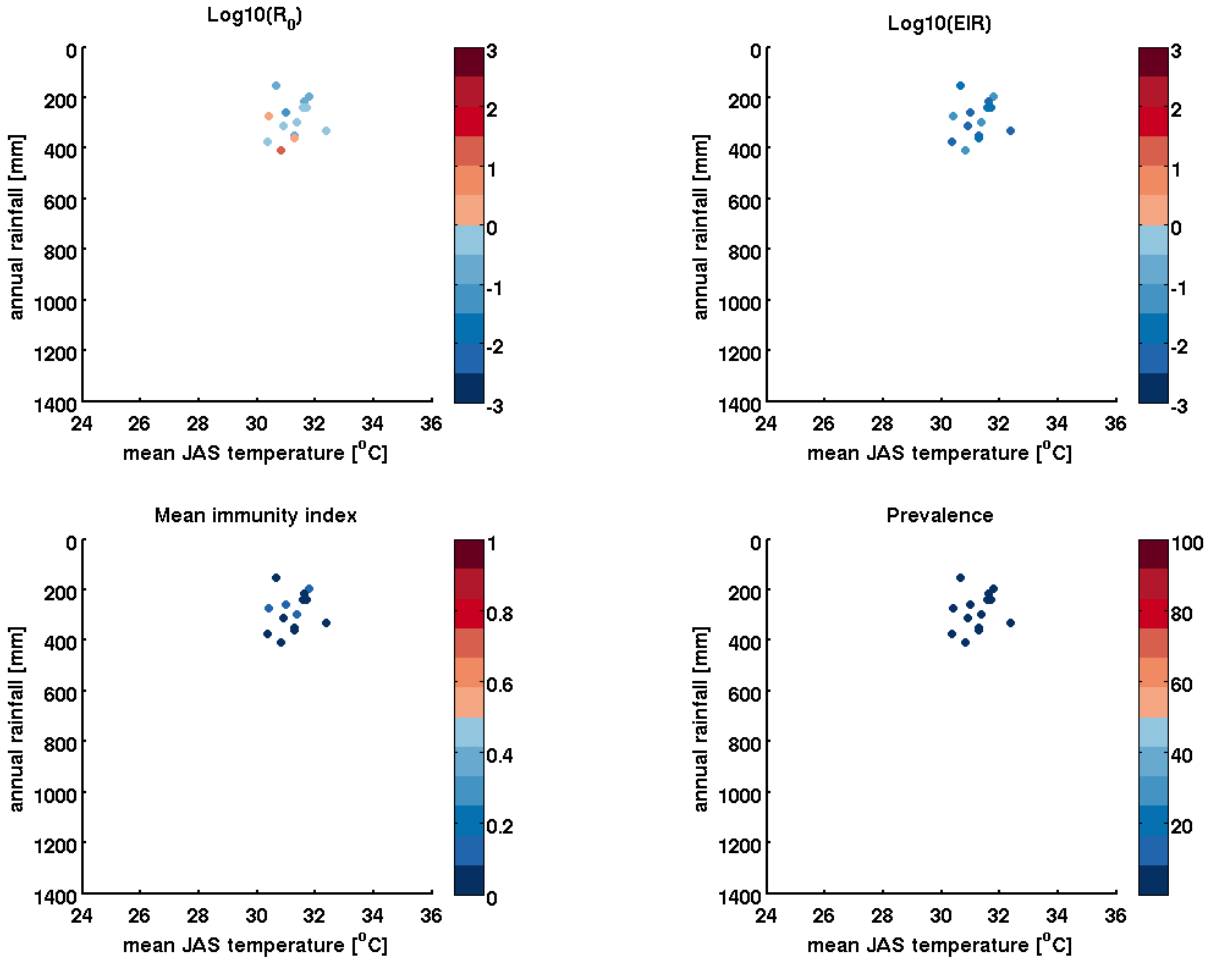

Figure 5.22 Malaria transmission indices for multiyear simulation at M3, a low transmission site

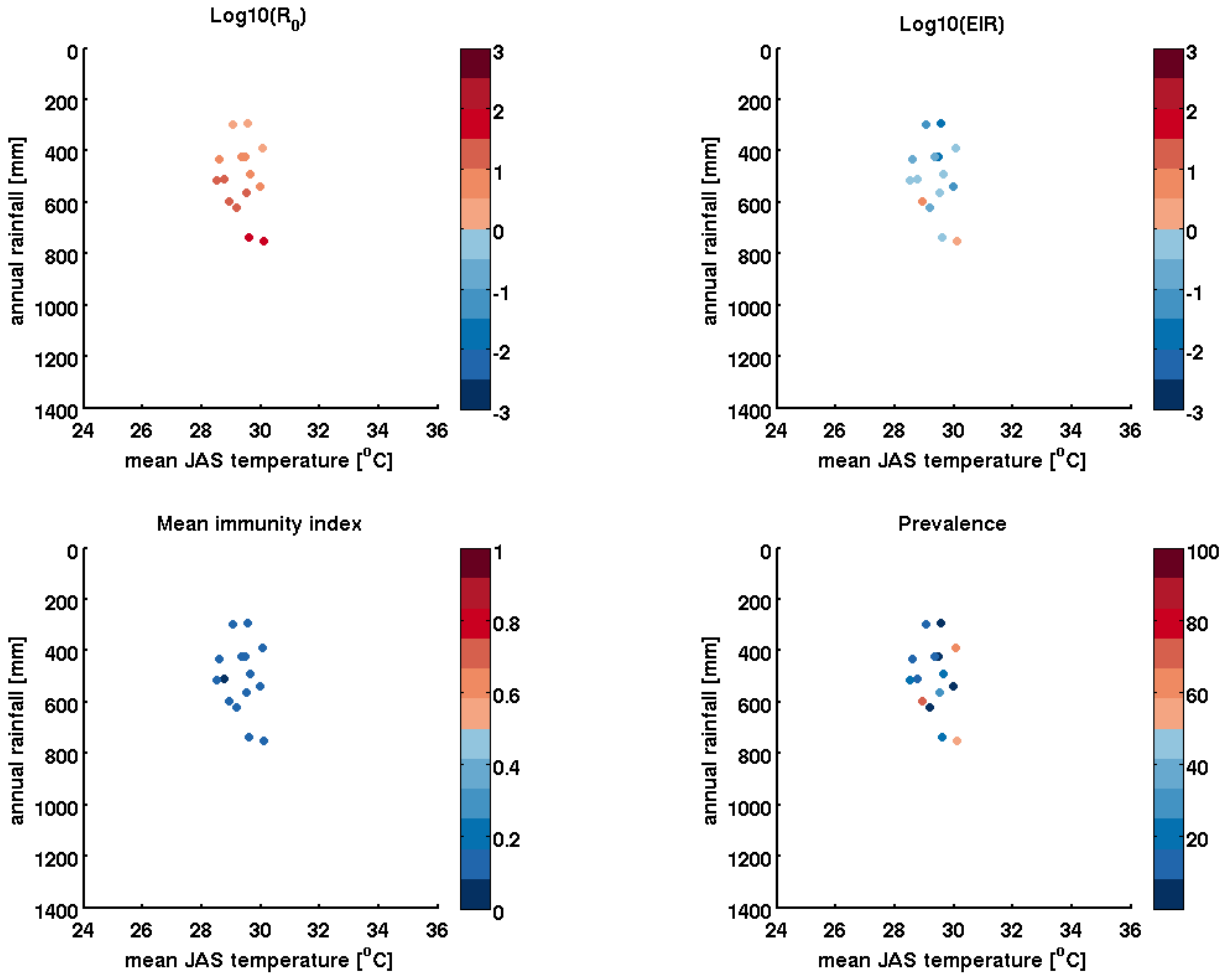

Figure 5.23 Malaria transmission indices at N3, a moderate transmission site

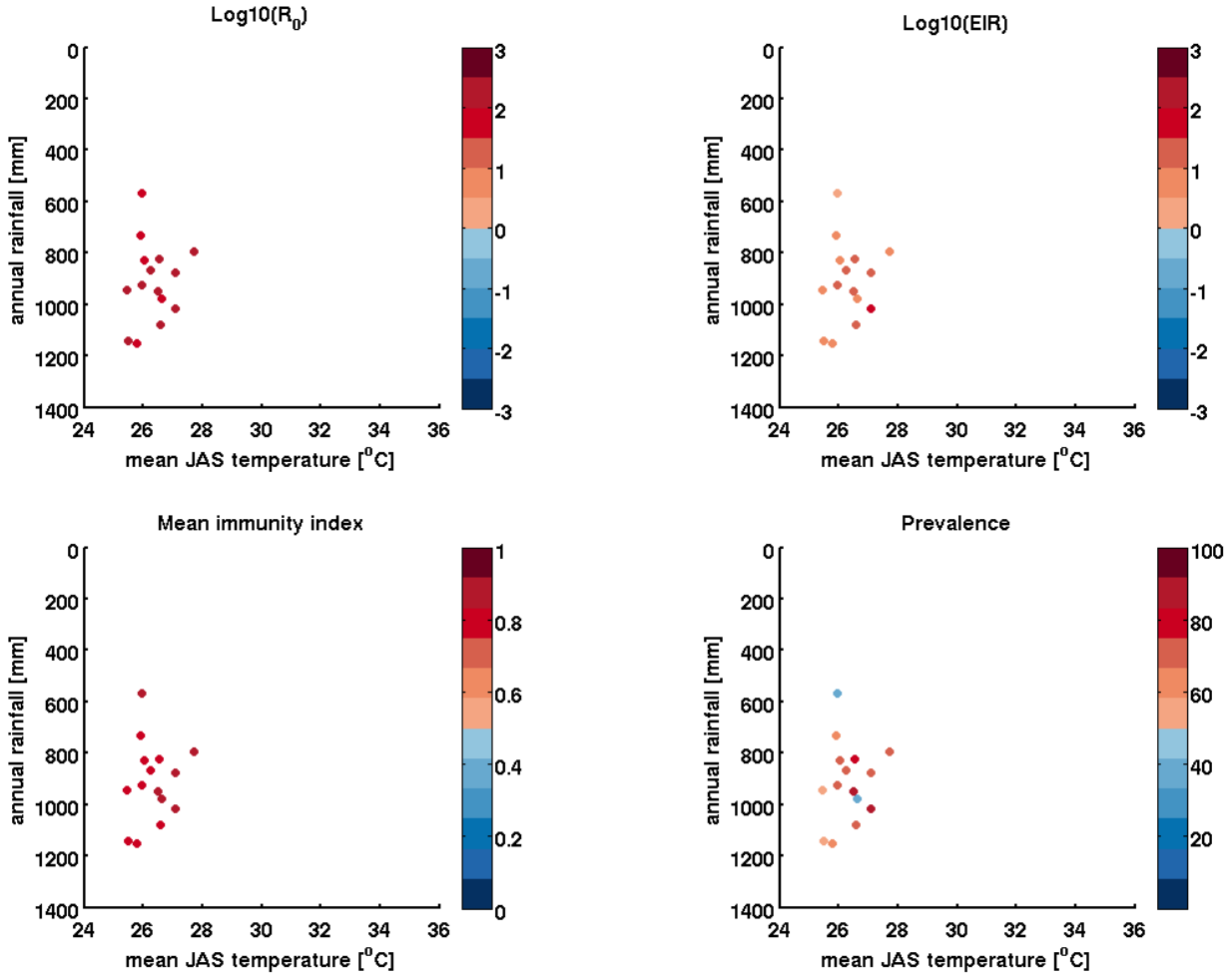

Figure 5.24 Malaria transmission indices at M6, a high transmission site

5.4.4 Establishing general relationships between climate and malaria transmission indices

The results shown in the previous section were used to fit linear regression models to predict R_0, EIR, immunity level and peak prevalence based on annual rainfall and July-September mean temperature. All four indices of malaria transmission were correlated with annual rainfall and TJAS, as well as with each other. The r-squared values are listed in Table 5.2.

Table 5.2 R-squared values for annual rainfall, TJAS and indices of malaria transmission

	Annual rainfall	TJAS	log10 (R0)	log10 (EIR)	Pr 2-10	Imm
Annual rainfall	1.00	0.51	0.72	0.81	0.62	0.68
TJAS	0.51	1.00	0.67	0.64	0.52	0.42
log10 (R0)	0.72	0.67	1.00	0.87	0.51	0.53
log10 (EIR)	0.81	0.64	0.87	1.00	0.70	0.81
Pr 2-10	0.62	0.52	0.51	0.70	1.00	0.65
Imm	0.68	0.42	0.53	0.81	0.65	1.00

Because annual rainfall and TJAS are correlated ($r^2 = .51$), it not possible to attribute variability in the transmission indices to rainfall independently of temperature, or vice versa; the Sahara is unsuitable for malaria transmission because it is both too hot and too dry. An analysis of the semipartial correlation between variables is shown in Figure 5.25. Covarying rainfall and temperature together accounted for between 42 and 47% of the variance in each of the four indices. After removing the common variance between rainfall and TJAS, residualized rainfall

explained an additional 15-30% of variance in the malaria indices, and residualized temperature explained an additional 1-7% of variance. The remaining 19-34% of variance was due to factors other than rainfall and TJAS. The r-squared value is highest for R_0 because this quantity depends on conditions of a given year, with little carry-over from one year to the next. Because EIR is very closely related to R_0, it is also strongly dependent on rainfall and temperature. However, prevalence and acquired immunity to malaria incorporate information about conditions in past years as well, as is discussed in greater detail in sections 5.1 and 5.5. As a result, these variables have a lower r-squared than EIR and R_0.

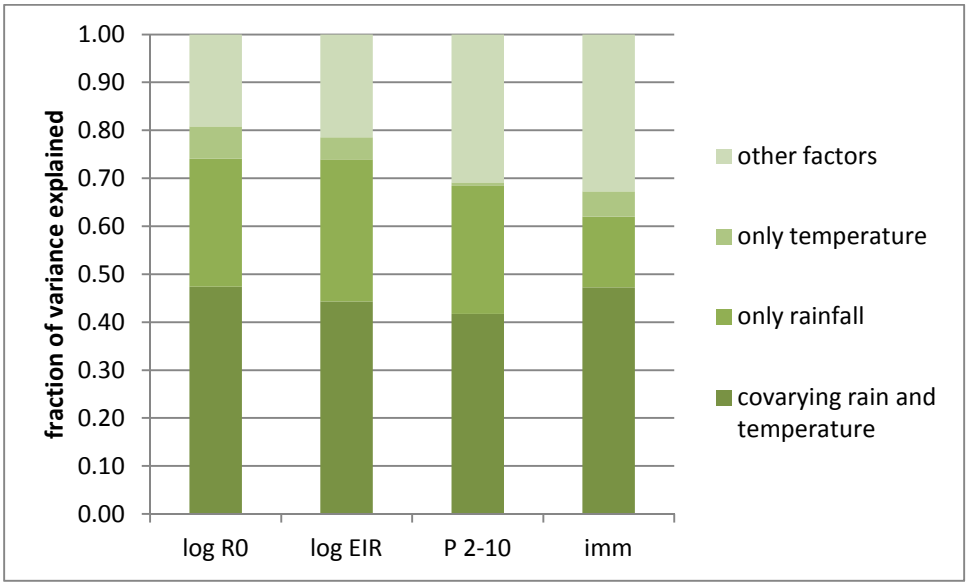

Figure 5.25 Contributions of rainfall and temperature to variability in malaria transmission indices

We developed a linear regression model for each of the malaria transmission indices. Annual rainfall was broken into segments that accounted for threshold effects and other nonlinearities between rainfall and predictor variables. For R_0, the slope of the least-squares regression line

was greater for annual rainfall values less than 690 mm than it was for higher values. In years with rainfall less than 690mm, mosquitoes were constrained by the availability and persistence of breeding sites. Additional rainfall made it more likely that a water pool will last long enough for larvae to emerge as adults, thus increasing R0. In years with heavy rainfall, mosquitoes had many water pools available for breeding, so the abundance was less sensitive to increases in rainfall. Excess rainfall can lead to pools that are too deep for Anopheles mosquitoes, which prefer to breed in shallow areas. Mosquito numbers are also regulated by the carrying capacity of breeding sites in years with ample rainfall.

The relationship between rainfall and EIR had two distinct segments. Rainfall was linearly correlated to the logarithm of EIR for annual rainfall up to 950 mm. Beyond this threshold, the two were no longer correlated, both because of the waning influence of rainfall on mosquito numbers at high rainfall, and also because prevalence did not increase with rainfall beyond this point.

The influence of rainfall on prevalence and the immunity index had three distinct segments. For rainfall values less than 415 mm per year, environmental and entomological conditions were generally insufficient to sustain transmission, resulting in near-zero values of EIR. There was a loose linear relationship between rainfall and malaria indices for annual totals between 415 mm and 950 mm. There was almost no correlation between rainfall greater than 950 mm and malaria transmission, due to the finite number of susceptible individuals, the upper limit of acquiring immunity, and the decreased sensitivity of mosquitoes to high levels of rainfall.

The coefficients and R-squared values for these regression models are listed in Table 5.3, in the form f(TJAS,rain)=a+b*TJAS+c*rain. Regression lines are shown in Appendix B.

Table 5.3 Coefficients and statistics of regression model. Regression models take the form of f(TJAS,rain)=a+b*TJAS+c*rain

	breakpoint	a	b	c	R-squared for segment	R-squared overall	RMSE
$\log_{10}$ R0	rain < 690	4.00E+00	-1.66E-01	3.76E-03	0.72	0.85	0.41
	rain > 690	3.03E+00	-7.71E-02	1.20E-03	0.44		
$\log_{10}$ EIR	rain < 950	1.77E+00	-1.38E-01	3.51E-03	0.75	0.80	0.55
	rain > 950	1.18E+00	-9.60E-03	2.25E-04	0.00		
prevalence	rain < 415	1.52E+01	-4.32E-01	1.24E-02	0.06	0.75	16.52
	415<rain<950	6.66E+01	-3.17E+00	1.06E-01	0.48		
	rain > 950	3.60E+01	1.42E+00	4.48E-04	0.02		
immunity index	rain < 415	7.31E-01	-1.84E-02	2.53E-05	0.24	0.74	0.16
	415<rain<950	1.89E+00	-6.33E-02	7.25E-04	0.53		
	rain > 950	1.16E+00	-1.81E-02	1.38E-04	0.05		

The regression models were used to create scatter plots similar to those shown in Figure 5.18 to Figure 5.21. The figures below compare the scatter plots simulated by HYDREMATS to the scatter plots from our regression models.

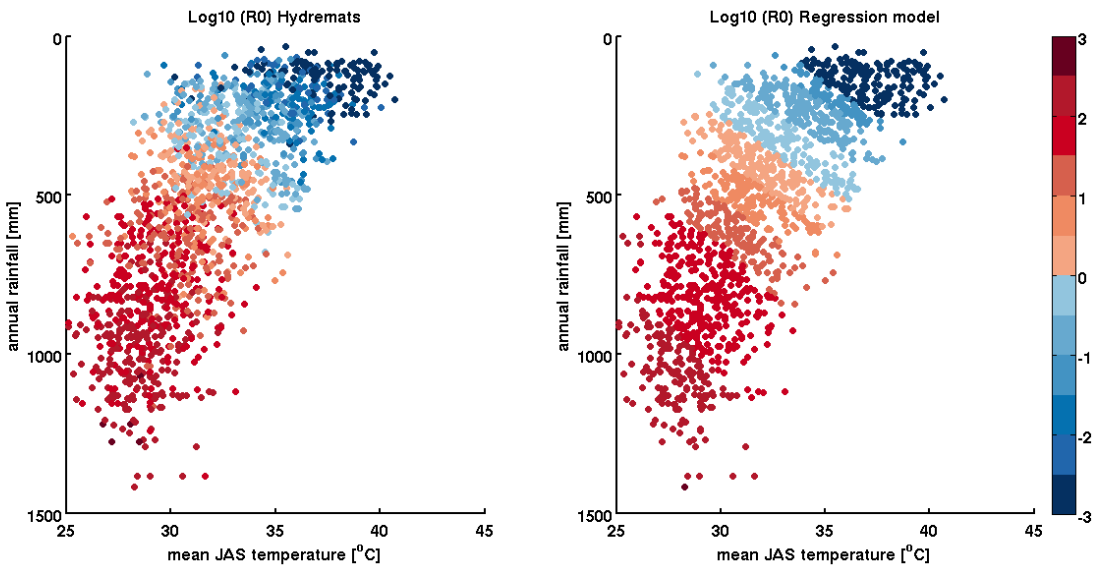

Figure 5.26 R0 as a function of rainfall and temperature simulated by HYDREMATS (left) and the regression model (right)

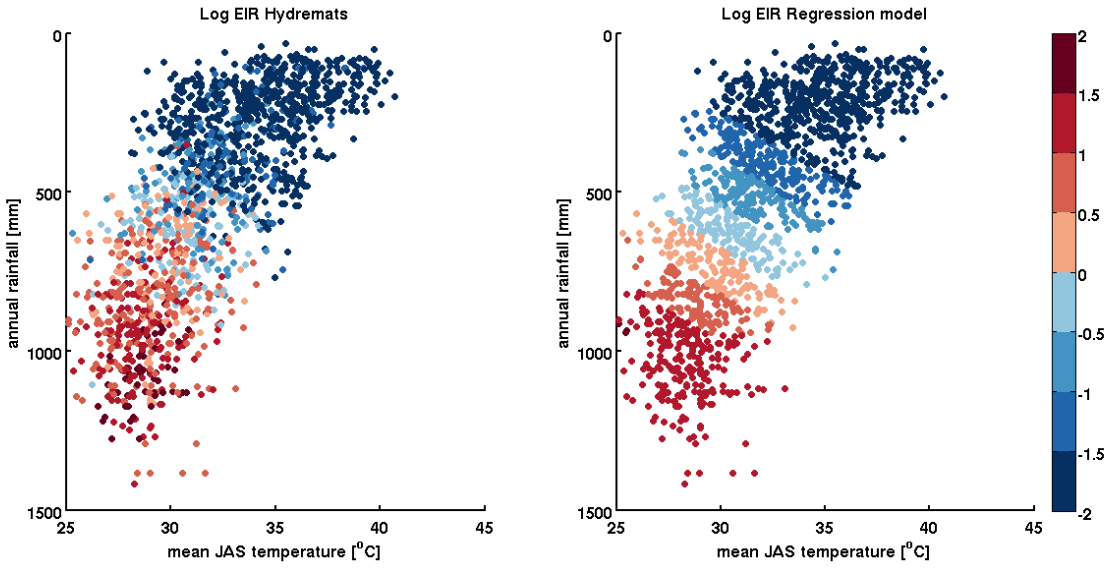

Figure 5.27 EIR as a function of rainfall and temperature simulated by HYDREMATS (left) and the regression model (right)

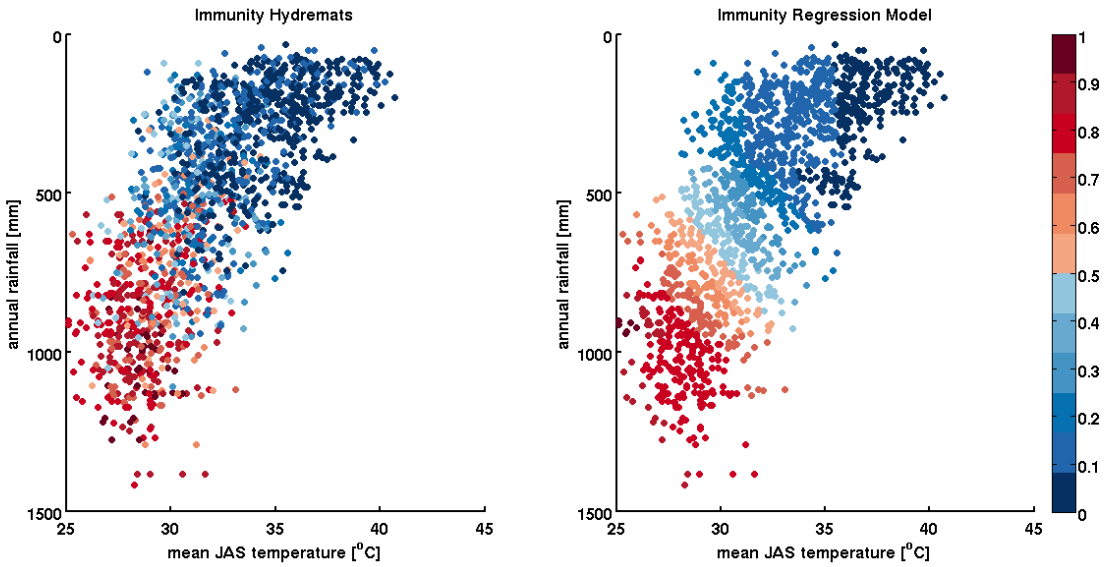

Figure 5.28 Immunity index as a function of rainfall and temperature simulated by HYDREMATS (left) and the regression model (right)

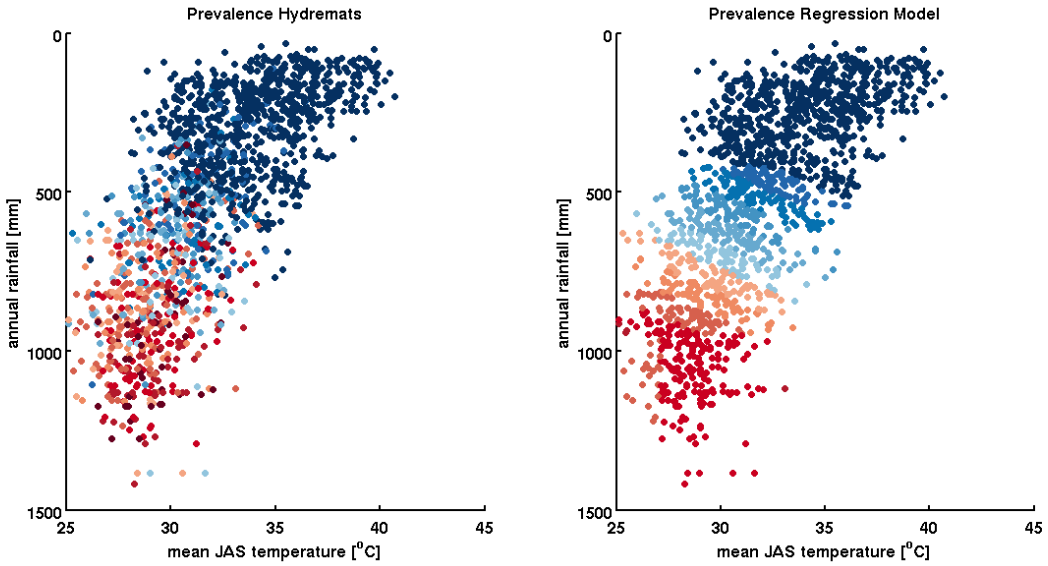

Figure 5.29 Malaria prevalence as a function of rainfall and temperature simulated by HYDREMATS (left) and the regression model (right)

These regression models can be used to estimate R_0, EIR, prevalence and the immunity index using annual rainfall and temperature data from historical climate observations or predictions from climate models.

5.4.5 Comparison between equilibrium and multiyear simulations

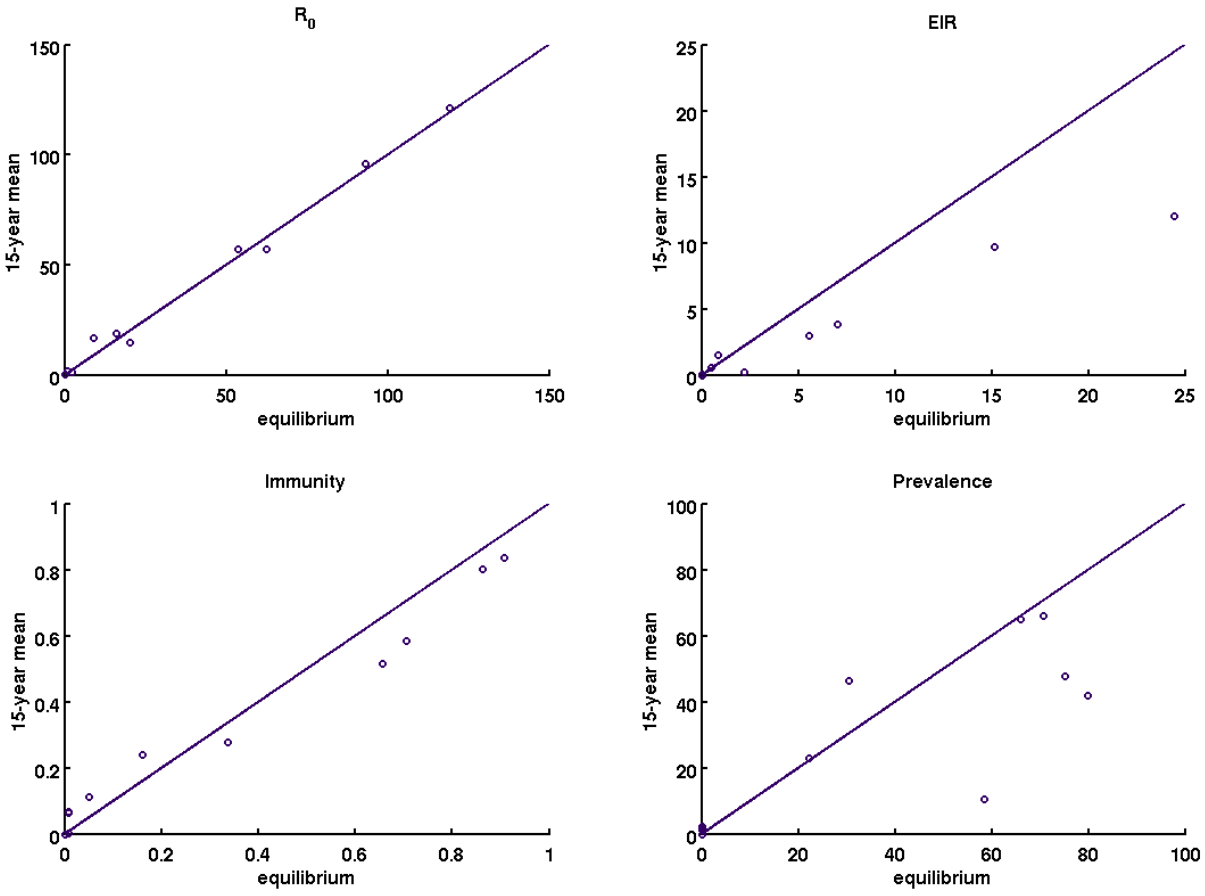

Figure 5.30 Comparison of results from the equilibrium year to the mean of the multiyear simulation. The solid line shows the y=x line for reference.

The previous results emphasize the extent of interannual variability in our simulations. Figure 5.30 shows how the equilibrium result compares to the mean of the multiyear simulation for each of the four malaria transmission indices. The equilibrium R0 matches well with the multiyear by

design; the equilibrium year was selected on the basis of having R0 closest to the 15 year mean. The equilibrium immunity was close to the interannual mean immunity. This was expected, as the slow-varying immunity index effectively incorporates information from all 15-years, making it less susceptible to short term fluctuations. For three locations, S1, M5 and NA1, the equilibrium prevalence was significantly higher than the mean of the multiyear simulation. This may be an example of the complexity of interannual variability in malaria transmission dynamics.

As an example, results from the multiyear simulation of the most obvious outlier, S1, is shown in Figure 5.31. As shown in the top plot, annual rainfall varied between 250 and 570 mm. During dry years, mosquito populations were limited, R0 is very low and very little malaria transmission occurred. As a result, prevalence fell to very low levels, and human immunity began to wane. In the final four years of the simulation, a succession of wet years with R0 values between 20 and 80 led to epidemics where the parasite spread to nearly half of the population. It is interesting to note that highest prevalence occurred in year 14, where R0 was 22. Years 4 and 8 also had R0 values of 22, but resulted in minimal disease transmission because the parasite rate was very low. The equilibrium simulation used climate input from year 7 of the multiyear simulation, with an R0 value of 20, and stabilized with a peak prevalence value of 58%. Similar figures are presented for the other 11 sites in Appendix C.

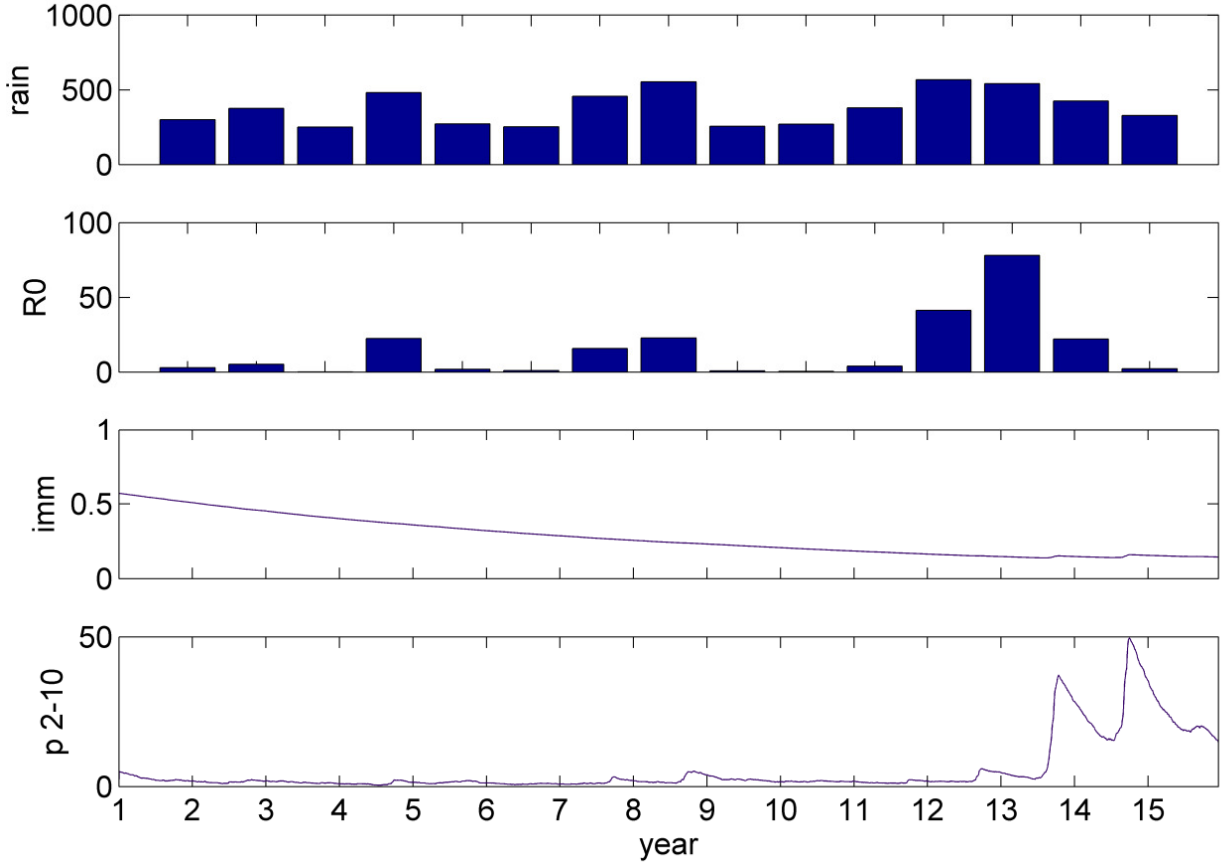

Figure 5.31 Interannual dynamics for site S1 multiyear simulation

5.5 Discussion

This chapter comprises of several major sections. This first was a comparison of simulated data to observations. While the model had been compared extensively to field data from Banizoumbou and Zindarou, two neighboring villages in southwestern Niger (Bomblies *et al.*, 2008; Bomblies *et al.*, 2009; Yamana *et al.*, 2013), it had not been tested outside of this region. By comparing HYDREMATS to entomological and epidemiological data from various sources

across multiple climate zones of West Africa, we increased our confidence in the model's ability to simulate malaria conditions in these areas. In particular, the results shown in Figure 5.12 serve as an important test of the immunity component of HYDREMATS. Like the hydrology and entomology components, the immunity component was parameterized using published estimates and fitting conditions from Banizoumbou and Niger (Yamana *et al.*, 2013). This result shows that the disease transmission model is able to simulate the feedbacks between inoculations, immunity and infections for a wide range of malaria transmission levels. These feedbacks are highly nonlinear, and are still not fully understood (Langhorne *et al.*, 2008). A recent paper tested the ability of five well known malaria transmission models to reproduce this relationship (Wallace *et al.*, 2014). The results of that comparison found that half of the models failed this basic test. While it is certainly possible to reproduce observed results for the wrong reasons, the similarity between our simulated results and observations, as well as our process-oriented modeling approach, suggest that HYDREMATS has a reasonable representation of the main processes linking the environmental, entomological, and immunological aspects of malaria transmission.

Our multiyear simulations highlighted the interannual variability in malaria transmission. This variability is not captured in estimates that give only a mean value of malaria transmission indices. Our simulations showed that R_0 routinely varied by as much as one or two orders of magnitude from year to year. In areas with very high or very low levels of R_0, these variations may be less important. However in the moderate transmission areas around the Sahel where R_0 is close to the threshold value of 1, these differences can make the difference between no malaria transmission and epidemics where more than half of the population is infected. The effects of these epidemics are exacerbated by the low levels of immunity within these populations, leading

to higher rates of severe forms of disease. In the context of climate change, we should focus on these locations where prevalence is most sensitive to changes in R_0.

The framework of analyzing malaria transmission indices as points on a rainfall-TJAS scatter plot developed in section 5.4.3 allows us to visualize interannual variability in climate and the corresponding variability in transmission indices by observing the spread between points for a single location. It also shows variability between years with similar climates by comparing adjacent points. While the annual entomological indices were closely related to corresponding annual rainfall and temperature, the immunological indices showed much greater variability. This is because the human immune system has a memory of past malaria exposure. The immunity index, a simplified measure we use to represent the level of acquired immunity in a population, operates on the timescale of years; human agents slowly build immunity with each infectious bite received over their lifetime. Outliers on the immunity scatter plot may represent years where the climate is more or less favorable for malaria transmission than usual. For example, a high-immunity point in the dry and hot portion of the scatter plot in Figure 5.20 could indicate a population with higher levels of immunity than would be expected for that climate due to high EIR in previous years.

Prevalence rates are influenced by entomological conditions and immunity levels in the human population, as well as the recent history of malaria within the population. While the entomological indices generally do not carry over from one wet season to the next, the malaria parasite in untreated humans can persist over the dry season and spread to new individuals when the mosquito population reestablishes itself the following wet season. As a result, malaria prevalence for a given year also reflects conditions of the previous year. Even given identical climate and entomological conditions and identical populations, the parasite rate can differ based

on the background parasite rate. For example, our simulations of the low transmission sites showed several examples of years where R_0 was greater than one but did not result in an epidemic. Even though there were many mosquitoes, the malaria parasite was only present in a small number of people, making it unlikely that the mosquitoes would pick up the infection. If more people were carrying the parasite at the beginning of the transmission season, it would have been much more likely that mosquitoes would have been infected early in the wet season and the disease would have spread.

The statistical analysis of our simulated results described in Section 5.4.4 show the strong influence of rainfall and temperature in determining various aspects of the malaria transmission cycle. These two variables alone accounted for 85% of the variability in R_0 between our simulations. The remaining 15% variability is likely due to the timing of rainfall within a wet season, soil and vegetation properties that influence infiltration and evaporation rates, other environmental inputs such as wind and humidity, and mosquito population dynamics. Unexplained variability in prevalence is likely due to complex interannual dynamics of the parasite within the human population discussed earlier in this chapter. It is important to note that there are many other factors that influence the malaria transmission that were not included in this study. We assumed constant microtopography, population size and age structure, and village layout in all of our simulations. Varying these factors would add variability to village scale R_0 which would be passed on to the other indices of transmission. Our focus is on the environmental determinants of malaria transmission. As such, we do not simulate varying levels of malaria control, which would certainly add significant variability to prevalence, EIR and the immunity index. Despite these caveats, the regression model we developed here provides a useful tool to estimate each of these indices of malaria transmission. The framework of plotting

years as points on a temperature-rainfall scatter plot developed here provide a useful way to visualize interannual variability at a single location as a cloud of points reflecting different rainfall and temperature conditions. It is also a useful way to visualize variability between points with similar mean climate, which helps to understand the uncertainty in estimates using these variables.

In the final section of this chapter, differences between the average transmission indices over the 15-year simulations were compared to the indices from our equilibrium simulations, where a year with mean climate conditions was repeated until a steady state was achieved. By studying the interannual dynamics at S1, a moderate transmission site where R_0 was less than one for about a quarter of the simulated years but as 80 other years, we noticed the importance of initial prevalence rates. Three years with nearly identical values of R0 led to drastically different outcomes, primarily due to the availability of the parasite within the population. The example of S1 also provides a cautionary tale for communities facing the prospect of malaria elimination. After a decade with almost no malaria infections, a succession of favorable years combined with waning immunity led to a rapid and drastic resurgence of disease.

5.6 Conclusions

In this chapter, we examined the malaria transmission dynamics at 12 West African locations across a range of climate zones, with a focus on areas where we expected malaria prevalence to be sensitive to changes in environmental conditions. We demonstrated that HYDREMATS is able to produce a reasonable representation of entomological and epidemiological conditions throughout our study area. We classified our 12 sites as having high, moderate or low transmission potential based on their levels of R_0.

We developed a framework of presenting results as scatter plots in rainfall-temperature space. This provides a convenient way to visualize interannual variability at a given location as a cloud within the rainfall-temperature space, and to assess the range of results that can occur under similar climate conditions.

We developed a regression models to estimate R_0, EIR, prevalence and immunity using annual rainfall and mean temperature between July-September that explained 74-85% of the variability in our simulated results.

Finally, we emphasized both the extent and the importance of interannual variability. We showed that R_0 can vary by several orders of magnitude at a single site, leading to very different potential malaria outcomes. As a result, single estimates of malaria transmission indices, whether based on mean conditions or coinciding with a field campaign, miss important details in describing malaria transmission dynamics.

6 Predicting the impacts of climate change on malaria transmission in West Africa

6.1 Introduction

Current trends in climate point towards a warmer future with altered rainfall. As these changes become increasingly likely, there has been significant interest in assessing the impacts of climate change on human aspects such as public health. If we understand the relationships between climate and disease, we can project these relationships into different climate scenarios and make comparisons between the old and new conditions. This type of study has become more common (for example, those reviewed in (Lafferty, 2009; Rohr *et al.*, 2011)). While many of these studies are usually very deliberate in developing and tuning their models of disease transmission, there is often less attention given to the selection of climate projections. Frequently, they use climate projections from one or two general circulation models (GCMs), with no explanation of how the GCMs were selected (Moore *et al.*, 2012; Parham & Michael, 2009; Peterson, 2009; Rogers & Randolph, 2000; Tanser *et al.*, 2003). The choice of climate projections is an important aspect of climate change studies, particularly in Africa, where there is substantial disagreement between GCMs (Roehrig *et al.*, 2013). In this chapter, we test the skill of climate models in their representation of historical climate variables most relevant to malaria transmission in West Africa. We then use the most credible climate predictions to predict the future of malaria transmission in this region.

6.2 Assessing skill of current climate models

We examined historical temperature and rainfall data simulated by 23 GCMs and ESMs from the Coupled Model Intercomparison Project Phase 5 (CMIP5) (Taylor *et al.*, 2012). We examined at least one GCM from each institution that had model output available in the Earth Systems Grid Federation data portal (http://dev.esg.anl.gov) as of August 2012. In cases where an institution provided multiple models or different versions of the same model, we selected the model with highest resolution, and the model that appeared to be featured most prominently in that institution's website. The models analyzed are listed in Table 6.1. The main features of the climate models are described in the IPCC Assessment Report 5, Working Group 1, Chapter 9 (Flato *et al.*, 2013).

In order to assess the skill of each model, we compared output from the models' CMIP5 historical simulations (Taylor *et al.*, 2012) to data from the Climatic Research Unit Time-Series Version 3.21 (CRU TS 3.21). The CMIP5 family of historical simulations runs from 1850 to 2005, forced by observed concentrations of greenhouse gasses.

The variables of interest were temperature and rainfall, as these are the variables most relevant to malaria transmission, and are required as inputs for HYDREMATS, our malaria transmission model. We defined the region of interest, West Africa, as the area bounded by 18^{o}W to 16^{o}E, and 11^{o}N and 21.5^{o}N. This area was further divided into three zones corresponding roughly to the Sahelo-Sahara (Zone 1: 18^{o}N-21.5^{o}N), Sahel (Zone 2: 14.5^{o}N-18^{o}N), and Soudan (Zone 3: 11^{o}N-14.5^{o}N) ecoclimate zones (Nicholson, 1993).

To test the ability of the models to reproduce the seasonal climate in this region, we calculated the average monthly rainfall and temperature from 1930-2005 using CRU TS 3.21, shown in

Figure 6.1 and Figure 6.2. We then compared the observed seasonal cycles to simulated average monthly rainfall and temperature from each of the 21 climate models. The models were ranked from best to worst based on the sum of squared errors (SSE) of average monthly rainfall and temperature.

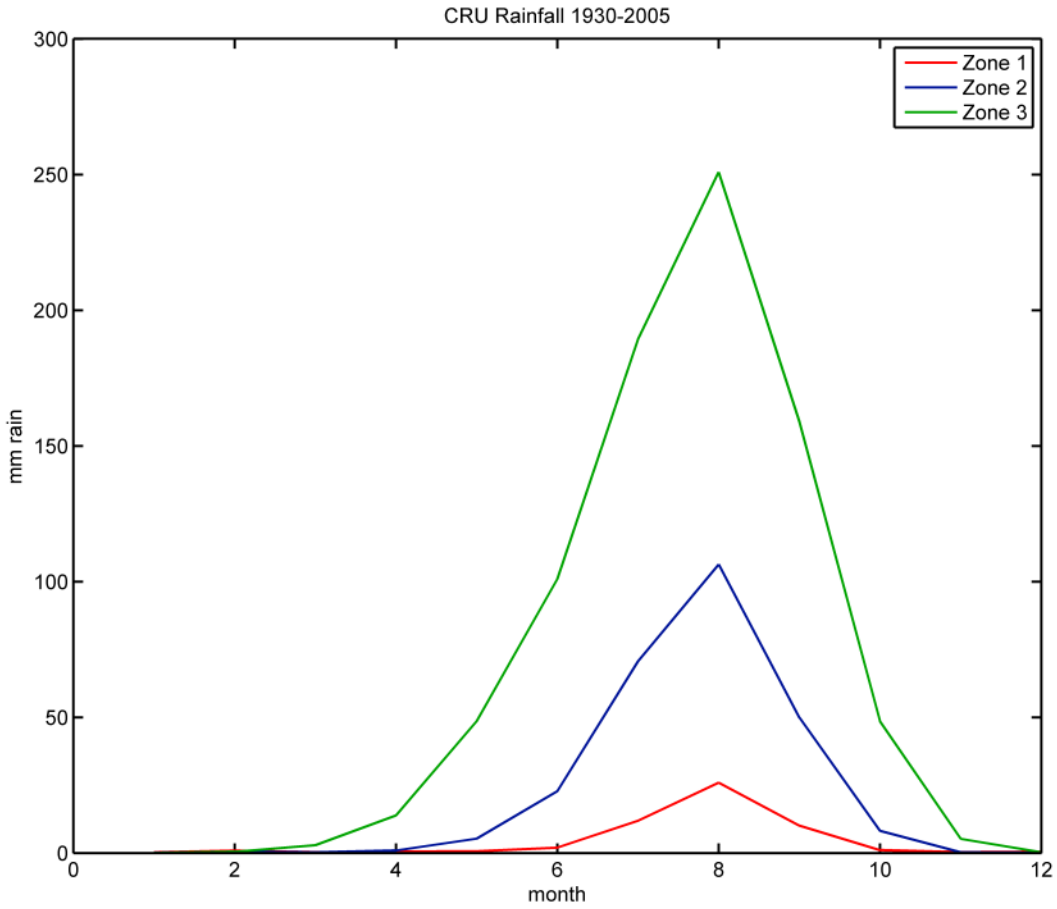

Figure 6.1 Historical monthly rainfall for Zones 1, 2 and 3

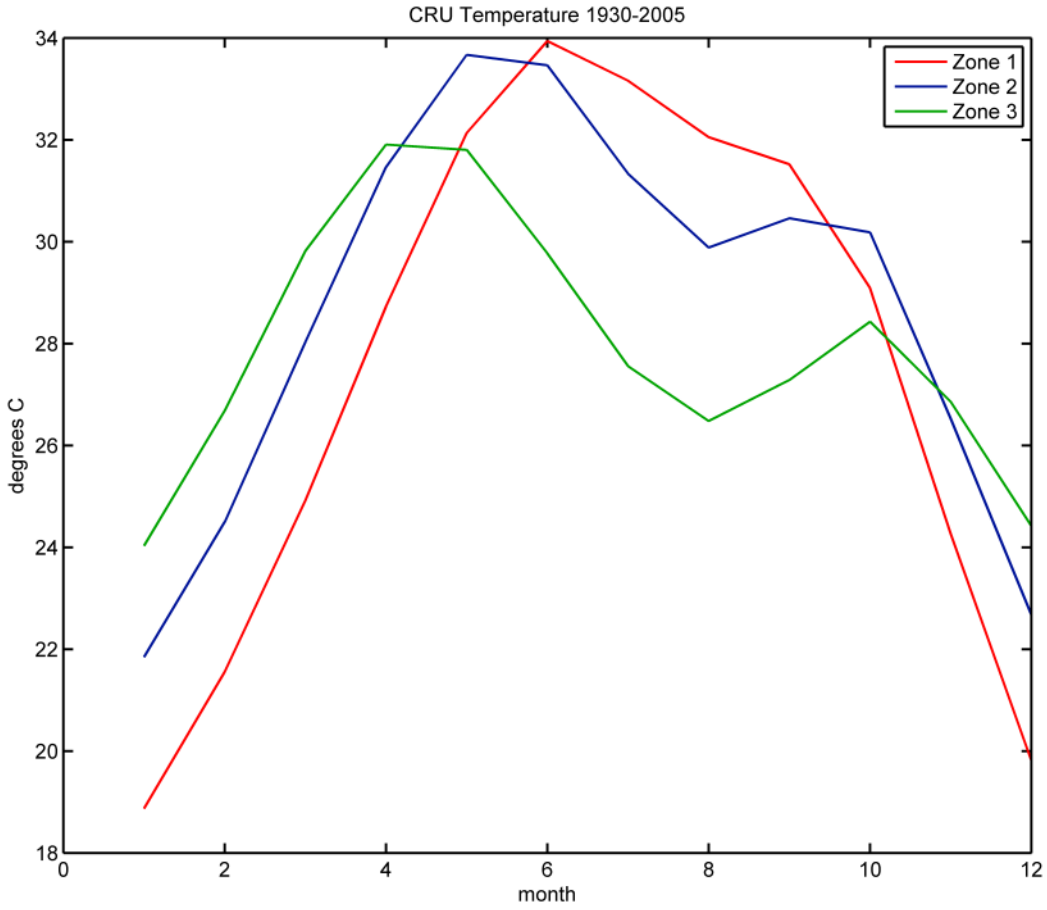

Figure 6.2 Historical monthly temperature for Zones 1, 2 and 3.

The SSE was computed for each model in each of six measurements: average monthly rainfall in Zones 1-3 and average monthly temperature in Zones 1-3. For each of six measures, the models were ranked from best to worst using the SSEs. We then assigned 1 point to the top six models for each measure, and subtracted 1 point for the bottom six models.

The highest scoring models were BNU-ESM (6 points), MIROC5 (5 points), MPI-ESM-MR (4 points), CANESM2 (3 points) and CCSM4 (3 points).

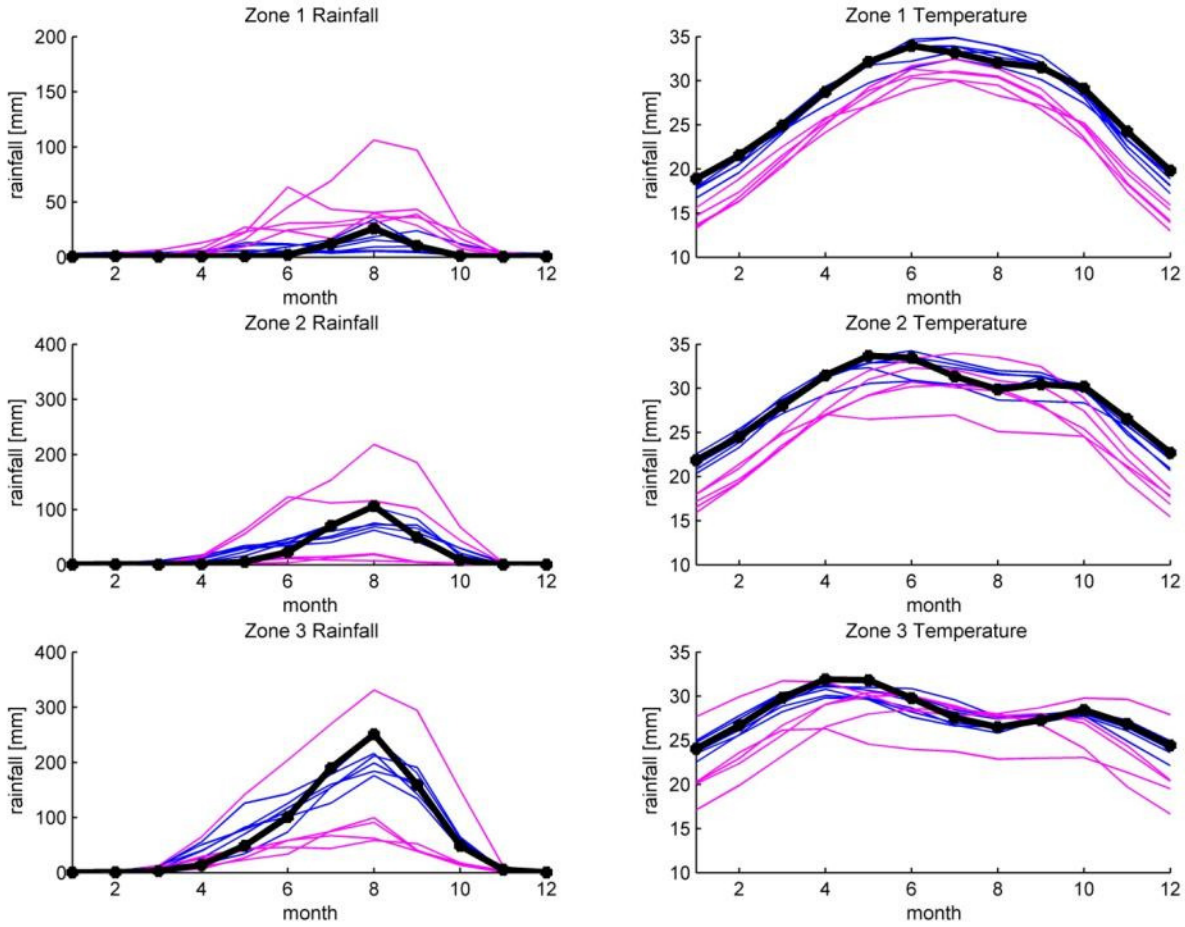

Figure 6.3 Monthly rainfall and temperature from CRU (black line), the six best models (blue), and the six worst models (pink)

Table 6.1 Performance of CMIP5 Climate Models

Model Name	Rainfall Score			Temperature Score			Total
	Zone 1	**Zone 2**	**Zone 3**	**Zone 1**	**Zone 2**	**Zone 3**	
BNU-ESM	1	1	1	1	1	1	6
MIROC5	1	1		1	1	1	5
MPI-ESM-MR	1		1	1	1		4
CANESM2				1	1	1	3
CCSM4	1	1	1				3
FGOALS-g2	-1	1		1	1		2
CESM1-CAM5		1	1				2
MIROC-ESM-CHEM						1	1
FIO-ESM	1						1
BCC-CSM1-1						1	1
CNRM-CM5	-1	1	1				1
CSIRO-Mk3-6-0	-1	-1		1	1	1	1
CMCC-CM							0
GFDL-CM3							0
GISS-E2-H						-1	-1
HadGEM2-AO				-1			-1
ACCESS		-1	-1				-2
MRI-CGCM3		-1	-1		-1		-3
EC-EARTH	-1		1	-1	-1	-1	-3
IPSL-CM5A-MR				-1	-1	-1	-3
GFDL-ESM2M	-1	-1	-1				-3
inmcm4	1		-1	-1	-1	-1	-3
HadGEM2-CC		-1	-1	-1	-1	-1	-5

We then examined mean annual rainfall from 1930 to 2005 for each of the top five models to see whether they reproduced the spatial characteristics of observed rainfall (Figure 6.4). Specifically, we were interested in whether the models could reproduce the observed gradient in rainfall travelling from north to south, while remaining relatively constant from east to west. We looked for the maxima along the Guinean coast. While MIROC5 performed well in the area used for our initial analysis, we eliminated this model because it greatly overestimated rainfall in the southern half of West Africa. We also eliminated CanESM because its rainfall extended too far north into the Sahara desert, and its isohyets peaked between 5^{o}W and 5^{o}E, unlike the roughly latitudinal isohyets in the observations.

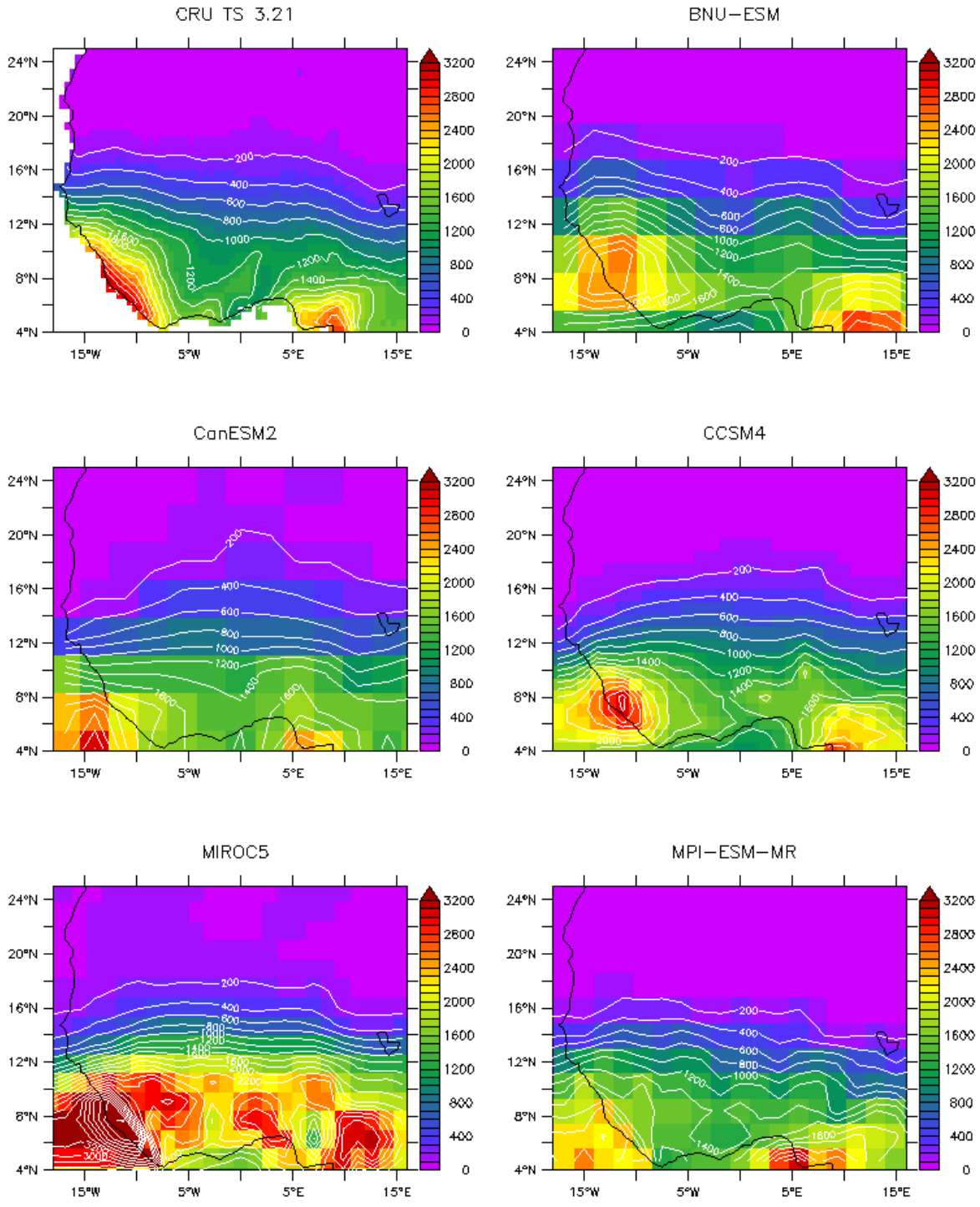

Figure 6.4 Observed and simulated mean annual rainfall over West Africa 1930-2005

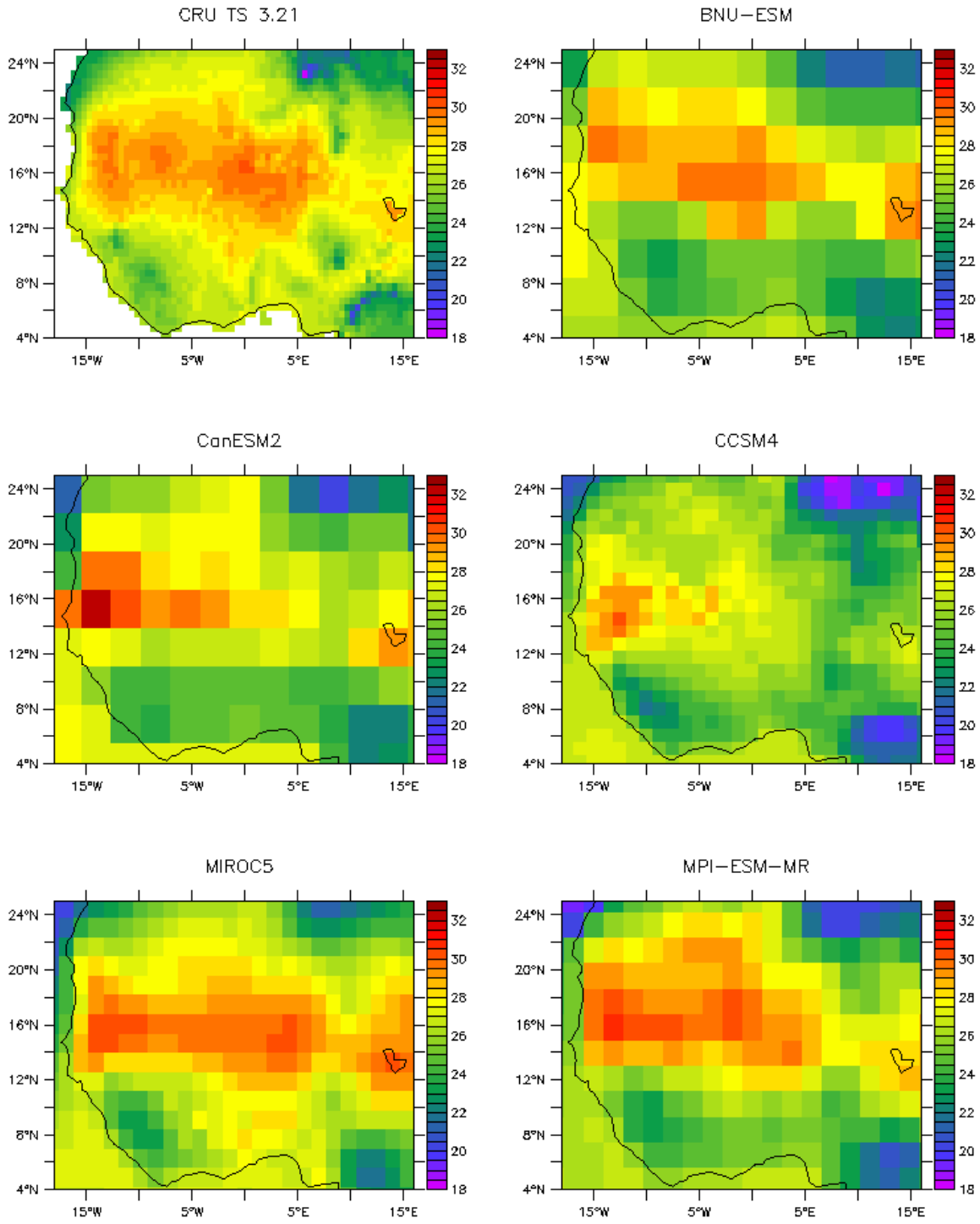

Figure 6.5 Observed and simulated mean temperature over West Africa 1930-2005

Based on this analysis, we determined that the following models had the best representation of the environmental variables related to malaria transmission in West Africa: BNU-ESM, CCSM4, and MPI-ESM-MR. However, a final literature review found that BNU-ESM had a large error in simulating the global atmospheric water balance, leading to a ghost source of precipitation and false latent cooling (Mariotti *et al.*, 2011). As a result, we eliminated BNU-ESM from further consideration.

As a final test, we examined the coefficient of variation (CV) in CRU and the final two models, shown in Figure 6.6. The very high values of the CV in the northernmost latitudes are due to near-zero value of mean rainfall in the denominator of the CV. Both models reproduce the general spatial patterns in the observed CV. CCSM4 underestimates the CV between 14-16 degrees N, while MPI-ESM-MR overestimates the CV north of 16 degrees N. As neither model appeared to be unreasonable in its representation of interannual variability, we proceeded with to use both models for our simulations of future malaria transmission.

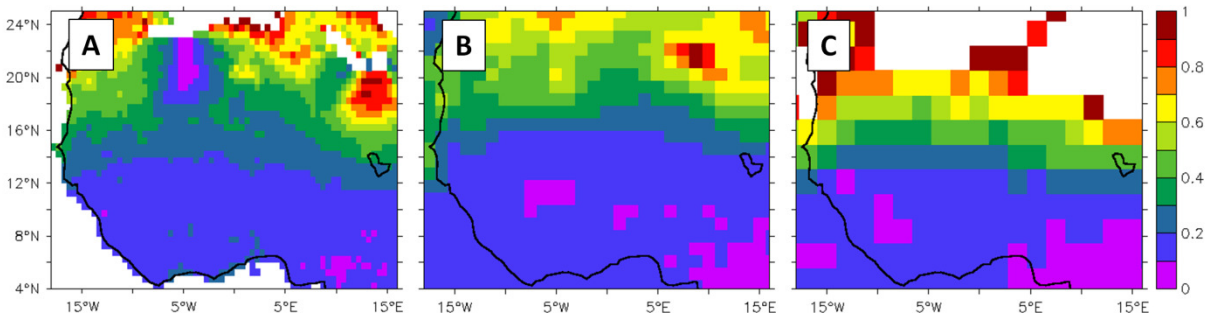

Figure 6.6 Coefficient of variation in historical rainfall. Box A shows observations, box B shows MPI-ESM-MR and box C shows CCSM4.White areas indicate CV values greater than 1.

6.3 Climate predictions for West Africa

We obtained monthly rainfall and temperature output for our selected climate models from the RCP 8.5 scenario, which represents a future with high greenhouse gas concentration levels, resulting in an increased radiative forcing of 8.5 W/m^2 by 2100 relative to preindustrial levels (Taylor *et al.*, 2012). We computed monthly and annual average rainfall and mean temperature between July and September (JAS; the peak malaria transmission season) over the short-term (2030-2060) and long-term (2070-2100), and compared to current values (1975-2005). Predicted changes in rainfall are shown in Figure 6.7 and predicted changes in temperature are shown in Figure 6.8. Both models show a general pattern of drying in the western portion of our study area, and wetting in the eastern and southern areas. This pattern of rainfall change is consistent with 75% of CMIP5 models analyzed by Roehrig et al. (2013).

The overall precipitation signal is stronger in CCSM4 than in MPI-ESM-MR. As a result, the average of the two models more closely resembles the pattern predicted by CCSM4. Temperatures generally increase more in the west than in the east. MPI-ESM-MR predicts JAS temperature increases between 0.8 and 2.9^{o}C by 2030-2060, and between 2.0 and 5.9^{o}C in 2070-2100, while CCSM4 predicts slightly less warming, between 0.5 and 2.8^{o}C in 2030-2060, and between 1.2 and 5.5^{o}C by 2070-2100.

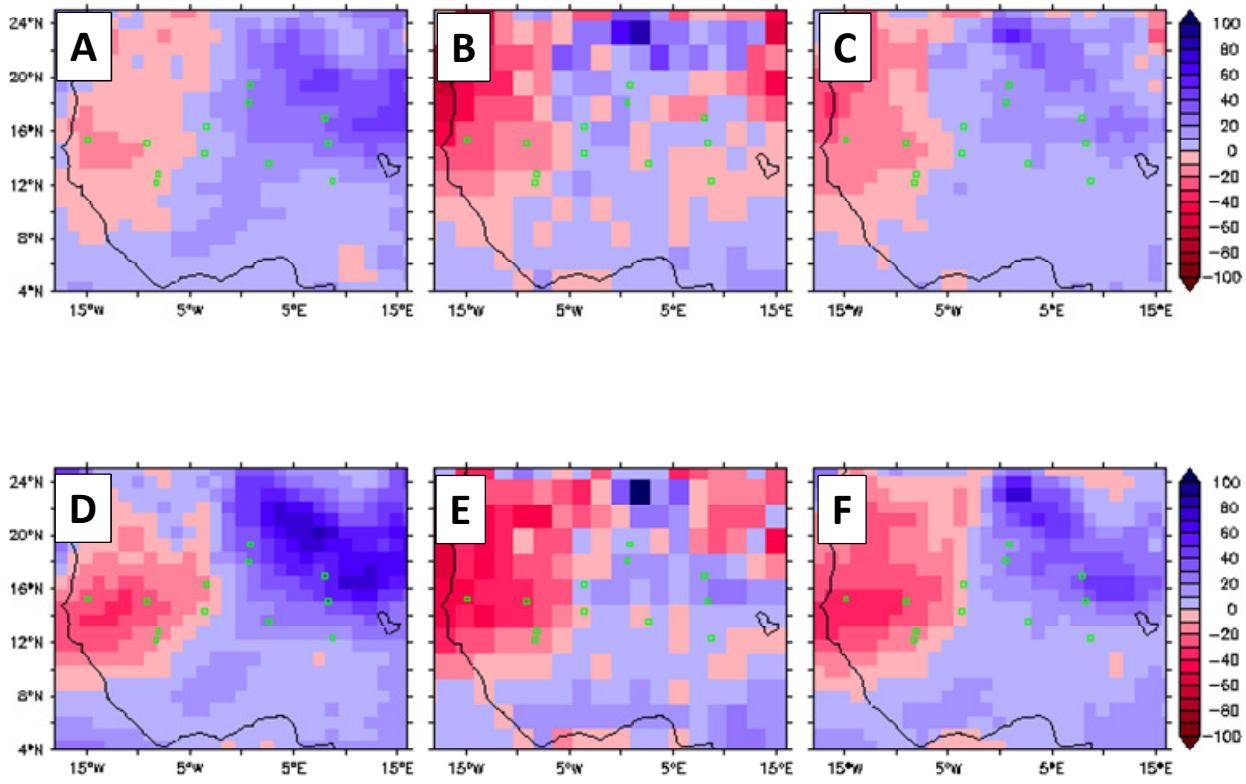

Figure 6.7 Predicted change in rainfall as a percentage of 1970-2000 mean rainfall. Boxes A and D show CCSM4, boxes B and E show MPI-ESM-MR, and the average between the two models is shown in boxes C and F. A-C show changes in the period 2030-2060, and D-F shows 2070-2100.

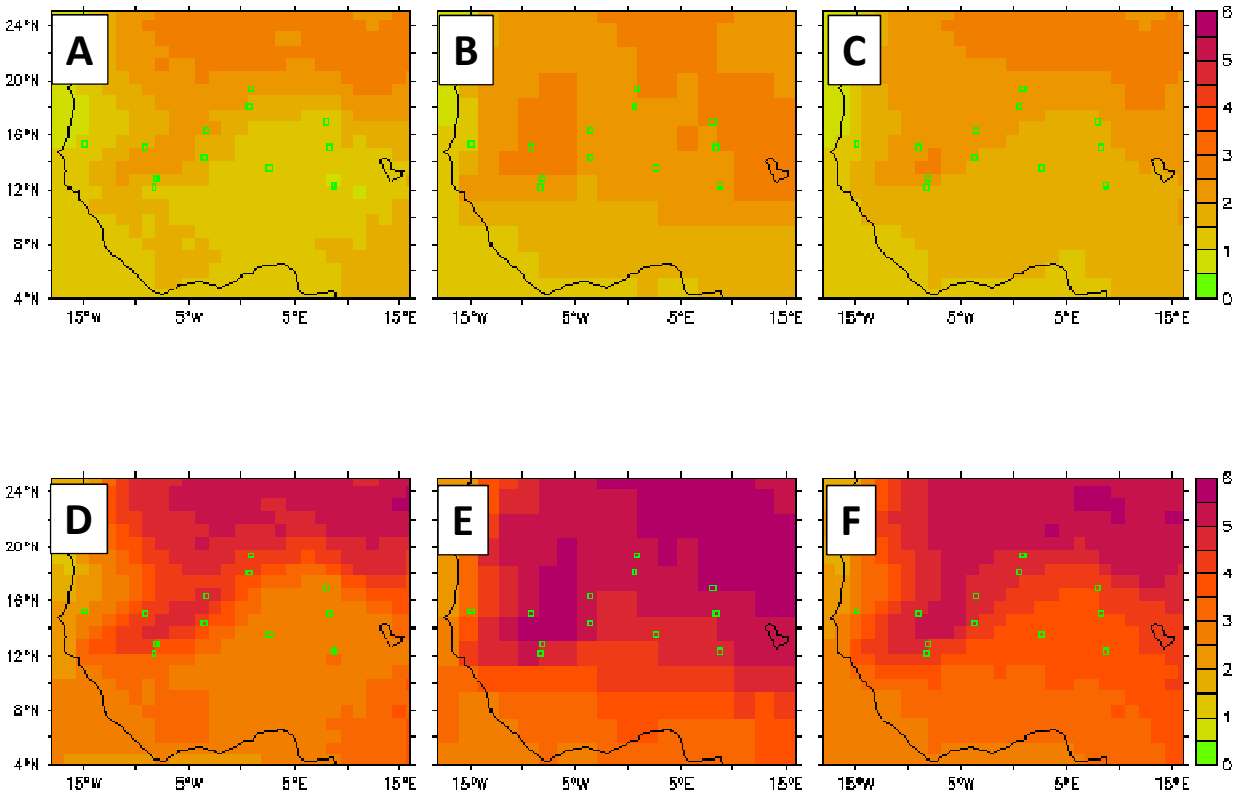

Figure 6.8 Predicted increase in JAS temperature compared to 1970-2000, in degrees Celsius. Boxes A and D show CCSM4, boxes B and E show MPI-ESM-MR, and the average between the two models is shown in boxes C and F. A-C show changes in the period 2030-2060, and D-F shows 2070-2100. The green points show the 12 study sites.

6.4 Simulating malaria transmission in future climates

6.4.1 Experiment design

In Chapter 5, we simulated malaria transmission in the current climate at 12 locations in West Africa where we anticipated the malaria prevalence level in the population would be sensitive to changes in the basic reproduction number (R_0). Using projections of rainfall and temperature from the two top-performing climate models, we simulate malaria transmission in the short-term (2030-2060) and in the long-term (2070-2100) for each of the 12 locations. Each simulation spanned 15 years.

As in Yamana et al. (2013), we assume that climate change will take the form of shifts in the north-south rainfall gradient, consistent with historical changes in rainfall regimes in this region (Bomblies & Eltahir, 2010; Irizarry-Ortiz *et al.*, 2003). The short-term and long-term precipitation time series were created by selecting a location directly north (for decreased rainfall) or south (for increased rainfall) of each site, where the current rainfall is equal to the short-term and long-term predictions of annual rainfall. We again disaggregate the coarse resolution rainfall data by applying the hourly patterns of rainfall observed by CMORPH. The hourly temperature inputs were obtained by adding the predicted short-term and long-term changes in temperature for each month to the baseline temperature time series.

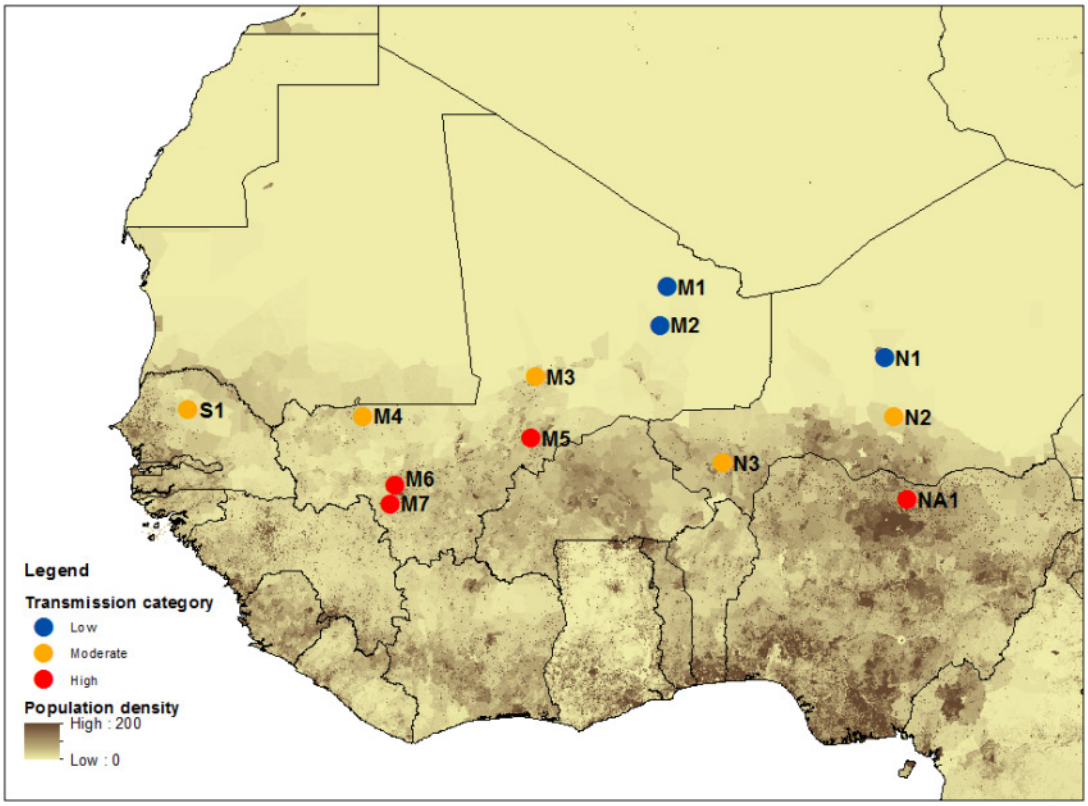

Figure 6.9 Site location. Colors show the transmission category of each site determined in Chapter 5. The background image shows population density data from the AfriPop database.

6.5 Results

The future climate for the 12 study sites varied by location; predicted changes in rainfall and JAS temperature are shown for CCSM4 in Figure 6.10 and for MPI-ESM-MR in Figure 6.11. The combination of warmer and drier conditions in the western portion of the study area is expected to cause the three sites in southwestern Mali and the site in Senegal to become less suitable for malaria transmission. However locations in Niger, Nigeria, and northern Mali are predicted to

have an increase in rainfall, which could increase vectorial capacity by providing mosquitoes with more water pools for breeding.

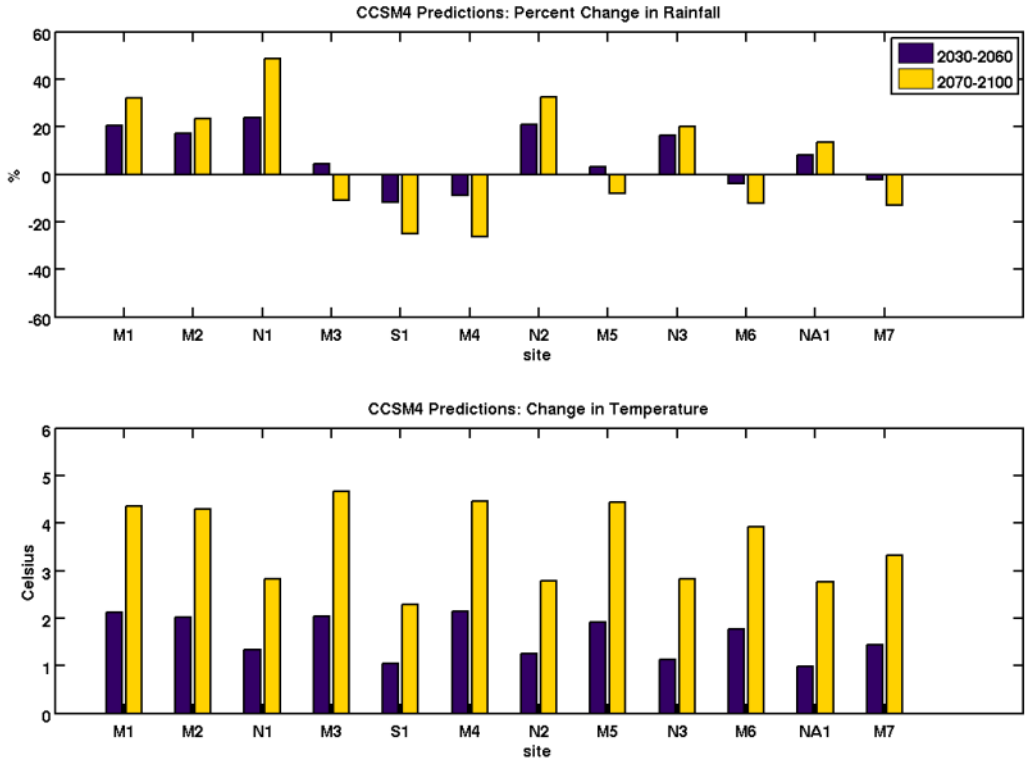

Figure 6.10 Changes in rainfall (top) and temperature (bottom) predicted by CCSM4 at the 12 study locations.

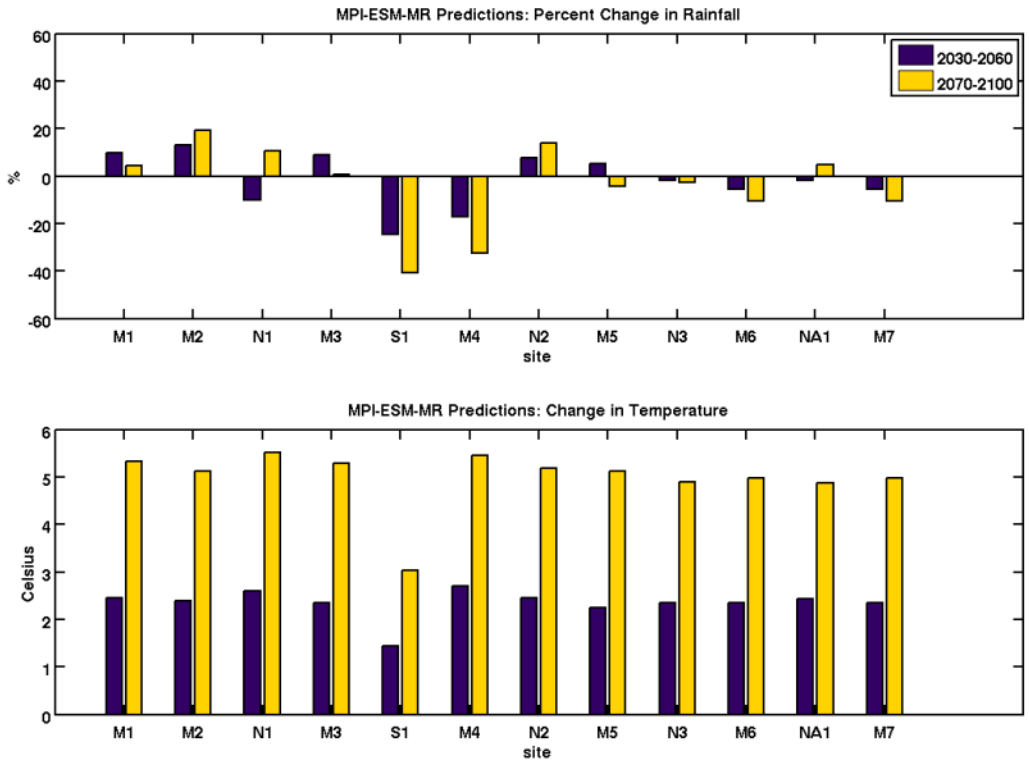

Figure 6.11 Changes in rainfall (top) and temperature (bottom) predicted by MPI-ESM-MR at the 12 study locations.

In Chapter 5, we classified our 12 sites according to the number of years with environmental conditions leading to R0 levels: low transmission sites (R_0 <1 more than half of the time), moderate transmission sites (R_0>1 more than half of the time, but always less than 10) and high transmission (R_0 almost always > 10). The location of these sites and their transmission categories are shown in Figure 6.9. We expect climate change to have the greatest impact in the moderate transmission sites. These areas are currently bordering the threshold of climate suitability to malaria, with possible occurrence of epidemics during some but not all years. Small changes in climate suitability could be enough to push the system above or below the

R_0=1 threshold, resulting in relatively large changes in malaria prevalence, should an epidemic occur. The sites with no current malaria transmission have R_0 values far below one; they would require several orders of magnitude increase in R_0 before malaria transmission is possible. High transmission sites already have well established malaria, and are less sensitive to changes in R_0.

6.5.1 Low or moderate transmission sites with increasing rainfall

Temperatures in M1 and M2 in northern Mali and N1 in northern Niger approached the limits of mosquito survival. Despite increases in rainfall, the overall effect was a decrease in R_0, and these sites remained unsuitable for malaria transmission. In N2 and N3, the effects of rainfall and temperature are of similar magnitude, roughly balancing each other. In our simulations, R_0 and prevalence in N2 increased in the short term, but by 2070-2100, conditions decreased and approached current levels. In N3, there was a small net decrease in R_0, which led to a decline in prevalence. Future rainfall predicted by CCSM4 and simulated R_0 and prevalence for low to moderate transmission sites with increasing rainfall are shown in Figure 6.12. The corresponding results using climate projections from MPI-ESM-MR are shown in Figure 6.13.

6.5.2 Low or moderate transmission with decreasing rainfall

Both climate models predicted a substantial decrease in rainfall for site M4 in western Mali and S1 in Senegal. Because both of these locations had R_0 values close to the threshold in the current climate, the decrease in rainfall led to a higher proportion of years with $R_0<1$. The result was a significant decrease in malaria prevalence. The change in rainfall was much smaller at M3, with both models predicting a small increase in the short term followed by a small decrease in the

long term climate. By 2070-2100, R_0 was below 1 for all years, making M3 unsuitable for malaria transmission. There was little effect on prevalence because current transmission was near zero despite occasional years with R_0 greater than 1. Results of these simulations are summarized in Figure 6.14 for CCSM4 and Figure 6.15 for MPI-ESM-MR.

6.5.3 High transmission sites

The four high transmission sites had the smallest relative changes in rainfall. Both models predicted that by 2070-2100, rainfall would decrease by 10-20% in M5, M6 and M7 and increase by less than 20% in NA1. These changes were small compared to current interannual variability and did not lead to notable change in any of the malaria transmission indices. Results are summarized in Figure 6.16 and Figure 6.17.

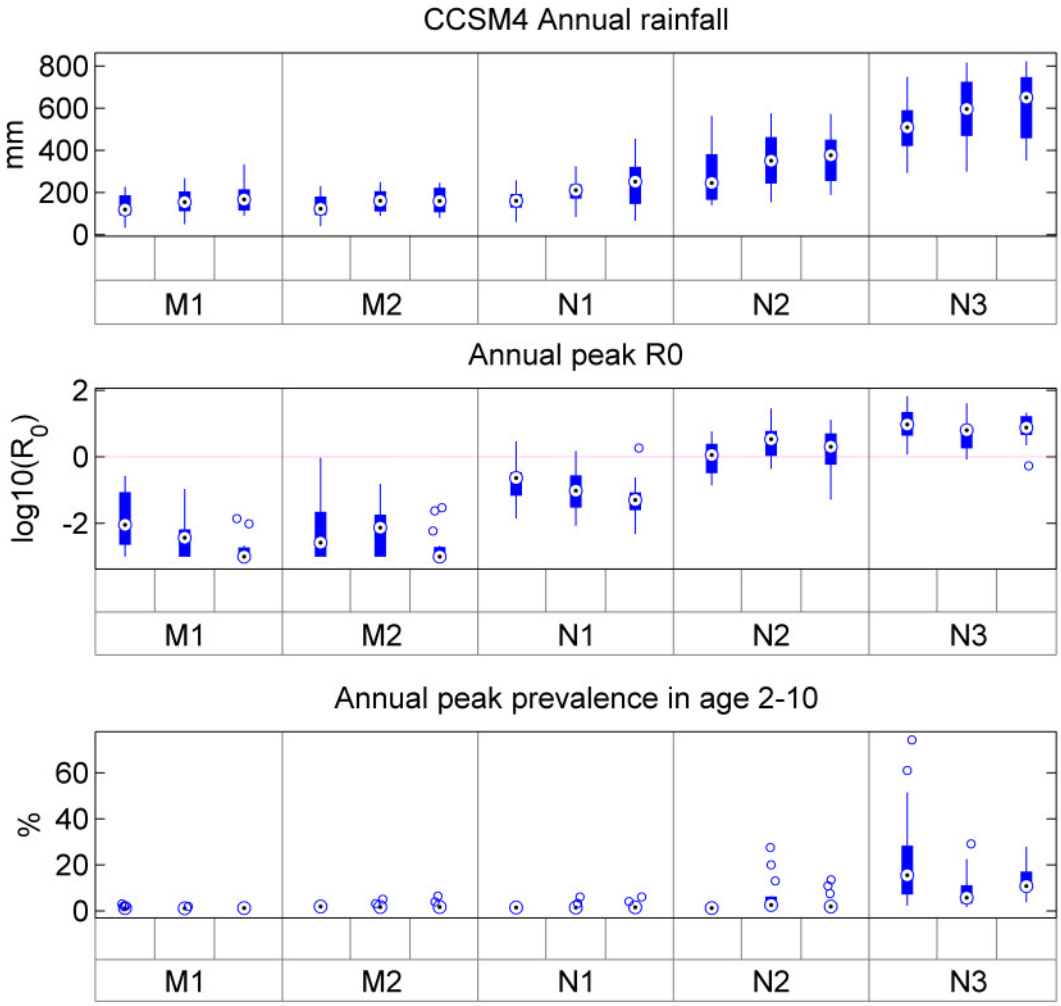

Figure 6.12 Summary of results using climate projections from CCSM4 for low and moderate transmission sites with increasing rainfall. Each location is represented by a set of three box plots of annual values for current climate (left), short term climate (center) and long term climate (right) simulations. The center dot of each boxplot indicates the median value over the 15 year simulation, the extent of the solid box corresponds to the limits of the 25th through 75th percentile values, and the solid lines (whiskers) extend to include roughly 99% of values if the data were normally distributed. Data points outside of the whiskers are considered outliers, and are denoted by open circles.

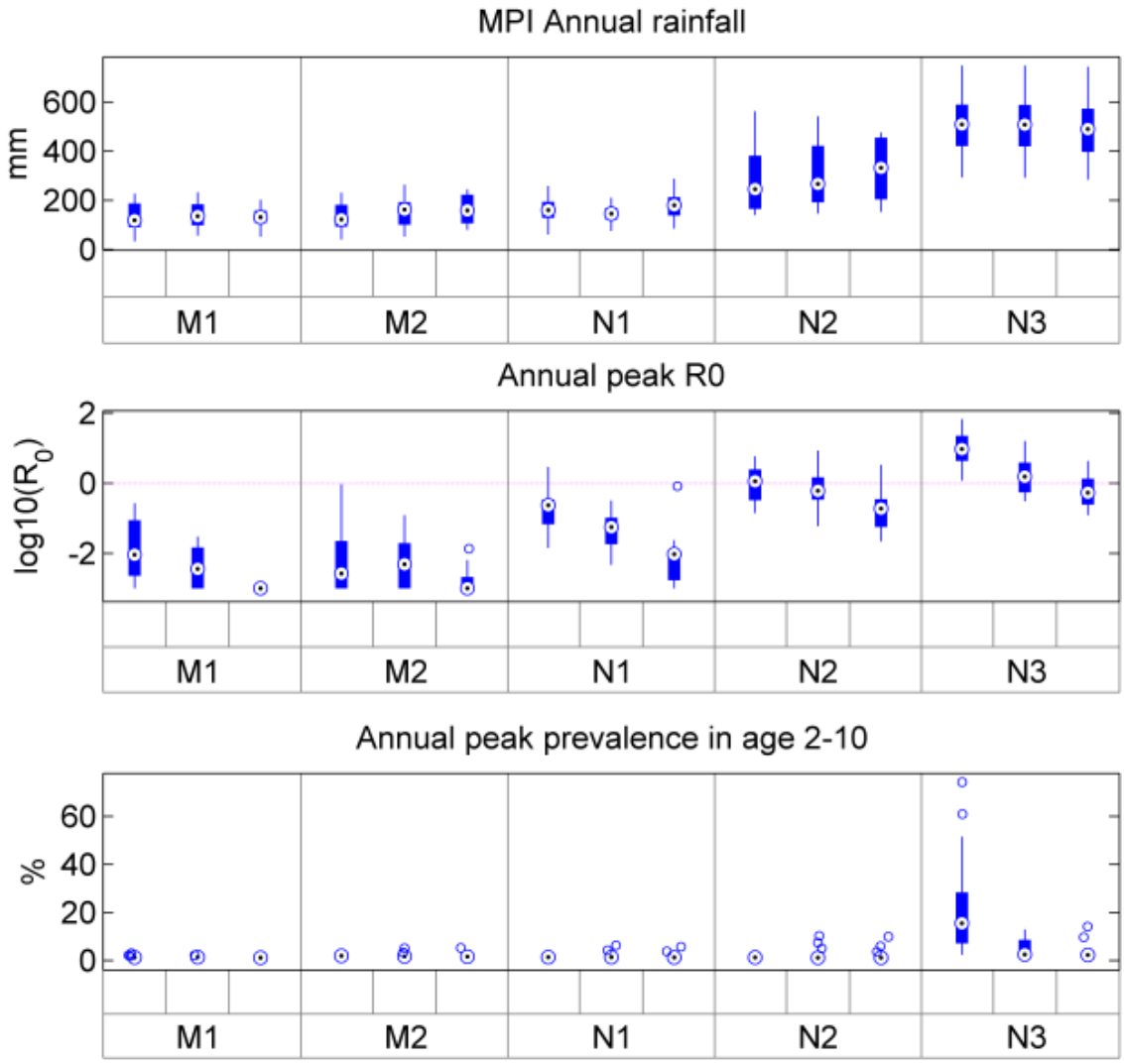

Figure 6.13 Summary of results using climate projections from MPI-ESM-MR for low and moderate transmission sites with increasing rainfall. Same as Figure 6.12 but for simulations using climate projections from MPI-ESM-MR.

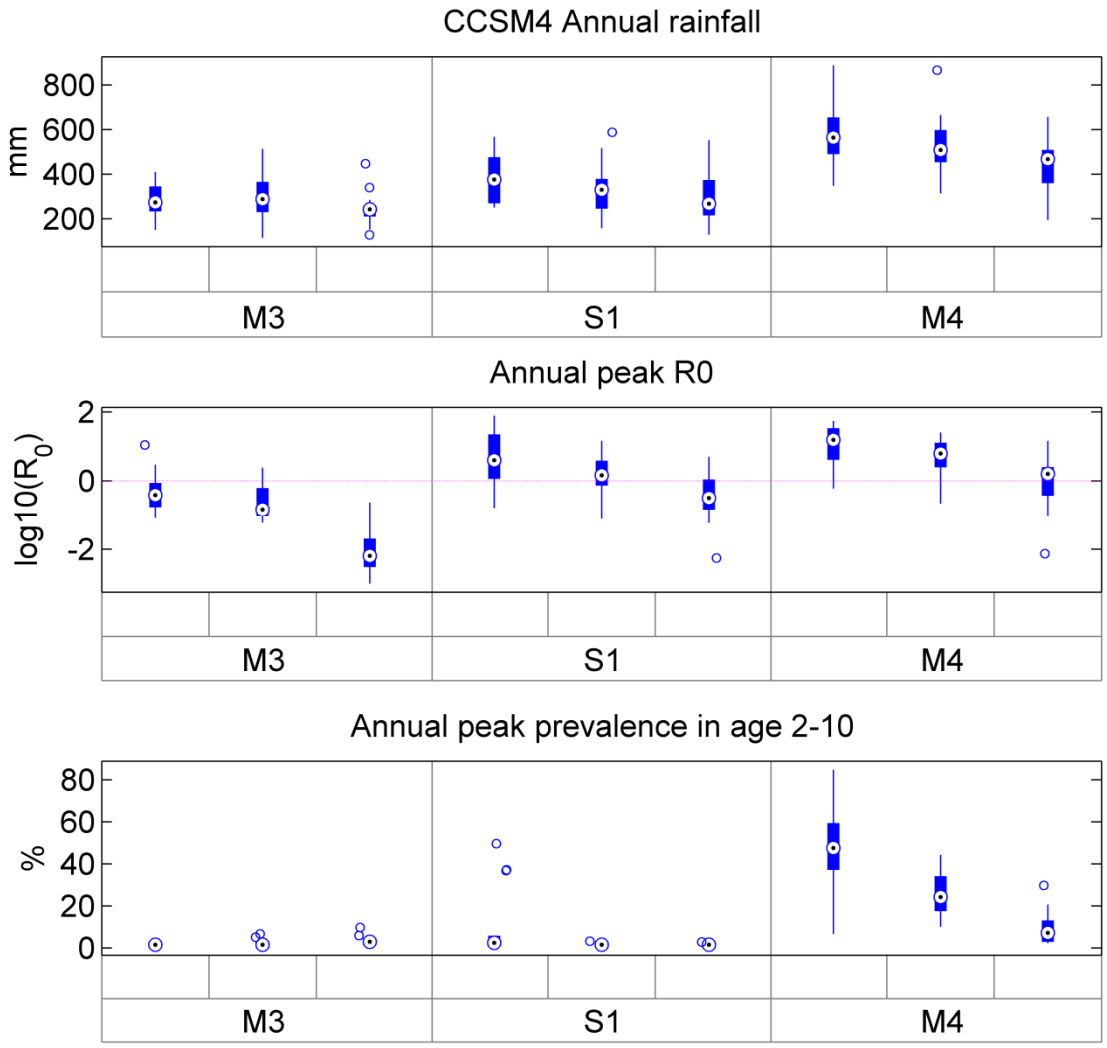

Figure 6.14 Summary of results using climate projections from CCSM4 for low and moderate transmission sites with decreasing rainfall. Same as Figure 6.12 but for sites with decreasing rainfall.

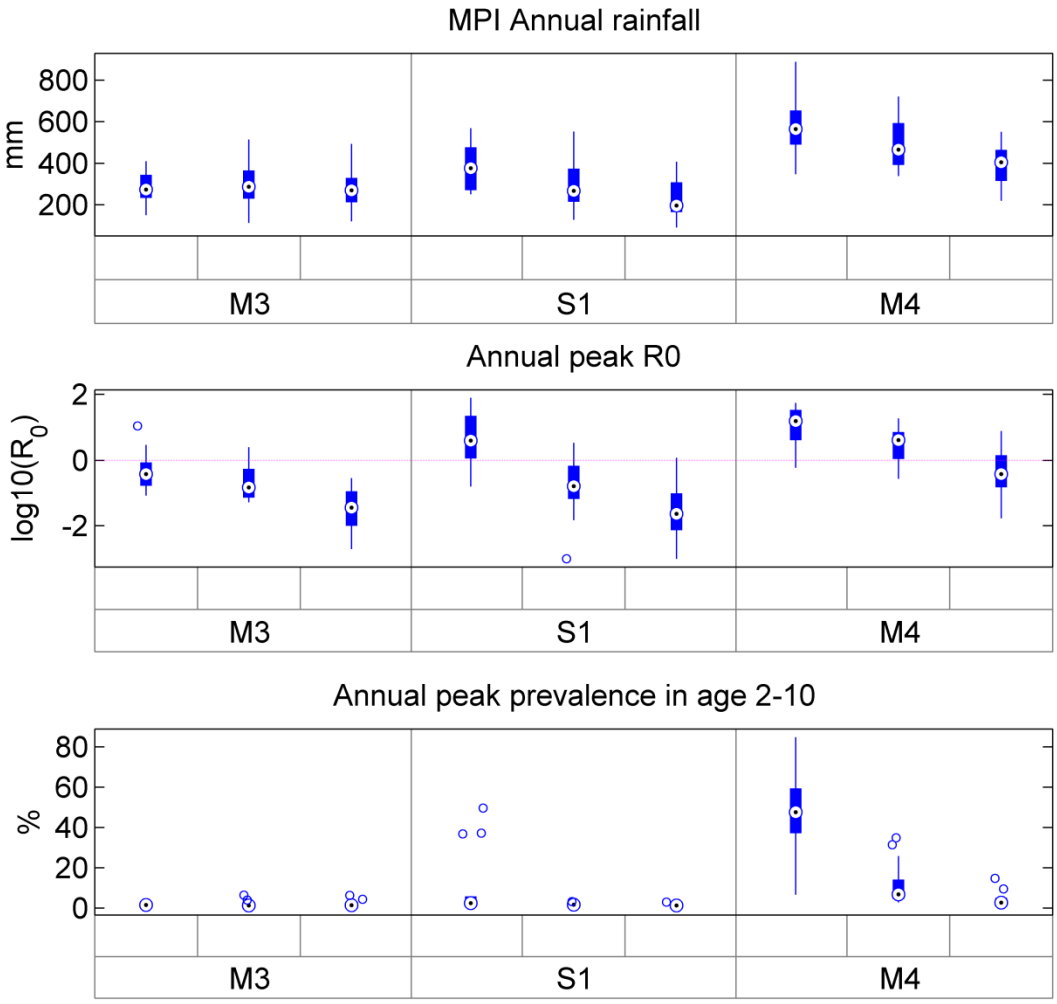

Figure 6.15 Summary of results using climate projections from MPI-ESM-MR for low and moderate transmission sites with decreasing rainfall. Same as Figure 6.14 but for simulations using climate projections from MPI-ESM-MR.

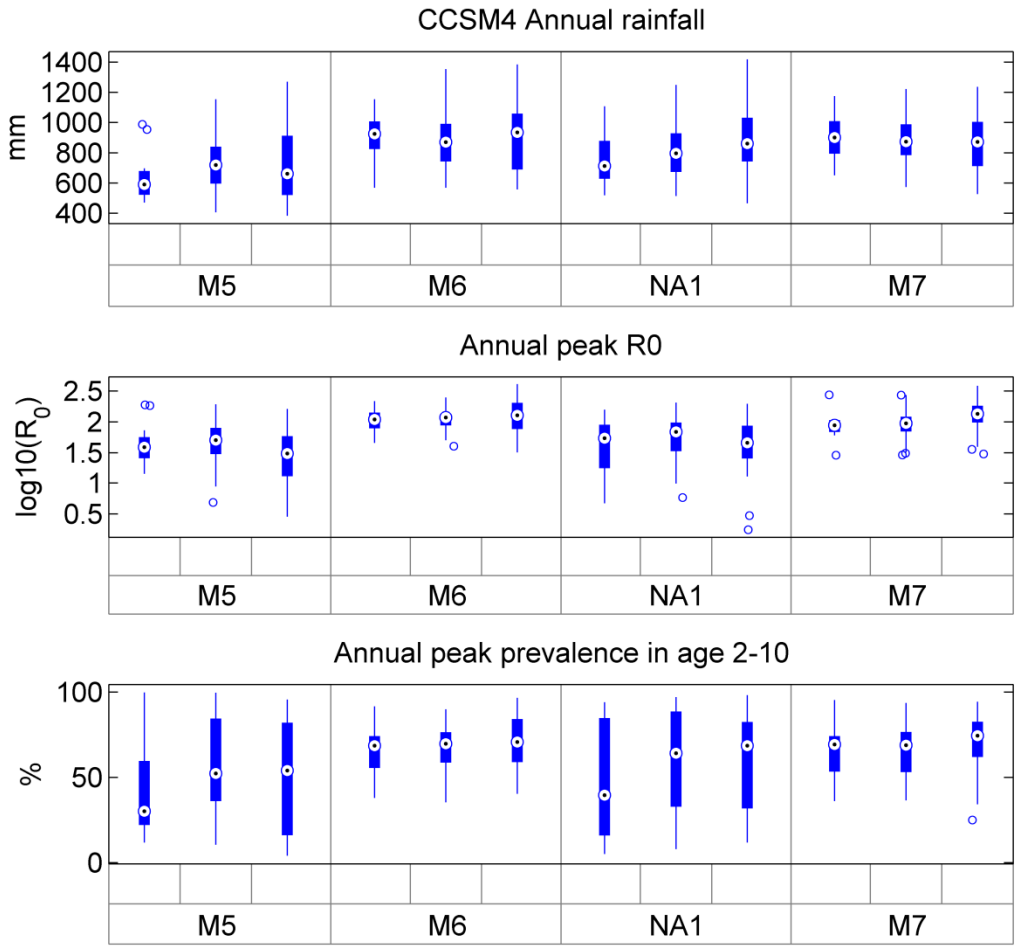

Figure 6.16 Summary of results using climate projections from CCSM4 for high transmission sites. Same as Figure 6.12 but for high transmission sites.

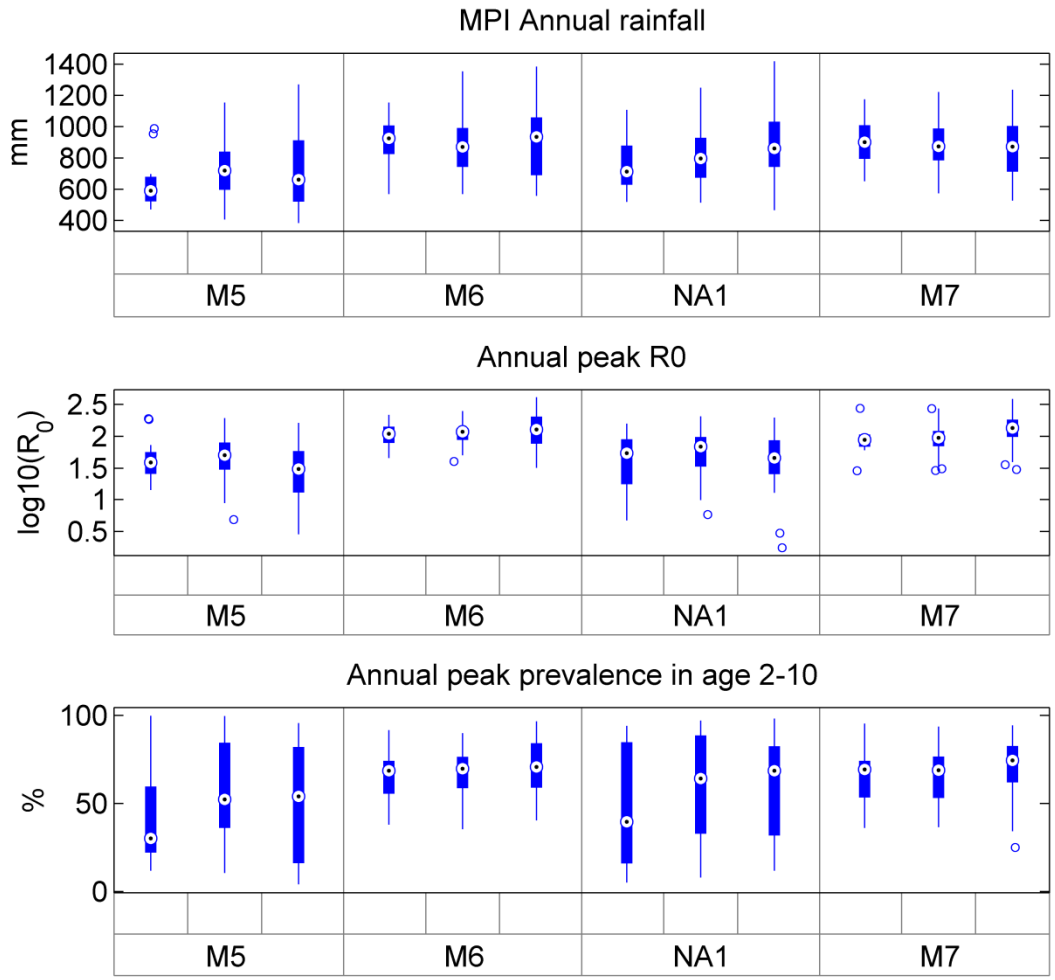

Figure 6.17 Summary of results using climate projections from MPI-ESM-MR for high transmission sites. Same as Figure 6.16 but for simulations using climate projections from MPI-ESM-MR.

The results of this experiment found several types of responses to climate change based on current suitability and predicted changes in climate, summarized in

Table 6.2. These categories are shown in Figure 6.18 and Figure 6.19.

Table 6.2 Responses of environmental suitability for malaria transmission to climate change

Response category	Current transmission classification	Sites	Change in rainfall	Change in suitability
A	Low	M1, M2, N1	Increase	Remains unsuitable
B	Moderate	N2, N3	Increase	Possible increase
C	Moderate	M4, S1	Decrease	Large decrease
D	Low	M3	Little change	Decrease
E	High	M5, M6, M7	Decrease	Little change
F	High	NA1	Increase	Little change

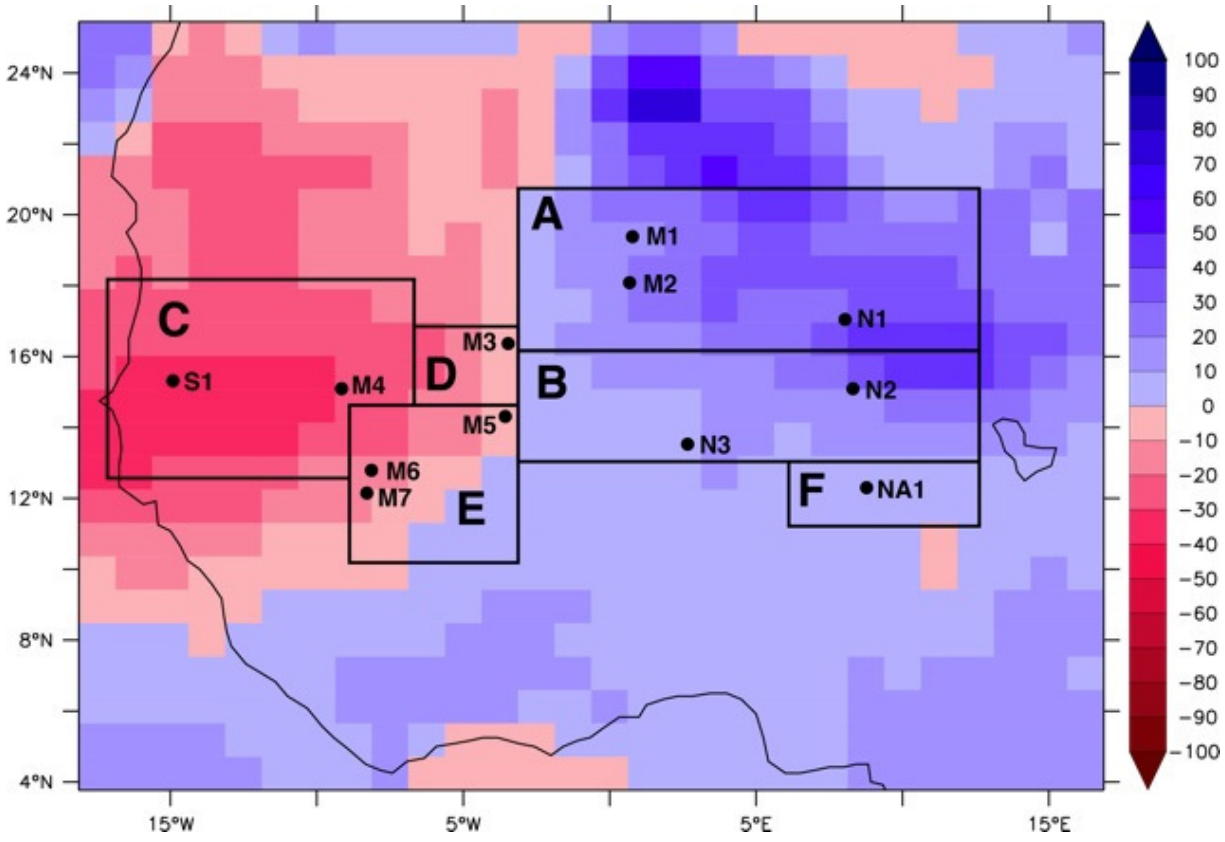

Figure 6.18 Study area response categories and long term percent change in rainfall averaged between MPI-ESM-MR and CCSM4.

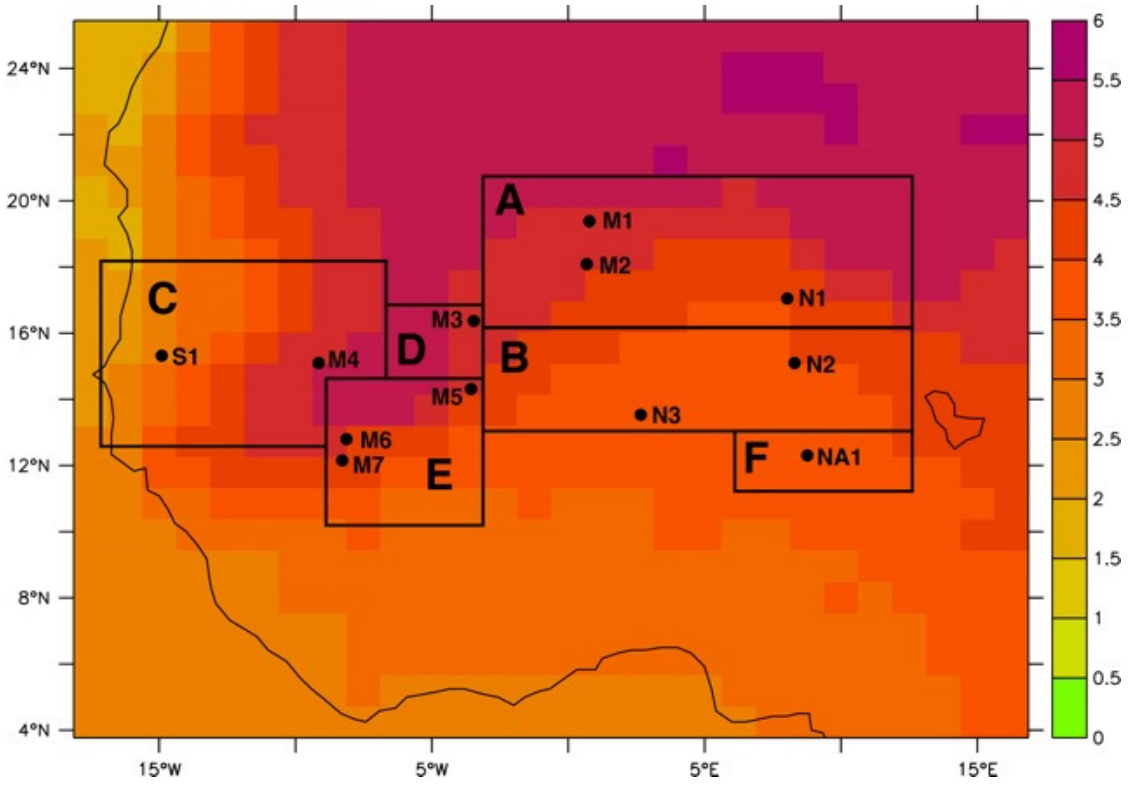

Figure 6.19 Study area response categories and long term temperature change averaged between MPI-ESM-MR and CCSM4

Changes in mean rainfall, $\log_{10}(R_0)$, and prevalence were compared to the standard deviation of the 15-year simulation of current conditions. The results of this analysis are shown in Table 6.3. With the exception of N1, S1 and M4, changes in rainfall were smaller than the standard deviation of current conditions. In the 2070-2100 simulations, future climate projections from both CCSM4 and MPI-ESM-MR led to a decrease of mean $\log_{10}(R_0)$ greater than the standard deviation of current conditions for sites in response category C and D, as well as site M1. The relatively warmer and drier projections from MPI-ESM-MR also led to a significant reduction in $\log_{10}(R_0)$ in all Category A and B sites, as well as M5. Changes in malaria prevalence were smaller than the standard deviation of current conditions, with an exception of a significant increase at N2 and a decrease at M4.

Table 6.3 Changes in rainfall, log10(R0) and prevalence compared to standard deviation in simulation of current climate.. Positive change greater than the standard deviation of current conditions are assigned a value of 1, negative changes greater than the standard deviation are shown as -1, and changes smaller than the standard deviation are shown as 0.

		Rainfall				Log10 (R0)				Prevalence in ages 2-10			
Site	Response	2030-2060		2070-2100		2030-2060		2070-2100		2030-2060		2070-2100	
		CCSM	MPI	CCSM	MPI	CCSM	MPI	CCSM	MPI	CCSM	MPI	CCSM	MPI
M1	A	0	0	0	0	0	0	-1	-1	0	0	0	0
M2	A	0	0	0	0	0	0	0	-1	0	0	0	0
N1	A	0	0	1	0	0	-1	0	-1	0	0	0	0
N2	B	0	0	0	0	0	0	0	-1	1	1	1	1
N3	B	0	0	0	0	0	-1	0	-1	0	0	0	0
S1	C	0	0	0	-1	0	-1	-1	-1	0	0	0	0
M4	C	0	0	-1	-1	0	0	-1	-1	0	-1	-1	-1
M3	D	0	0	0	0	0	0	-1	-1	0	0	0	0
M5	E	0	0	0	0	0	0	0	-1	0	0	0	0
M6	E	0	0	0	0	0	0	0	0	0	0	0	0
M7	E	0	0	0	0	0	0	0	0	0	0	0	0
NA1	F	0	0	0	0	0	0	0	0	0	0	0	0

Simulation results can be visualized as points on the rainfall-temperature scatter plots developed in Chapter 5. An example is shown for site M4 in Figure 6.20, the location with the most dramatic change in R_0 and prevalence. The images on the left show the spread of temperature and rainfall in the current climate, and the corresponding values of R_0 and prevalence. The center and right hand boxes show how the cloud of points moves to the left in response to increasing temperatures, and upwards in response to decreasing rainfall. As a result, R_0 goes from being greater than one for all years to being less than one for more than half of the years by 2070-2100. As a result, prevalence rates fall from the 40-60% range to the 0-20% range. Corresponding figures for the all twelve sites are shown in Appendix D.

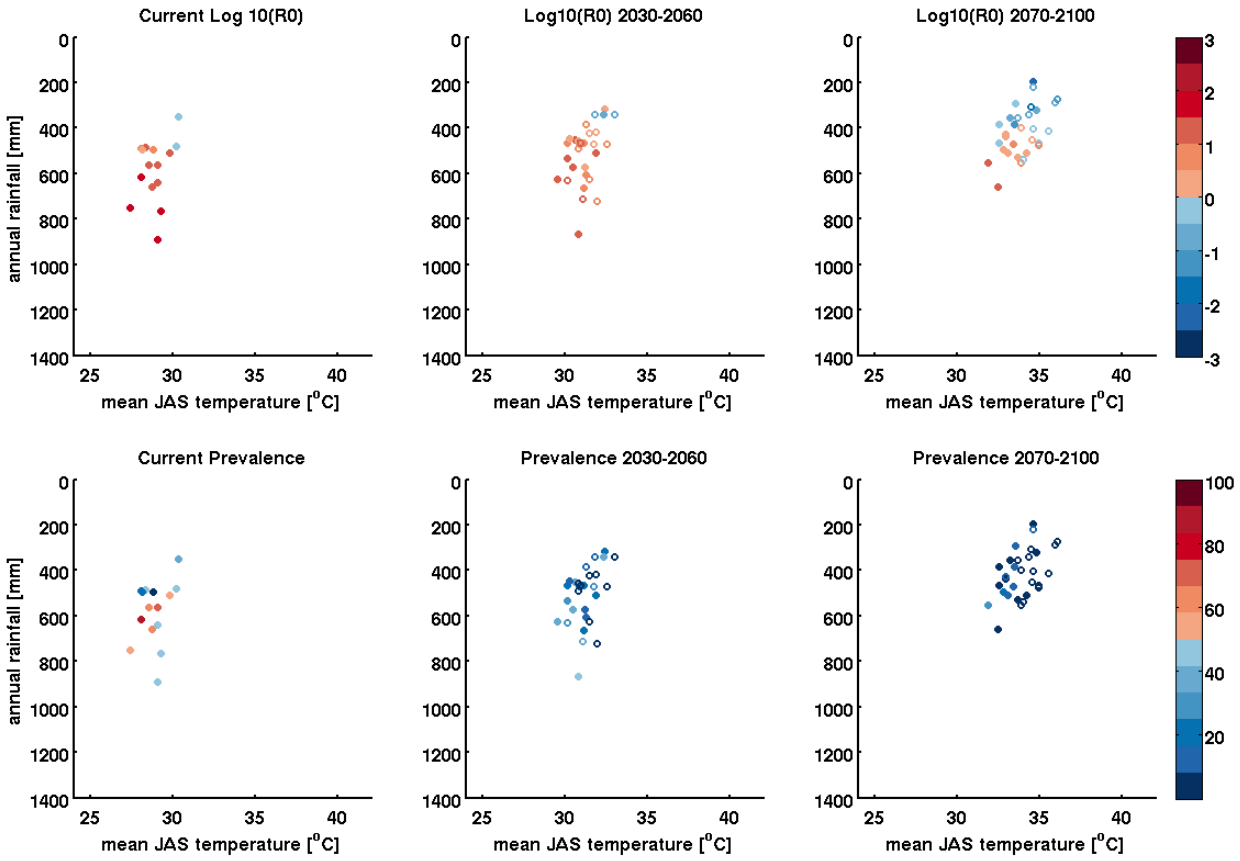

Figure 6.20 Annual R0 and prevalence for M4. The top row shows log10 (R0) and the bottom row shows prevalence in children aged 2-10. Current conditions are shown on the left, short term conditions in the center, and long term conditions on the right. Closed circles are results from the simulation using CCSM4 climate predictions and open circles used MPI-ESM-MR predictions.

6.6 Discussion

Our analysis of climate models demonstrated the CMIP5 models continue to vary in their ability to simulate current climate in West Africa, a fact often neglected in studies of climate change impacts. This emphasizes the importance of selecting an appropriate model for predicting results. Despite the wide spread in climate predictions discussed Chapter 4, the two models that ranked highest in our screening had similar predictions for the future climate.

In simulating future malaria conditions, we emphasize that this study considered only the environmental aspects of malaria transmission and climate change. We did not include malaria control interventions or housing improvements, which can have a very large impact on malaria transmission dynamics. We neglect population growth, migration and urbanization. We also do not consider the extreme effects of climate change, such as changes in frequency of droughts and floods.

The northernmost locations (categories A and D), where current temperatures are already close to the upper limits of mosquito survival, became less suitable for malaria transmission even when rainfall increased. The southernmost locations (categories E and F) where climate is currently highly suitable for transmission were least sensitive to changes in climate. Temperatures became warmer but remained within the mosquito's survival limits. Changes in rainfall were modest, and we found in Chapter 5 that malaria transmission indices were less sensitive to climate in these wetter regions. As a result, there was little change in malaria transmission in these locations.

Category C saw the most dramatic changes. In the current climate, we simulated moderate malaria transmission in these locations. R_0 was above 1 for most years, but within the range that is still sensitive to changes in climate. The increase in temperature and decrease in precipitation

both contributed to decreases in mosquito populations and R_0. As a result, malaria transmission decreased.

Finally, Category B represents the most critical scenario. Detailed results of mosquito density, R_0 and malaria prevalence at N2 and N3, the two sites in this category, are shown in Figure 6.21and Figure 6.22, respectively. In the current climate, these locations have modest malaria transmission. Immunity levels are relatively low, and transmission varies greatly from year to year. In our simulations, we found that the effects of rainfall and temperature were of similar magnitude, leading to uncertainty in the change in R_0. Site N3 generally had R_0 greater than 1 during all three simulation periods, and there was little change in the 15-year mean of R_0. Site N_3 had a more pronounced increase in R_0, particularly in the 2030-2060 simulation. However conditions remained highly unstable in all three time periods. The increase in mean prevalence at N2 was the result of a single epidemic in each of the future simulations that boosted prevalence levels for the following one or two years. Because R_0 at N2 is close to the threshold value, malaria transmission is very unstable and epidemics of the size observed in the short term climate simulation could have occurred under current conditions. Our simulation length of 15 years may be insufficient to determine whether the frequency of such epidemics will increase in the future. Small differences in the climate predictions or in the malaria model used could tip the balance in favor of malaria transmission leading to dangerous increase in disease transmission. Because of these uncertainties and potentially harmful changes, we recommend that this area be monitored as a potential hotspot for increase in malaria transmission due to climate change.

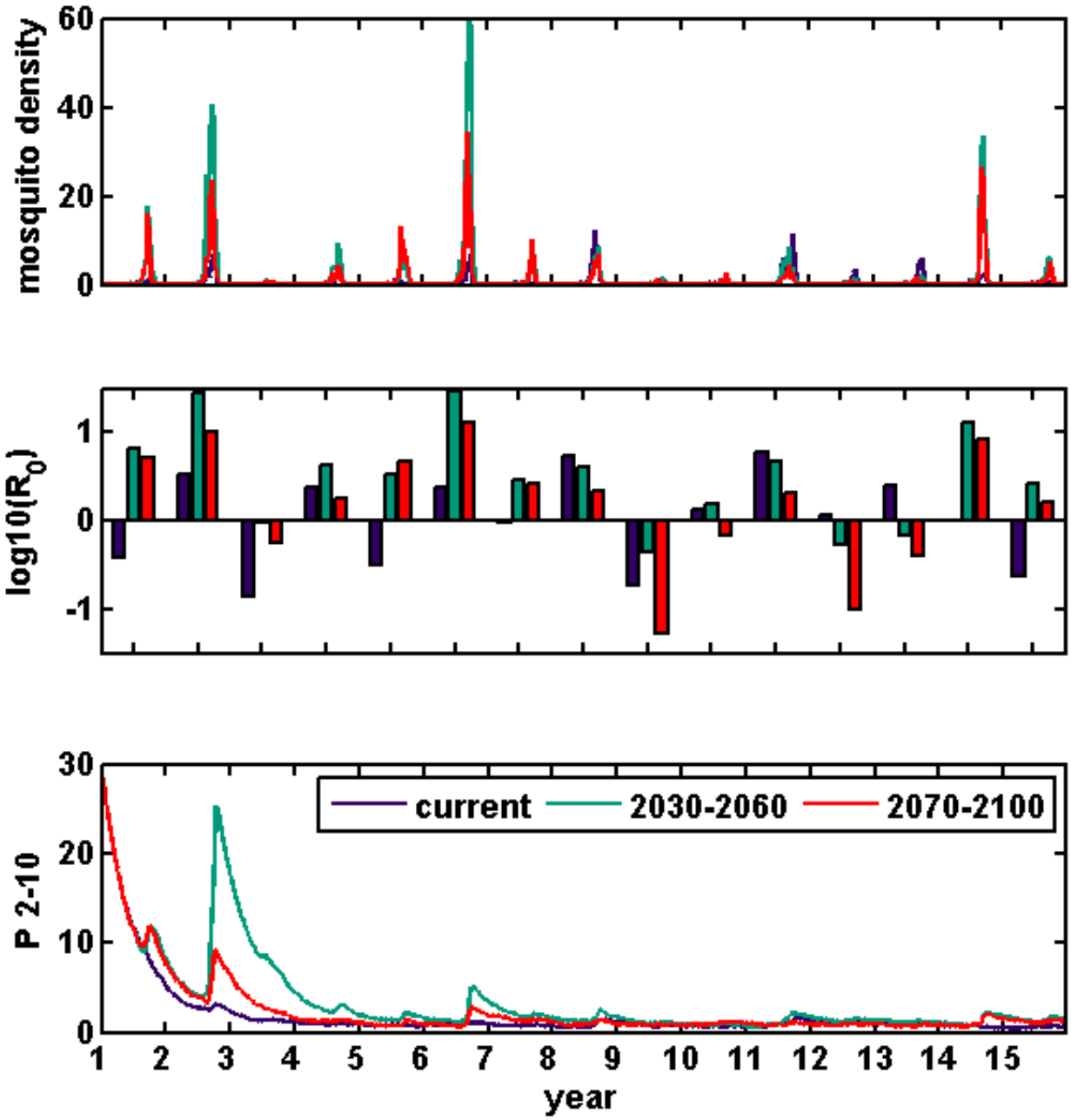

Figure 6.21 Detailed simulation results for Site N2 in current (blue), short term future (green), and long term future(2070-2100) climates using projections from CCSM4. The top figure shows weekly mosquito density. The middle figure shows annual log10(R0). The bottom figure shows weekly malaria prevalence in children aged 2-10.

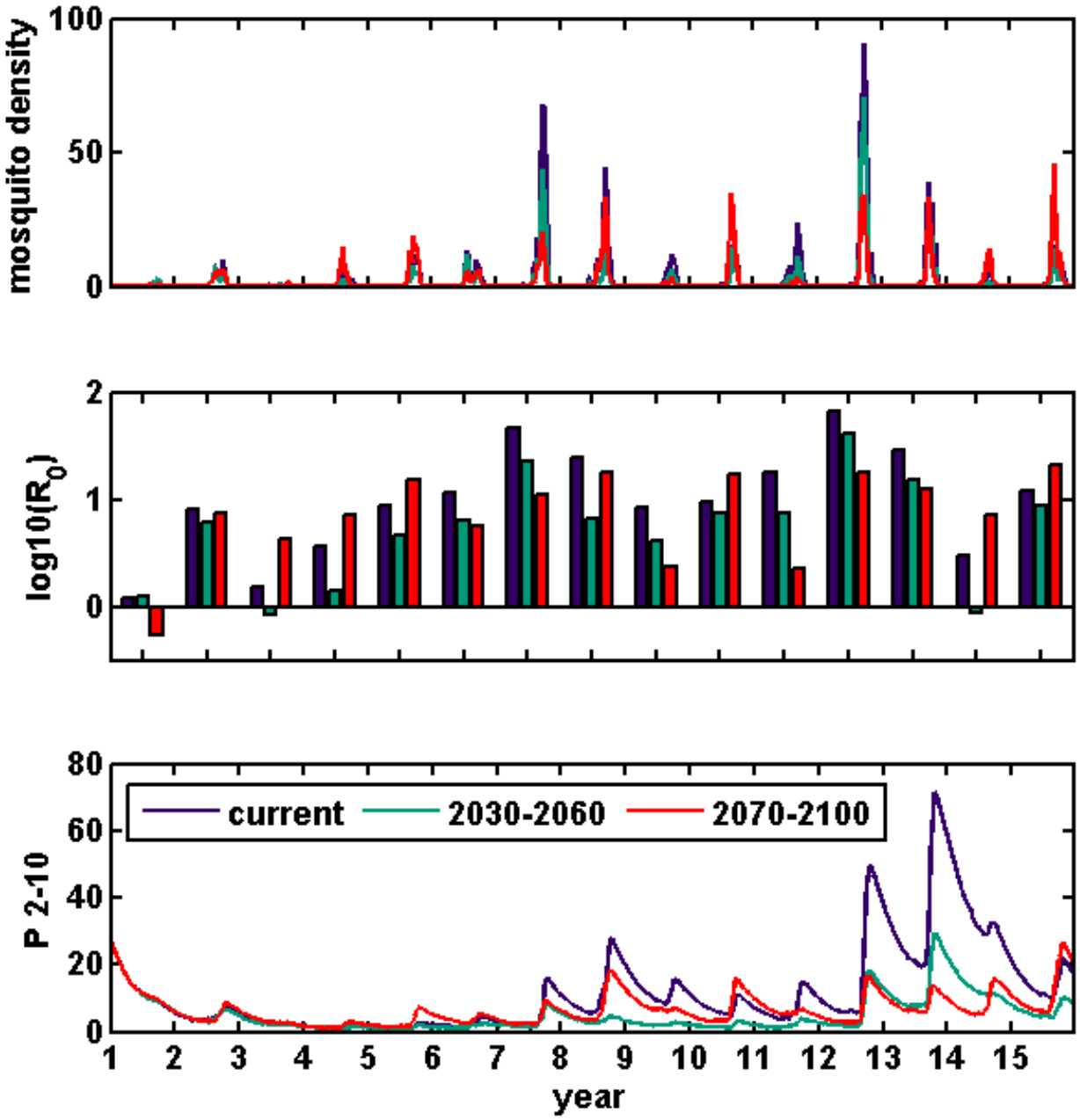

Figure 6.22 Detailed simulation results for Site N3 in current (blue), short term future (green), and long term future(2070-2100) climates using projections from CCSM4. The top figure shows weekly mosquito density. The middle figure shows annual log10(R0). The bottom figure shows weekly malaria prevalence in children aged 2-10.

6.7 Conclusions

The analysis of climate models presented here was an important advancement over previous work analyzing malaria and climate change, as there are still major differences in the ability of CMIP5 models in simulating the climate of West Africa. We identified two models CCSM4 and MPI-ESM-MR as being the most credible in this region. Climate predictions from these two models showed drier conditions in the western portion of our study area and wetter conditions in the east. These changes in rainfall combined with warmer temperatures are expected to affect environmental suitability for malaria transmission in some parts of our study area. The northern and southern extents of our study area are not expected to change significantly, as the north remains unsuitable and the south remains highly suitable. However, we identified two areas where significant changes can occur. The first is the low to moderate transmission areas in the western portion of our study area, including Senegal and western Mali, where we expect malaria transmission to decrease. The second area is in the eastern Sahel where rainfall is likely to increase. Although our simulations predicted little change in this region, we recommend further monitoring of this region.

7 Conclusions

7.1 Summary of results

The goal of this thesis was to improve understanding of the relationships between environment, entomology, and malaria transmission in the current and future climates of West Africa. This was done using HYDREMATS, a highly detailed mechanistic modelling tool. Chapters 2 and 3 described improvements made to HYDREMATS. Improvements to the model's efficiency described in Chapter 2 were essential in enabling the long term simulations in Chapters 4 through 6, capturing far more information about each location's malaria transmission dynamics than would have been possible in a simulation of only two or three years. Improvements to the representation of the human population in HYDREMATS allowed a more realistic simulation of the complex interactions between previous exposure, immunity and malaria prevalence.

Chapter 4 described a first-order approximation to the impacts of climate change on malaria transmission in West Africa. This chapter highlighted the high uncertainty in GCM predictions of future climate in this region and showed expected changes in malaria transmission under the best and worst case scenarios. Despite the uncertainties in climate predictions, we found that even the worst case scenario in terms of increased suitability for malaria transmission was not expected to lead to significant increases in disease prevalence. A separation of the effects of rainfall and temperature in shaping the response of vectorial capacity to climate change emphasized the value of a hydrologic modelling tool in studies of climate change impacts.

Chapter 5 presented a detailed study of current entomological and epidemiological conditions across West Africa. Comparison of model results to observational data showed the validity of

HYDREMATS across a range of ecoclimate zones. The interannual variability of the basic reproduction number and malaria transmission was examined, and locations were classified based on the level of these indices over a 15-year period. As the computational requirements of HYDREMATS remain prohibitive for the simulation of entire countries or continents, linear regression models were developed to relate rainfall and temperature to key malaria indices. These models were able to explain 74-85% of variability in simulated results and provide a tool that can be used to estimate malaria transmission in current or future climate, perhaps narrowing down wide areas into critical zones to simulate in greater detail.

Chapter 6 described predictions of the effects of climate change on malaria transmission in West Africa. Based on an evaluation of current climate models, two models, CCSM4 and MPI-ESM-MR were identified as being the most credible in simulating the current and future climate of West Africa. Projections from these models indicate that the western half of the Sahel is expected to become drier while the eastern half is expected to become wetter. Wet season temperatures are expected to increase by 2.5 to 5.7^{o}C by 2070-2100. The northern area of West Africa was expected to remain unsuitable for malaria transmission regardless of future rainfall due to temperatures exceeding mosquito tolerance. Changes in climate did not lead to significant changes in malaria prevalence in the high transmission areas in the southern portion of West Africa. Drier and hotter conditions in the moderate transmission areas in the western Sahel were expected to decrease malaria transmission. In the eastern Sahel, the positive effects of increasing rainfall on vectorial capacity were of similar magnitude of the negative effects of increasing temperature, leading to uncertainty in future malaria transmission. As a result, we recommend continued monitoring in the eastern Sahel.

7.2 Major contributions

This thesis contributed to the development of the HYDREMATS modelling tool in three key areas:

The effects of humidity on mosquito survival placed an important constraint on vector populations and malaria transmission during the dry season. This was shown to improve simulation of the seasonality in areas where hydrological conditions allow potential mosquito breeding sites to persist into the dry season.

The improvement of the immunity component in HYDREMATS allowed us to move beyond entomological measures such as mosquito density and vectorial capacity to analyzing the prevalence of the malaria parasite within human populations. The result is a novel modelling tool that mechanistically simulates all of the key processes linking environment to malaria transmission.

A comparison of simulation results to observational data of entomological and epidemiological variables across West Africa established the ability of HYDREMATS to simulate malaria transmission dynamics across a range of ecoclimate zones. This, combined with the methodology developed here of incorporating data from satellites, reanalysis models and archived datasets as model inputs, greatly increases the significance of HYDREMATS, as it allows simulation under a far wider range of conditions than was previously possible.

The enhanced version of HYDREMATS was applied to improve understanding of the impact of natural interannual variability of climate on the dynamics of malaria transmission in the current climate of West Africa.

Areas where populations are at greatest risk of increased malaria transmission due changes in environmental conditions were identified. These areas include the northern extent of malaria transmission in the Sahel, where the current climate leads to basic reproduction number close to the threshold that would allow the disease to spread.

Linear regression models were developed in order to predict key malaria transmission indices using historical or predicted data of annual rainfall and mean wet season temperature.

Finally, this work improved on previous understanding of the impacts of climate change on malaria transmission in West Africa.

Climate models were screened for their ability to simulate climate in West Africa, resulting in a best estimate of future climate in this region. This is the first time to our knowledge that a study of climate change impacts on malaria tested the credibility of a climate model before using its projections to predict impacts on disease transmission.

The framework of mechanistic modelling to translate changes in rainfall and temperature due to increased greenhouse gas emissions into changes in mosquito density, vectorial capacity and malaria transmission is an improvement over previous work that had relatively crude representations of rainfall.

7.3 Recommendations for future work

7.3.1 Further investigations of human immunity

The improved human immunity component of HYDREMATS presents numerous opportunities for future work. An important application of HYDREMATS is its potential to provide *a priori* assessments of malaria control interventions. The hydrology and entomology components of the model alone can be used to determine the effect of vector control operations, such as application of larvicide or use of mosquito nets, on vector populations. The immunology component of the model enables the extension of these predictions to the effect of interventions on malaria prevalence. This is especially important given the nonlinearities between vectorial capacity and malaria transmission. Even large scale mosquito control efforts may have little effect if they fail to drive the basic reproduction number below one. Malaria control activities targeted at the human population, such as vaccination or case detection and treatment, can be evaluated in conjunction with vector control and environmental management initiatives.

The improved modelling tool can be used to explore interesting questions relating to the long lasting memory of acquired immunity to malaria. An issue that has been important in the historical context of malaria control has been the interruption of malaria interventions due to diminished political incentive or financial resources. In these cases, a sudden increase in vectorial capacity in a population with reduced immunity to the disease can cause a dangerous resurgence of malaria. HYDREMATS can be used to predict and mitigate such resurgences.

Future improvements to the immunity model include simulating parasite densities with human agents over the course of an infection. The parasite density may affect the probability the disease is passed to mosquitoes during bloodmeals. We do not currently differentiate between

symptomatic and asymptomatic disease, or provide estimates on severe forms of disease. Inclusion of this aspect would be useful in determining the burden of disease in a population.

7.3.2 Extending predictions of climate change impacts on malaria transmission

We showed that malaria prevalence is most vulnerable in areas where current environmental conditions lead to basic reproduction numbers close to the threshold value. While we are able to approximate the location of these areas, it was not possible based on this analysis to specify the exact areas. Recent advances in computational resources and the improvements to model efficiency greatly increased the number of simulations that could be conducted. However, we were still limited to selecting representative villages in various climate zones. An improved future study would cover greater spatial areas to better delineate this sensitive region. We found a delicate balance between increase in mosquito populations due to higher rainfall and decrease in vectorial capacity due to exceedingly high temperatures. It is possible that there are parts of the eastern Sahel where the effects of rainfall dominate. A larger scale simulation would identify these areas.

While this study was careful in selecting the most credible general circulation models to drive our estimates of climate impacts, there are still known biases in the entire ensemble of CMIP5 GCMs. As these climate models improve, the assessment of impact on malaria transmission should be updated. In downscaling model predictions of future rainfall, we made the assumption that changes in precipitation would take the form of climate shifts so that future precipitation in a given location will resemble current conditions directly to the north (for drier conditions) or south (for wetter conditions). However it is possible that climate change will alter the temporal

pattern of precipitation. This can have significant implications for mosquito populations as it would affect pool persistence and the length of the breeding season. Future work should therefore include an analysis of changes to the temporal pattern of future rainfall.

Appendix A Bias-correction for CMORPH rainfall

Like most satellite rainfall products, CMORPH is known to have a positive bias compared to rain gauge data in West Africa, primarily due to overestimation of high-intensity rainfall (Gosset *et al.*, 2013). However, after a simple bias-correction, CMORPH can be used as in input to HYDREMATS to reasonably simulate water pools and mosquito populations (Yamana & Eltahir, 2011).

While Yamana & Eltahir (2011) used a single bias-correction factor for all rainfall estimates regardless of intensity, here we used a probability matching technique (Wolff *et al.*, 2005) so that the cumulative distribution function (CDF) of corrected hourly CMORPH data matched that of the ground observations. This method is preferable to applying a single correction factor because the bias differs by rainfall intensity. Variations of the probability matching technique have recently been used to correct biases in CMORPH using rain gauge data (De Vera & Terra, 2012; Guilloteau *et al.*, 2014).

Ground observations measured by Institut de Recherche pour le Développement of Niger, Mali, and Benin were obtained through the African Monsoon and Multidisciplinary Analyses (AMMA) database for the time period 2006 through 2008 and pooled together. The five locations were: Banizoumbou and Zindarou in Niger, Agoufou and Bamba in Mali, and Djougou in Benin. Hourly rainfall data measured by ground rain gauges from five West African locations were paired with corresponding hourly CMORPH rainfall data. The cumulative density functions (CDF) of rainfall intensity for the two datasets are shown in Figure A.1. The pair of

CDFs were used to create a look-up table, Table A.1, such that raw CMORPH hourly rainfall values are multiplied by a bias correction factor (BCF) to obtain the correct CDF.

$$CMORPH_{corrected} = CMORPH_{raw} \times BCF(CMORPH_{raw})$$

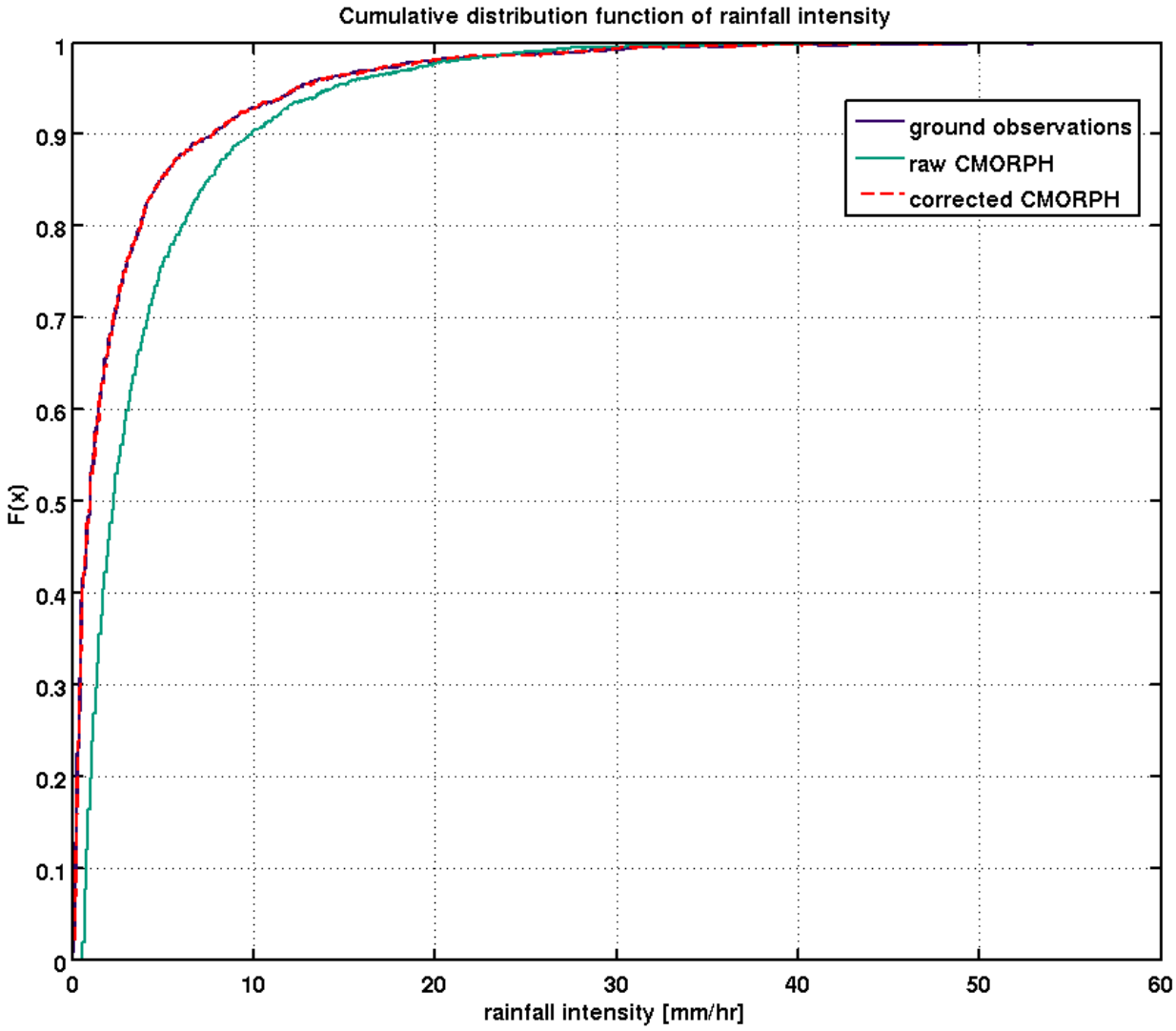

Figure A.1 Cumulative density function of non-zero rainfall values from ground observations (blue) and CMORPH estimates (green)

Hourly CMORPH data were extracted for our 12 sites for the 15-year time period 1998 through 2012, and corrected using Table A.1. While hourly rainfall measurements from meteorological stations were not available for these locations, comparison with annual rainfall data from CRU, shown in Figure A.2, shows that the correction method greatly improved the accuracy of total annual rainfall.

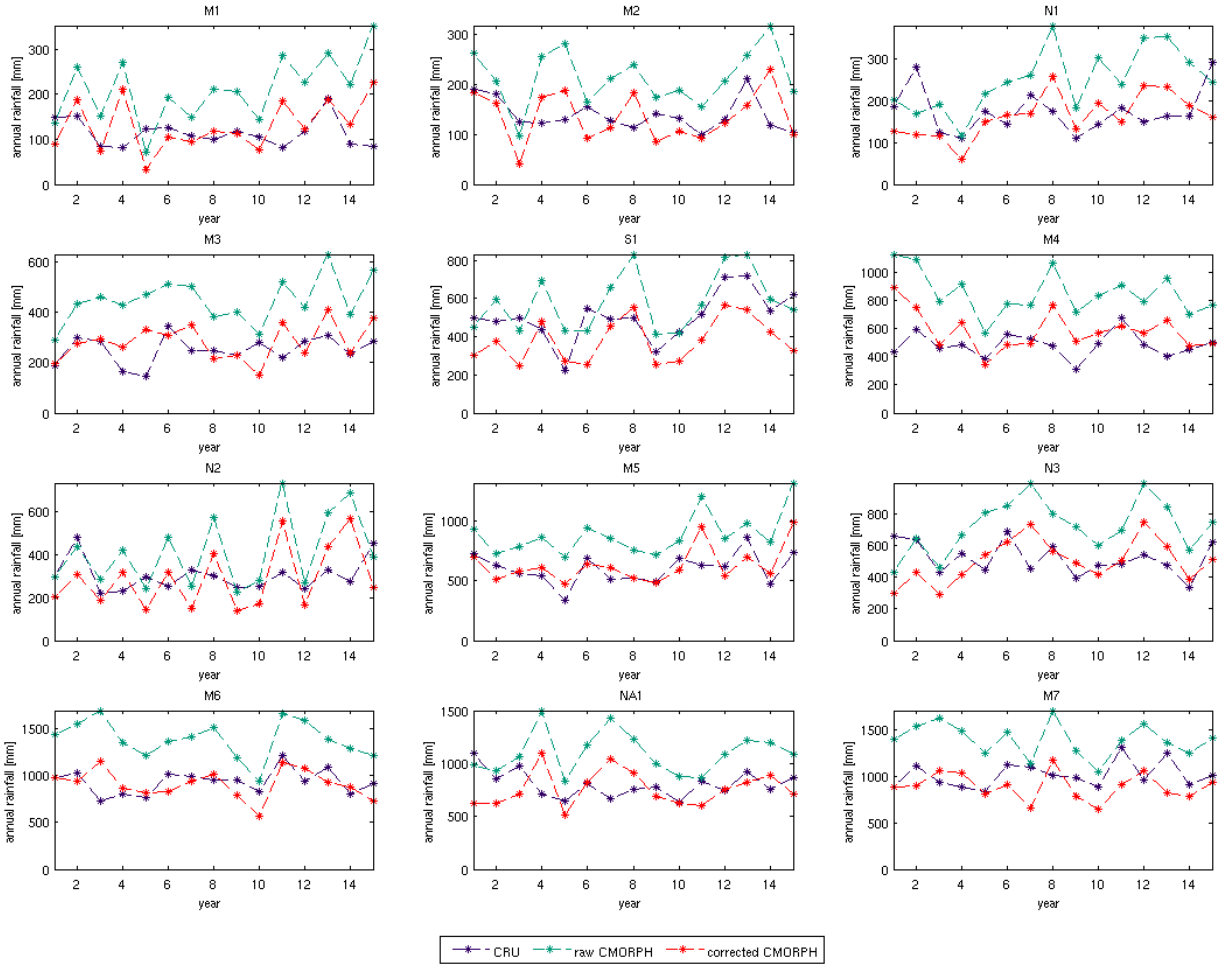

Figure A.2 Annual rainfall at each location from CRU (blue), raw CMORPH (green), and bias-corrected CMORPH (red).

Table A.1 Bias-correction factor for CMORPH rainfall

Rainfall intensity [mm/hr]			BCF
0.0	to	0.5	0.00
0.6	to	0.6	0.03
0.7	to	0.7	0.23
0.8	to	0.8	0.25
0.9	to	0.9	0.27
1.0	to	1.0	0.27
1.1	to	1.1	0.29
1.2	to	1.2	0.33
1.3	to	1.3	0.31
1.4	to	1.4	0.34
1.5	to	1.5	0.33
1.6	to	1.6	0.31
1.7	to	1.7	0.33
1.8	to	1.8	0.36
1.9	to	1.9	0.39
2.0	to	2.0	0.38
2.1	to	2.1	0.40
2.2	to	2.2	0.45
2.3	to	2.3	0.43
2.4	to	2.4	0.42
2.5	to	2.5	0.46
2.6	to	2.6	0.45
2.7	to	2.7	0.46
2.8	to	2.8	0.45
2.9	to	2.9	0.47
3.0	to	3.0	0.49
3.1	to	3.1	0.48
3.2	to	3.2	0.49
3.3	to	3.3	0.50
3.4	to	3.4	0.51
3.5	to	3.5	0.50
3.6	to	3.7	0.53
3.8	to	3.8	0.53
3.9	to	3.9	0.53
4.0	to	4.0	0.55
4.1	to	4.2	0.55
4.3	to	4.3	0.57
4.4	to	4.4	0.57
4.5	to	4.6	0.57
4.7	to	4.7	0.59
4.8	to	4.8	0.60
4.9	to	5.1	0.60
5.2	to	5.3	0.60
5.4	to	5.6	0.61
5.7	to	5.9	0.62
6.0	to	6.2	0.62
6.3	to	6.4	0.62
6.5	to	6.7	0.61
6.8	to	6.9	0.62
7.0	to	7.2	0.64
7.3	to	7.7	0.65
7.8	to	8.0	0.67
8.1	to	8.4	0.69
8.5	to	8.8	0.71
8.9	to	9.5	0.74
9.6	to	10.1	0.79
10.2	to	11.0	0.79
11.1	to	11.5	0.81
11.6	to	12.4	0.86
12.5	to	13.6	0.88
13.7	to	15.1	0.87
15.2	to	17.2	0.88
17.3	to	19.7	0.90
19.8	to	23.4	0.94
23.5	to	Inf	1.10

Appendix B Regression relationships for variables in Chapter 5

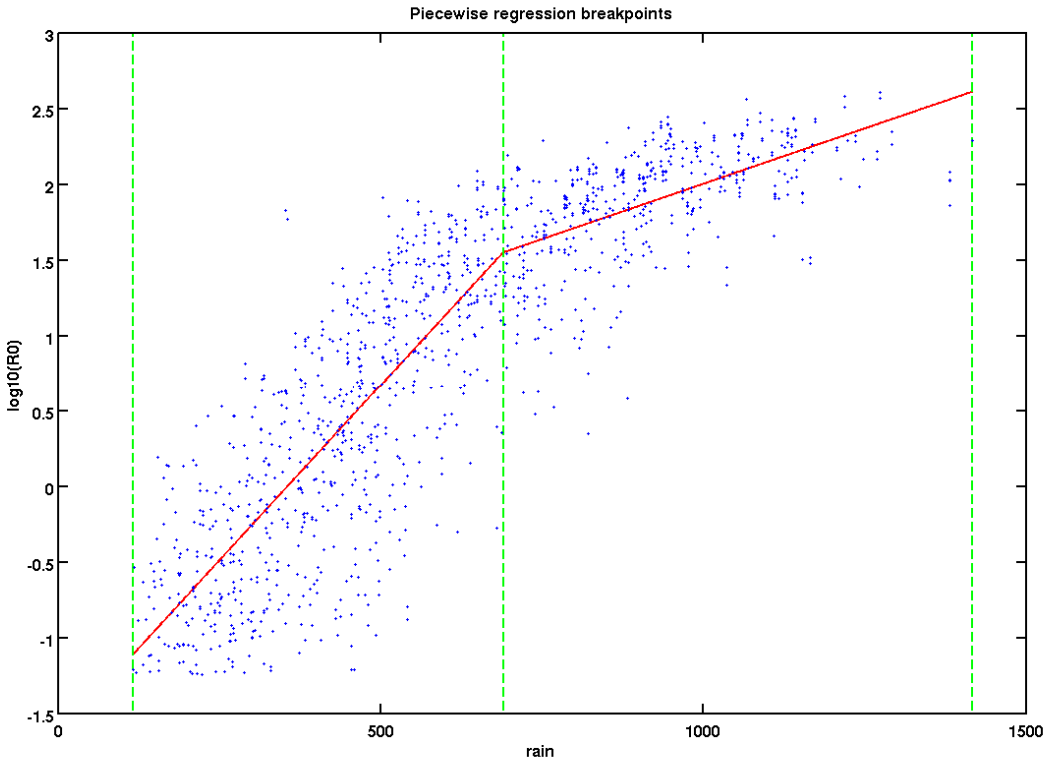

Figure B.1 Annual rainfall versus annual $\log_{10}(R_0)$

Regression equation in the form f(x)=a*x+b

x	a	b
rain<690	4.64E-03	-1.65E+00
rain>690	1.46E-03	5.44E-01

RMSE: 0.13

R^2: 0.79

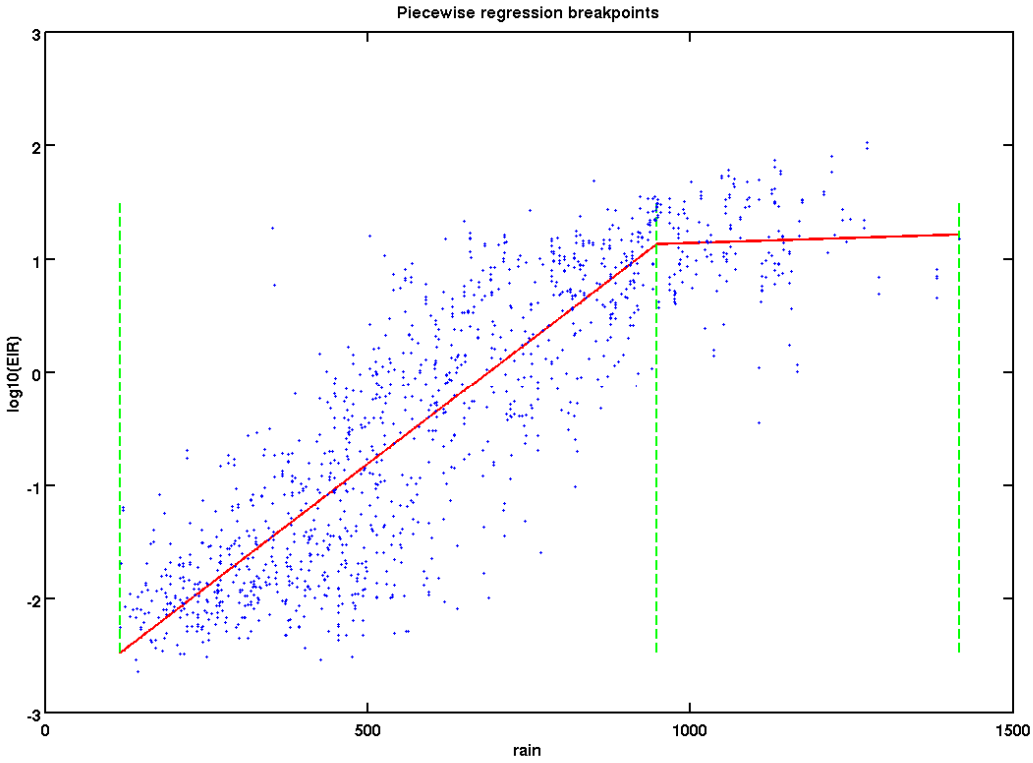

Figure B.2 Annual rainfall versus annual Log_{10}(EIR)

Regression equation in the form f(x)=a*x+b

x	a	b
rain<950	4.34E-03	-2.98E+00
rain>950	1.79E-04	9.61E-01

RMSE: 0.13

R^2: 0.76

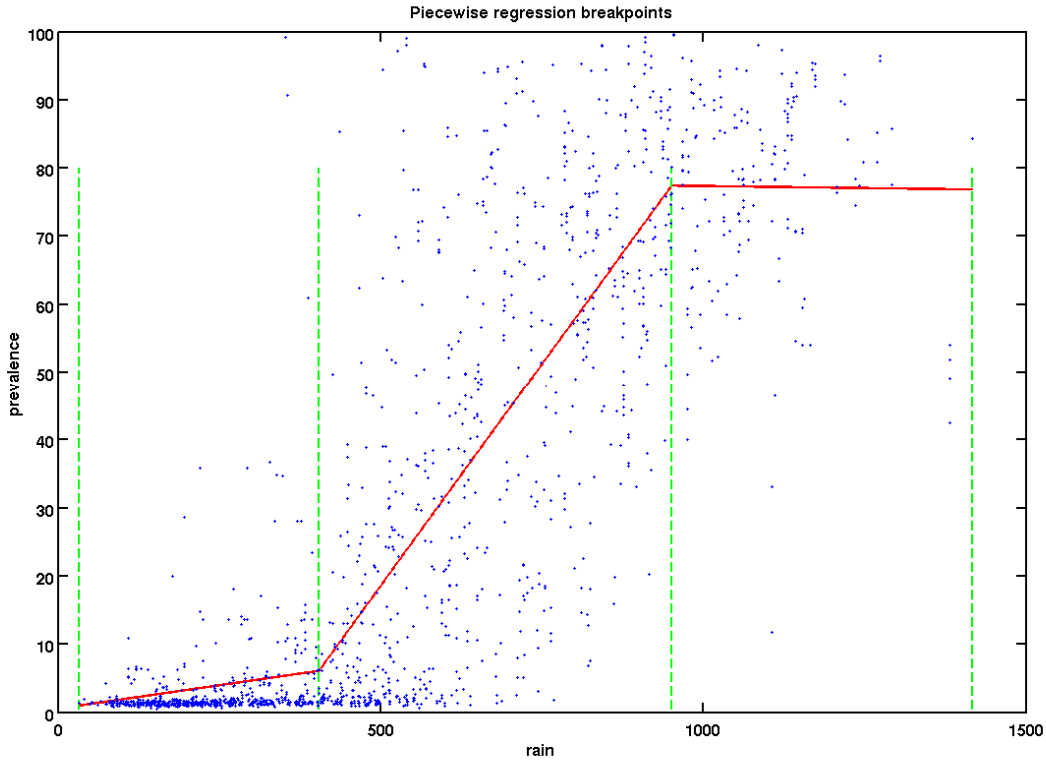

Figure B.3 Annual rainfall versus annual peak malaria prevalence in children ages 2-10

Regression equation in the form f(x)=a*x+b

x	a	b
rain < 415	1.37E-02	5.50E-01
415<rain<950	1.31E-01	-4.67E+01
rain > 950	-1.21E-03	7.86E+01

RMSE: 0.17

R^2: 0.72

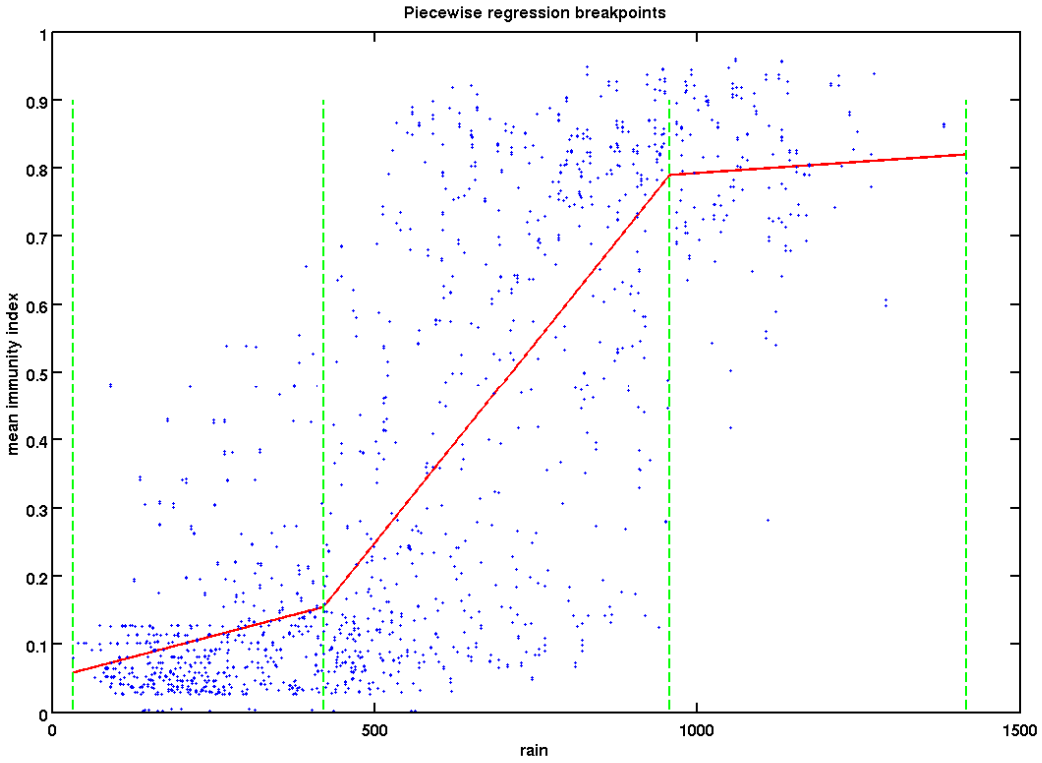

Figure B.4 Annual rainfall versus annual mean population immunity index

Regression equation in the form f(x)=a*x+b

x	a	b
rain < 415	2.48E-04	5.02E-02
415<rain<950	1.18E-03	-3.44E-01
rain > 950	6.55E-05	7.27E-01

RMSE: 0.20

R^2: 0.65

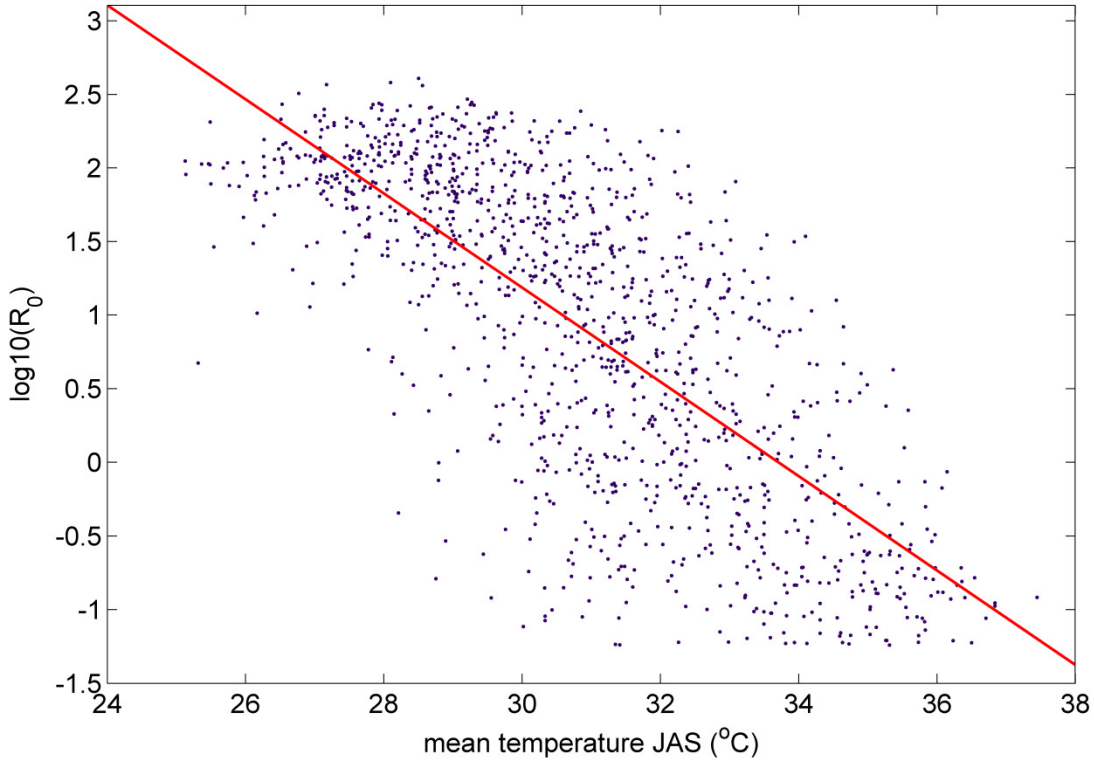

Figure B.5 Mean July-September temperature versus annual log10(R0). The red line is the least-squares regression line.

Regression equation in the form f(x)=a*x+b

x	a	b
tjas	-3.20E-01	1.08E+01

R^2= 0.54

RMSE=2.75

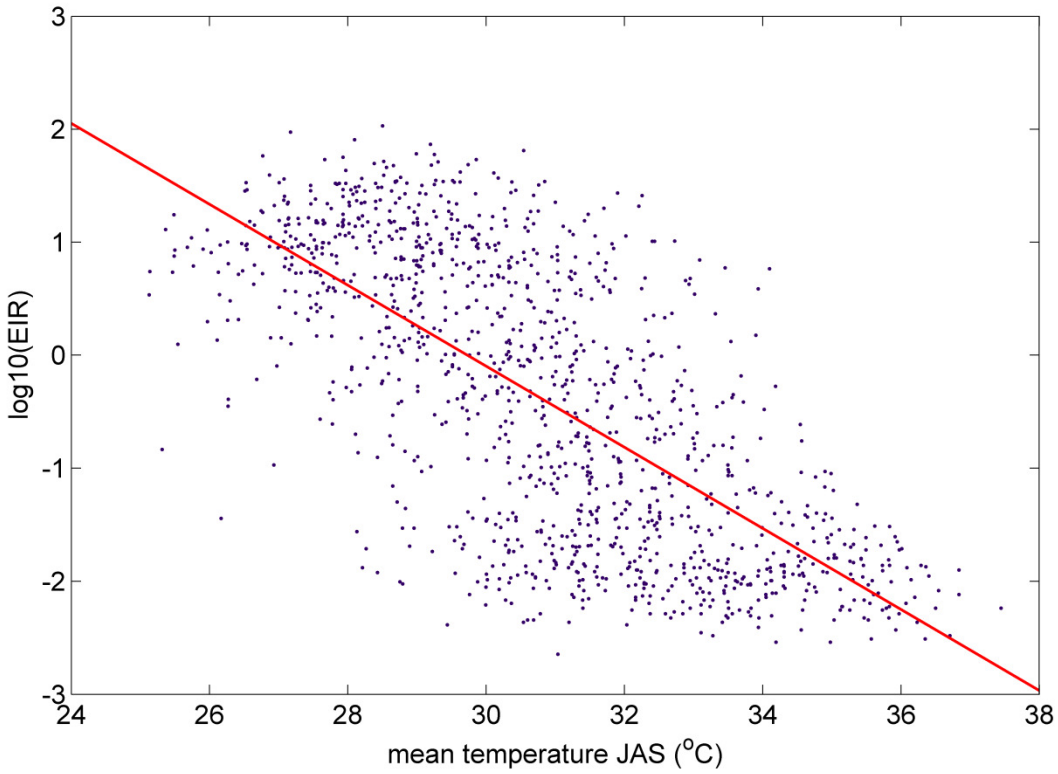

Figure B.6 Mean July-September temperature versus annual log10(EIR)

Regression equation in the form f(x)=a*x+b

x	a	b
tjas	-3.59E-01	1.07E+01

R^2= 0.49

RMSE=4.16

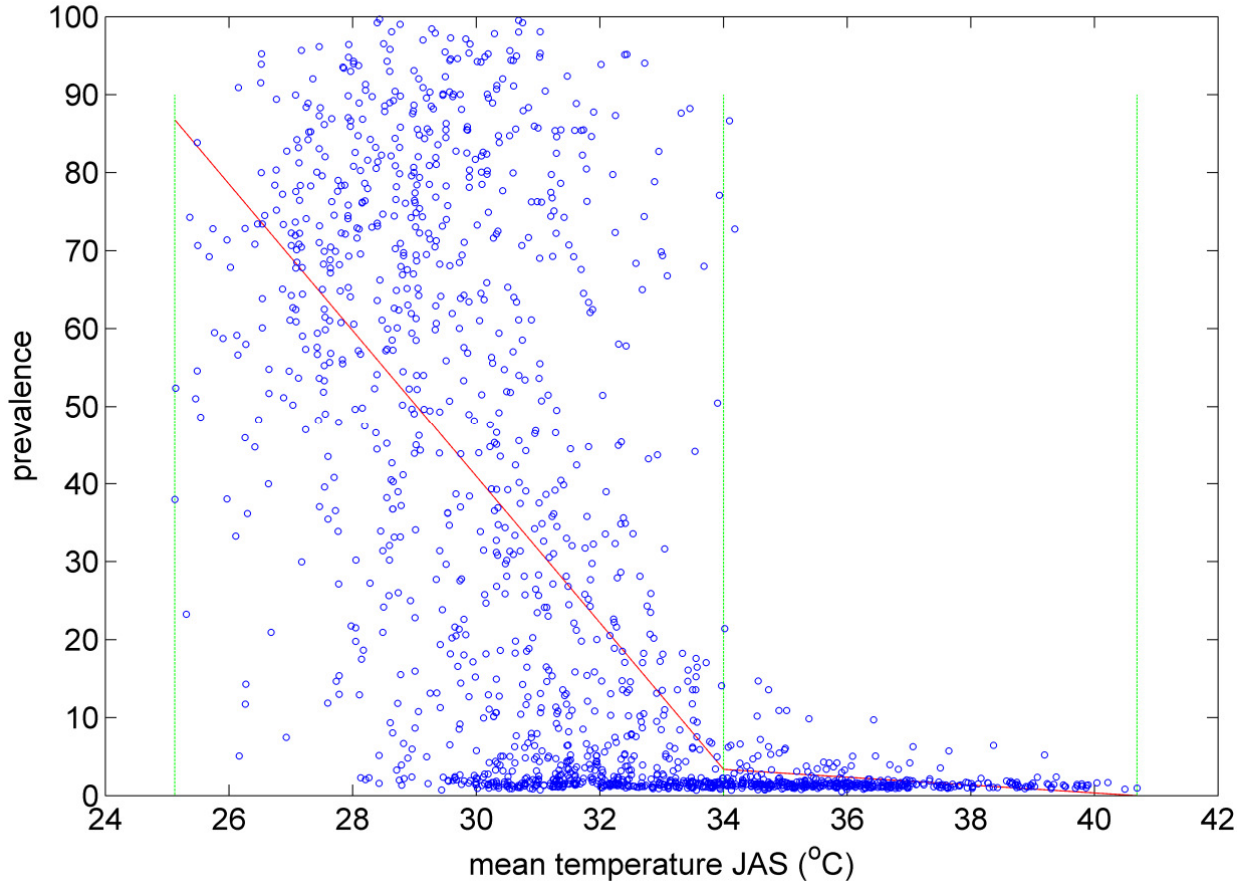

Figure B.7 Mean July-September temperature versus annual peak malaria prevalence in children ages 2-10.

Regression equation in the form f(x)=a*x+b

x	a	b
tjas<34	-9.40E+00	3.23E+02
tjas>34	-5.04E-01	2.05E+01

RMSE: 0.24

R^2: 0.47

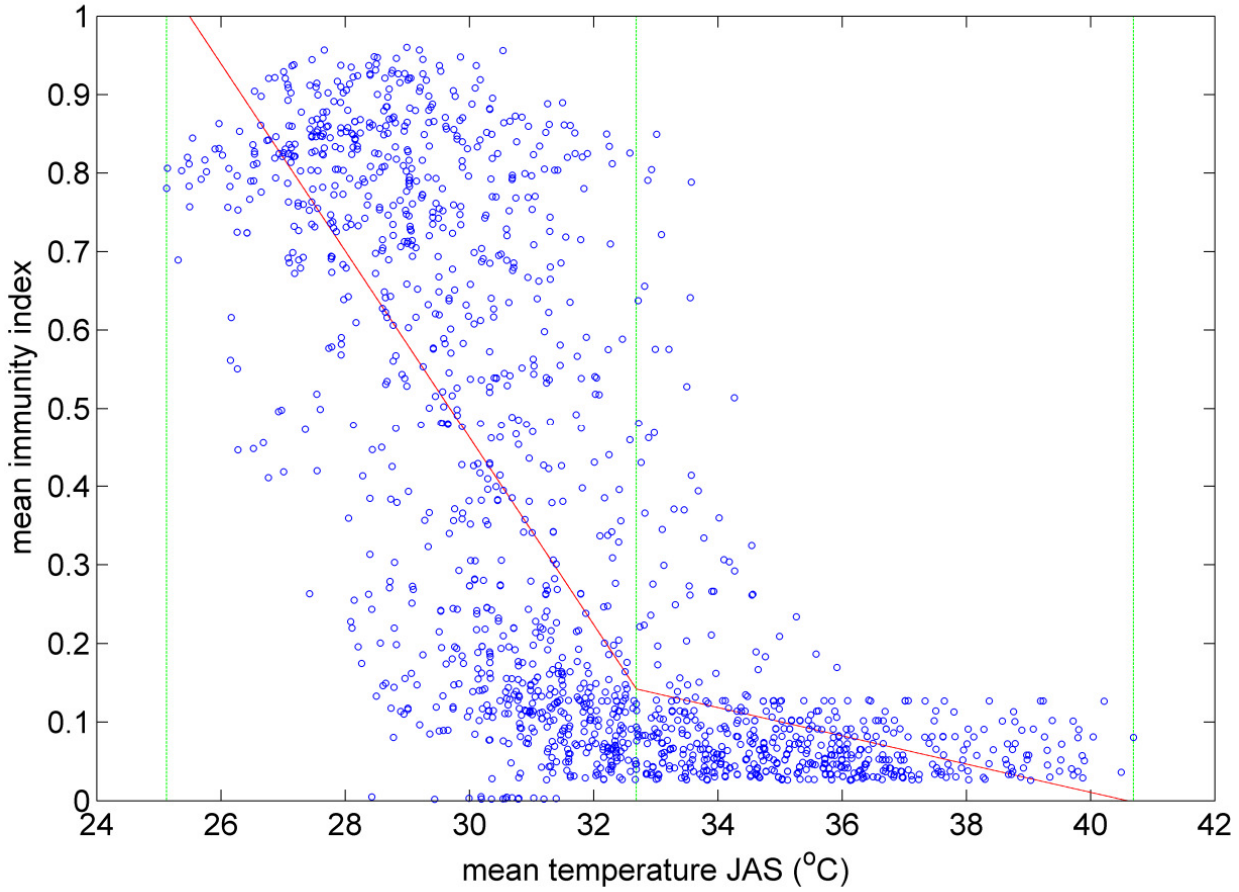

Figure B.8 Mean July-September temperature versus annual mean population immunity index.

Regression equation in the form f(x)=a*x+b

x	a	b
tjas < 32.7	-1.19E-01	4.04E+00
tjas > 32.7	-1.80E-02	7.29E-01

RMSE: 0.21

R^2: 0.60

Appendix C Additional results for malaria transmission in current climate conditions

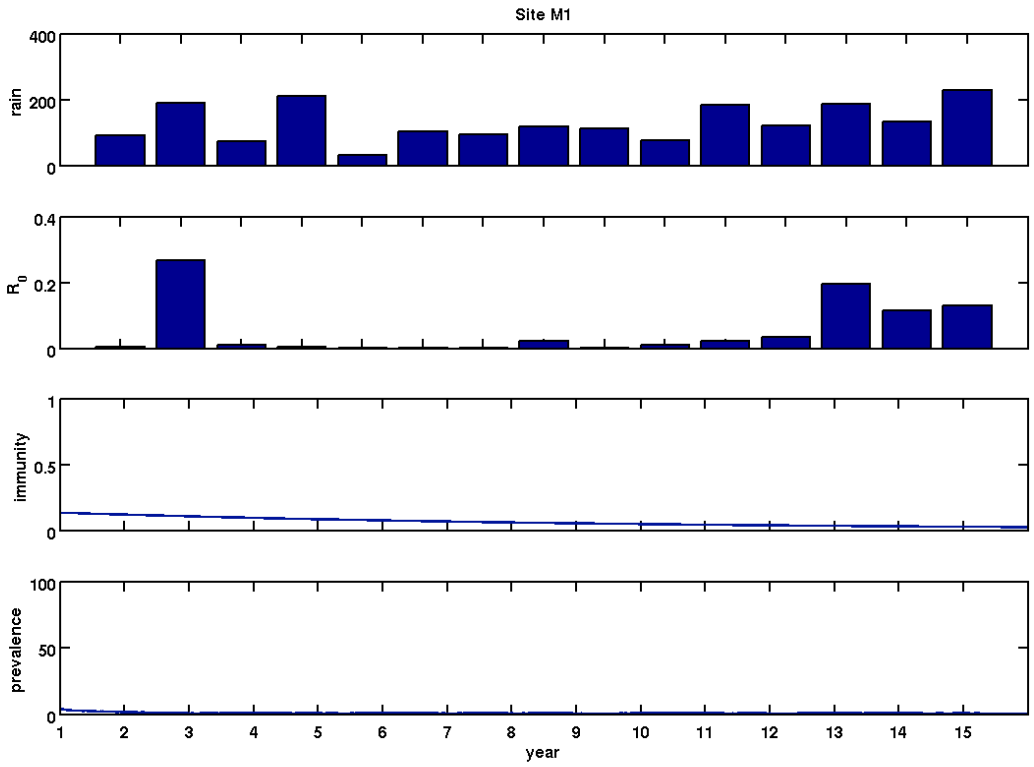

Figure C.1 Simulation results for site M1. From top to bottom, the sub figures show annual rainfall, peak annual R_0, daily mean population immunity index, and daily malaria prevalence in children aged 2-10.

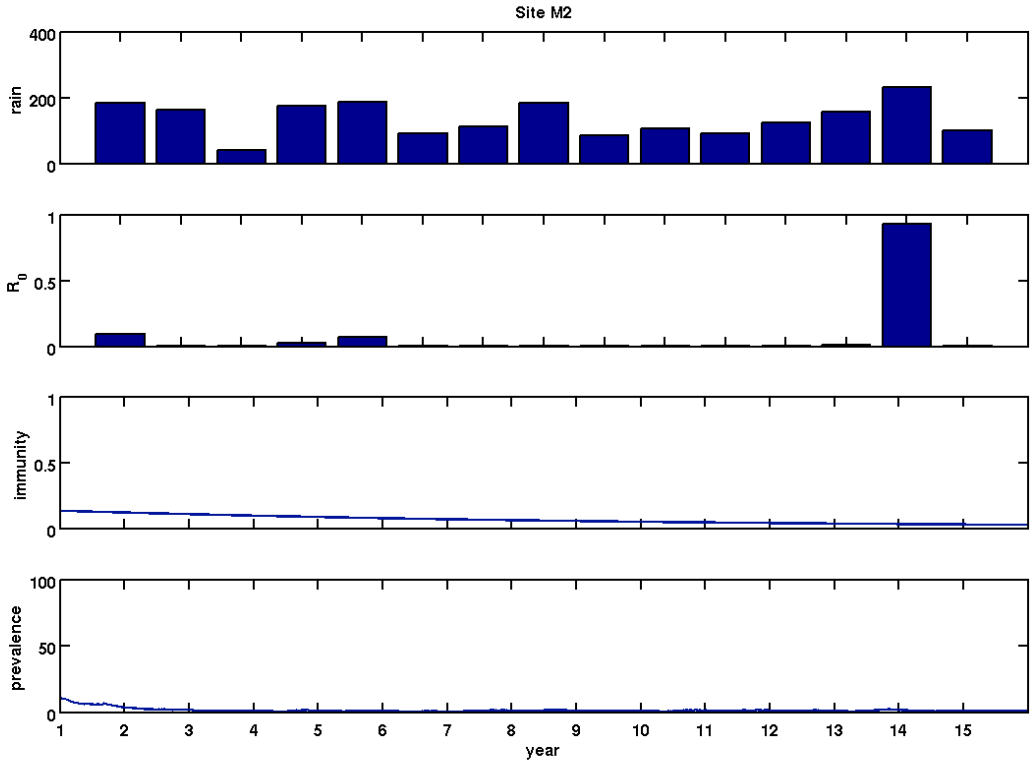

Figure C.2 Simulation results for site M2. From top to bottom, the sub figures show annual rainfall, peak annual R_0, daily mean population immunity index, and daily malaria prevalence in children aged 2-10.

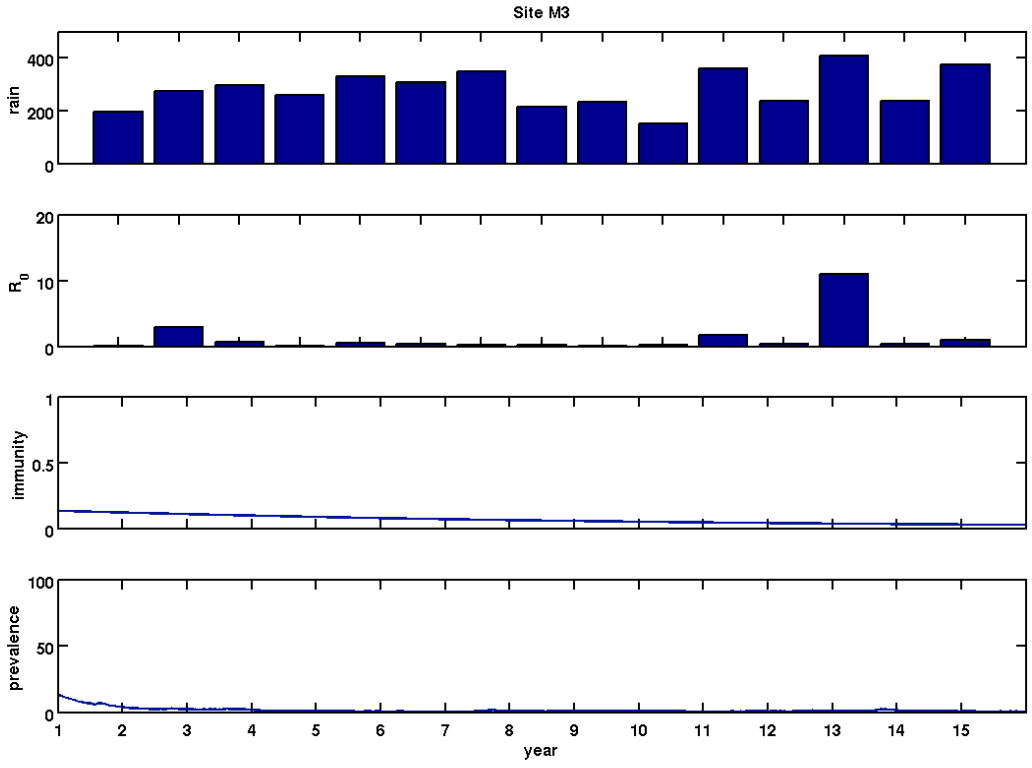

Figure C.3 Simulation results for site M3. From top to bottom, the sub figures show annual rainfall, peak annual R_0, daily mean population immunity index, and daily malaria prevalence in children aged 2-10.

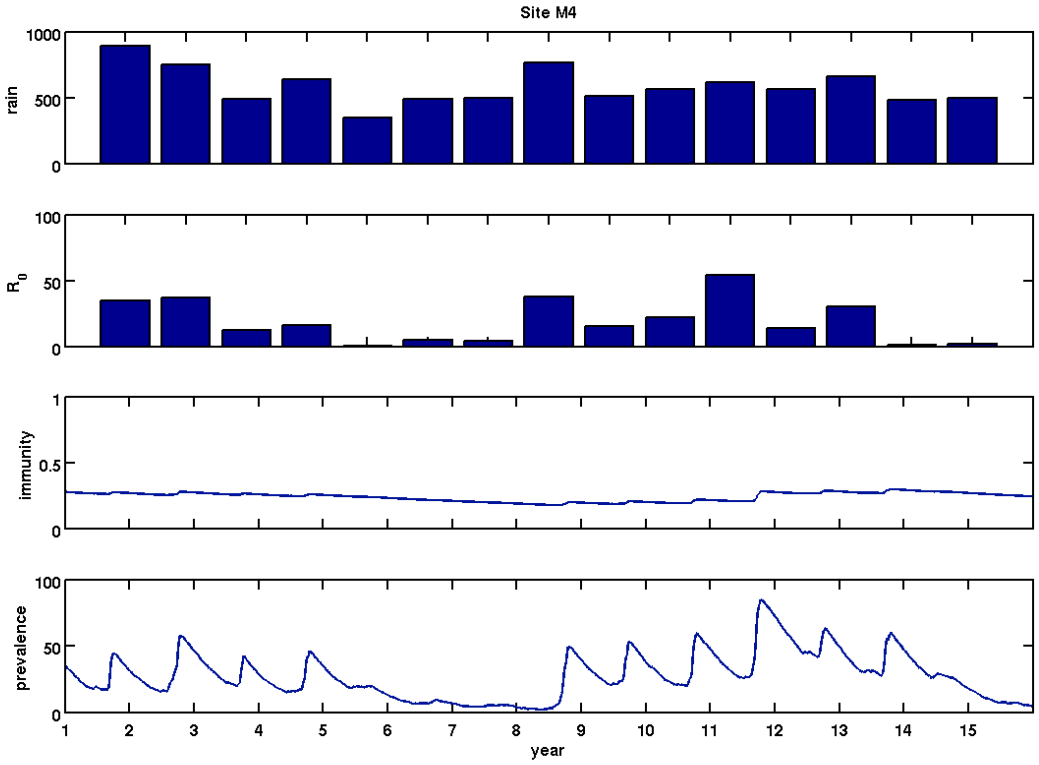

Figure C.4 Simulation results for site M4. From top to bottom, the sub figures show annual rainfall, peak annual R_0, daily mean population immunity index, and daily malaria prevalence in children aged 2-10.

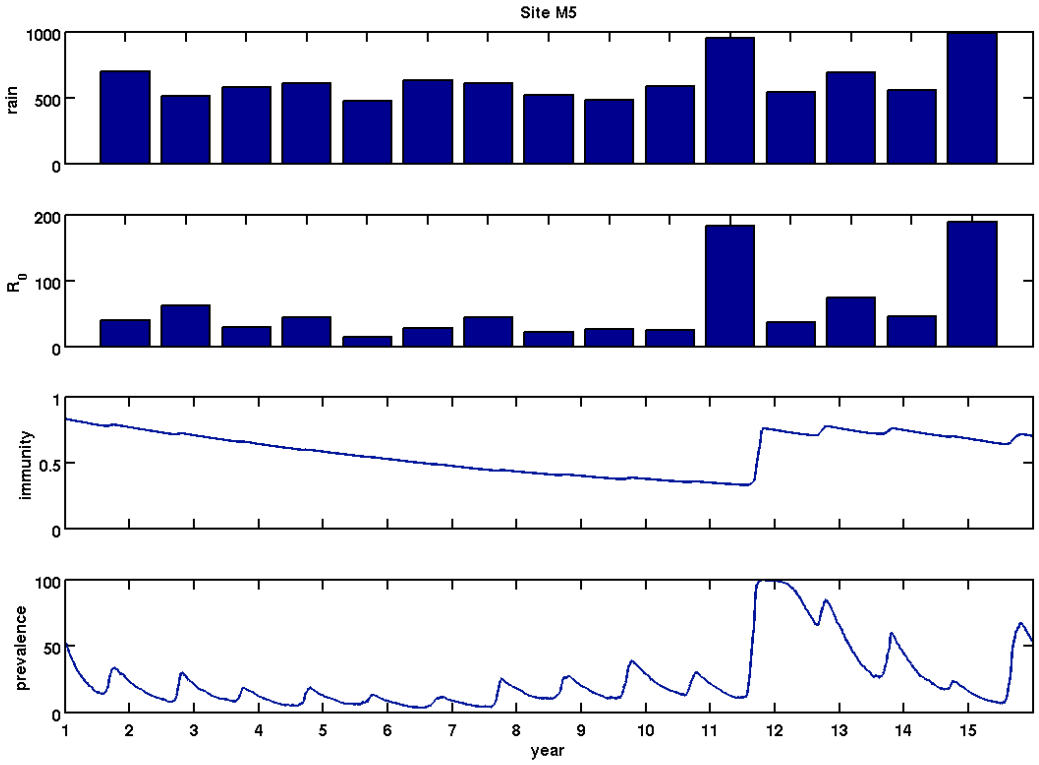

Figure C.5 Simulation results for site M5. From top to bottom, the sub figures show annual rainfall, peak annual R_0, daily mean population immunity index, and daily malaria prevalence in children aged 2-10.

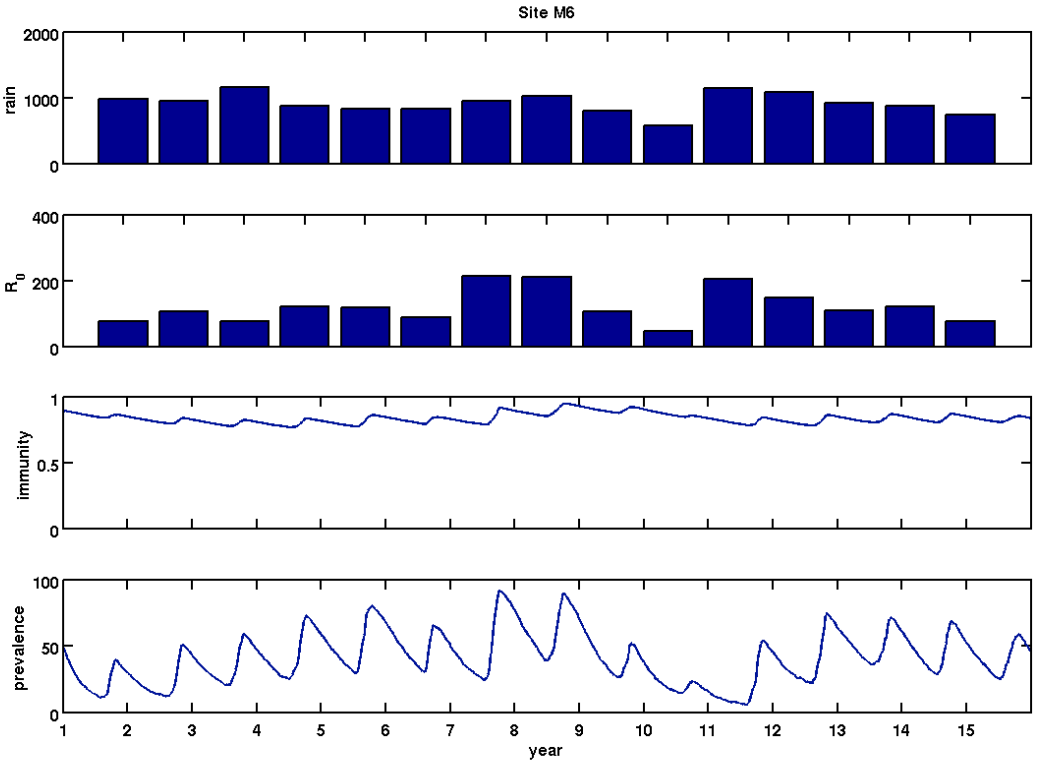

Figure C.6 Simulation results for site M6. From top to bottom, the sub figures show annual rainfall, peak annual R_0, daily mean population immunity index, and daily malaria prevalence in children aged 2-10.

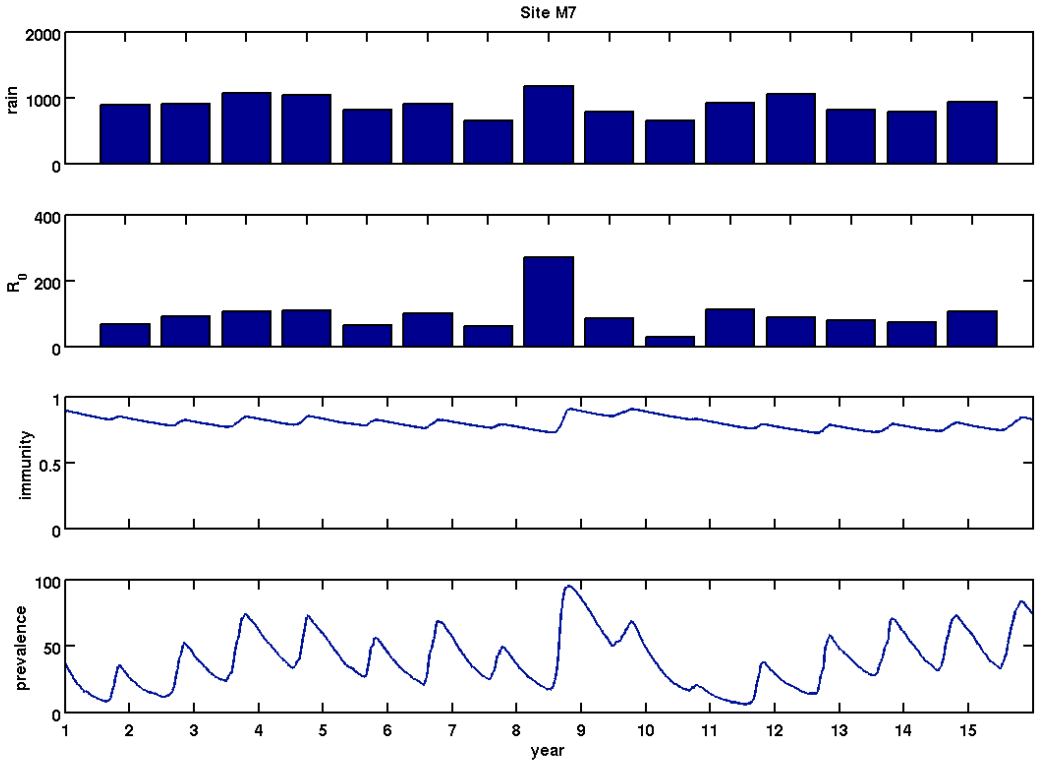

Figure C.7 Simulation results for site M7. From top to bottom, the sub figures show annual rainfall, peak annual R_0, daily mean population immunity index, and daily malaria prevalence in children aged 2-10.

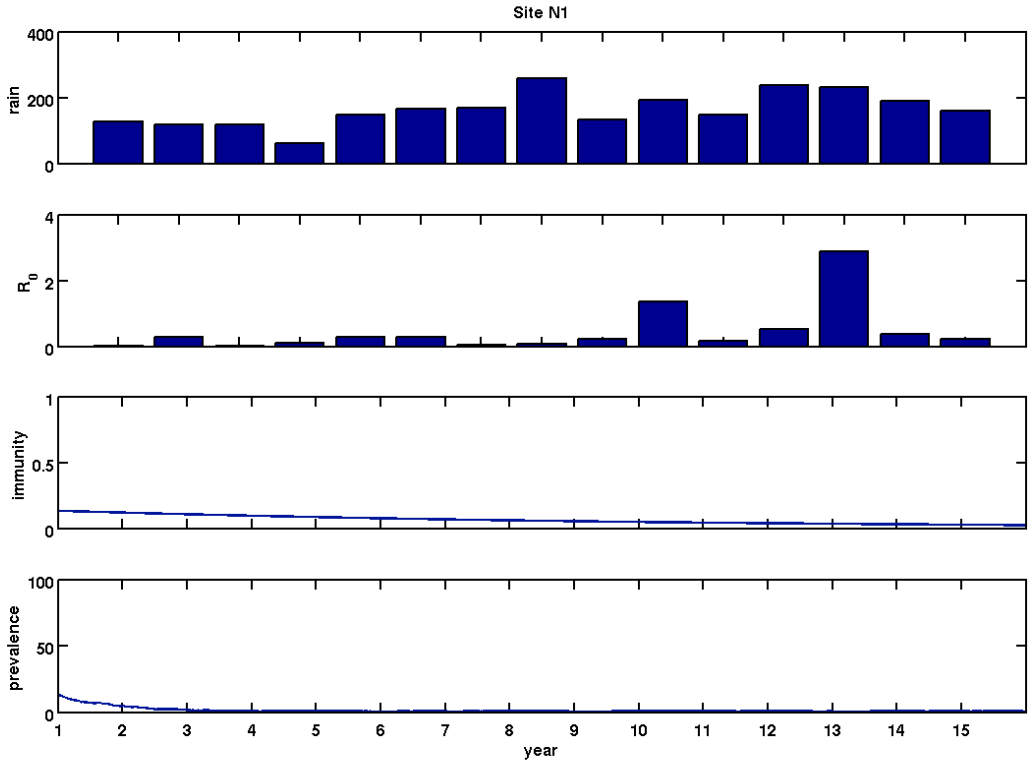

Figure C.8 Simulation results for site N1. From top to bottom, the sub figures show annual rainfall, peak annual R_0, daily mean population immunity index, and daily malaria prevalence in children aged 2-10.

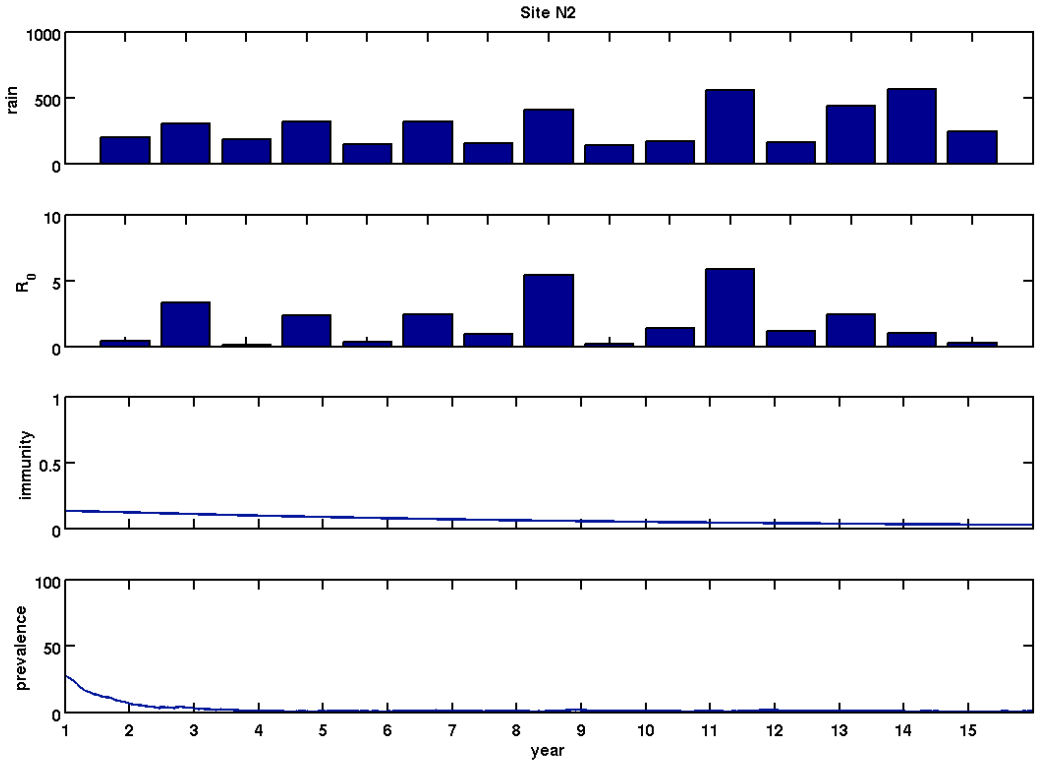

Figure C.9 Simulation results for site N2. From top to bottom, the sub figures show annual rainfall, peak annual R_0, daily mean population immunity index, and daily malaria prevalence in children aged 2-10.

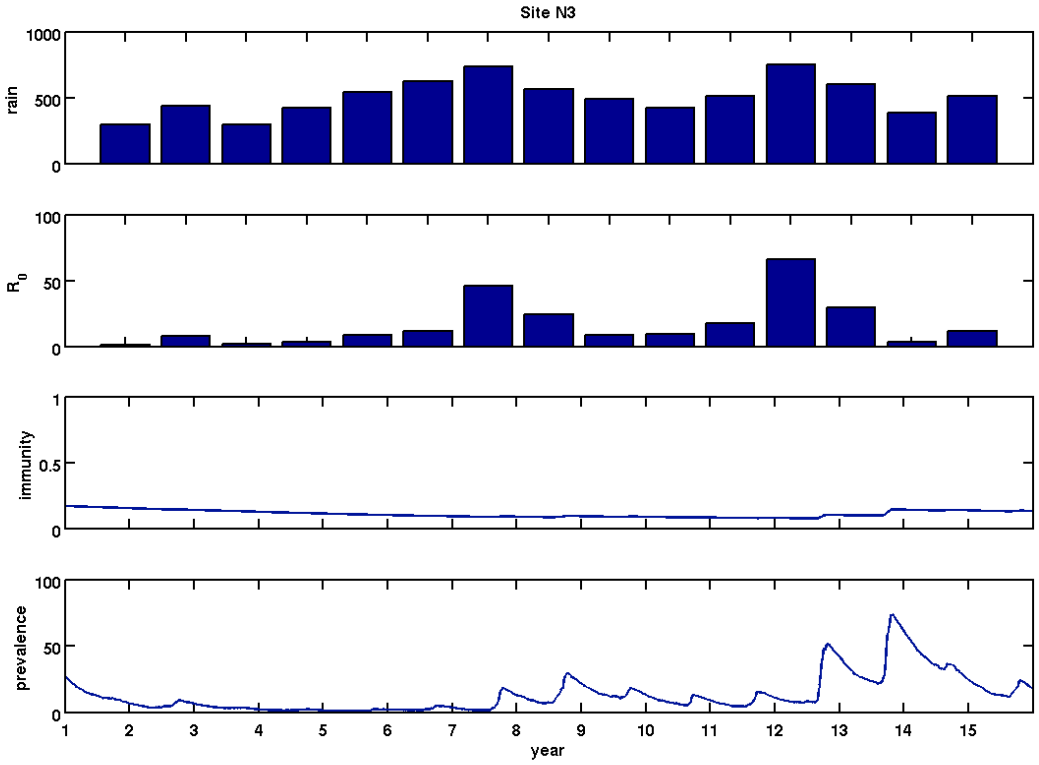

Figure C.10 Simulation results for site N3. From top to bottom, the sub figures show annual rainfall, peak annual R_0, daily mean population immunity index, and daily malaria prevalence in children aged 2-10.

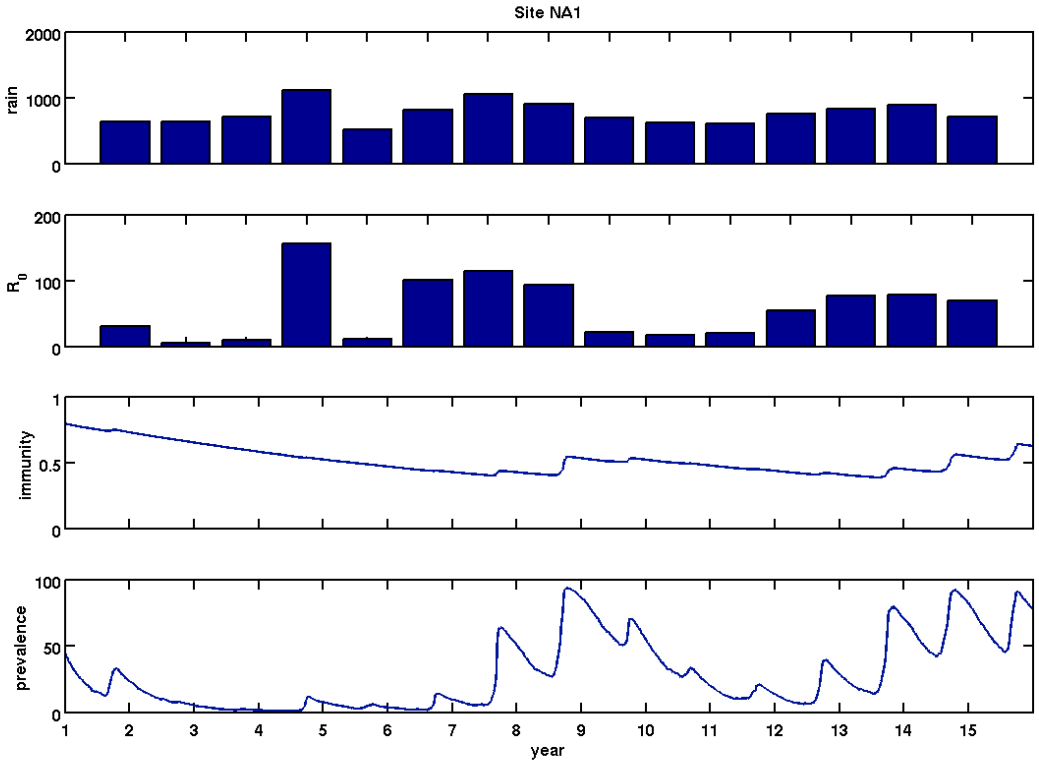

Figure C.11 Simulation results for site NA1. From top to bottom, the sub figures show annual rainfall, peak annual R_0, daily mean population immunity index, and daily malaria prevalence in children aged 2-10.

Appendix D Additional results for malaria transmission in future climate conditions

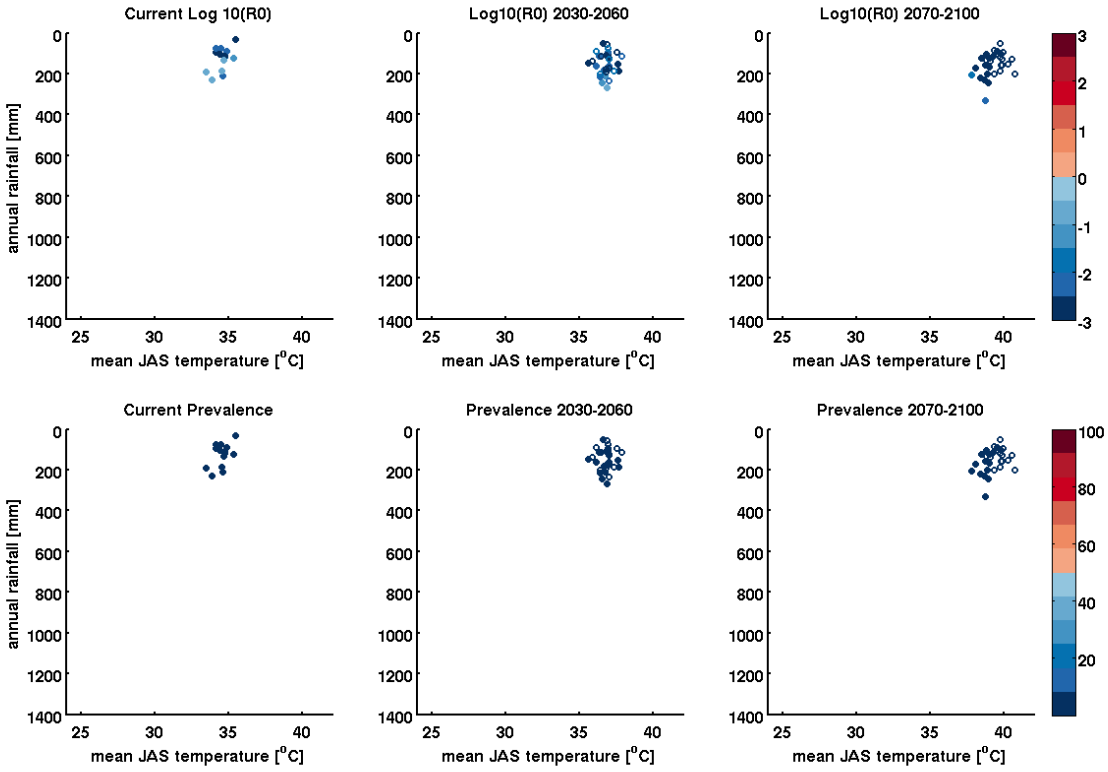

Figure D.1 Simulation results for site M1. The top row shows log10 (R_0) and the bottom row shows prevalence in children aged 2-10. Current conditions are shown on the left, short term conditions in the center, and long term conditions on the right. Closed circles are results from the simulation using CCSM4 climate predictions and open circles used MPI-ESM-MR predictions.

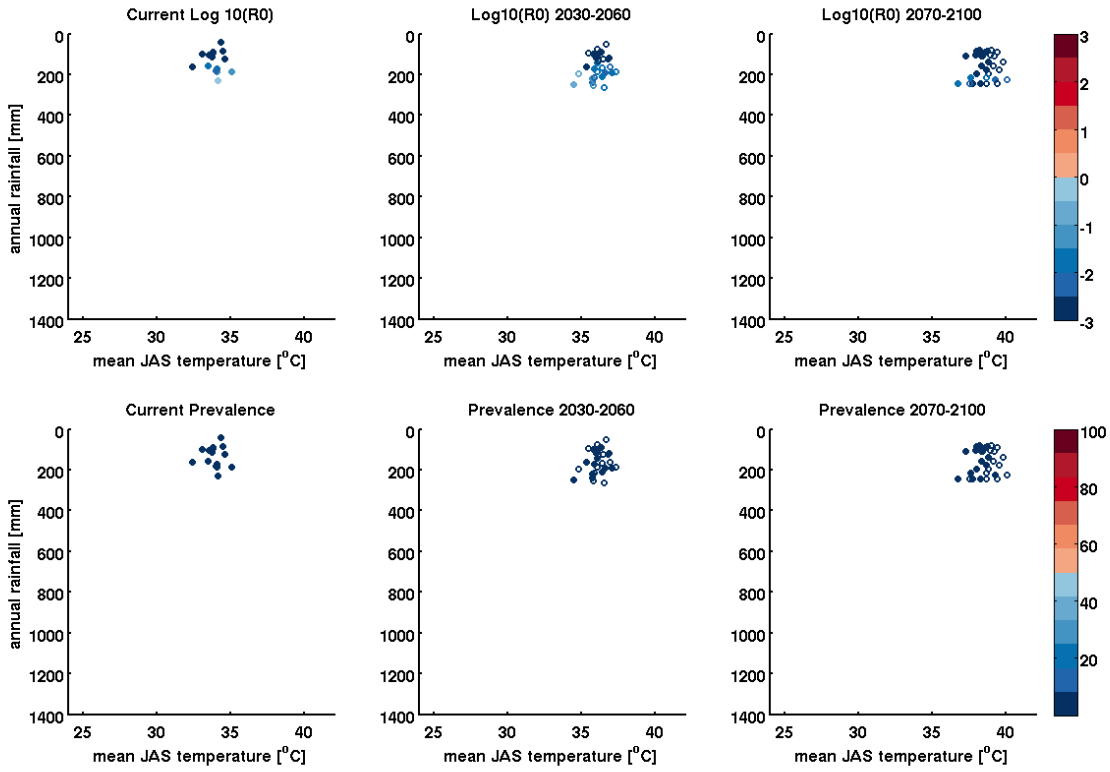

Figure D.2 Simulation results for site M2. The top row shows log10 (R_0) and the bottom row shows prevalence in children aged 2-10. Current conditions are shown on the left, short term conditions in the center, and long term conditions on the right. Closed circles are results from the simulation using CCSM4 climate predictions and open circles used MPI-ESM-MR predictions.

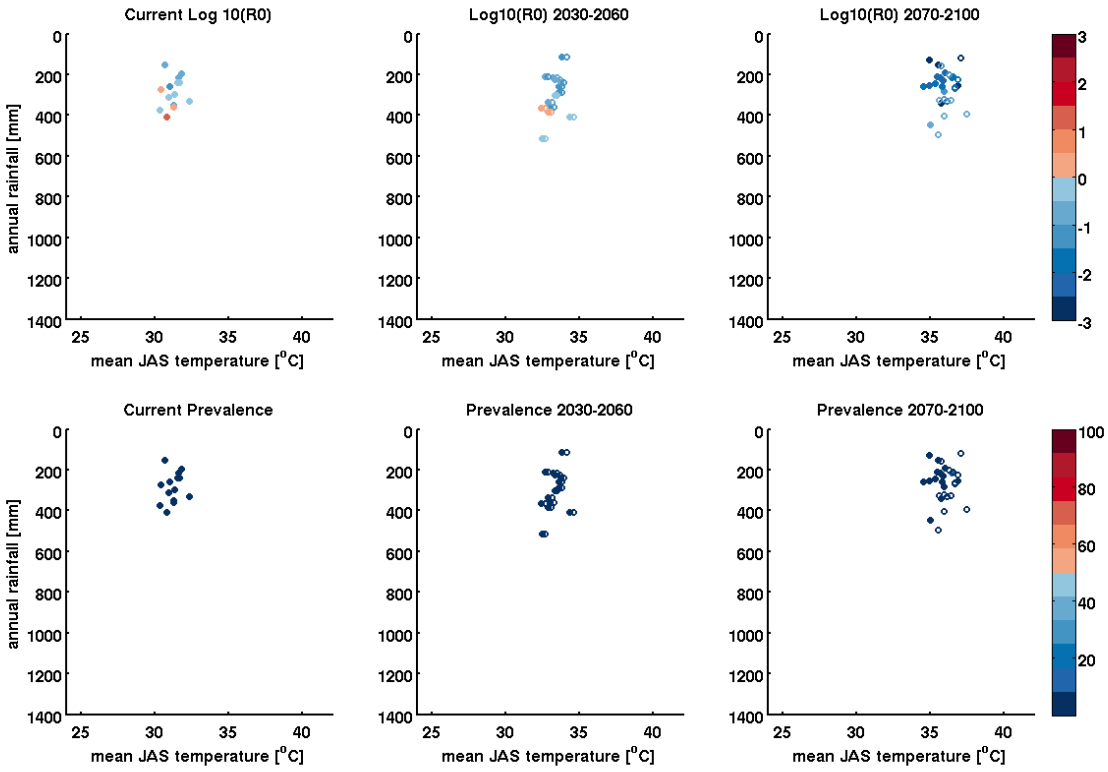

Figure D.3 Simulation results for site M3. The top row shows log10 (R_0) and the bottom row shows prevalence in children aged 2-10. Current conditions are shown on the left, short term conditions in the center, and long term conditions on the right. Closed circles are results from the simulation using CCSM4 climate predictions and open circles used MPI-ESM-MR predictions.

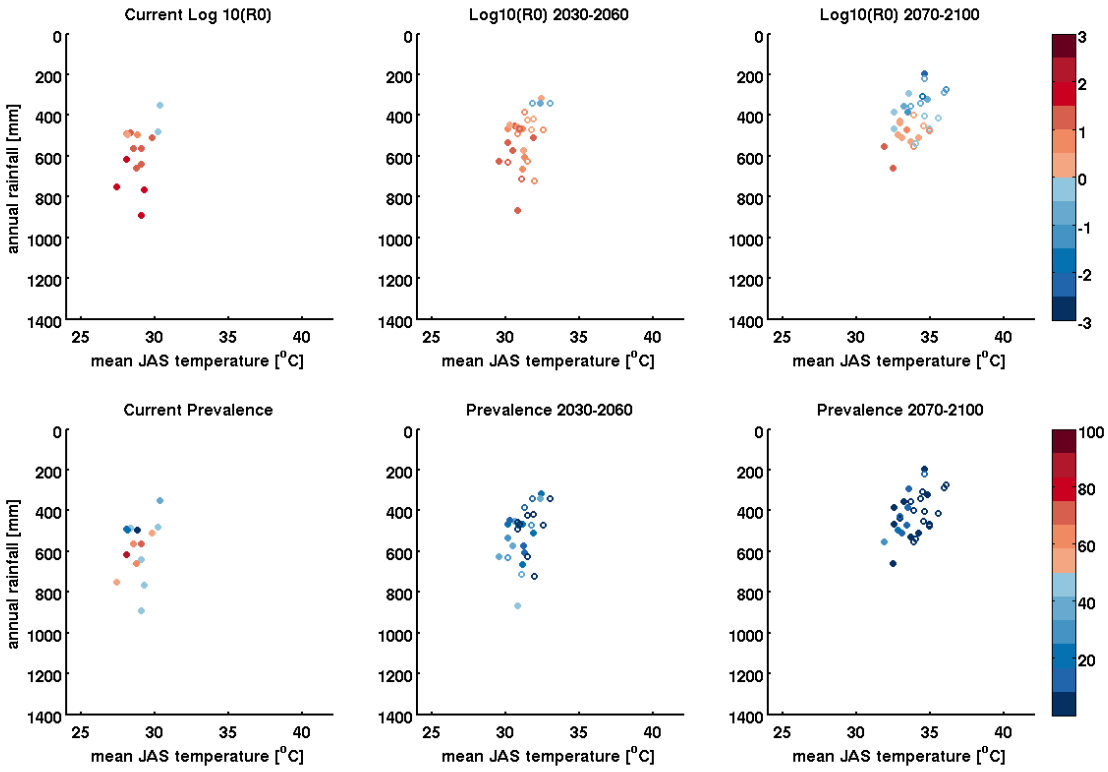

Figure D.4 Simulation results for site M4. The top row shows log10 (R_0) and the bottom row shows prevalence in children aged 2-10. Current conditions are shown on the left, short term conditions in the center, and long term conditions on the right. Closed circles are results from the simulation using CCSM4 climate predictions and open circles used MPI-ESM-MR predictions.

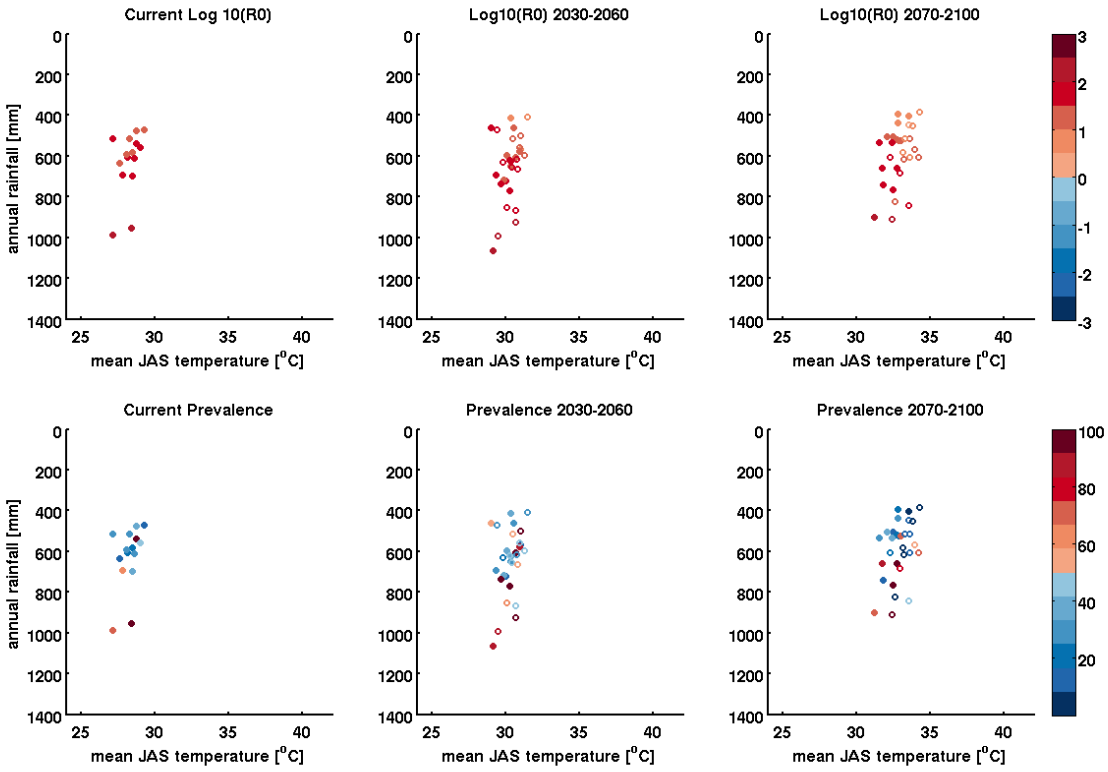

Figure D.5 Simulation results for site M5. The top row shows log10 (R_0) and the bottom row shows prevalence in children aged 2-10. Current conditions are shown on the left, short term conditions in the center, and long term conditions on the right. Closed circles are results from the simulation using CCSM4 climate predictions and open circles used MPI-ESM-MR predictions.

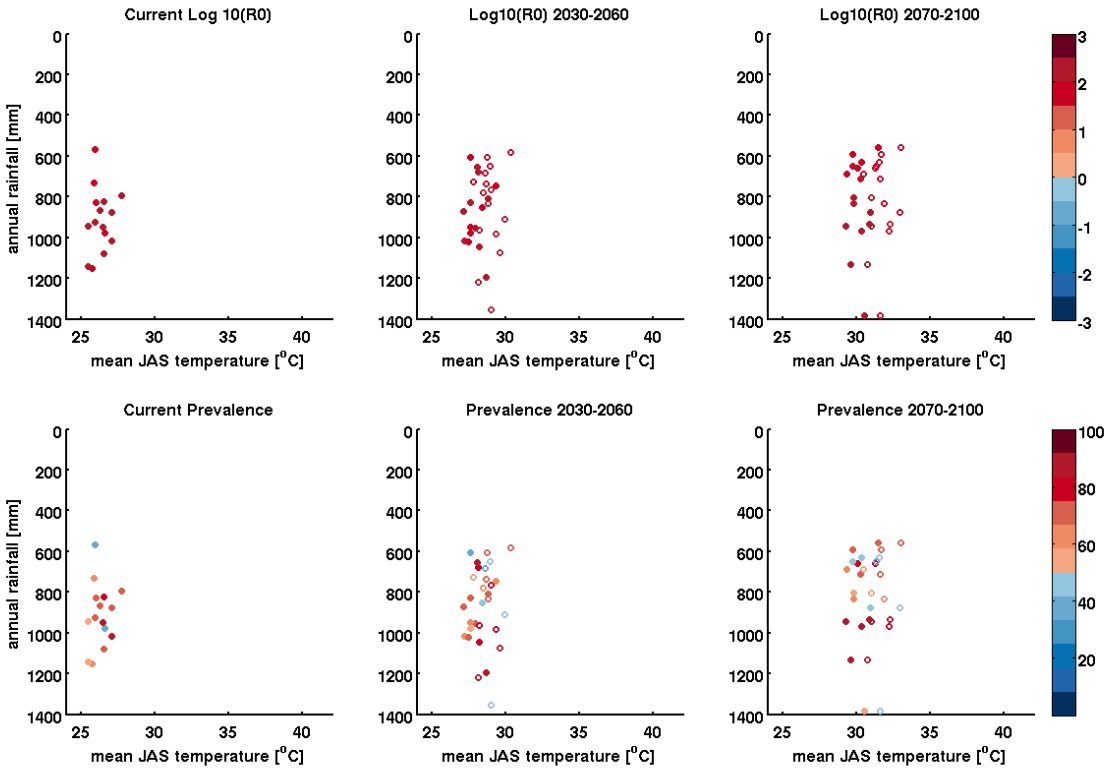

Figure D.6 Simulation results for site M6. The top row shows log10 (R_0) and the bottom row shows prevalence in children aged 2-10. Current conditions are shown on the left, short term conditions in the center, and long term conditions on the right. Closed circles are results from the simulation using CCSM4 climate predictions and open circles used MPI-ESM-MR predictions.

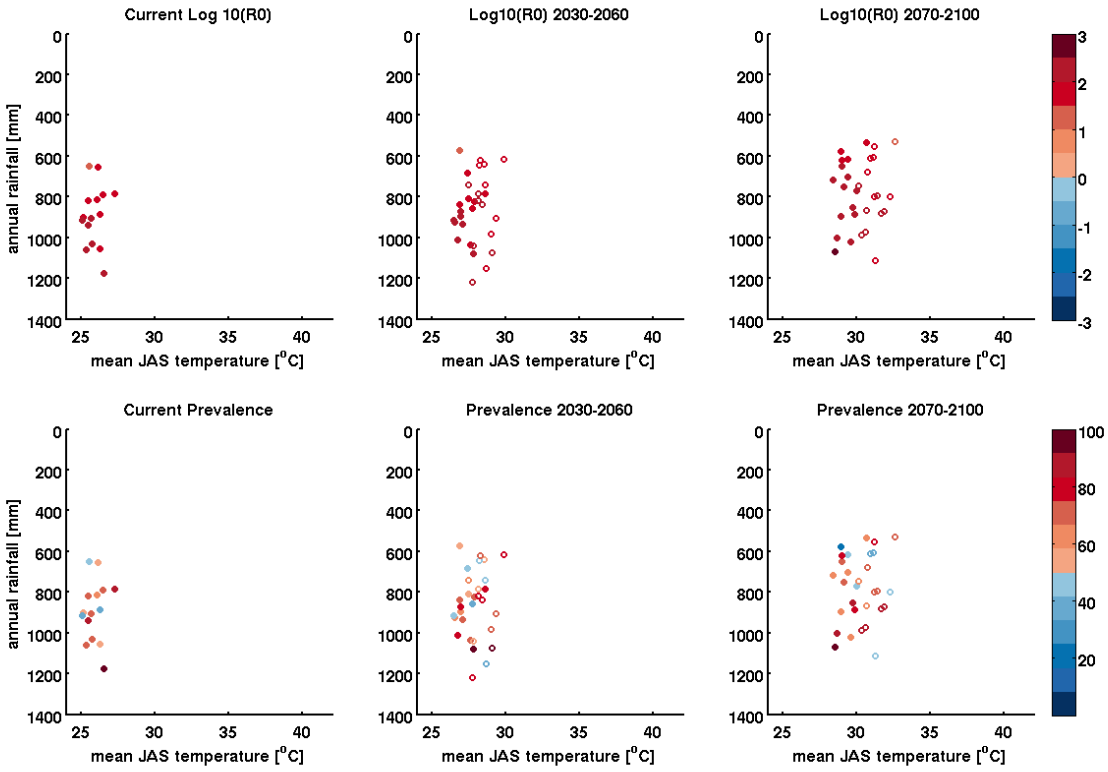

Figure D.7 Simulation results for site M7. The top row shows log10 (R_0) and the bottom row shows prevalence in children aged 2-10. Current conditions are shown on the left, short term conditions in the center, and long term conditions on the right. Closed circles are results from the simulation using CCSM4 climate predictions and open circles used MPI-ESM-MR predictions.

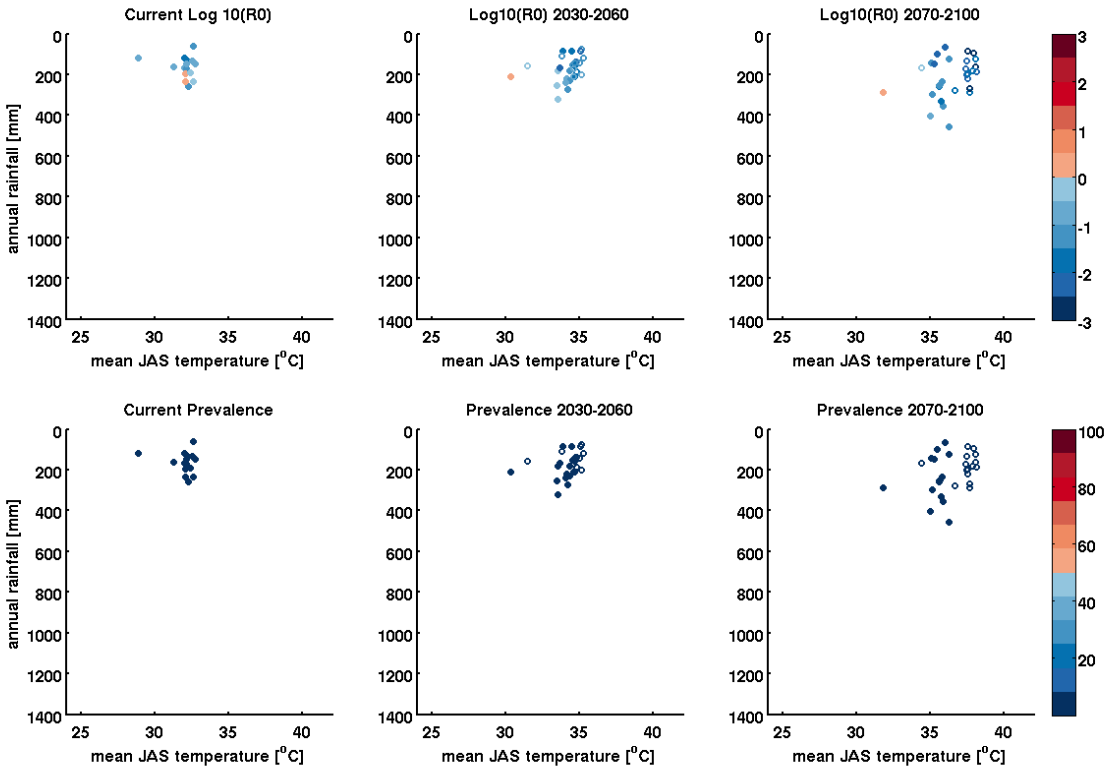

Figure D.8 Simulation results for site N1. The top row shows log10 (R_0) and the bottom row shows prevalence in children aged 2-10. Current conditions are shown on the left, short term conditions in the center, and long term conditions on the right. Closed circles are results from the simulation using CCSM4 climate predictions and open circles used MPI-ESM-MR predictions.

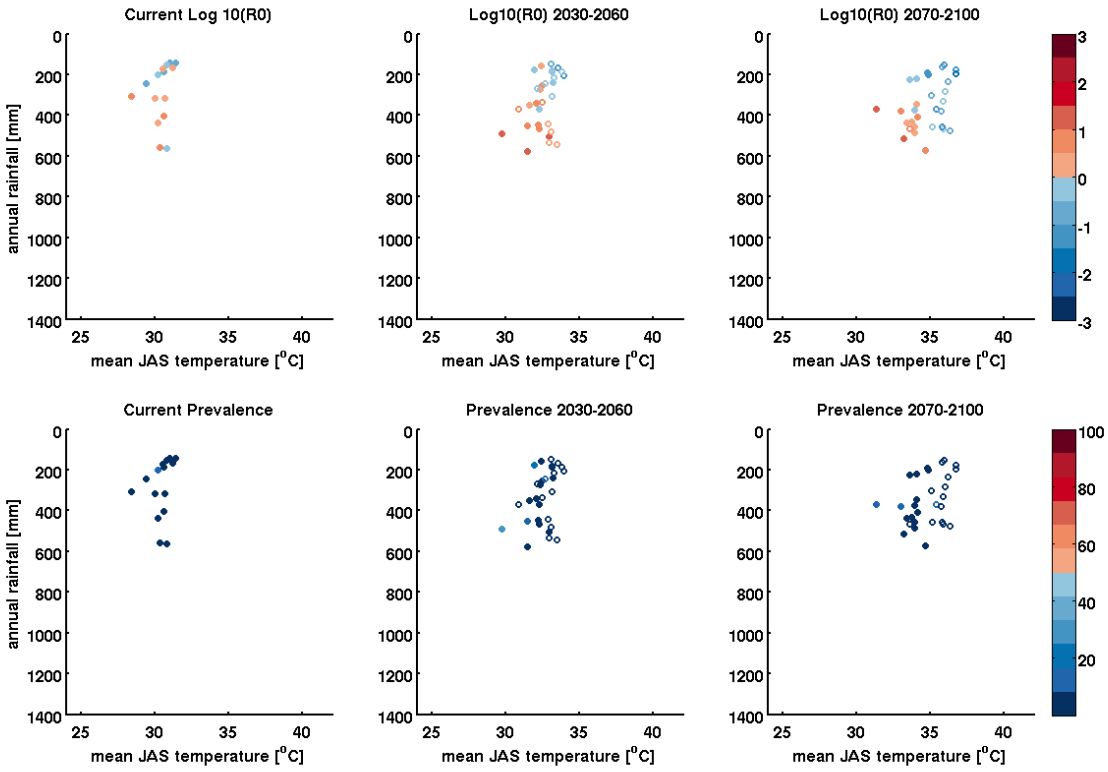

Figure D.9 Simulation results for site N2. The top row shows log10 (R_0) and the bottom row shows prevalence in children aged 2-10. Current conditions are shown on the left, short term conditions in the center, and long term conditions on the right. Closed circles are results from the simulation using CCSM4 climate predictions and open circles used MPI-ESM-MR predictions.

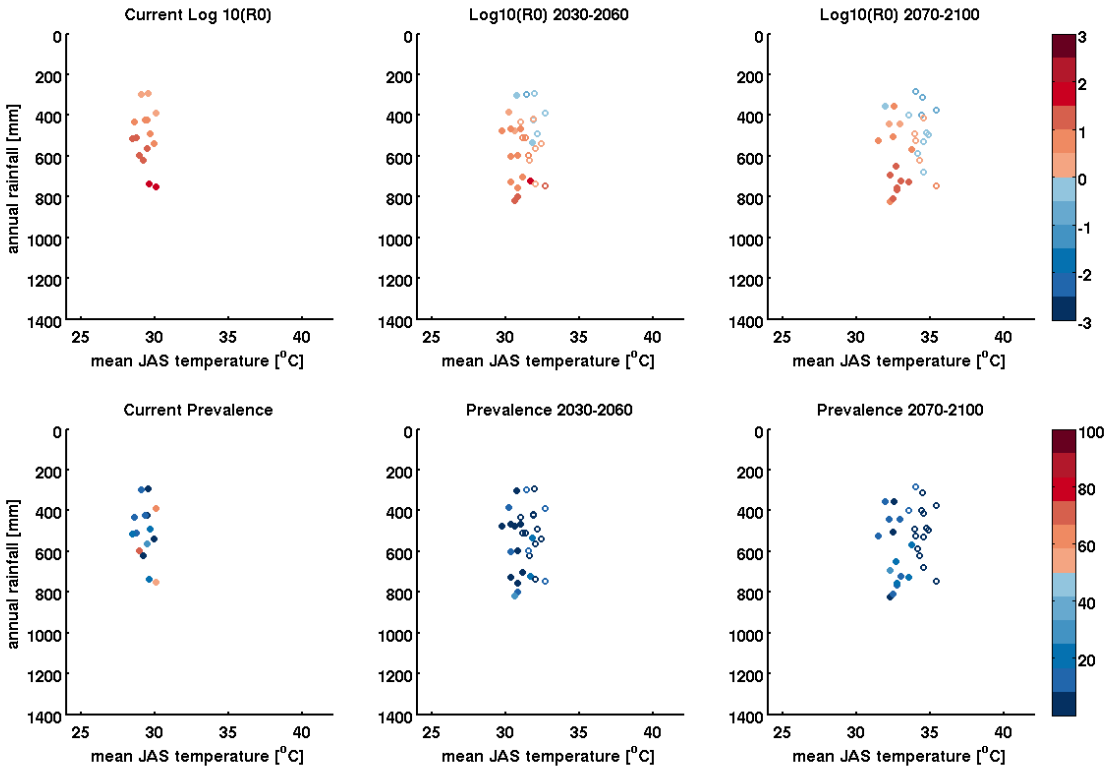

Figure D.10 Simulation results for site N3. The top row shows log10 (R_0) and the bottom row shows prevalence in children aged 2-10. Current conditions are shown on the left, short term conditions in the center, and long term conditions on the right. Closed circles are results from the simulation using CCSM4 climate predictions and open circles used MPI-ESM-MR predictions.

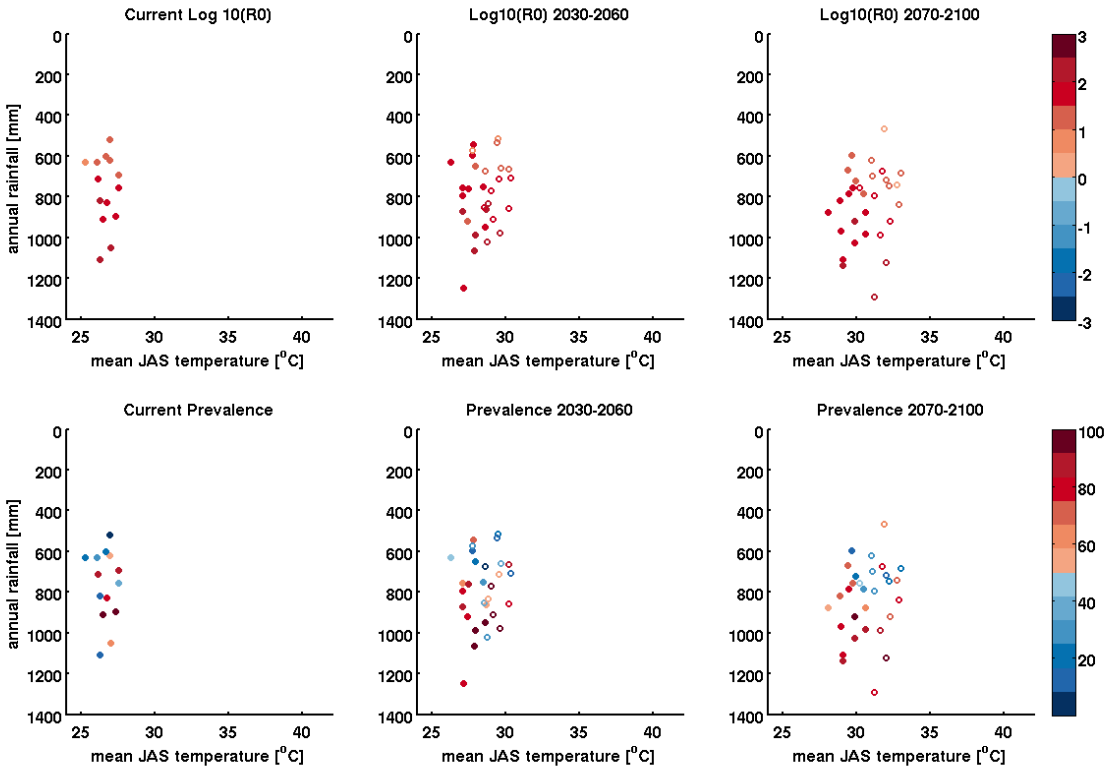

Figure D.11 Simulation results for site NA1. The top row shows log10 (R_0) and the bottom row shows prevalence in children aged 2-10. Current conditions are shown on the left, short term conditions in the center, and long term conditions on the right. Closed circles are results from the simulation using CCSM4 climate predictions and open circles used MPI-ESM-MR predictions.

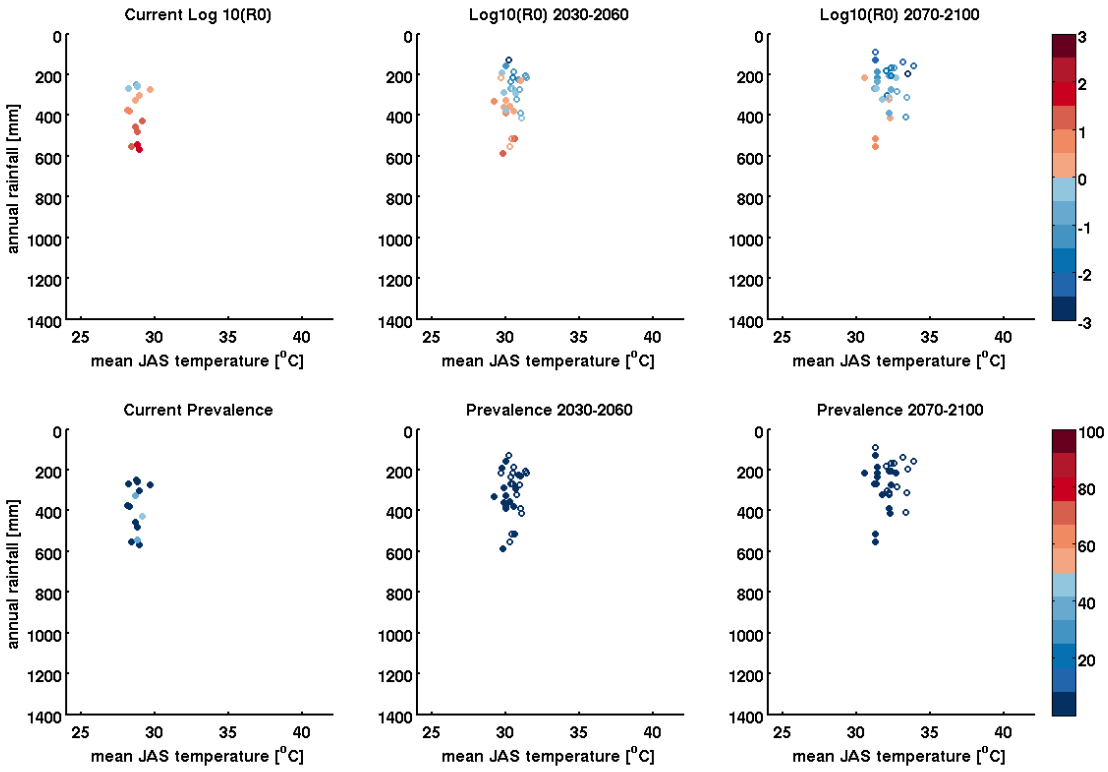

Figure D.12 Simulation results for site S1. The top row shows log10 (R_0) and the bottom row shows prevalence in children aged 2-10. Current conditions are shown on the left, short term conditions in the center, and long term conditions on the right. Closed circles are results from the simulation using CCSM4 climate predictions and open circles used MPI-ESM-MR predictions.

Appendix E Model code and input files

Simulation code and input files used in this thesis are available at:

\afs\athena.mit.edu\e\l\eltahir\yamana_code

References

Agnandji, S. T., Lell, B., Soulanoudjingar, S. S., Fernandes, J. F., Abossolo, B. P., Conzelmann, C., et al. (2011). First results of phase 3 trial of RTS,S/AS01 malaria vaccine in African children. *The New England Journal of Medicine, 365*(20), 1863-1875.

Águas, R., White, L. J., Snow, R. W., & Gomes, M. G. M. (2008). Prospects for malaria eradication in sub-Saharan Africa. *PLoS One, 3*(3), e1767.

Aron, J. L. (1988). Mathematical modelling of immunity to malaria. *Mathematical Biosciences, 90*(1-2), 385-396.

Bayoh, M. N. (2001). Studies on the development and survival of Anopheles gambiae sensu stricto at various temperatures and relative humidities. (PhD thesis, University of Durham). *Durham: University of Durham, 134*

Beier, J. C., Killeen, G. F., & Githure, J. I. (1999). Short report: entomologic inoculation rates and Plasmodium falciparum malaria prevalence in Africa. *The American Journal of Tropical Medicine and Hygiene, 61*(1), 109-113.

Bekessy, A., Molineaux, L., & Storey, J. (1976). Estimation of incidence and recovery rates of Plasmodium falciparum parasitaemia from longitudinal data. *Bulletin of the World Health Organization, 54*(6), 685.

Bicheron, P., Defourny, P., Brockmann, C., Schouten, L., Vancutsem, C., Huc, M., et al. (2008). Globcover: products description and validation report. *MEDIAS France, Toulouse,*

Bo, Z., Islam, S., & Eltahir, E. (1994). Aggregation-disaggregation properties of a stochastic rainfall model. *Water Resources Research, 30*(12), 3423-3435.

Bomblies, A. (2009). The hydrology of malaria: field observations and mechanistic modeling of the malaria transmission response to environmental climatic variability. (PhD thesis, Massachusetts Institute of Technology, Department of Civil & Environmental Engineering).

Bomblies, A. (2012). Modeling the role of rainfall patterns in seasonal malaria transmission. *Climatic Change, 112*(3-4), 673-685.

Bomblies, A., Duchemin, J. B., & Eltahir, E. A. B. (2008). Hydrology of malaria: Model development and application to a Sahelian village. *Water Resour.Res, 44*(12)

Bomblies, A., Duchemin, J. B., & Eltahir, E. A. B. (2009). A mechanistic approach for accurate simulation of village-scale malaria transmission. *Malaria Journal, 8*(1), 223.

Bomblies, A., & Eltahir, E. A. B. (2010). Assessment of the impact of climate shifts on malaria transmission in the Sahel. *EcoHealth, 6*(3), 426-437.

Bonnet, S., Gouagna, L., Paul, R., Safeukui, I., Meunier, J. Y., & Boudin, C. (2003). Estimation of malaria transmission from humans to mosquitoes in two neighbouring villages in south Cameroon: evaluation and comparison of several indices. *Transactions of the Royal Society of Tropical Medicine and Hygiene, 97*(1), 53-59.

Buckling, A., & Read, A. F. (2001). The effect of partial host immunity on the transmission of malaria parasites. *Proceedings of the Royal Society of London.Series B: Biological Sciences, 268*(1483), 2325.

Chitnis, N., Hyman, J. M., & Cushing, J. M. (2008). Determining important parameters in the spread of malaria through the sensitivity analysis of a mathematical model. *Bulletin of Mathematical Biology, 70*(5), 1272-1296.

Chiyaka, C., Garira, W., & Dube, S. (2007). Transmission model of endemic human malaria in a partially immune population. *Mathematical and Computer Modelling, 46*(5-6), 806-822.

Christensen, J. H., Hewitson, B., Busuioc, A., Chen, A., Gao, X., Held, R., et al. (2007). Regional climate projections. In S. Solomon (Ed.), *Climate Change 2007: The Physical Science Basis. Contribution of Working Group I to the Fourth Assessment Report of the Intergovernmental Panel on Climate Change* (). Cambridge, UK and New York, NY, USA: Cambridge University Press.

Coetzee, M., & Fontenille, D. (2004). Advances in the study of Anopheles funestus, a major vector of malaria in Africa. *Insect Biochemistry and Molecular Biology, 34*(7), 599-605.

Collins, M., Knutti, R., Arblaster, J., Dufresne, J. -., Fichefet, T., Friedlingstein, P., et al. (2013). Long-term climate change: Projections, commitments and irreversibility. In T. F. Stocker, et al. (Ed.), *Climate Change 2013: The Physical Science Basis. Contribution of Working Group I to the Fifth Assessment Report of the Intergovernmental Panel on Climate Change*

(pp. 1029–1136-12). Cambridge, United Kingdom and New York, NY, USA: Cambridge University Press.

Confalonieri, U., Menne, B., Akhtar, R., Ebi, K. L., Hauengue, M., Kovats, R. S., et al. (2007). Human health. Climate Change 2007: Impacts, Adaptation and Vulnerability. Contribution of Working Group II to the Fourth Assessment Report of the Intergovernmental Panel on Climate Change, ML Parry, OF Canziani, JP Palutikof, PJ van der Linden and CE Hanson, Eds., 391-431.

Cook, K. H., & Vizy, E. K. (2006). Coupled model simulations of the West African monsoon system: Twentieth-and twenty-first-century simulations. *Journal of Climate, 19*(15), 3681-3703.

Craig, M. H., Snow, R. W., & le Sueur, D. (1999). A climate-based distribution model of malaria transmission in sub-Saharan Africa. *Parasitology Today, 15*(3), 105-111.

Dagum, L., & Menon, R. (1998). OpenMP: an industry standard API for shared-memory programming. *Computational Science & Engineering, IEEE, 5*(1), 46-55.

De Bruin, H., & Moore, C. (1985). Zero-plane displacement and roughness length for tall vegetation, derived from a simple mass conservation hypothesis. *Boundary-Layer Meteorology, 31*(1), 39-49.

De Vera, A., & Terra, R. (2012). Combining CMORPH and rain gauges observations over the Rio Negro Basin. *Journal of Hydrometeorology, 13*(6), 1799-1809.

De Wit, M., & Stankiewicz, J. (2006). Changes in surface water supply across Africa with predicted climate change. *Science, 311*(5769), 1917-1921.

Dee, D. P., Uppala, S. M., Simmons, A. J., Berrisford, P., Poli, P., Kobayashi, S., et al. (2011). The ERA-Interim reanalysis: configuration and performance of the data assimilation system. *Quarterly Journal of the Royal Meteorological Society, 137*(656), 553-597.

Depinay, J. M., Mbogo, C. M., Killeen, G., Knols, B., Beier, J., Carlson, J., et al. (2004). A simulation model of African Anopheles ecology and population dynamics for the analysis of malaria transmission. *Malaria Journal, 3*, 29.

Desconnets, J., Taupin, J., Lebel, T., & Leduc, C. (1997). Hydrology of the HAPEX-Sahel Central Super-Site: surface water drainage and aquifer recharge through the pool systems. *Journal of Hydrology, 188*, 155-178.

Detinova, T. S. (1962). Age-grouping methods in Diptera of medical importance with special reference to some vectors of malaria. *Monograph Series.World Health Organization, 47*, 13-191.

Dietz, K., Molineaux, L., & Thomas, A. (1974). A malaria model tested in the African savannah. *Bulletin of the World Health Organization, 50*(3-4), 347.

Diuk-Wasser, M., Bagayoko, M., Sogoba, N., Dolo, G., Touré, M., Traoré, S., et al. (2004). Mapping rice field anopheline breeding habitats in Mali, West Africa, using Landsat ETM sensor data. *International Journal of Remote Sensing, 25*(2), 359.

Drakeley, C., Sutherland, C., Bousema, J. T., Sauerwein, R. W., & Targett, G. A. T. (2006). The epidemiology of Plasmodium falciparum gametocytes: weapons of mass dispersion. *Trends in Parasitology, 22*(9), 424-430.

Eltahir, E. A. B., & Gong, C. (1996). Dynamics of wet and dry years in West Africa. *Journal of Climate, 9*(5), 1030-1042.

Ermert, V., Fink, A., Jones, A., & Morse, A. (2011). Development of a new version of the Liverpool Malaria Model. I. Refining the parameter settings and mathematical formulation of basic processes based on a literature review. *Malaria Journal, 10*(1), 35.

Ermert, V., Fink, A. H., Morse, A. P., & Paeth, H. (2012). The impact of regional climate change on malaria risk due to greenhouse forcing and land-use changes in tropical Africa. *Environmental Health Perspectives, 120*(1), 77-84.

FAO. (1998). *Sahel weather and crop situation - june 1998* No. 1)Food and Agriculture Organization (FAO).

Filipe, J. A. N., Riley, E. M., Drakeley, C. J., Sutherland, C. J., & Ghani, A. C. (2007). Determination of the processes driving the acquisition of immunity to malaria using a mathematical transmission model. *PLoS Computational Biology, 3*(12), e255.

Flato, G., Marotzke, J., Abiodun, B., Braconnot, P., Chou, S. C., Collins, W., et al. (2013). Evaluation of climate models. In T. F. Stocker, et al. (Ed.), *Climate Change 2013: The Physical Science Basis. Contribution of Working Group I to the Fifth Assessment Report of*

the Intergovernmental Panel on Climate Change (pp. 741–866-9). Cambridge, United Kingdom and New York, NY, USA: Cambridge University Press.

Fouet, C., Gray, E., Besansky, N. J., & Costantini, C. (2012). Adaptation to aridity in the malaria mosquito Anopheles gambiae: Chromosomal inversion polymorphism and body size influence resistance to desiccation. *PLoS One, 7*(4), e34841.

Gaaboub, I., El-Sawaf, S., & El-Latif, M. (1971). Effect of different relative humidities and temperatures on egg-production and longevity of adults of Anopheles (Myzomyia) pharoensis Theob. *Zeitschrift Für Angewandte Entomologie, 67*(1-4), 88-94.

Garrett-Jones, C., & Grab, B. (1964). The assessment of insecticidal impact on the malaria mosquito's vectorial capacity, from data on the proportion of parous females. *Bull World Health Organ, 31*, 71-86.

Gething, P. W., Smith, D. L., Patil, A. P., Tatem, A. J., Snow, R. W., & Hay, S. I. (2010). Climate change and the global malaria recession. *Nature, 465*(7296), 342-345.

Gething, P. W., Patil, A. P., Smith, D. L., Guerra, C. A., Elyazar, I., Johnston, G. L., et al. (2011). A new world malaria map: Plasmodium falciparum endemicity in 2010. *Malar J, 10*(378), 1475-2875.

Giannini, A., Salack, S., Lodoun, T., Ali, A., Gaye, A., & Ndiaye, O. (2013). A unifying view of climate change in the Sahel linking intra-seasonal, interannual and longer time scales. *Environmental Research Letters, 8*(2), 024010.

Gillies, M. T. (1953). The duration of the gonotrophic cycle in Anopheles gambiae and Anopheles funestus, with a note on the efficiency of hand catching. *East African Medical Journal, 30*(4), 129-135.

Githeko, A., Brandling-Bennett, A., Beier, M., Atieli, F., Owaga, M., & Collins, F. (1992). The reservoir of Plasmodium falciparum malaria in a holoendemic area of western Kenya* 1. *Transactions of the Royal Society of Tropical Medicine and Hygiene, 86*(4), 355-358.

Gosset, M., Viarre, J., Quantin, G., & Alcoba, M. (2013). Evaluation of several rainfall products used for hydrological applications over West Africa using two high-resolution gauge networks. *Quarterly Journal of the Royal Meteorological Society, 139*(673), 923-940.

Gray, E. M., & Bradley, T. J. (2005). Physiology of desiccation resistance in Anopheles gambiae and Anopheles arabiensis. *The American Journal of Tropical Medicine and Hygiene, 73*(3), 553.

Gray, E. M., Rocca, K., Costantini, C., & Besansky, N. J. (2009). Inversion 2La is associated with enhanced desiccation resistance in Anopheles gambiae. *Malar J, 8*, 215.

Griffin, J. T., Hollingsworth, T. D., Okell, L. C., Churcher, T. S., White, M., Hinsley, W., et al. (2010). Reducing Plasmodium falciparum malaria transmission in Africa: a model-based evaluation of intervention strategies. *PLoS Med, 7*(8), 1-27.

Gu, W., & Novak, R. J. (2005). Habitat-based modeling of impacts of mosquito larval interventions on entomological inoculation rates, incidence, and prevalence of malaria. *The American Journal of Tropical Medicine and Hygiene, 73*(3), 546.

Guilloteau, C., Gosset, M., Vignolles, C., Alcoba, M., Tourre, Y. M., & Lacaux, J. (2014). Impacts of satellite-based rainfall products on predicting spatial patterns of the Rift Valley Fever vectors. *Journal of Hydrometeorology,* (2014)

Gupta, S., Snow, R. W., Donnelly, C. A., Marsh, K., & Newbold, C. (1999). Immunity to non-cerebral severe malaria is acquired after one or two infections. *Nature Medicine, 5*(3), 340-343.

Hansen, M., DeFries, R., Townshend, J., & Sohlberg, R. (2000). Global land cover classification at 1 km spatial resolution using a classification tree approach. *International Journal of Remote Sensing, 21*(6), 1331-1364.

Hay, S. I., Guerra, C. A., Gething, P. W., Patil, A. P., Tatem, A. J., Noor, A. M., et al. (2009). A world malaria map: Plasmodium falciparum endemicity in 2007. *PLoS Medicine, 6*(3), e1000048.

Hay, S. I., Smith, D. L., & Snow, R. W. (2008). Measuring malaria endemicity from intense to interrupted transmission. *The Lancet Infectious Diseases, 8*(6), 369-378.

Hay, S. I., Okiro, E. A., Gething, P. W., Patil, A. P., Tatem, A. J., Guerra, C. A., et al. (2010). Estimating the global clinical burden of Plasmodium falciparum malaria in 2007. *PLoS Medicine, 7*(6), e1000290.

Hoerling, M., Hurrell, J., Eischeid, J., & Phillips, A. (2006). Detection and attribution of twentieth-century northern and southern African rainfall change. *Journal of Climate, 19*(16), 3989-4008.

Hoffman, S. L., Oster, C. N., Plowe, C. V., Woollett, G. R., Beier, J. C., Chulay, J. D., et al. (1987). Naturally acquired antibodies to sporozoites do not prevent malaria: vaccine development implications. *Science (New York, NY), 237*(4815), 639.

Horsfall, W. R. (1943). Some responses of the malaria mosquito to light. *Annals of the Entomological Society of America, 36*(1), 41-45.

Irizarry-Ortiz, M. M., Wang, G., & Eltahir, E. A. B. (2003). Role of the biosphere in the mid-Holocene climate of West Africa. *J.Geophys.Res, 108*, 4042.

Jeffery, G. M., & Eyles, D. E. (1954). The duration in the human host of infections with a Panama strain of Plasmodium falciparum. *The American Journal of Tropical Medicine and Hygiene, 3*(2), 219-224.

Jepson WF, Moutia A, Courtois C. (1947). The malaria problem in Mauritius: the bionomics of Mauritian anophelines. *Bull. Entomol. Res, 38*, 117:208.

Joyce, R. J., Janowiak, J. E., Arkin, P. A., & Xie, P. (2004). CMORPH: A method that produces global precipitation estimates from passive microwave and infrared data at high spatial and temporal resolution. *Journal of Hydrometeorology, 5*(3), 487-503.

Kreuels, B., Kobbe, R., Adjei, S., Kreuzberg, C., von Reden, C., Bäter, K., et al. (2008). Spatial variation of malaria incidence in young children from a geographically homogeneous area with high endemicity. *Journal of Infectious Diseases, 197*(1), 85-93.

Lafferty, K. D. (2009). The ecology of climate change and infectious diseases. *Ecology, 90*(4), 888-900.

Lal, A. M. W. (1998). Performance comparison of overland flow algorithms. *Journal of Hydraulic Engineering, 124*(4), 342-349.

Langhorne, J., Ndungu, F. M., Sponaas, A. M., & Marsh, K. (2008). Immunity to malaria: more questions than answers. *Nature Immunology, 9*(7), 725-732.

Lee, Y., Meneses, C. R., Fofana, A., & Lanzaro, G. C. (2009). Desiccation resistance among subpopulations of Anopheles gambiae ss from Selinkenyi, Mali. *Journal of Medical Entomology, 46*(2), 316-320.

Lehmann, T., Dao, A., Adamou, A., Kassogue, Y., Diallo, M., Sékou, T., et al. (2010). Aestivation of the African malaria mosquito, Anopheles gambiae in the Sahel. *The American Journal of Tropical Medicine and Hygiene, 83*(3), 601-606.

Lindsay, S., & Martens, W. (1998). Malaria in the African highlands: past, present and future. *Bulletin of the World Health Organization, 76*(1), 33.

Liu, K., Tsujimoto, H., Cha, S. J., Agre, P., & Rasgon, J. L. (2011). Aquaporin water channel AgAQP1 in the malaria vector mosquito Anopheles gambiae during blood feeding and humidity adaptation. *Proceedings of the National Academy of Sciences, 108*(15), 6062.

Lobell, D. B., & Burke, M. B. (2008). Why are agricultural impacts of climate change so uncertain? The importance of temperature relative to precipitation. *Environmental Research Letters, 3*(3), 034007.

Lunde, T. M., Bayoh, M. N., & Lindtjørn, B. (2013). How malaria models relate temperature to malaria transmission. *Parasites & Vectors, 6*(1), 1-10.

Lunde, T. M., Korecha, D., Loha, E., Sorteberg, A., & Lindtjørn, B. (2013). A dynamic model of some malaria-transmitting anopheline mosquitoes of the Afrotropical region. I. Model description and sensitivity analysis. *Malaria Journal, 12*(1), 28.

Lysenko, A., & Semashko, I. (1968). Geography of malaria. A medico-geographic profile of an ancient disease. *Itogi Nauki: Medicinskaja Geografija.Moscow: Academy of Sciences, USSR,* , 25–146.

Macdonald, G. (1950). The analysis of infection rates in diseases in which super infection occurs. *Tropical Diseases Bulletin, 47*, 907-915.

Macdonald, G. (1955). The measurement of malaria transmission. *Proceedings of the Royal Society of Medicine, 48*(4), 295.

Macdonald, G. (1956). Epidemiological basis of malaria control. *Bull World Health Organ, 15*, 613-626.

Machault, V., Vignolles, C., Borchi, F., Vounatsou, P., Briolant, S., Lacaux, J., et al. (2011). The use of remotely sensed environmental data in the study of malaria. *Geospatial Health, 5*(2), 151-168.

Mackay, N., Chandler, R., Onof, C., & Wheater, H. (2001). Disaggregation of spatial rainfall fields for hydrological modelling. *Hydrology and Earth System Sciences Discussions, 5*(2), 165-173.

Maire, N., Smith, T., Ross, A., Owusu-Agyei, S., Dietz, K., & Molineaux, L. (2006). A model for natural immunity to asexual blood stages of Plasmodium falciparum malaria in endemic areas. *The American Journal of Tropical Medicine and Hygiene, 75*(2 suppl), 19.

Margulis, S. A., & Entekhabi, D. (2001). Temporal disaggregation of satellite-derived monthly precipitation estimates and the resulting propagation of error in partitioning of water at the land surface. *Hydrology and Earth System Sciences, 5*, 27-38.

Mariotti, L., Coppola, E., Sylla, M. B., Giorgi, F., & Piani, C. (2011). Regional climate model simulation of projected 21st century climate change over an all-Africa domain: Comparison analysis of nested and driving model results. *Journal of Geophysical Research: Atmospheres (1984–2012), 116*(D15)

Martens, P., Kovats, R., Nijhof, S., De Vries, P., Livermore, M., Bradley, D., et al. (1999). Climate change and future populations at risk of malaria. *Global Environmental Change, 9*, S89-S107.

Martens, W. J. (1997). Health impacts of climate change and ozone depletion: An eco-epidemiological modelling approach. (PhD thesis, University of Maastricht, Dept. of Mathematics).

Martens, W., Niessen, L., Rotmans, J., Jetten, T., & McMichael, A. (1995). Potential impact of global climate change on malaria risk. *Environmental Health Perspectives, 103*(5), 458.

Martens, W. (1998). Health impacts of climate change and ozone depletion: an ecoepidemiologic modeling approach. *Environmental Health Perspectives, 106*, 241-251.

Martin, P., & Lefebvre, M. (1995). Malaria and climate: sensitivity of malaria potential transmission to climate. *Ambio (Sweden),*

Mayne, B. (1930). A study of the influence of relative humidity on the life and infectibility of the mosquito. *Indian Journal of Medical Research, 17*(4), 1119-1137.

McMichael, A. J., Woodruff, R. E., & Hales, S. (2006). Climate change and human health: present and future risks. *The Lancet, 367*(9513), 859-869.

Menendez, C., Kahigwa, E., Hirt, R., Vounatsou, P., Aponte, J. J., Font, F., et al. (1997). Randomised placebo-controlled trial of iron supplementation and malaria chemoprophylaxis for prevention of severe anaemia and malaria in Tanzanian infants. *The Lancet, 350*(9081), 844-850.

Midega, J. T., Mbogo, C. M., Mwambi, H., Wilson, M. D., Ojwang, G., Mwangangi, J. M., et al. (2007). Estimating dispersal and survival of Anopheles gambiae and Anopheles funestus

along the Kenyan Coast by using mark–release–recapture methods. *Journal of Medical Entomology, 44*(6), 923.

Mitchell, T. D., & Jones, P. D. (2005). An improved method of constructing a database of monthly climate observations and associated high-resolution grids. *International Journal of Climatology, 25*(6), 693-712.

Mockenhaupt, F. P., Reither, K., Zanger, P., Roepcke, F., Danquah, I., Saad, E., et al. (2007). Intermittent preventive treatment in infants as a means of malaria control: a randomized, double-blind, placebo-controlled trial in northern Ghana. *Antimicrobial Agents and Chemotherapy, 51*(9), 3273-3281.

Molineaux, L., & Gramiccia, G. (1980). *The Garki Project*. Geneva: World Health Organization.

Montosi, E., Manzoni, S., Porporato, A., & Montanari, A. (2012). An ecohydrological model of malaria outbreaks. *Hydrol.Earth Syst.Sci, 16*, 2759-2769.

Moore, S., Shrestha, S., Tomlinson, K. W., & Vuong, H. (2012). Predicting the effect of climate change on African trypanosomiasis: integrating epidemiology with parasite and vector biology. *Journal of the Royal Society, Interface / the Royal Society, 9*(70), 817-830.

Mordecai, E. A., Paaijmans, K. P., Johnson, L. R., Balzer, C., Ben-Horin, T., Moor, E., et al. (2013). Optimal temperature for malaria transmission is dramatically lower than previously predicted. *Ecology Letters, 16*(1), 22-30.

Morin, J. (1993). Soil crusting and sealing. Soil tillage in Africa: needs and challenges. *FAO Soils Bulletin (FAO), 69*, 41-41-67.

Morita, M., & Chie Yen, B. (2000). Numerical methods for conjunctive two-dimensional surface and three-dimensional sub-surface flows. *International Journal for Numerical Methods in Fluids, 32*(8), 921-957.

Mouchet, J., Carnevale, P., & Manguin, S. (2008). *Biodiversity of malaria in the world* John Libbey Eurotext.

Muirhead-Thomson, R. C. (1957). The malarial infectivity of an African village population to mosquitoes (Anopheles gambiae): a random xenodiagnostic survey. *The American Journal of Tropical Medicine and Hygiene, 6*(6), 971.

Nachtergaele, F., & Batjes, N. (2012). *Harmonized world soil database* FAO.

Nicholson, S. E. (1993). An overview of African rainfall fluctuations of the last decade. *Journal of Climate, 6*(7), 1463-1466.

Niger. Bureau Central du Recensement, & Niger. Ministère de l'Economie et des Finances. Sécretariat Général. (2005). *Résultats définitifs: répartition par sexe et par groupe d'âges, selon la situation matrimoniale de la population du Niger en 2001*. Niamey, Niger: Bureau central du recensement.

Omer, S. M., & Cloudsley-Thompson, J. (1970). Survival of female Anopheles gambiae Giles through a 9-month dry season in Sudan. *Bulletin of the World Health Organization, 42*(2), 319.

Paaijmans, K. P., Read, A. F., & Thomas, M. B. (2009). Understanding the link between malaria risk and climate. *Proceedings of the National Academy of Sciences, 106*(33), 13844.

Parham, P. E., & Michael, E. (2009). Modelling the Effects of Weather and Climate Change on Malaria Transmission. *Environ Health Perspect, 118*(5), 620-626.

Parham, P. E., Pople, D., Christiansen-Jucht, C., Lindsay, S., Hinsley, W., & Michael, E. (2012). Modeling the role of environmental variables on the population dynamics of the malaria vector Anopheles gambiae sensu stricto. *Malaria Journal, 11*(1), 1-13.

Peterson, A. T. (2009). Shifting suitability for malaria vectors across Africa with warming climates. *BMC Infectious Diseases, 9*, 59.

Pollard, D., & Thompson, S. L. (1995). Use of a land-surface-transfer scheme (LSX) in a global climate model: the response to doubling stomatal resistance. *Global and Planetary Change, 10*(1-4), 129-161.

Porphyre, T., Bicout, D., & Sabatier, P. (2005). Modelling the abundance of mosquito vectors versus flooding dynamics. *Ecological Modelling, 183*(2), 173-181.

Reiter, P. (2008). Global warming and malaria: knowing the horse before hitching the cart. *Malaria Journal, 7*(Suppl 1), S3.

Reiter, P., Thomas, C. J., Atkinson, P. M., Hay, S. I., Randolph, S. E., Rogers, D. J., et al. (2004). Global warming and malaria: a call for accuracy. *The LANCET Infectious Diseases, 4*(6), 323-324.

Roehrig, R., Bouniol, D., Guichard, F., Hourdin, F., & Redelsperger, J. (2013). The present and future of the West African monsoon: a process-oriented assessment of CMIP5 simulations along the AMMA transect. *Journal of Climate,* (2013)

Rogers, D. J., & Randolph, S. E. (2000). The global spread of malaria in a future, warmer world. *Science, 289*(5485), 1763.

Rohr, J. R., Dobson, A. P., Johnson, P. T., Kilpatrick, A. M., Paull, S. H., Raffel, T. R., et al. (2011). Frontiers in climate change–disease research. *Trends in Ecology & Evolution, 26*(6), 270-277.

Ross, A., Killeen, G., & Smith, T. (2006). Relationships between host infectivity to mosquitoes and asexual parasite density in Plasmodium falciparum. *The American Journal of Tropical Medicine and Hygiene, 75*(2 suppl), 32.

Sachs, J., & Malaney, P. (2002). The economic and social burden of malaria. *Nature, 415*(6872), 680-685.

Schofield, L., & Grau, G. E. (2005). Immunological processes in malaria pathogenesis. *Nature Reviews Immunology, 5*(9), 722-735.

Segond, M., Neokleous, N., Makropoulos, C., Onof, C., & Maksimovic, C. (2007). Simulation and spatio-temporal disaggregation of multi-site rainfall data for urban drainage applications. *Hydrological Sciences Journal, 52*(5), 917-935.

Serrat-Capdevila, A., Valdes, J. B., & Stakhiv, E. Z. (2014). Water management applications for satellite precipitation products: Synthesis and recommendations. *JAWRA Journal of the American Water Resources Association, 50*(2), 509-525.

Service, M. (1993). *Mosquito ecology: field sampling methods* (2nd ed.). London, U.K.: Elsevier Applied Science.

Shaman, J., Stieglitz, M., Stark, C., Le Blancq, S., & Cane, M. (2002). Using a dynamic hydrology model to predict mosquito abundances in flood and swamp water. *Emerging Infectious Diseases, 8*(1), 8.

Smith, T., Killeen, G. F., Maire, N., Ross, A., Molineaux, L., Tediosi, F., et al. (2006). Mathematical modeling of the impact of malaria vaccines on the clinical epidemiology and natural history of Plasmodium falciparum malaria: Overview. *The American Journal of Tropical Medicine and Hygiene, 75*(2 suppl), 1.

Smith, T., Maire, N., Dietz, K., Killeen, G. F., Vounatsou, P., Molineaux, L., et al. (2006). Relationship between the entomologic inoculation rate and the force of infection for Plasmodium falciparum malaria. *The American Journal of Tropical Medicine and Hygiene, 75*(2 suppl), 11.

Smith, T., Maire, N., Ross, A., Penny, M., Chitnis, N., Schapira, A., et al. (2008). Towards a comprehensive simulation model of malaria epidemiology and control. *Parasitology, 135*(13), 1507-1516.

Snow, R. W., Omumbo, J. A., Lowe, B., Molyneux, C. S., Obiero, J. O., Palmer, A., et al. (1997). Relation between severe malaria morbidity in children and level of< i> Plasmodium falciparum transmission in Africa. *The Lancet, 349*(9066), 1650-1654.

Solomon, S., Qin, D., Manning, M., Chen, Z., Marquis, M., Averyt, K., et al. (2007). *Climate Change 2007: The Physical Science Basis. Contribution of Working Group I to the Fourth Assessment Report of the Intergovernmental Panel on Climate Change*. Cambridge, United Kingdom and New York, NY, USA: Cambridge University Press.

Struik, S. S., & Riley, E. M. (2004). Does malaria suffer from lack of memory? *Immunological Reviews, 201*(1), 268-290.

Sultan, B., & Janicot, S. (2003). The West African monsoon dynamics. Part II: The "preonset" and "onset" of the summer monsoon. *Journal of Climate, 16*(21), 3407-3427.

Tanser, F. C., Sharp, B., & le Sueur, D. (2003). Potential effect of climate change on malaria transmission in Africa. *The Lancet, 362*(9398), 1792-1798.

Taylor, K. E., Stouffer, R. J., & Meehl, G. A. (2012). An overview of CMIP5 and the experiment design. *Bulletin of the American Meteorological Society, 93*(4), 485-498.

Thomas, C. J., Davies, G., & Dunn, C. E. (2004). Mixed picture for changes in stable malaria distribution with future climate in Africa. *Trends in Parasitology, 20*(5), 216-220.

Thomas, C., & Lindsay, S. (2000). Local-scale variation in malaria infection amongst rural Gambian children estimated by satellite remote sensing. *Transactions of the Royal Society of Tropical Medicine and Hygiene, 94*(2), 159-163.

Thomson, M., Doblas-Reyes, F., Mason, S., Hagedorn, R., Connor, S., Phindela, T., et al. (2006). Malaria early warnings based on seasonal climate forecasts from multi-model ensembles. *Nature, 439*(7076), 576-579.

Thomson, M. C., Connor, S. J., Milligan, P. J., & Flasse, S. P. (1996). The ecology of malaria--as seen from Earth-observation satellites. *Annals of Tropical Medicine and Parasitology, 90*(3), 243-264.

Tonnang, H. E. Z., Kangalawe, R. Y. M., & Yanda, P. Z. (2010). Predicting and mapping malaria under climate change scenarios: the potential redistribution of malaria vectors in Africa.

Trape, J., Tall, A., Diagne, N., Ndiath, O., Ly, A. B., Faye, J., et al. (2011). Malaria morbidity and pyrethroid resistance after the introduction of insecticide-treated bednets and artemisinin-based combination therapies: a longitudinal study. *The Lancet Infectious Diseases, 11*(12), 925-932.

Van Lieshout, M., Kovats, R., Livermore, M., & Martens, P. (2004). Climate change and malaria: analysis of the SRES climate and socio-economic scenarios. *Global Environmental Change, 14*(1), 87-99.

Wallace, D. I., Southworth, B. S., Shi, X., Chipman, J. W., & Githeko, A. K. (2014). A comparison of five malaria transmission models: benchmark tests and implications for disease control. *Malaria Journal, 13*, 268-2875-13-268.

Wang, M. H., Marinotti, O., Vardo-Zalik, A., Boparai, R., & Yan, G. (2011). Genome-wide transcriptional analysis of genes associated with acute desiccation stress in Anopheles gambiae. *PLoS One, 6*(10), e26011.

Wigglesworth, V. (1939). *The Principles of Insect Physiology*. London: Methuen & Co. Ltd.

Wijesundera Mde, S. (1988). Malaria outbreaks in new foci in Sri Lanka. *Parasitology Today (Personal Ed.), 4*(5), 147-150.

Wolff, D. B., Marks, D., Amitai, E., Silberstein, D., Fisher, B., Tokay, A., et al. (2005). Ground validation for the tropical rainfall measuring mission (TRMM). *Journal of Atmospheric and Oceanic Technology, 22*(4), 365-380.

World Health Organization. (2014). *World malaria report 2014*. Geneva, Switzerland: WHO Press.

Yamana, T. K., & Eltahir, E. A. B. (2011). On the use of satellite-based estimates of rainfall temporal distribution to simulate the potential for malaria transmission in rural Africa. *Water Resources Research, 47*(2), W02540.

Yamana, T. K., Bomblies, A., Laminou, I. M., Duchemin, J., & Eltahir, E. A. (2013). Linking environmental variability to village-scale malaria transmission using a simple immunity model. *Parasites & Vectors, 6*, 226.

Yamana, T. K., & Eltahir, E. A. (2013). Projected impacts of climate change on environmental suitability for malaria transmission in West Africa. *Environ Health Perspect, 121*(10), 1179-1186.

Yang, H. M. (2000). Malaria transmission model for different levels of acquired immunity and temperature-dependent parameters (vector). *Revista De Saúde Pública, 34*(3), 223-231.